File Copy

37TH LUNAR AND PLANETARY SCIENCE CONFERENCE PROGRAM TO TECHNICAL SESSIONS

SPONSORED BY
LUNAR AND PLANETARY INSTITUTE
NASA JOHNSON SPACE CENTER

NASA

LPI

THIRTY-SEVENTH LUNAR AND PLANETARY SCIENCE CONFERENCE

Program to Technical Sessions

March 13–17, 2006

Sponsored by

Lunar and Planetary Institute
NASA Johnson Space Center

Program Committee

Stephen Mackwell, Co-Chair, *Lunar and Planetary Institute*
Eileen Stansbery, Co-Chair, *NASA Johnson Space Center*
John Armstrong, *Weber State University*
Nancy Chabot, *Johns Hopkins University*
Harold Connolly, *Kingsborough College of the City University of New York*
Catherine Corrigan, *Johns Hopkins University*
David Draper, *University of New Mexico*
Herbert Frey, *NASA Goddard Space Flight Center*
Yulia Goreva, *University of Arizona*
Tracy Gregg, *University at Buffalo*
Ross Irwin, *Smithsonian Institution*
Randy Korotev, *Washington University*
Don Korycansky, *University of California–Santa Cruz*
Dennis Matson, *Jet Propulsion Laboratory*
Greg Neumann, *NASA Goddard Space Flight Center*
Daniel Nunes, *Lunar and Planetary Institute*
Robert Pappalardo, *University of Colorado*
Elisabetta Pierazzo, *University of Arizona*
Frans Rietmeijer, *University of New Mexico*
David Senske, *Jet Propulsion Laboratory*
Stephanie Shipp, *Lunar and Planetary Institute*
Brad Thomson, *Lunar and Planetary Institute*
Michael Weisberg, *Kingsborough College of the City University of New York*
David Williams, *Arizona State University*
James Zimbelman, *Smithsonian Institution*

South Shore Harbour Resort and Conference Center

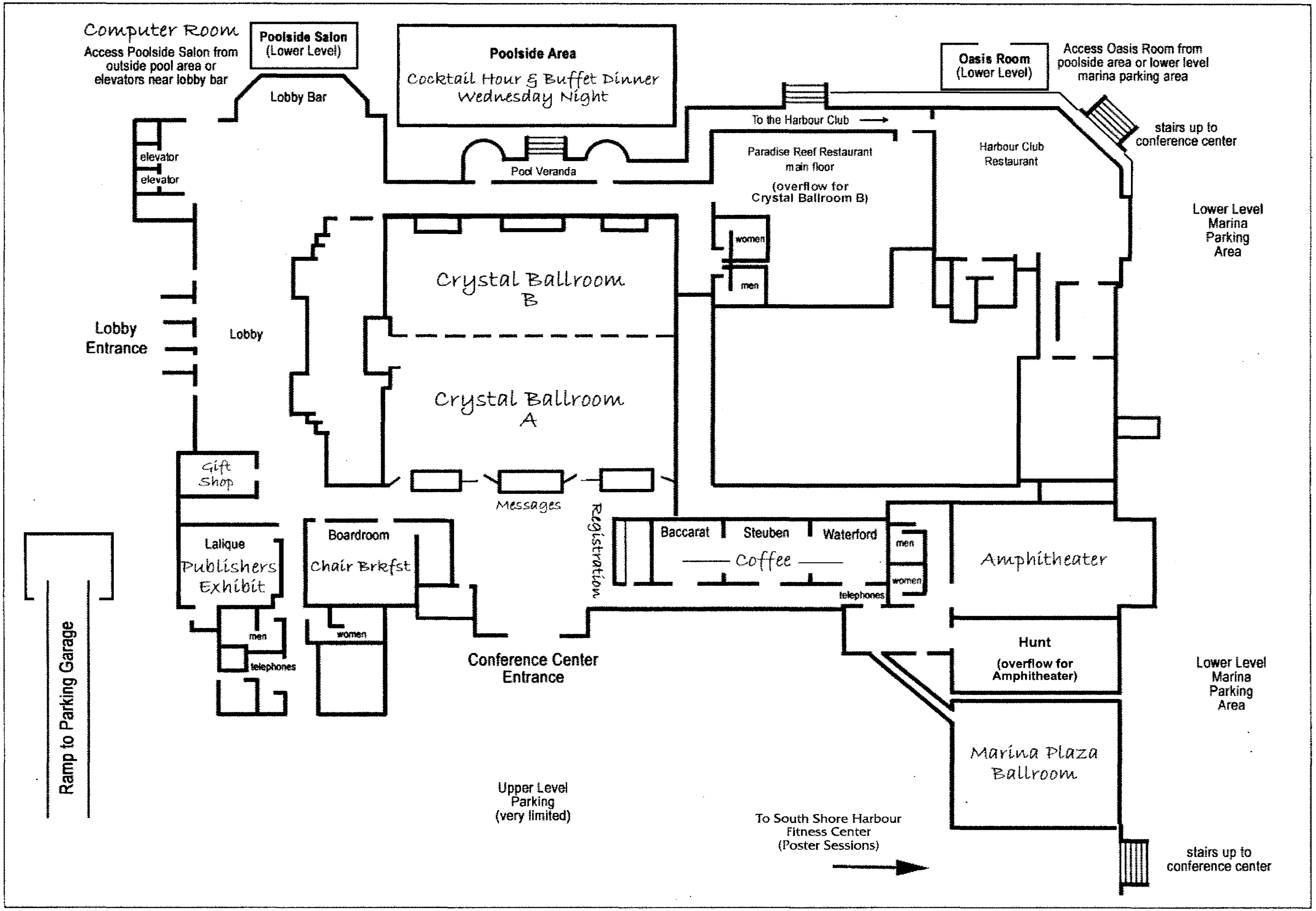

CONFERENCE INFORMATION

Registration — LPI Open House

A combination Registration/Open House will be held Sunday, March 12, 2006, from 5:00 p.m. until 8:00 p.m. at the Lunar and Planetary Institute. Registration will continue at the South Shore Harbour Resort and Conference Center, Monday through Thursday, 8:00 a.m. to 5:00 p.m., and Friday, 8:00 a.m. to noon. A shuttle bus will be available to transport participants between the LPI and local hotels Sunday evening from 4:45 p.m. to 8:30 p.m.

Business Center

Fax and copy services will not be available at the LPSC registration desk. These services are available for a fee at the hotel business center or you may use the LPI facilities (see note about daily shuttle service to the LPI below). Anyone needing to contact attendees during the conference may call 281-334-1000. These messages will be posted on the message board located next to the conference registration desk.

Shuttle Bus Service

A shuttle bus service between the LPI, South Shore Harbour, and various hotels will operate daily. A detailed schedule of the shuttle routes is in your registration packet and is available at the registration desk.

GUIDE TO TECHNICAL SESSIONS AND ACTIVITIES

Wednesday Morning, 8:30 a.m.

Wednesday Afternoon, 1:30 p.m.

Wednesday Evening, 5:30 p.m.

Wednesday Evening, 6:00–9:30 p.m.

Poolside	Cocktail Hour followed by Buffet Dinner	

Thursday Morning, 8:30 a.m.

Thursday Afternoon, 1:30 p.m.

Thursday Evening, 5:30 p.m.

Thursday Evening, 7:00–9:30 p.m.

Fitness Center Poster Session II

Friday Morning, 8:30 a.m.

Friday Afternoon, 1:30 p.m.

Print-only presentations are listed on pages 151 – 162

** Denotes speaker*

OPEN HOUSE EDUCATION AND PUBLIC OUTREACH DISPLAYS
Sunday, 5:00 p.m., LPI

Shaner A. J.   Laura M.   Wilkins K.   Tidwell L.   Lombardi D.
MarsBots: A National Robotics Education Learning Module for Grades 3 and 4 **[#1023]**
Developed by Phoenix Mission E/PO, MarsBots is an interdisciplinary learning module designed to engage elementary students in simulated investigations of the Martian environment and the robotic technologies of space exploration.

Hudoba Gy.   Hegyi S.   Hargitai H.   Gucsik A.   Józsa S.   Kereszturi A.   Sik A.   Szakmány Gy.   Földi T.   Gadányi P.   Bérczi Sz.
Planetary Analog Studies and Simulations: Materials, Terrains, Morphologies, Processes: Concise Atlas in the Solar System (9), Eötvös University, Hungary **[#1114]**
In this third *Concise Atlas (9) of the Solar System* planetary analog studies are focused on planetary materials, terrains, morphologies and processes comparisons and it includes planetary study simulations, too.

Buxner S. R.   Keller J. M.   Enos H. L.   Boynton W. V.
Mars GRS Curriculum Materials Educational Products **[#1958]**
The Mars Odyssey GRS (Gamma Ray Spectrometer) team will present our main educational products as a result of our E/PO efforts. These include six curriculum activities and two interactive web products that have been field tested in classrooms.

Stewart S. T.   Griswold A.   Sacco J. C.   Leinhardt Z. M.
IMPACT! The Making of a Meteorite — New Visualizations for Museums and Classrooms **[#1991]**
We present a new 7-minute DVD video providing a self-contained explanation of the "lifetime" of a meteor, which is part of a larger E/PO educational package on scientifically accurate visualizations of impact processes.

Croft S. K.   Pompea S. M.
Astronomy Village: Experiencing the Process of Science in a Multimedia Environment **[#2234]**
Two exciting multimedia environments have been developed to introduce middle and high school students to the research process in earth science and astronomy.

Klug S. L.   Christensen P. R.   Valderrama P.   Grigsby B.   Gootee B.   Rogers L.
A Model for Engaging Teachers and Students in Authentic STEM Research: The Mars Student Imaging Project **[#2448]**
The Mars Student Imaging Project has engaged over 11,000 students (grades 5–14) across the U.S. in authentic science research by allowing them to access the THEMIS camera currently in orbit around Mars and research the image they target.

STARDUST: MISSION ACCOMPLISHED
Monday, 8:30 a.m., Crystal Ballroom A

Chairs: **D. E. Brownlee and P. Tsou**

8:30 a.m. Brownlee D. E. *   Flynn G.   Hörz F.   Keller L.   McKeegan K.   Sandford S.   Tsou P.   Zolensky M. E.
Comet Samples Returned by the Stardust Mission **[#2286]**
Stardust has returned samples from comet Wild 2. The particles captured from the coma of a Kuiper belt comet should provide an intimate view of the initial solid building materials of the solar system that existed beyond the orbit of Neptune.

8:45 a.m. Tsou P. *   Brownlee D. E   Flynn G. J.   Hörz F.   Keller L.   McKeegan K.   Sandford S. A.   Zolensky M. E.
STARDUST's Comet Wild 2 and Contemporary Interstellar Stream Sample Status **[#2189]**
STARDUST's Wild 2 and interstellar samples returns to Earth. The preliminary number of samples, condition of the samples and their tracks will be presented.

9:00 a.m. Flynn G. J. * Borg J. Bleuet P. Brenker F. Brennan S. Daghlian C. Djouadi Z. Ferroir T. Gallien J.-P. Gillet Ph. Grant P. G. Grossemy F. Herzog G. F. Ishii H. A. Khodja H. Lanzirotti A. Leitner J. Lemelle L. Luening K. MacPherson G. Marcus M. Matrajt G. Nakamura T. Nakano T. Newville M. Pianetta P. Rao W. Rost D. Sheffield-Parker J. Simionovici A. Stephan T. Sutton S. R. Taylor S. Tsuchiyama A. Uesugi K. Westphal A. Vicenzi E. Vincze L.
Chemical Analysis of Wild-2 Samples Returned by Stardust **[#1217]**
The Stardust Composition Preliminary Analysis Team will report on preparations for the chemical analysis of the samples of comet Wild-2 collected by NASA Stardust spacecraft, and present the preliminary results.

9:15 a.m. Zolensky M. * Bland P. Bradley J. Brearley A. Brennan S. Bridges J. Brownlee D. Butterworth A. Dai Z. Ebel D. Genge M. Gounelle M. Graham G. Grossman L. Harvey R. Ishii H. Kearsley A. Keller L. Krot A. Lanzirotti A. Leroux H. Messenger K. Mikouchi T. Nakamura T. Ohsumi K. Okudaira K. Perronnet M. Rietmeijer F. Simon S. Stephan T. Stroud R. Taheri M. Tomeoka K. Toppani A. Tsou P. Tsuchiyama A. Weber I. Weisberg M. Westphal A. Yano H. Zega T.
Mineralogy and Petrology of Comet Wild2 Nucleus Samples **[#1203]**
First mineralogy and petrology results from the Stardust Mission.

9:30 a.m. Keller L. P. * Bajt S. Baratta G. A. Borg J. Brucato J. Burchell M. J. Colangeli L. d'Hendecourt L. Djouadi Z. Ferrini G. Flynn G. Franchi A. Fries M. Grady M. M. Graham G. Grossemy F. Kearsley A. Matrajt G. Mennella V. Nittler L. Palumbo M. E. Rotundi A. Wopenka B. Zolensky M.
Infrared, UV/VIS and Raman Spectroscopy of Comet Wild-2 Samples Returned by the Stardust Mission **[#2062]**
Results from the preliminary examination of Stardust samples obtained using various spectroscopic methods will be presented.

9:45 a.m. Sandford S. A. * Aleon J. Alexander C. Butterworth A. Clemett S. J. Cody G. Cooper G. Dworkin J. P. Flynn G. J. Gilles M. K. Glavin D. P. Jacobsen C. Matrajt G. Robert F. Spencer M. K. Stephan T. Westphal A. Wirick S. Zare R. N.
The Preliminary Examination of Organics in the Returned Stardust Samples from Comet Wild 2 **[#1124]**
The preparations for and latest results of the study of the organic portion of the samples of Comet Wild 2 returned by the Stardust Mission will be discussed.

10:00 a.m. Hörz F. * Borg J. Bradley J. P. Bridges J. Brownlee D. E. Burchell M. J. Cole M. J. Dai Z. R. Djouadi Z. Floss C. Franchi I. A. Graham G. A. Green S. F. Heck P. Hoppe P. Kearsley A. T. Leitner J. Leroux H. Teslich N. Marhas K. K. Schwandt C. S. See T. H. Stadermann F. J. Stephan T. Troadec D. Tsou P. Zolensky M. E. Stardust Cratering Team
Microcraters in Aluminum Foils Exposed by Stardust **[#1148]**
We will present preliminary results on the nature and size frequency distribution of microcraters that formed in aluminum foils during the flyby of comet Wild 2 by the Stardust spacecraft.

10:15 a.m. Leitner J. * Stephan T. Hörz F.
TOF-SIMS Analysis of Residues of Projectiles Shot onto Stardust Aluminum Foil **[#1576]**
Crater residues on Stardust Al foil from impact experiments using three different materials were analyzed by TOF-SIMS. Goal of this investigation is to evaluate the reproducibility of the chemical composition of the projectiles by TOF-SIMS analysis.

10:30 a.m. Hoppe P. * Heck P. Hörz F. Huth J. Marhas K. K. Messenger K. Snead C. Westphal A.
NanoSIMS Studies of Dust Projectile Shots into Stardust-type Aerogel and Aluminum Foils **[#1546]**
We present results of a feasibility study of isotopic analyses on Stardust samples, aimed at the discovery of presolar grains, with the NanoSIMS ion microprobe.

10:45 a.m. Bridges J. C. * Franchi I. A. Green S. F.
Extraction and Analysis of Microcrater Residues Using Focused Ion Beam Microscopy **[#1664]**
We describe results from a new technique using dual beam FIB/SEM with which impact residues can be extracted from microcraters and analysed by EDS. This will allow the determination of residue compositions from Stardust craters.

11:00 a.m. Stephan T. * Butterworth A. L. Snead C. J. Srama R. Westphal A. J.
TOF-SIMS Analysis of Aerogel Picokeystones — An Analogue to Stardust's Interstellar Dust Collection **[#1448]**
Tracks from ~0.5 μm particles, shot at ~20 km/s into aerogel to simulate Stardust's interstellar dust collection, were analyzed with TOF-SIMS. Particle residues distributed heterogeneously along the tracks can be localized and identified by TOF-SIMS.

11:15 a.m. Grady M. M. * Morlok A. Fernandes C. D. Johnson D.
Spectroscopy of Stardust from 200nm to 16μm (With a Gap in the Middle) **[#2032]**
UV/Vis and IR spectroscopy are complementary, non-destructive techniques that can be used to identify the presence of a range of organic and inorganic, hydrated and anhydrous minerals within micron-sized grains. We look forward to applying these techniques to the Stardust materials.

11:30 a.m. Fairey S. Burchell M. J. *
Impacts in Aerogel at Low Temperatures **[#1570]**
The effect of the aerogel temperature on dust capture in aerogel is reported. Aerogel temperatures in the range 175–293 K were used. No significant influence on particle capture (track length, entrance hole, captured particle size) was found.

MARS EXPRESS: PROBING THE DEPTHS
Monday, 8:30 a.m., Crystal Ballroom B

Chairs: J. J. Plaut and A. F. Chicarro

8:30 a.m. Chicarro A. F. *
Mars Express Scientific Overview After One Martian Year in Orbit **[#1061]**
A scientific overview of the consolidated results from all seven experiments onboard the ESA Mars Express spacecraft after more than one Martian year in orbit is given.

8:45 a.m. Plaut J. J. * Picardi G. Cicchetti A. Clifford S. Edenhofer P. Farrell W. Federico C. Frigeri A. Heggy E. Herique A. Ivanov A. Jordan R. Kofman W. Leuschen C. Marinangeli L. Nielsen E. Ori G. Orosei R. Pettinelli E. Phillips R. Plettemeier D. Safaeinili A. Seu R. Stofan E. Vannaroni G. Watters T. Williams I.
MARSIS Subsurface Sounding Observations of the South Polar Layered Deposits of Mars **[#1212]**
MARSIS on Mars Express has observed the south polar layered deposits with subsurface sounding radar. The radar penetrates to the base of the deposits and detects multiple internal layers.

9:00 a.m. Watters T. R. * Leuschen C. J. Plaut J. J. Picardi G. Safaeinili A. Clifford S. M. Farrell W. M. Ivanov A. B. Phillips R. J. Stofan E. R.
Evidence of Buried Basins in the Northern Lowlands of Mars from the MARSIS Radar Sounder **[#1693]**
The Mars Advanced Radar for Subsurface and Ionospheric Sounding (MARSIS) has returned the first subsurface data on the shallow crust in northern lowlands. MARSIS has revealed buried impact basins in the northern lowlands with little or no surface expression.

9:15 a.m. Ivanov A. B. * Safaeinili A. Picardi G. Plaut J. J.
Observations of the "Stealth" Radar Feature in the Mars Express MARSIS Investigation **[#1946]**
We will present the latest observations of the "Stealth" radar feature by the MARSIS radar.

9:30 a.m. Neukum G. * Basilevsky A. T. van Gasselt S. Greeley R. Hauber E. Head J. W. Hoffmann H. Ivanov B. A. Jaumann R. McCord T. B. Preuschmann S. Werner S. Williams D. A. Wolf U. HRSC Co-Investigator Team
New Insights into the Geological Evolution of Mars Through the Mars Express High Resolution Stereo Camera (HRSC) **[#2379]**
Mars fell dry on a global scale by 3.5 Ga ago, but there has been episodic volcanic, hydrothermal, fluvial, and glacial activity throughout the whole history of Mars though declining in magnitude through time in the past, becoming confined more and more to certain regions or locales.

9:45 a.m. McCord T. B. * Adams J. B. Hansen G. B. Combe J.-P. Bellucci G. Jaumann R. Neukum G. Poulet F. Gillespie A. R.
Mars Surface Compositional Units from the Mars Express High Resolution Stereo Camera **[#1757]**
Mars Express HRSC color data are used to define and map compositional units. These maps suggest there are only a few basic units for most of the surface but their distributions require revising some existing geologic maps and interpretations.

10:00 a.m. Pinet P. C. * Jehl A. Cord A. Daydou Y. D. Baratoux D. Chevrel S. C. Manaud N. Greeley R. Hoffmann H. Gwinner K. Scholten F. Roatsch T. Jaumann R. Neukum G. Bell J. F. Arvidson R. E. Johnson J. R. Squyres S. W. Mars Express HRSC Co-Investigator Team MER Science Team
Mars Express/HRSC Imaging Photometry and MER Spirit/PANCAM In Situ Spectrophotometry Within Gusev **[#1220]**
High resolution (100 m/pixel) mapping of surface physical properties derived from orbital HRSC multi-angular observations reveals different behaviours for the Columbia Hills and Plains materials in Gusev, complementing *in situ* Spirit observations.

10:15 a.m. Bibring J.-P. * Langevin Y. Poulet F. Gondet B. Gendrin A. Mustard J. Mangold N. Arvidson R. OMEGA Science Team
The Mars History Derived from the Mineralogical Data of OMEGA/MEx Acquired During the First Martian Year of Operations **[#2276]**
The OMEGA mineralogical data acquired so far enable to describe the global Mars history in three eras, characterized by the formation of phyllosilicates first, followed by that of sulfates in an acidic environment, and finally the formation of anhydrated ferric oxides.

10:30 a.m. Gendrin A. * Bibring J.-P. Quantin C. Mangold N. Le Mouelic S. Hauber E. Gondet B. Langevin Y. Poulet F. Arvidson R.
Two Years of Sulfate Mapping in Valles Marineris and Terra Meridiani as Seen by OMEGA/Mars Express **[#1872]**
We describe an updated view of the sulfate distribution associated to layered deposits, as seen by OMEGA/Mars Express.

10:45 a.m. Noe Dobrea E. Z. * Poulet F. Malin M. C.
Omega Analysis of Light-Toned Outcrops in the Chaotic Terrain of the Eastern Valles Marineris Region **[#2068]**
We investigate the compositional, morphologic, and stratigraphic relationships of light-toned outcrops in the chaotic terrain of the eastern Valles Marineris region using OMEGA, MOC, and MOLA data.

11:00 a.m. Fishbaugh K. E. * Poulet F. Langevin Y. Chevrier V. Bibring J.-P.
The Origin of Gypsum in the Mars North Polar Region **[#1642]**
The largest gypsum deposit on Mars, discovered by OMEGA, is mixed with the mafic north polar sand sea emanating from the Basal Unit. We discuss the origin of the gypsum as an evaporite deposit, formed in conditions unique to the region.

11:15 a.m. Poulet F. * Bibring J.-P. Langevin Y. Gondet B. Mustard J. Gendrin A. Mangold N. Loizeau D. Arvidson R. Chevrier V.
The Distribution of Phyllosilicates on Mars from the OMEGA-MEx Imaging Spectrometer **[#1698]**
New identifications by OMEGA of phyllosilicate minerals are presented and discussed, along with new evidence for regions containing hydrated minerals.

11:30 a.m. Langevin Y. * Poulet F. Vincendon M. Bibring J.-P. Gondet B. Schmitt B. Douté S.
New Observations of CO_2 and H_2O Ice by OMEGA/MEx in the South Polar Region of Mars During Late Summer (November/December 2005) **[#1744]**
We compare the late 2005 observations and the early 2004 observations of the Martian south polar cap by OMEGA over significant fractions of the cap.

LUNAR HISTORY FROM SAMPLES
Monday, 8:30 a.m., Marina Plaza Ballroom

Chairs: **R. A. Zeigler and V. A. Fernandes**

8:30 a.m. Jones J. H. *
The Dos and Don'ts of How to Build a Planet, Using the Moon as an Example **[#1354]**
In calculations of planetary bulk compositions, Mg/Al is good and Mg/Si is bad.

8:45 a.m. Jolliff B. L. *
What is the Composition of the Moon's Lower Crust? **[#2346]**
The composition of materials excavated by South Pole-Aitken basin from LP-GRS data, coupled with information from lunar samples, indicates that the lower crust beneath the FHT is ferroan and that extended magmatic activity was constrained to the PKT.

9:00 a.m. Borg L. E. * Wadhwa M.
ε^{142}Nd-ε^{143}Nd Isotopic Evidence for Protracted Lunar Differentiation **[#1154]**
Nd isotopic compositions are reported for lunar basalts (low-Ti, high-Ti and KREEP). Based upon these data, implications for the crystallization age of the lunar magma ocean are presented.

9:15 a.m. Rankenburg K. * Brandon A. D. Neal C. R.
Constraints on the Formation of the Moon from High-Precision Nd-Isotope Measurements of Lunar Basalts **[#1348]**
High-precision samarium-neodymium isotope data for six lunar basalts show that the bulk Moon has a ^{142}Nd/^{144}Nd ratio indistinguishable from chondritic meteorites.

9:30 a.m. Fernandes V. A. * Burgess R.
Ar-Ar Studies of Two Lunar Mare Rocks: LAP02205 and EET96008 **[#1145]**
Ar-Ar experiments have been conducted on two lunar meteorites, LAP02205 and EET96008, to determine the age of the formation and later events on the history of these meteorites. Age for LAP is ~2.92 Ga and for EET is 3.22 Ga. Final work is underway.

9:45 a.m. Terada K. * Sasaki Y. Sano Y.
In-Situ U-Pb Dating of Phosphates in Lunar Basaltic Breccia Yamato 981031 **[#1665]**
The lunar meteorites have been valuable sources for understanding the evolution of the Moon's crust. In this paper, we report ion microprobe U-Pb isotopic analyses of the phosphates in brecciated lunar meteorite Yamato 981031, which includes VLT mare basalt.

10:00 a.m. Vaughan J. P. * Nemchin A. A. Pidgeon R. T. Meyer C.
U-Pb Ages of Lunar Apatites **[#1606]**
U-Pb dating of apatites and zircons from two breccia samples shows that the U-Pb systems in the apatites have been reset during the impact, whereas the zircons preserve primary crystallization ages.

10:15 a.m. Korotev R. L. *
Geochemistry of a Unique Lunar Meteorite from Oman, a Crystalline Impact-Melt Breccia Dominated by Magnesian Anorthosite **[#1402]**
Fifteen Dhofar lunar meteorite stones are samples of a feldspathic, magnesian anorthosite that is largely unlike samples from the Apollo collection.

10:30 a.m. Zeigler R. A. * Korotev R. L. Jolliff B. L.
Geochemistry and Petrography of High-Th, Mafic Impact-Melt Breccia from Apollo 12 and Sayh Al Uhaymir 169 **[#2366]**
Here we characterize a new group of high-Th (30 ppm) impact-melt breccias found at Apollos 12 and 14 and compare them to the impact-melt breccia lithology of lunar meteorite SaU 169, which is compositionally identical.

10:45 a.m. Day J. M. D. * Pearson D. G. Taylor L. A.
Accretion, Differentiation, and Late Bombardment History of the Moon Deduced from Re-Os Isotope Systematics of Mare Basalts **[#2253]**
Using new precise Re-Os isotope data for Apollo 15 and 17 mare basalts we provide important constraints on the initial composition of the Earth-Moon system, and the controls of a putative lunar core and late accretionary materials on the HSE composition of the Moon.

11:00 a.m. Zellner N. E. B. * Delano J. W. Swindle T. D. Barra F. Olsen E. Whittet D. C. B.
Did a Transient Increase in the Impact Flux Occur 800 Ma Ago? **[#1745]**
Lunar impact glasses and other lunar samples from four Apollo landing sites suggest that there may have been a transient increase in the impact flux ~800 Ma ago.

11:15 a.m. Trail D. * Mojzsis S. J. Harrison T. M. Levison H. F.
Do Hadean Zircons Retain a Record of the Late Heavy Bombardment on Earth? **[#2139]**
Hadean zircons record overgrowths contemporaneous with the hypothesized Late Heavy Bombardment. The dynamics and implications of this result are investigated.

11:30 a.m. Nemchin A. A. * Whitehouse M. J. Pidgeon R. T. Meyer C.
Heavy Isotope Composition of Oxygen in Zircon from Soil Sample 14163: Lunar Perspective of an Early Ocean on the Earth **[#1593]**
New analyses of zircon from the lunar soil sample show elevated $\delta^{18}O$, similar to that observed in some >4.0 Ga zircons from Western Australia, implying that the oxygen data alone are not sufficient to support the presence of an ocean on the early Earth.

ASTEROIDS: OBSERVATIONS AND EXPERIMENTS
Monday, 8:30 a.m., Amphitheater

Chairs: **A. S. Rivkin and L. F. Lim**

8:30 a.m. Buczkowski D. L. * Prockter L. Barnouin-Jha O. S.
Mapping Lineaments on 433Eros: Process, Results, and Implications **[#1330]**
We identify lineaments on the surface of Eros and classify them according to type and region. We compare lineament orientation to impact craters to determine if there is a causal relationship and what effect lineaments have on crater shape.

8:45 a.m. Riner M. A. * Eckart J. M. Digilio J. G. Robinson M. S.
Global Study of Small-scale Color Features on 433 Eros, the Effect of Residual Scattered Light and Implications for Ponded Deposit Formation Mechanisms **[#2291]**
Utilizing all viable MSI color image sequences, we cataloged every resolvable spectral/albedo unit on Eros. A new detailed analysis of residual scattered light is presented and used to constrain interpretations of the spectral ratios.

9:00 a.m. Sasaki S. * Nimura T. Hiroi T. Ishiguro M. Hirata N. Abe M. Ueda Y. Yamamoto A. Clark B. E.
Space Weathering of Rock Surface Without Regolith: Laboratory Simulation of Spectral Change **[#1705]**
Laboratory space weathering simulation shows that small less-regolith asteroids with silicate composition may change their brightness and color by space weathering, although their weathering degree would be weaker than regolith-covered asteroids.

9:15 a.m. Vilas F. * Hendrix A. R.
Space Weathering on Asteroids: New Results from the Ultraviolet **[#2447]**
We explore the effects of space weathering on asteroids in the ultraviolet wavelength range, using existing observations from IUE and new observations from HST. These are compared with space weathering trends seen in lunar samples.

9:30 a.m. Reddy V. * Gaffey M. J. Abell P. A. Hardersen P. S.
Compositional Investigation of Near-Earth Asteroids 6456 Golombek, (5660) 1974 MA, (13553) 1992 JE **[#1746]**
Near-Earth Asteroids are the most important, yet least understood class objects. Of the ~3600 NEAs, only few have mineralogic and compositional information. We present our results from compositional studies of three NEAs: 6456 Golombek, 1974 MA, 1992 JE.

9:45 a.m. Rivkin A. S. * Volquardsen E. L.
What is the Surface Composition of Ceres? **[#1822]**
After staying up all night watching the world Ceres, we will make our pitch for new interpretations of its surface composition (iron-rich clays?) and highlight evidence for previously-unknown consituents (carbonates?).

10:00 a.m. Fieber-Beyer S. K. * Gaffey M. J. Hardersen P. S.
Near-Infrared Spectroscopic Analysis of Mainbelt M-Asteroid 755 Quintilla **[#1315]**
The mainbelt M-type asteroid 755 Quintilla exhibits an unusual set of absorption features suggesting that spinel may be a spectrally important mineral phase on its surface.

10:15 a.m. Lim L. F. * Emery J. E. McConnochie T. H.
Mid-IR Spectroscopy of M Asteroids with the Spitzer IRS: Preliminary Results **[#2148]**
Preliminary results from a survey of the emission spectra of 27 class M asteroids using the Spitzer Infrared Spectrograph (IRS; 5.2–38 μm) will be presented.

10:30 a.m. Hardersen P. S. * Gaffey M. J. Cloutis E. A. Abell P. A. Reddy V.
Discovering Spectral and Mineralogical Diversity Among the M-Asteroid Population **[#1106]**
Continuing spectral study of the M-asteroid population is finding significant diversity among these objects. A variety of spectral features suggest that M-asteroids have varying surface abundances of pyroxene, olivine, and phyllosilicate minerals.

10:45 a.m. Emery J. P. * Cruikshank D. P. Van Cleve J.
Structure and Composition of the Surfaces of Trojan Asteroids from Reflection and Emission Spectroscopy **[#2075]**
Comparisons with spectral libraries are not able to completely explain thermal emission spectra of several dark asteroids, including three Trojans (from Spitzer). We suggest this is due to the surface structure, and offer a couple of hypotheses.

11:00 a.m. Klima R. L. * Pieters C. M. Dyar M. D.
Pyroxene Spectroscopy at Visible Wavelengths: Effect of Iron Content on Spin Forbidden Absorption Features **[#1637]**
Spin-forbidden absorptions at visible wavelengths are one indicator of the form and chemistry of pyroxenes on an asteroid or planet's surface. We analyze synthetic Ca-free pyroxenes to systematically investigate how Fe^{2+} content affects these bands.

11:15 a.m. Lawrence S. J. * Lucey P. G. Taylor G. J.
Asteroid Surface Mineralogy Using Hapke Mixing Models: The Spectral Effects of Coarse-Grained Metal **[#1670]**
A new theoretical treatment for the spectral effects of coarse-grained Fe,Ni-metal is presented, and its implications are discussed.

11:30 a.m. Gaffey M. J. *
A Plethora of Partially Melted Asteroids? **[#1223]**
Asteroid spectral analyses suggest that partially melted asteroids are relatively common in contrast to the rarity of such assemblages among meteorites. The normal melting behavior of heated asteroids should produce abundant partially melted objects.

PLENARY SESSION: MASURSKY LECTURE AND DWORNIK AWARDS
Monday, 1:30 p.m., Crystal Ballroom A

Chairs: **S. K. Mackwell and E. K. Stansbery**

Presentation of the 2005 GSA Stephen E. Dwornik U.S. Citizen Student Award Winners

Masursky Lecture:

Masursky Lecture by Jonathan I. Lunine: "Beyond the Asteroid Belt: What to Do Next in the Outer Solar System, and Why?"

MARS: VOLCANISM AND TECTONICS
Monday, 2:15 p.m., Crystal Ballroom A

Chairs: **S. E. H. Sakimoto and L. S. Glaze**

2:15 p.m. Burt D. M. * Wohletz K. H. Sheridan M. F.
"Water-laid Tuff" of the Utah Desert and Similar Surge Deposit Misinterpretations: A Possible Lesson for Mars? **[#2295]**
More than 25 years ago, finely stratifed, cross-bedded, altered, mineralized surge deposits at Spor Mt., Utah, were widely interpreted to be water-laid. The alluvial or eolian misinterpretation was common at the time. Has a similar misinterpretation now been made on Mars?

2:30 p.m. Glaze L. S. * Baloga S. M.
Topographic Variability: Implications for Lava Flow Modeling **[#1302]**
We develop a statistic that relates lava flow thickness to surrounding topography. The statistic can be used to better understand the influence of topography on lava flow emplacement, e.g., extracting inferences about rheologic changes and interpreting the style of emplacement.

2:45 p.m. Byrnes J. M. * Finnegan D. C. Anderson S. W. Ramsey M. S.
Analyses of Amboy Crater, Mojave Desert, California, as an Analog for Small Martian Volcanoes **[#1205]**
This investigation presents a remote sensing data fusion approach for examining Amboy Crater as an analog for small Martian volcanoes, using laboratory, airborne, and spaceborne instruments to study VNIR, SWIR, TIR, and topographic characteristics.

3:00 p.m. Morris A. R. * Anderson F. S. Mouginis-Mark P. J. Haldemann A. F. C. Gregg T. K. P.
Initial Analysis of Topographic Roughness of Martian and Hawaiian Terrains **[#2064]**
We develop maps of roughness statistics of analog lava flows in Hawaii to identify the topographic resolution required to constrain the emplacement of volcanic features on the surface of Mars.

3:15 p.m. Vaucher J. * Baratoux D. Pinet P. C. Mangold N. Ceuleneer G. Gregoire M. Daydou Y. Chevrel S. Neukum G. HRSC Co-Investigator Team
Cerberus Plains, Mars: Chronology of Volcanic Event and Evidence of Recent Tectonic Activity **[#1851]**
We constrain the volcanic history from a new statistical approach giving a probability law associated with each lava surface age. Lava cut by fractures evidence very recent tectonic activities.

3:30 p.m. Sakimoto S. E. H. *
Constraints on the Origins of Platy Flows on Mars: Mud, Lava, Frozen Sea, Or . . . ? **[#2384]**
This is a progress report on a joint quantitative study of martian platy flows examining constraints on origins from fluvial, volcanic, debris (mud), and ice (frozen sea) perspectives.

3:45 p.m. Woodcock B. L. * Sakimoto S. E. H.
Lava Tube Flow: Constraints on Maximum Sustained Eruption Rates for Major Martian Volcanic Edifices **[#1992]**
Modeling maximum volcanic flow rates of large martian volcanoes yields an inverse relationship between edifice size and flow rate . . . low rates (often lava tubes) yield the largest edifice volumes; higher rates (usually channels) produce the smallest.

4:00 p.m. Bleacher J. E. * Greeley R. Williams D. A. Neukum G. HRSC Co-Investigator Team
Comparison of Effusive Volcanism at Olympus, Arsia, Pavonis, and Ascraeus Montes, Mars from Lava Flow Mapping Using Mars Express HRSC Data **[#1182]**
HRSC data enable lava flow mapping at high resolution with regional context. Results show a flank transition to channel-forming eruptions, followed by rift apron development where each volcano displays different morphologies and flow relationships.

4:15 p.m. Vidal A. * Mueller K. J. Golombek M. P.
Constraining Crustal Thickness and Hesperian Heat Flow on Solis Planum, Mars Using Depth to Detachment Mapping on Blind Thrust Faults **[#1712]**
We examine uncertainty in measurements of wrinkle ridge width on Solis Planum, Mars and their implications for fault modeling and heat flow calculations in the Hesperian.

MARS: CORE TO CLOUDS
Monday, 2:15 p.m., Crystal Ballroom B

Chairs: G. A. Neumann and R. J. Lillis

2:15 p.m. Fei Y. * Zhang L. Komabayashi T. Sata N. Bertka C. M.
Evidences for a Liquid Martian Core **[#1500]**
We present new melting data in the system Fe-Ni-S at Martian core pressures, using multi-anvil apparatus and laser-heated diamond-anvil cell. The data provide fundamental understanding of the relationships among the temperature, composition, and physical state of the martian core.

2:30 p.m. Lillis R. J. * Frey H. V. Manga M. Mitchell D. L. Lin R. P. Acuna M. H.
Bracketing the End of the Martian Dynamo: The Ages and Magnetic Signatures of Hellas and Ladon Basins **[#2183]**
We use visible and buried craters to compare crater retention ages of the magnetized Ladon basin and the demagnetized Hellas Basin to bracket the end of the martian dynamo era.

2:45 p.m. Hood L. L. *
East-West Trending Magnetic Anomalies in the Southern Hemisphere of Mars: Modeling Analysis and Interpretation **[#2203]**
The east-west trending anomalies in the Terra Sirenum region can be explained as due to their location near the martian paleoequator so that magnetization directions are nearly in the north or south directions. No elongated sources are required.

3:00 p.m. Voorhies C. V. *
Thickness of the Magnetic Crust of Mars from Magneto-Spectral Analysis **[#1426]**
Magnetic spectra from six analyses of MGS-MAG/ER data are fitted with that expected from both compact and extended sources. Magnetic crustal thickness is put at 47.8 ± 8.2 km. Extended sources are typically 650 km across. How did such vast regions form?

3:15 p.m. Bridges J. C. * Wright I. P.
Atmospheric Thickness on Ancient Mars: Constraints from SNC Meteorites **[#1990]**
We use carbonate abundance in an SNC meteorite as a guide to the carbonate abundances in the upper 7 km of Mars crust. This in turn is equivalent to an atmosphere pCO_2 of 2.3 bar >3.8Ga and total early Mars CO_2 inventory of 45 bar CO_2.

3:30 p.m. Chappelow J. E. * Sharpton V. L.
The Event That Produced Heat Shield Rock and Its Implications **[#1431]**
The discovery of the iron meteorite "Heat Shield Rock" in Terra Meridiani led to speculation that its presence implies Mars must once have had a denser atmosphere. However, to date no quantitative work addressing this theory has been presented.

3:45 p.m. Santiago D. L. * Colaprete A. Haberle R. M. Sloan L. C. Asphaug E. I.
Clouds, Cap, and Consequences: Outflow Events and Mars Hesperian Climate **[#1484]**
We focus on how outflows relate to past climate using a MGCM with cloud scheme. Early runs show water goes to the poles with current orbital configurations. We run the model for five years with a northern water ice cap then release the outflow, and will present these results.

4:00 p.m. Kreslavsky M. A. * Head J. W.
Evolution and Inner Structure of the Polar Layered Deposits on Mars: A Simple Deposition/Ablation Balance Model **[#2058]**
We show that simple changing climate-controlled balance of sublimation and ablation with albedo feedback and slope effect explains many characteristic properties of the polar layered deposits on Mars.

4:15 p.m. Neumann G. A. * Wilson R. J.
Night and Day: The Opacity of Clouds Measured by the Mars Orbiter Laser Altimeter (MOLA) **[#2330]**
MOLA uniquely provides atmospheric column opacity measurements both night and day. We contrast the pronounced nighttime opacity of the aphelion season tropical water ice clouds, and the enigmatic low opacity of the southern polar winter dry ice clouds.

VENUS
Monday, 2:15 p.m., Marina Plaza Ballroom

Chairs: D. C. Nunes and M. R. Warner

2:15 p.m. Bondarenko N. V. * Head J. W.
Roughness Asymmetry as a Clue to the Evolution of Crater-associated Dark Diffuse Features on Venus **[#1494]**
We analyze anisotropy of radar backscattering from Venus surface using both Magellan radar altimeter and SAR data. Reworking of surficial deposits of loose material by wind is responsible for degradation of crater-related parabolas.

2:30 p.m. Herrick R. R. *
Updates Regarding the Resurfacing of Venusian Impact Craters **[#1588]**
Results are summarized from an expanded data set of stereo-derived DEMs of Venusian craters, and geologic histories have been studied for several large craters. Most craters are not at the top of the stratigraphic column and many have complex histories.

2:45 p.m. Bond T. M. Warner M. R. *
Dating Venus: Statistical Models of Magmatic Activity and Impact Cratering **[#1957]**
Statistical modelling of the magmatic and impact history of Venus demonstrates that no rapid resurfacing event is required to match the impact crater record.

3:00 p.m. Ivanov M. A. * Head J. W.
Testing Directional (Evolutionary) and Non-Directional Models of the Geologic History of Venus: Results of Mapping in a Geotraverse Along the Equator of Venus **[#1366]**
A global equatorial geotraverse representing ~39% of the surface of Venus was mapped to test directional and non-directional geological evolution models. Major units showed global and generally continuous lateral geological correlation.

3:15 p.m. Ivers C. B. * McGill G. E.
Kinematics of a Tessera Inlier, Southwest Vellamo Planitia (V-12) Quadrangle, Venus **[#1248]**
Kinematic analysis indicates significant age overlap of tessera structures with formation of surrounding regional plains. Abrupt changes in fabric orientation across domain boundaries suggests significant lateral displacement of these domains.

3:30 p.m. Ghail R. C. *
Catastrophe Not Required: A New Steady-State Model of Venus **[#1269]**
New cosmochemical models of Venus indicate that it has a smaller core than Earth but bigger mantle. High temperatures decouple the crust and mantle allowing steady-state cooling by subcrustal plate tectonics. >2 Ga ago crustal recycling occurred.

3:45 p.m. Basilevsky A. T. * Abdrakhimov A. M.
Geochemistry of Venus Crust as Revealed by the Venera-Vega Analyses **[#1079]**
The Venera-Vega analyses are compared with the appropriate compositional data for the Earth, the Moon, Mars and meteorites. Most of the Venus' materials show similarities with geochemically evolved terrestrial rocks of island arcs and hot spots and one (Venera 14) shows similarity with MORBs.

4:00 p.m. Solomon S. C. * Anderson B. J. Domingue D. L. Gold R. E. Izenberg N. R. Leary J. C. McAdams J. V. McClintock W. E. McNutt R. L. Jr. Neumann G. A. Prockter L. M. Robinson M. S. Starr R. D. Taylor T. H. Williams B. G.
The MESSENGER Venus Flybys: Opportunities for New Venus Observations **[#1413]**
NASA's MESSENGER spacecraft, launched in August 2004, will pass as close as 300 km to Venus in June 2007. This flyby will provide a range of opportunities for new scientific observations of the Venus environment, atmosphere, and surface.

IMPACTS AND SMALL BODIES POTPOURRI
Monday, 2:15 p.m., Amphitheater

Chairs: M. J. Burchell and Z. M. Leinhardt

2:15 p.m. Britt D. T. * Consolmagno G. J. Merline W. J.
Small Body Density and Porosity: New Data, New Insights **[#2214]**
New data on the bulk density of small bodies from the NEA, comet, and KBO populations have provided some remarkable insights on the structure and porosity of comets and asteroids. Comets and mid-sized KBOs appear to have porosities of >60%.

2:30 p.m. Consolmagno G. J. SJ * Tegler S. C. Romanishin W. Britt D. T.
Shape, Spin, and the Structure of Asteroids, Centaurs, and Kuiper Belt Objects **[#1222]**
We compare the shapes and spin states of well-characterized asteroids with the stress/spin curves of Holsapple (2004). Applying these trends to centaurs and KBOs we infer that most have densities <1 g/cc, but the largest may be denser.

2:45 p.m. Scheeres D. J. *
Stability of Binary Asteroids Formed Through Fission **[#1632]**
The evolution of NEA contact binaries to orbital binaries due to spin-up effects (such as YORP) is discussed. The stability of the resulting systems indicate a strong preference for the formation of binary systems with non-elongate primaries.

3:00 p.m. Holsapple K. A. * Michel P.
Tidal Disruptions: Applications of an Analytical Theory for Solid Bodies **[#1026]**
We present results from a theory of tidal disruptions of solid bodies using an appropriate model for dry granular materials such as sands and rocks, for rubble-pile asteroids and comets, and for all larger satellites, asteroids and comets.

3:15 p.m. Leinhardt Z. M. * Stewart S. T.
Numerical Simulations of the Collisional Evolution of Cometesimals **[#2414]**
To further our understanding of the initial conditions that produced our solar system we present preliminary results from numerical simulations to model the chemical and physical alteration of Oort Cloud comets and Kuiper Belt Objects (KBOs) as the result of collisional evolution.

3:30 p.m. Lightwing A. Burchell M. J. *
Catastrophic Disruption of Mixed Ice: Sand Bodies **[#1565]**
The catastrophic disruption energy for mixed ice:silicate bodies is found by impact experiments in the laboratory. Impact speeds are 1–7 km/s. The resulting critical energy is found to be significantly greater than for pure water ice bodies.

3:45 p.m. Schultz P. H. * Harris R. S.
Argentine Impact Record: Implications for the Late Cenozoic Cratering Rates **[#2361]**
The large number of preserved impact glass layers in the Argentine loess-like sediments indicates that models of atmospheric entry need to be revised or that the Earth has had an enhanced flux over the late Cenozoic.

4:00 p.m. Xie Z. * Sharp T. G.
Ringwoodite Lamellae in Olivine from the L6 S6 Chondrite Tenham: Constraints on the Transformation Mechanism **[#2306]**
Here, we document the occurrence of ringwoodite lamellae in partially transformed olivine in Tenham, and discuss the likely transformation mechanism as incoherent transformation along distinct crystallographic planes in olivine, rather than coherent intracrystalline transformation.

4:15 p.m. Barnouin-Jha O. S. * Yamamoto S. Toriumi T. Sugita S. Matsui T.
Non-Intrusive Measurements of Crater Growth **[#1243]**
A new experimental technique to measure crater growth is presented whereby a high speed video captures profiles of a crater forming after impact obtained using a vertical laser sheet centered on the impact point.

NASA HEADQUARTERS BRIEFING
Monday, 5:00 p.m., Crystal Ballroom A

Led by Dr. Mary Cleave, Associate Administrator, Science Mission Directorate

ODYSSEY: A NEW VIEW OF THE MARS SURFACE
Tuesday, 8:30 a.m., Crystal Ballroom A

Chairs: **D. A. Senske and M. L. Litvak**

8:30 a.m. Senske D. A. * Plaut J. J.
The Mars Odyssey Mission, Two Mars Years of Observations **[#1452]**
In August of 2006, Mars Odyssey will complete its first extended mission. The results from the THEMIS, GRS and MARIE/MRME investigations continue to significantly advance the understanding of Mars and its environment.

8:45 a.m. Bell J. F. III* Bender K. C. Caplinger M. Cherednik L. L. Christensen P. R. Dombovári A. Glotch T. Hamilton V. E. Ivanov A. B. McConnochie T. McEwen A. Mehall G. Malin M. Million C. Murray K. Savransky D. Skok J. R. Wolff M. J. THEMIS Science Team
High Spatial Resolution Visible Wavelength Orbital Multispectral Imaging of Mars from the Mars Odyssey THEMIS-VIS Instrument **[#1653]**
This presentation shows examples of visible wavelength multispectral variations in Mars Odyssey THEMIS-VIS images that may be related to mineralogic variations at sub-100-meter scales on Mars.

9:00 a.m. Michalski J. R. * Ruff S. W. Christensen P. R.
TES and THEMIS Analysis of Martian Clay-bearing Deposits Discovered by Mars Express OMEGA **[#1242]**
We use thermal infrared emission data from the TES and THEMIS instruments to further constrain the mineralogy and geologic origin of clay-bearing deposits previously discovered by the OMEGA team.

9:15 a.m. Wagstaff K. L. * Bandfield J. L. Castano R. Chien S. Smith M. D.
Dust Storms and Water Ice Clouds: Feature Detection for Use Onboard THEMIS **[#2287]**
We present results from three regression models that can detect atmospheric features such as dust storms and water ice clouds on Mars. These models show promise for future use onboard THEMIS.

9:30 a.m. Taylor G. J. * Martel L. M. V. Boynton W. V.
Mapping Mars Geochemically **[#1981]**
Using multivariate analysis we made maps of Mars from elemental concentrations determined by Mars Odyssey GRS. Some units correspond to mapped geologic units, while others do not. It appears TES-derived Surface Type 1 is not compositionally uniform.

9:45 a.m. Gasnault O. *
Unsupervised Definition of Chemically Distinct Provinces at Mars **[#2328]**
A multivariate analysis of the Martian maps of H, Si, Fe, Cl, Th, and K shows that seven large provinces chemically distinct can be defined. The dimensionality of the problem can be reduced to 5, or even to 3, through a principal component analysis.

10:00 a.m. Keller J. M. * Boynton W. V. Williams R. M. S. Karunatillake S. GRS Science Team
Analysis of Layering at Mars Near-Surface Using Attenuation of Chlorine Gamma Rays **[#2343]**
Using model calculations and Mars GRS data, we investigate surface attenuation of high and low energy chlorine gamma rays as an indicator for layering within the upper few tens of cm of the martian surface. We do not find significant evidence for large scale regional layering of chlorine.

10:15 a.m. Karunatillake S. * Squyres S. Taylor J. Keller J. Gasnault O. Evans L. G. Reedy R. C. Starr R. Boynton W. Janes D. M. Kerry K. E. Dohm J. M. Sprague A. L. Hahn B. Hamara D. Mars Odyssey Team
Northern Low Albedo Regions of Mars: GRS Implications **[#2070]**
GRS results, showing significant enrichment of K and Th in northern low-albedo regions of Mars characterized by higher areal abundances of surface type 2, are more consistent with an igneous origin to surface type 2 than aqueous alteration of basalts.

10:30 a.m. Hahn B. C. * McLennan S. M. GRS Science Team
Gamma-Ray Spectrometer Elemental Abundance Correlations with Martian Surface Age: Implications for Martian Crustal Evolution **[#1904]**
We examine and report initial results of correlations between element abundances and martian apparent surface age. Secular changes in element abundances may reveal information about crustal and planetary formation and evolution.

10:45 a.m. Litvak M. L. * Mitrofanov I. G. Kozyrev A. S. Sanin A. B. Tretyakov V. Boynton W. V. Hamara D. K. Shinohara C. Saunders R. S.
Long Term Observations of Southern Winters on Mars: Evolution from Year to Year **[#1720]**
In this presentation we focused our efforts on estimation of CO_2 deposit column density and mass to make numerical comparison between southern winters of two successive martian years.

11:00 a.m. Mitrofanov I. G. * Boynton W. Litvak M. Kozyrev A. Sanin A. Saunders R. S.
Water Content in the Arabia Soil **[#1643]**
The HEND/Odyssey data analysis will allow us to determine the best model of soil in Arabia among Depth Homogeneous, Double Layers and Gradient Layer models, and using this model to provide the most reliable estimation of content of water in the Arabia soil.

11:15 a.m. Maurice S. * Feldman W. C. Gasnault O. Elphic R. C. Lawrence D. J. Prettyman T. H.
Stratigraphy of the Hydrogen Distribution at Equatorial Latitudes on Mars **[#2222]**
A simple one-dimensional model of water-equivalent-hydrogen abundance and stratigraphy is described and presented using Mars Odyssey Neutron Spectrometer data.

11:30 a.m. Feldman W. C. * Elphic R. C. Gasnault O. Hagerty J. J. Lawrence D. J. Maurice S. Mellon M. T.
Stratigraphy of Water-equivalent Hydrogen at High Northern Latitudes on Mars **[#2246]**
Measurements of the three neutron currents using the Mars Odyssey Neutron Spectrometer are used to determine the abundance and stratigraphy of hydrogen at high northern latitudes.

INTERPLANETARY DUST PARTICLES
Tuesday, 8:30 a.m., Crystal Ballroom B

Chairs: G. Matrajt and F. J. M. Rietmeijer

8:30 a.m. Toppani A. Dukes C. Baragiola R. Bradley J. P. *
Segregation of Mg, Ca, Al and Ti in Silicates During Ion Irradiation **[#2056]**
We report refractory element segregation in silicates exposed to ionizing ratiation in IDPs, lunar solar grains and mineral standards. The results may provide insight about the origin of GEMS.

8:45 a.m. Rietmeijer F. J. M. * Pun A. Nuth J. A. III
Initial Results on CaSiO Vapor Condensates: Potential Implications for Dust in Chondritic Aggregate Particles **[#1117]**
Deep metastable eutectic condensates in a CaSiO vapor: Oxygen fugacity and the annealing of novel, primitive extraterrestrial silicates.

9:00 a.m. Tsuchiyama A. * Uesugi K. Nakano T. Okazaki T. Nakamura K. Nakamura T. Noguchi T. Yano H.
Three-Dimensional Structures of Interplanetary Dust Particles and IDP-like Large Micrometeorites Using Synchrotron Radiation Microtomography **[#2001]**
3-D structures (porosities and fractal dimensions) of IDPs and IDP-like micrometeorites were examined. Although the spatial resolution is not sufficient for fine textures, we can obtain non-destructive 3-D information complimentary to TEM and SEM.

9:15 a.m. Joswiak D. J. * Brownlee D. E.
Non-GEMS Silicate Glasses in Chondritic Porous Interplanetary Dust Particles **[#2190]**
At least two populations of non-GEMS silicate glasses are present in chondritic porous interplanetary dust particles, a bulk silicate glass free of nanophase Fe-rich inclusions and an Al-rich interstitial glass which typically occurs between Fe-rich olivines.

9:30 a.m. Flynn G. J. * Lanzirotti A. Sutton S. R.
Chemical Compositions of Large Cluster IDPs **[#1216]**
We performed X-ray fluorescence spectroscopy on two large cluster IDPs, which sample the IDP parent body at a mass scale two orders-of-magnitude larger than ~10 µm IDPs, allowing proper incorporation of larger mineral grains into the bulk composition of the parent body.

9:45 a.m. Floss C. * Stadermann F. J. Wopenka B.
The Presence and Absence of Different Isotopically Anomalous Phases in the Primitive Interplanetary Dust Particle Tiberius **[#1290]**
Tiberius contains presolar corundum and SiC, and ^{15}N-rich hotspots, but presolar silicate grains are absent. The presence of phyllosilicates suggests aqueous alteration may have destroyed presolar silicates, but not more refractory presolar phases.

10:00 a.m. Christoffersen R. * Keller L. P.
Space Plasma Ion Processing of IDP Sulfides: A Comparison to Silicates Based on In-Situ TEM Ion Irradiation Experiments **[#1738]**
Pyrrhotite in IDPs shows relative less evidence of space radiation processing than silicates. We have calibrated and confirmed pyrrhotite's resistance to radiation-induced amorphization relative to silicates in a series of *in-situ* TEM irradiation experiments.

10:15 a.m. Matrajt G. * Brownlee D. Sadilek M. Kruse L.
The Fate of Organic Phases in Porous IDPs and Micrometeorites During Atmospheric Entry: A Pulse-heating Study **[#1006]**
We performed pulse-heating experiments on three organic molecules loaded in a porous substrate to investigate their survival by imitating the processes of atmospheric entry heating experienced by IDPs and micrometeorities.

10:30 a.m. Aléon J. * McKeegan K. D. Leshin L.
Oxygen Isotopes in Chondritic Interplanetary Dust: Parent-Bodies and Nebular Oxygen Reservoirs **[#1921]**
High precision oxygen isotope measurements of chondritic interplanetary dust particles reveal that all particles including porous anhydrous cluster particles of potential cometary origin have a composition typical of bulk carbonaceous chondrites.

10:45 a.m. Alexander C. M. O'D. * Keller L. P.
Are There Clues to the Dust 'Annealing' Process in Protoplanetary Disks in IDPs? **[#2325]**
We review the properties CP-IDPs and their components to determine whether they hold clues to the process responsible for the "annealing" seen in dust in protoplanetary disks.

11:00 a.m. Nittler L. R. * Busemann H. Hoppe P.
Isotopic and Micro-Raman Investigation of Interplanetary Dust Particles Collected During 2003 Earth Passage Through Comet Grigg-Skjellerup Dust Stream **[#2301]**
We report microscale H and N isotopic and Raman spectral data for IDPs collected in April 2003. The samples show extreme D and ^{15}N enrichments carried by very primitive organic matter. A high abundance of D anomalies might indicate a cometary origin.

11:15 a.m. Genge M. J. *
Ordinary Chondrite Micrometeorites from the Koronis Asteroids **[#1759]**
Seventy percent of coarse-grained micrometeorites are shown to have affinities to ordinary chondrites.

11:30 a.m. Maurette M. Brack A. Duprat J. Engrand C. *
Kerogen-rich Micrometeorites and Crude Petroleum in Hadean Time **[#1583]**
Antarctic micrometeorites can be assimilated to a kind of cosmic kerogen-rich "shales" when deposited on the sea floor, and trapped in sediments that get steadily buried. They could thus have formed huge amounts of crude petroleum on the young Earth.

CHONDRITES: METAL-RICH, SHOCK EFFECTS, METAMORPHISM, AND CLASSIFICATION
Tuesday, 8:30 a.m., Marina Plaza Ballroom

Chairs: M. K. Weisberg and M. Gounelle

8:30 a.m. Petaev M. I. *
Modeling Major and Trace Element Chemistry of Zoned Metal Grains from the CH and CB Chondrites **[#1681]**
To place better constraints on the origin of zoned metal grains from the CH and CB chondrites their major and trace element chemistry is modeled with the undated ZONMET code, which now includes 33 elements as well as new diffusion and activity coefficients.

8:45 a.m. Ivanova M. A. * Kononkova N. N. Franchi I. A. Verchovsky A. B. Korochantseva E. V. Trieloff M. Krot A. N. Brandstaetter F.
Isheyevo Meteorite: Genetic Link Between CH and CB Chondrites? **[#1100]**
Based on the mineralogy, petrography, bulk chemical, oxygen, and nintrogen isotopic compositions and ^{40}Ar-^{39}Ar age, Isheyevo is genetically related to CH and CB carbonaceous chondrites and provides a link between these group of pristine meteorites.

9:00 a.m. Krot A. N. * Ulyanov A. A. Ivanova M. A. Russell S. S.
Origins of Chondrules in the Metal-rich Carbonaceous Chondrites **[#1224]**
The CH/CB-like chondrite Isheyevo contains chondrules of several generations, which could have formed by different mechanisms and later accreted together with metal grains, CAIs, and heavily-hydrated matrix lumps into the Isheyevo parent body.

9:15 a.m. Weisberg M. K. * Kimura M. Suzuki A. Ohtani E. Sugiura N.
Discovery of Coesite and Significance of High Pressure Phases in the Gujba CB Chondrite **[#1788]**
We report clusters of coesite and coesite mixed with quartz in the Gujba CB chondrite, the first discovery of coesite in a meteorite. We previously found majorite-pyrope$_{ss}$ and wadsleyite. These high-pressure phases record a range of shock pressures.

9:30 a.m. Gounelle M. * Young E. D. Shahar A. Kearsley A.
Magnesium Isotopic Composition of CAIs and Chondrules from CB$_b$ Chondrites **[#2014]**
We measured magnesium isotope ratios in 17 chondrules and 3 CAIs from the CB$_b$ chondrites HH 237 and QUE 94411 by LA-MC-ICPMS. We find no detectable ^{26}Al excesses in the three CAIs and approximately normal (chondritic) $\delta^{25}Mg$ in CAIs and chondrules.

9:45 a.m. Zipfel J. * Weyer S.
Impact or Solar Nebula Origin of CB Chondrites? Evidence from Fe Isotopes **[#1902]**
Whether CB chondrites have an impact or solar nebula origin is explored by evaluating evidence from bulk Fe isotopes. Mass dependent Fe isotope compositions with increasingly lighter Fe from Gujba through Hammadah al Hamra 237 and Isheyevo are observed.

10:00 a.m. Swindle T. D. * Kring D. A. Olson E. K. Isachsen C. E.
Ar-Ar Dating of Shock-melted Ordinary Chondrites: Chronology of Asteroidal Impacts **[#1454]**
Three samples of H impact melt LAP 02240 have Ar-Ar plateaus at ~3900 Ma, consistent with the "lunar cataclysm" and other meteorite impact ages. LL impact melt breccia NWA 1701 records an ~1000 Ma impact, which degassed melt more thoroughly than clasts.

10:15 a.m. Perronnet M. * Zolensky M. E.
Characterization and Quantification of Metallic and Mineral Phases in the Highly Hydrated Grosvenor Mountains 95577 CR1 Chondrite **[#2402]**
Metallic and mineral phases of CR1 GRO 95577 have been quantified using X-ray elemental maps. The abundance of calcite, magnetite and intermediate sulfides plus the relatively low microprobe analysis total support a high degree of aqueous alteration.

10:30 a.m. Abreu N. M. * Brearley A. J.
Early Solar System Processes Recorded in the Matrices of CR2 Chondrites MET 00426 and QUE 99177 **[#2395]**
TEM and HRTEM observations of matrix and dark inclusions in the MET 00426 and QUE 99177 indicate that the fine-grained component of these meteorites is largely composed of amorphous silicate material. This amorphous material is the potential precursor of phyllosilicates.

10:45 a.m. Mikouchi T. * Zolensky M. Tachikawa O. Komatsu M. Ivanova M. A. Le L. Gounelle M.
Electron Back-Scatter Diffraction (EBSD) Analysis of Two Unusual Minerals in Carbonaceous Chondrites **[#1855]**
We report application of EBSD to identify two possible new minerals in carbonaceous chondrites (Fe-Cr phosphide in Kaidun and Ca-Al oxide in NWA470). The presence of these unique phases offers useful information on the formation of these meteorites.

11:00 a.m. Kimura M. * Grossman J. N. Weisberg M. K.
Fe-Ni Metal in Primitive Chondrites: Indicators of Classification and Metamorphic Conditions **[#1260]**
We report the relationship between metamorphic grade and the characteristic features of Fe-Ni metal in O and CO chondrites, in order to explore the classification criteria and metamorphic conditions of the highly primitive chondrites.

11:15 a.m. Grossman J. N. * Rubin A. E.
Dominion Range 03238: A Possible Missing Link in the Metamorphic Sequence of CO3 Chondrites **[#1383]**
DOM 03238 is probably CO3, but metal has been largely converted to magnetite. Olivine and matrix chemistry show it to be the first CO3.1 chondrite. The early metamorphic changes in the CO group are identical to those in ordinary chondrites.

11:30 a.m. Friedrich J. M. *
Impact-related Metal/Silicate Segregation in L Chondrites Falls: Clues from Major Elements **[#2084]**
Using bulk chemical analyses and analyzed sample size, one can place a limit on the scale of shock-related metal/silicate segregation. Results suggest shock-related heating could have played a role in early differentiation of solar system materials.

11:45 a.m. Schrader D. L. * Schmidt B. E. Lauretta D. S.
Oxidation and Sulfidation-Oxidation of Fe-based Alloys in H_2-H_2S-CO_2 Gas Mixtures **[#2256]**
We present the results of an experimental study of corrosion at 700°–1000°C in gases with enhanced O/H and at 1000°C in gases with enhanced (O+S)/H ratios, compared to solar abundances.

IMPACT CRATERING: OBSERVATIONS
Tuesday, 8:30 a.m., Amphitheater

Chairs: J. G. Spray and B. M. Simonson

8:30 a.m. Dulin S. A. * Elmore R. D.
Paleomagnetic Constraints on the Age of the Decaturville Impact Structure, Southwest Missouri **[#1246]**
A mixed breccia at the Decaturville impact structure in Missouri contains a post-depositional mid Permian magnetization which, along with stratigraphic data, constrains the timing of the impact to the Pennsylvanian-mid Permian.

8:45 a.m. Milam K. A. * Deane B. King P. L. Lee P. C. Hawkins M.
From the Inside of a Central Uplift: The View from Hawkins Impact Cave **[#1211]**
Hawkins Impact Cave is the only cave in the world known to have formed in the central uplift of a complex crater. The subterranean view it provides offers a unique, three-dimensional view into central uplift formation.

9:00 a.m. Misra S. * Bose T. Newsom H. E. Sengupta D.
Geochemistry of Impact Ejecta from Lonar Crater, India — More Clues to Crater Evolution **[#2123]**
The geochemistry of fines from between basalt blocks in the ejecta blanket of the Lonar crater provides only limited evidence for post-impact aqueous alteration, arguing against hydrothermal processes in the ejecta blanket on the crater rim.

9:15 a.m. Spray J. G. *
Ultrametamorphism of Impure Carbonates Beneath the Manicouagan Impact Melt Sheet: Evidence for Superheating **[#2385]**
Ultrametamorphism of impure carbonates by impact melt at Manicouagan has yielded refractory Ca-Mg alumino-silicates and *in situ* partial melts that attained >900°C. This indicates that the melt sheet cooled from >1800°C and was superheated.

9:30 a.m. Osinski G. R. * Bunch T. E. Wittke J.
Proximal Ejecta at Meteor Crater, Arizona: Discovery of Impact Melt-bearing Breccias **[#1005]**
Impact melt-bearing breccias have been discovered within the proximal ejecta blanket of Meteor Crater, Arizona, for the first time. They contain melt derived from a combination of the projectile and various sedimentary target rocks, including carbonates.

9:45 a.m. Plescia J. B. *
Kelly West Impact Structure, Australia, Gravity **[#1259]**
Gravity data for the Kelly West impact structure define a central positive anomaly over the central uplift with an inset low and an exterior annular low. A diameter of 6.6 km is estimated for the structure based on the gravity data.

10:00 a.m. Nelson M. J. * Newsom H. E.
Yaxcopoil-1 Impact Melt Breccias: Silicate Melt Clasts Among Dolomite Melt and Implications for Deposition **[#2081]**
Microprobe and XRD results suggest Chicxulub Yax-1 melt breccia consists of silicate melt clasts with K-rich rims amongst quenched dolomite melt. A depositional model includes brecciation of silicate melt by seawater and infilling by dolomite melt.

10:15 a.m. Guillemette R. N. * Yancey T. E.
Microaccretionary and Accretionary Carbonate Spherules of the Chicxulub Impact Event from Brazos River, Texas, and Bass River, New Jersey **[#1779]**
Small accretionary carbonate spherules of low-Mg calcite and clay are common in deposits of the Chicxulub impact. These form as primary calcite in the vapor plume, indicating much carbonate was preserved as particles and not as carbon dioxide.

10:30 a.m. Harris R. S. * Schultz P. H.
Airesites: A New Class of Late Miocene Tektites from Argentina **[#2272]**
Two new splashform tektites have been discovered attached to 5.28 Ma impact glass collected from the vicinity of Bahia Blanca, Argentina. Their occurrence, composition, and implications are discussed.

10:45 a.m. Skála R. * Čada M.
A Layered Moldavite from the Cheb Basin **[#1833]**
A layered moldavite was found in the Cheb Basin. It displays a layering on a millimeter to sub-millimeter scale and a significant chemical heterogeneity. This moldavite may indicate an incomplete mixing of parent rocks like Muong Nong tektites.

11:00 a.m. Sheffer A. A. * Dyar M. D. Sklute E. C.
Lightning Strike Glasses as an Analog for Impact Glasses: ^{57}Fe Mössbauer Spectroscopy of Fulgurites **[#2009]**
We present the results of microprobe and ^{57}Fe Mössbauer spectroscopy studies on eight fulgurites and Trinitite and their country rocks. Six glasses have lower Fe^{3+} or formed Fe metal. The chemistry of a lightning strike is similar to an impact.

11:15 a.m. Simonson B. M. * Sumner D. Y. Beukes N. J. Hassler S. Kohl I. Jones-Zimberlin S. Johnson S. Scally A. Gutzmer J.
Correlating Multiple Neoarchean-Paleoproterozoic Impact Spherule Layers Between South Africa and Western Australia **[#1489]**
Well-preserved early Precambrian successions on two continents each contain spherule layers from three large impacts. Although the layers occur in roughly coeval pairs, closer analysis suggests four impacts were involved.

11:30 a.m. Becker L. * Shukolyukov A. Macaissic C. Lugmair G. Poreda R.
ET Extraterrestrial Chromium at the Graphite Peak P/Tr Boundary and in the Bedout Impact Melt Breccia **[#2321]**
We present ET chromium isotopes as direct evidence of an impact event associated with sediments at the Permian-Triassic boundary at Graphite Peak Antarctica and in the Bedout impact melt breccia.

MARS: ANALOG STUDIES AND AEOLIAN DEPOSITION/EROSION
Tuesday, 1:30 p.m., Crystal Ballroom A

Chairs: **P. Lee and R. A. Beyer**

1:30 p.m. Lee P. * Glass B. J. Osinski G. R. Parnell J. Schutt J. W. McKay C. P.
Gullies on Mars: Fresh Gullies in Dirty Snow, Devon Island, High Arctic, as End-Member Analogs **[#1818]**
We report new observations of freshly-formed gullies in dirty snow on Devon Island, High Arctic, that may serve as end-member analogs for gullies on Mars. The dirty snow gullies on Devon are of surficial origin and are transient on annual timescales.

1:45 p.m. Irwin R. P. III * Howard A. D. Craddock R. A.
Theater-Headed Valleys: The Roles of Overland Flow and Groundwater Sapping **[#1912]**
At theater-headed valleys in Utah and Arizona, we found diversity relative to the Laity-Malin sapping model, large discharges of ephemeral contributing streams from the plateau surface, and substantial erosion of vegetated alluvial fill since 1985.

2:00 p.m. Craddock R. A. * Irwin R. P. III Williams R. Swanson D. Howard A. D. Quantin C. Zimbelman J. R.
Topical Martian Field Studies in the Ka'u Desert, Hawaii **[#1384]**
We are conducting field studies in the Ka'u Desert, Hawaii to understand the history of gully development, eolian reworking of fluvial materials, and alluvial fan formation. The geologic processes in this area make it a good analog for understanding surficial processes on Mars.

2:15 p.m. Clifford S. M. * Heggy E. Ali M. Ciarletti V. Corbel C. Dinwiddie C. L. Dolon F. Le Gall A. Grimm R. E. McGinnis R. N. Ney R. Sandberg S. K.
Mars Analog Investigations of the West Egyptian Desert Utilizing Multifrequency GPR and Other Electromagnetic Sounding Techniques **[#2442]**
We present results from geophysical sounding investigations of two locations in the West Egyptian Desert as potential geologic and hydrologic analogs of Mars.

2:30 p.m. Dinwiddie C. L. * Sandberg S. K. McGinnis R. N. Grimm R. E.
Geophysical Field Investigation of a Potential Hyper-Arid Desert Analog to Mars: The Western Desert of Egypt **[#2335]**
We are conducting transient electromagnetic and vertical electrical soundings of potential Mars analog sites to quantify the geoelectrical characteristics of the subsurface as a complement to radar soundings. This paper summarizes our recent work in the western desert of Egypt.

2:45 p.m. Quinn R. C. * Ehrenfreund P. Grunthaner F. J. Taylor C. L. Zent A. P.
Decomposition of Organic Compounds in Aqueous Conditions in the Chilean Atacama Desert and on Mars **[#1778]**
We report on the degradation kinetics of organics added to Atacama soils and compare our results to the Viking LR decomposition rates. We find that the overall rate of organic decomposition by some Atacama soils exceeds that of the Viking samples.

3:00 p.m. Parteli E. J. R. * Durán O. Herrmann H. J.
The Shape of the Barchan Dunes in the Arkhangelsky Crater on Mars **[#1827]**
We use a dune model to calculate dunes on Mars, and find that an astonishing difference based on the efficiency of the wind in carrying grains into saltation resolves the discrepancy between previously estimated and observed dune sizes on Mars.

3:15 p.m. Bourke M. C. *
A New Model for Linear Dune Formation: Merged Barchan Convoys on Mars **[#2432]**
MOC images indicate that dunes on Mars display a range of morphodynamics. These include merging, extension and calving. A new model is presented whereby linear dunes form by the collision and merging of barchan and dome dune convoys.

3:30 p.m. Zimbelman J. R. * Williams S. H.
Aeolian Ripples on Earth and Mars: Scale Diversity and Implications for Modes of Particulate Transport **[#2047]**
Granule ripples at Great Sand Dunes National Park were documented to move over a one-year interval, which is relevant to better understanding ripple and dune features of many length scales on Mars.

3:45 p.m. Bridges N. T. * Kushunapally R. Razdan A. Stone A. Laity J. Greeley R. Addleman D.
Quantifying Abrasion Maturity Using High Resolution Laser Scanning: Preliminary Quantitative Results and Applications to Terrestrial and Martian Studies **[#2065]**
Using laser scanning and mathematical algorithms, we show that abraded analog targets undergo an evolution in textural form that can be quantified using simple parameters. These results can be extended to constrain the abrasion maturity of ventifacts on Earth and Mars.

4:00 p.m. Beyer R. A. *
Erosion, Burial, and Exhumation at Ganges Mensa, Mars **[#1914]**
The slopes and surfaces of Ganges Mensa show evidence for aeolian erosion, burial, and exhumation. This indicates that its shape and surfaces are not primary features, but have been modified by the same forces that alter terrain elsewhere on Mars.

4:15 p.m. Ori G. G. * Komatsu G. Pacifici A. Hauber E. Gwinner K. Neukum G. HRSC Co-Investigator Team
Deltaic, Sebkha and Aeolian Sedimentation in Juventae Chasma and Their Stratigraphic Relationships (Mars) **[#1247]**
The High Resolution Stereo Camera has remarkable stereo capabilities and it allows three-dimensional analysis of Martian outcrops in cliffs and slopes in a way similar to the study of large terrestrial outcrops or seismic lines.

4:30 p.m. Venechuk E. M. * Allen C. C. Oehler D. Z.
Widespread Layers in Arabia Terra: Implications for Martian Geologic History **[#1380]**
Mars Orbital Camera high-resolution images indicate extensive layers across Arabia Terra, with the exception of an altitude-dependent region in the eastern half. Three different types of layers suggest varied formational environments.

GENESIS MISSION
Tuesday, 1:30 p.m., Crystal Ballroom B

Chairs: **D. S. Burnett and A. J. G. Jurewicz**

1:30 p.m. Jurewicz A. J. G. * Burnett D. S. Guan Y. G. Woolum D. S.
Elemental Solar Wind Fluences of Fe and Mg from Genesis Samples **[#2106]**
Preliminary Fe and Mg fluences in the bulk solar wind have been determined from Genesis fragments, and are applied to understanding fractionation of solar-wind from the average photosphere. The fragments analyzed by SIMS were of "average" to "fair" quality and underwent a standard wash.

1:45 p.m. Reisenfeld D. B. * Wiens R. C. Barraclough B. L. Steinberg J. T. DeKoning C. Raines J. Zurbuchen T. H. Burnett D. S.
The Genesis Mission: The Effects of Solar Wind Conditions on the Deposition and Interpretation of the Genesis Samples **[#1830]**
Our analysis of Genesis samples has been complemented by composition data from the SWICS instrument on ACE. We have used the ACE data to make comparisons between *in situ* composition measurements and abundances determined from the Genesis samples.

2:00 p.m. Calaway W. F. * Veryovkin I. V. Tripa C. E. Savina M. R. Pellin M. J. Burnett D. S.
The Elemental Abundance of Magnesium in Solar Wind Samples Returned by Genesis **[#1814]**
The composition of ^{24}Mg versus depth in a Si Genesis Discovery mission solar wind collector was measured using resonance ionization mass spectrometry. Integration of the data yields a dose of 1.02×10^{12} atoms/cm^2 for the 27 month exposure.

2:15 p.m. Nishiizumi K. * Reedy R. C. Burnett D. S. Komura K. Welten K. C.
Solar Cosmic Ray Production Rate on Genesis Quartz Target **[#2420]**
Radionuclides made in a SiO_2 slab flown on Genesis have been measured. The ^{7}Be/^{10}Be ratio is that for galactic cosmic rays. Excess activities of ^{26}Al and ^{22}Na are consistent with production by independently-measured solar-proton fluxes.

2:30 p.m. Heber V. S. * Wiens R. C. Burnett D. S. Baur H. Wiechert U. Wieler R.
Solar Wind Neon in the Genesis Concentrator Gold Cross by UV Laser Ablation: First Preliminary Data **[#2175]**
Neon was analysed along the radius of one arm of the Genesis concentrator gold cross. ^{20}Ne amounts are in agreement with predicted values. The reproducibility of ^{20}Ne/^{22}Ne is about 0.1%. But fractionation is different as predicted for O isotopes.

2:45 p.m. Grimberg A. * Bühler F. Burnett D. S. Jurewicz A. J. G. Hays C. C. Bochsler P. Heber V. S. Baur H. Wieler R.
Solar Wind Helium and Neon from Metallic Glass Flown on Genesis — Preliminary Bulk and Velocity-dependent Data **[#1782]**
He and Ne data have been obtained from a metallic glass flown on Genesis. We present preliminary total extraction data from the bulk solar wind and first results from studies on the putative solar energetic particle component.

3:00 p.m. Hohenberg C. M. * Meshik A. P. Marrocchi Y. Mabry J. C. Pravdivtseva O. V. Allton J. H. Burnett D. S.
Light Noble Gases from Solar Wind Regimes Measured in Genesis Collectors from Different Arrays **[#2439]**
We report He and Ne results from the Genesis regime samples. Fluences for all but the bulk collectors agree well with those predicted, however, the bulk fluence seems somewhat higher than predicted. No isotopic distinctions between the different regimes are apparent.

ASTROBIOLOGY: MARS, EARTH ANALOGS, AND THE SEARCH FOR LIFE
Tuesday, 3:30 p.m., Crystal Ballroom B

Chairs: **J. L. Vago and J. Parnell**

3:30 p.m. Stoker C. R. * Lemke L. G. Cannon H. Glass B. Dunagan S. Zavaleta J. Miller D. Gomez-Elvira J.
The Search for Subsurface Life on Mars: Results from the MARTE Analog Drill Experiment in Rio Tinto, Spain **[#1537]**
The Mars Analog Research and Technology (MARTE) experiment has developed an automated drilling system on a simulated Mars lander platform including drilling, sample handling, core analysis and down-hole instruments relevant to searching for life in the Martian subsurface.

3:45 p.m. Vago J. L. * Gardini B. Baglioni P. Kminek G. Gianfiglio G. ExoMars Project Team
ExoMars: ESA's Mission to Search for Signs of Life on the Red Planet **[#1871]**
ExoMars is a newly approved ESA mission scheduled to be launched in 2011. Its goal will be to land a rover on Mars to search for signs of past and present life, on the shallow subsurface and in exposed bedrock formations.

4:00 p.m. Parnell J. * Bowden S. A. Cockell C. S. Osinski G. R. Lee P.
Surface Mineral Crusts: A Priority Target in Search for Life on Mars **[#1049]**
Mineral crusts are strong candidates in the search for evidence of life during planetary exploration, and should be an important target for examination in impact craters. Crusts in the Haughton crater readily yield a biological signature.

4:15 p.m. Weinstein S. Pane D. Ernst L. A. Minkley E. Lanni F. Wettergreen D. S. Wagner M. Heys S. Teza J. Waggoner A. S. *
Autonomous Daylight Detection of Life by Fluorescence Imaging **[#2462]**
An integrated fluorescence imaging system was used to detect biomarkers from extant microbial colonies and biofilms during autonomous rover exploration. Chlorophyll and other biomarkers were visualized autonomously.

4:30 p.m. Smith T. * Thompson D. R. Weinstein S. Wettergreen D.
Autonomous Rover Detection and Response Applied to the Search for Life Via Chlorophyll Fluorescence in the Atacama Desert **[#2072]**
We describe autonomous rover detection and response capabilities applied to the search for Atacama Desert life. The rover could detect chlorophyll fluorescence and respond with more in-depth study, including application of fluorescent dyes.

4:45 p.m. Skelley A. M. * Aubrey A. D. Willis P. Amaskhukeli X. Ponce A. Ehrenfreund P. Grunthaner F. J. Bada J. L. Mathies R. A.
Detection of Trace Biomarkers in the Atacama Desert with a Novel In Situ Organic Compound Analysis System **[#2270]**
Detection of trace biomarkers in the Atacama Desert with a novel *in situ* organic compound analysis system.

TERRESTRIAL PLANET FORMATION AND DIFFERENTIATION
Tuesday, 1:30 p.m., Marina Plaza Ballroom

Chairs: **C. A. Hier-Majumder and T. Kleine**

1:30 p.m. Machida R. * Abe Y.
Formation of Terrestrial Planets in a Cold Nebula **[#1615]**
Recent studies show that protoplanetary disk is initially opaque, and water condenses at terrestrial planet formation region. Then, planetesimals mainly composed of ice should be formed in this region. Such planetesimals may form water ball planets.

1:45 p.m. Stimpfl M. * de Leeuw N. H. Deymier P. Drake M. J. Walker A. M.
In the Beginning There Was Water and Dust: A Look into Adsorption as a Mechanism to Explain Water in the Inner Solar System **[#1395]**
Atomistic techniques are employed to study the interaction between water and olivine surfaces with the aim to explore if water gas adsorbed onto the dust in the accretion disk could be a possible source for water in the inner solar system.

2:00 p.m. O'Brien D. P. * Morbidelli A. Levison H. F.
Simulations of Terrestrial Planet Formation with Strong Dynamical Friction: Implications for the Origin of the Earth's Water **[#2347]**
With numerical simulations of terrestrial planet accretion for different outer planet configurations, we find that an initially circular and co-planar Jupiter and Saturn are most consistent with the abundance of water on Earth.

2:15 p.m. Kleine T. * Halliday A. N. Palme H. Mezger K. Markowski A.
Hf-W Chronometry of the Accretion and Thermal Metamorphism of Ordinary Chondrite Parent Bodies **[#1884]**
Hf-W data for ordinary chondrites of different petrological type contrain the timescales of accretion and thermal metamorphism. The data indicate that core formation in some asteroids predated the accretion of chondrite parent bodies.

2:30 p.m. Humayun M. * Simon S. B. Grossman L.
Tungsten and Hafnium Distribution in Calcium-Aluminum Inclusions (CAIs) from Allende and Efremovka **[#2338]**
Hf and W distribution in CAI minerals shows that W appears to have diffused into silicates, which has implications for Hf-W chronology.

2:45 p.m. Nimmo F. * Agnor C. B. Raymond S.
Hf/W Isotopic Evolution from N-Body Accretion Simulations: Constraints on Equilibration Processes During Large Impacts **[#1390]**
We incorporate Hf/W isotopic evolution calculations into an N-body accretion code. Matching the observations requires that even the largest impactors undergo re-equilibration with the target mantle.

3:00 p.m. Jacobsen B. * Yin Q.-Z. Tinker D. Lesher C. E.
Tungsten (W) Self-Diffusion and Metal-Silicate Equilibration **[#2410]**
We performed the first of its kind W self-diffusion experiments and apply the results to address the question of metal-silicate equilibration during planet building processes.

3:15 p.m. Berthet S. * Malavergne V. Righter K. Corgne A. Combes R.
The Evolution of the EH4 Chondrite Indarch at High Pressure and Temperature: The First Experimental Results **[#2026]**
To derive constraints on the understanding of early planetary differentiation processes, HP-HT experiments have been performed on the EH4 chondrite Indarch. Melting relations and equilibrium partitioning behavior in this material have been studied.

3:30 p.m. Hier-Majumder C. A. * Hustoft J. W. Solomon S. C.
Core Formation by Percolation of Iron-rich Liquids **[#1329]**
Experimental and numerical modeling evidence supports the hypothesis that core formation in planetesimals and planets can occur by the percolation of iron-rich liquids through a deforming, solid silicate layer that compacts as the liquid core grows.

3:45 p.m. Asahara Y. Rubie D. C. * Frost D. J. Langenhorst F.
Oxygen Solubility in Liquid Iron and Consequences for the Early Differentiation of Earth and Mars **[#1162]**
Oxygen solubility in liquid Fe decreases with pressure up to 10–15 GPa and then increases at higher pressures. The metal-silicate partitioning of oxygen during core formation has a major effect on chemical differentiation of terrestrial planets.

4:00 p.m. Kegler Ph. * Holzheid A. Palme H.
The FeO, NiO and CoO Contents of Solar System Basalts and Their Significance for Core Formation in Planetary Bodies **[#1785]**
The difference in Ni and Co contents of eucrites, lunar and martian basalts can only be understood by considering the recently discovered steep decline of Ni and Co metal-silicate partition coefficients between 1 atmosphere and 5 GPa.

4:15 p.m. Mills N. M. * Agee C. B. Draper D. S.
Metal-Silicate Partitioning of Cesium — Implications for Planetary Core Formation **[#1709]**
These experiments provide a data set for the metal-silicate partitioning of cesium, a mantle-depleted lithophile element, and discuss its implications for core formation processes.

4:30 p.m. Righter K. *
Depletion of Vanadium in Planetary Mantles: Controlled by Metal, Oxide, or Silicate? **[#2259]**
Vanadium can be compatible in both FeNi metal and mantle phases such as spinel, magnesiowustite and garnet. In this paper consideration of depletions due to metal, oxide and silicate are critically evaluated and applied to Earth, Moon, Mars and Vesta.

IMPACT CRATERING: MODELING AND EXPERIMENTS
Tuesday, 1:30 p.m., Amphitheater

Chairs: O. S. Barnouin-Jha and D. G. Korycansky

1:30 p.m. Bray V. J. * Collins G. S. Morgan J. V.
Numerical Modelling of Impact Cratering on the Moon and Icy Satellites **[#1175]**
This work describes numerical simulations of cratering on the Moon and icy satellites using the SALE hydrocode, with the ultimate aim of inferring the thickness of Europa's ice crust.

1:45 p.m. Baldwin E. C. * Vocadlo L. Crawford I. A.
Reviewing the Impact Parameters for Meteor Crater Using AUTODYN **[#1835]**
There are a wide range of parameters suggested for the projectile that created Meteor Crater. We consider projectiles of varying size and velocity to determine AUTODYN's suitability for replicating large scale planetary impact events.

2:00 p.m. Morgan J. * Lana C. Artemieva N.
Shocked Minerals in the K-T Boundary: Implications for Obliquity of Impact **[#1281]**
This study combines observational data on the distribution of the coarse ejecta within the global K-T boundary layer with numerical modeling of vertical and oblique impacts, in an attempt to constrain the direction and angle of impact at Chicxulub.

2:15 p.m. Ohno S. * Sugita S.
Rapid Fall of the K/T Sulfuric Acid Aerosols and Oceanic pH Reduction **[#1699]**
We estimate the fall time of the K/T sulfuric acid aerosols considering the interaction with silicate condensates. We found that more than 70% of sulfuric acid aerosols would have fallen within two days and that oceanic pH decreases dramatically.

2:30 p.m. Gisler G. R. * Weaver R. P. Gittings M. L.
Energy Partitions in Three-Dimensional Simulations of the Chicxulub Meteor Impact **[#2095]**
We did three-dimensional simulations of the meteor impact at Chicxulub with the compressible multiphase multifluid hydrocode SAGE at four different angles. Steeper angles more likely account for the observations of widely dispersed material.

2:45 p.m. Abramov O. * Kring D. A.
Numerical Modeling of Impact-induced Hydrothermal Activity at the Chicxulub Crater **[#2102]**
Impact-induced hydrothermal activity at the Chicxulub crater was modeled using a finite-difference computer code constrained with geologic data. Duration of activity, system temperatures and dynamics, and biological implications are discussed.

3:00 p.m. Korycansky D. G. * Lynett P. J. Ward S. N.
Runup from Impact Tsunami **[#1255]**
We present results of the calculation of the on-shore runup of waves generated by the deep-ocean impact of a 300-m-diameter asteroid.

3:15 p.m. Wright S. P. * Vesconi M. A. Gustin A. Williams K. K. Ocampo A. C. Cassidy W. A.
Revisiting the Campo Del Cielo, Argentina Crater Field: A New Data Point from a Natural Laboratory of Multiple Low Velocity, Oblique Impacts **[#1102]**
In 2005, a ~15 metric ton meteorite was recovered from the Campo del Cielo crater field, Argentina for comparisons to previous excavations and calculations of energies of crater formation.

3:30 p.m. Cooke W. J. * Suggs R. M. Swift W. R.
A Probable Taurid Impact on the Moon **[#1731]**
On November 7, 2005, at 23:41:52 UT, observers located at the Marshall Space Flight Center captured the flash produced by a kilogram-sized meteoroid striking the lunar surface. Photometric analysis of the event video yields a mass of approximately 3.8 kg.

3:45 p.m. Kenkmann T. Thoma K. Deutsch A. * MEMIN-Team
Hypervelocity Impact into Dry and Wet Sandstone **[#1587]**
Experiments with 1-cm-sized steel spheres impacting dry and wet sandstone blocks at 5.3 km/s are presented. Differences in shape and size of the craters and in the ejection flow indicate the influence of pore fluids on the cratering process.

4:00 p.m. Yamamoto S. * Kadono T. Sugita S. Matsui T.
Cumulative Mass-Velocity Distribution of Impact Ejecta in Oblique Impacts **[#1164]**
We measured the cumulative mass-velocity distribution of ejecta with velocities of a few m/s (low-velocity ejecta) for impacts at various impact angles into soda-lime glass spheres.

4:15 p.m. Hamano K. * Abe Y.
Pressure Dependence of Atmospheric Loss by Impact-induced Vapor Expansion **[#1562]**
Atmospheric pressure differs by planets and could change through its evolution. We calculated atmospheric motion with vapor expansion with a 2-D cylindrical hydrocode and investigated the pressure dependence of the mass of the atmospheric loss.

4:30 p.m. Ishibashi K. * Ohno S. Sugita S. Kadono T. Matsui T.
Oxidation of Carbon Compounds by SiO_2-derived Oxygen Within Laser-induced Vapor Clouds **[#1721]**
We conducted laser heating experiments that simulate impact-induced vaporization to investigate the effects of SiO_2-derived oxygen on carbon chemistry within vapor clouds. The results indicate that SiO_2-derived oxygen oxidizes carbon significantly.

SPECIAL SESSION: PHOENIX LANDING SITE
Tuesday, 5:30 p.m., Marina Plaza Ballroom

Chairs: R. E. Arvidson and L. K. Tamppari

5:30 p.m. Smith P. H. *
Science Considerations Driving the Choice of the Phoenix Mission Landing Site **[#1910]**
The Phoenix mission will study the subsurface ice discovered in 2002 by the Odyssey orbiter. There are a number of scientific objectives concerning the chemistry and mineralogy of this region that require careful attention to the selection of a landing site in the northern plains.

5:45 p.m. Arvidson R. E. * Barge L. Barnes J. Boynton W. Friedson J. Golombek M. P. Guinn J. Kass D. M. Kirk R. Malin M. Mellon M. Michaels T. Paige D. Parker T. J. Rafkin S. Seelos K. Smith M. D. Smith P. H. Tamppari L. Tyler D.
Overview of Mars Exploration Program 2007 Phoenix Mission Landing Site Selection **[#1328]**
This abstract focuses on the 2007 Phoenix Lander site selection work, including entry, descent, and landing (EDL)-based requirements, analyses of candidate sites, and a summary of what has been accomplished to date.

6:00 p.m. Smith P. H. Arvidson R. E. Golombek Guinn J.
Panel Discussion (30 Minutes)

POSTER SESSION I
Tuesday, 7:00 p.m., Fitness Center

EVERYTHING VENUS

Carter L. M. Campbell D. B. Margot J.-L. Campbell B. A.
Mapping the Topography of Maxwell Montes Using Ground-based Radar Interferometry **[#2261]**
We use ground-based radar interferometry to map the topography of Maxwell Montes at a higher spatial resolution than Magellan. The data have a spatial resolution of ~2 km and can be used to study the relationship between emissivity and altitude on a more localized scale than was previously possible.

Bleamaster L. F. III
Geologic Mapping of Isabella Quadrangle (V50), Venus **[#2233]**
Geologic mapping of the Isabella Quadrangle (V50) provides tests of wrinkle ridge and shield formation mechanisms and temporal relations, impact crater-volcanic construct interactions, and structural reactivation.

Ivanov M. A. Head J. W. III
Mapping in V-3 and V-56 Quadrangles, Venus: Assessment of Evolution of the Topography of the Midlands **[#1111]**
Venus quadrangles representing midlands are mapped in opposite hemispheres. Formation and timing of characteristic midlands features are documented; significant topography formed prior to regional plains emplacement and is preserved today.

Törmänen T. Aittola M. Kostama V.-P. Raitala J.
Topographic Characteristics of Multiple Coronae on Venus **[#1725]**
We have studied the topographic characteristics of the multiple coronae on Venus. Initial results are presented including topographic classification and comparison with the total corona population.

Kryuchkov V. P. Raitala J. Törmänen T.
New Data on Coronae Bring Up New Questions and Tasks in Research of Venus **[#1657]**
Venusian coronae in plan view are mostly ellipses. This shape reflects deformation in a surface stress field. The corona ellipses have different orientations and this reflects different deformation in different surface areas.

Bannister R. A. Hansen V. L.
Geologic Analysis of Deformation in the Interior Region of Artemis (Venus, 34°S 132°E) **[#1370]**
Geologic observations of Artemis, Venus from NASA Magellan data and discussion/evaluation of four hypotheses for its formation.

Wilson L. Head J. W. III
Lateral Dike Injection and Magma Eruption Around Novae and Coronae on Venus **[#1125]**
The pattern of radiating fractures leading to distal fissure vents seen in novae and some coronae on Venus is shown to be a consequence of the high atmospheric pressure influencing conditions in the shallow parts of laterally propagating dikes.

Grosfils E. B.
New Insights into the Failure of Magma Reservoirs on the Terrestrial Planets **[#1015]**
Results from published elastic models of magma reservoirs are often contradictory. Based on a numerical effort to understand and resolve these issues, I describe new insights into reservoir failure on the terrestrial planets.

McGovern P. J.
Flexural Stresses and Magma Ascent at Large Volcanoes on Venus **[#2459]**
I examine in detail the ways in which lithospheric flexural stresses influence magma ascent at Venusian volcanoes. I present two forms of magma-stalling "stress traps" and discuss how they may affect the growth of several types of volcano on Venus.

Lang N. P. Hansen V. L. Swenson J. B. Bannister R. A.
Can Venusian Channels Form by Subsurface Thermal Erosion? **[#1763]**
We present our initial results for 1-D modeling of venusian channel formation as a thermal erosive process.

MERCURY

Helbert J. Moroz L. V. Maturilli A. Bischoff A. Warell J. Sprague A. Palomba E.
A Set of Laboratory Analogue Materials for the MERTIS Instrument on the ESA BepiColombo Mission to Mercury **[#1662]**
The MERTIS instrument on BepiColombo will study the surface of Mercury in the TIR. We will present a list of analog material compiled to support the development of analytic tools, planned ground based observations and a cross calibration with other instruments on BepiColombo and MESSENGER.

Kozyrev A. S. Mitrofanov I. G. Litvak M. L. Sanin A. B. Tretyakov V. I. Rogozhin A. A. Gurvits L. I. Schvetsov V. N. Leleux P.
The Mercury Gamma-Ray and Neutron Spectrometer (MGNS) for the ESA BepiColombo Mission **[#1696]**
The Mercury Gamma-ray and Neutron Spectrometer (MGNS) has been selected for the payload of the ESA Mercury Planetary Orbiter of the BepiColombo mission for providing mapping of soil composition of Mercury and testing possible hydrogen/water deposits at cold traps around the planetary poles.

André S. L. Watters T. R.
Depth to Diameter Measurements of Mercurian Mature Complex Craters **[#2054]**
We present depth/diameter crater measurements from digital elevation models derived from Mariner 10 stereo imagery.

LUNAR SAMPLE STUDIES

Korotev R. L.
New Geochemical Data for Some Poorly Characterized Lunar Meteorites **[#1404]**
New compositional data for lunar meteorites Dar al Gani 996, Dhofar stones 280, 910, 961, and 1084, and NWA stones 2200 and 3163 are presented.

Takeda H. Arai T. Yamaguchi A. Mikouchi T.
Important Lithologies of the Lunar Farside Crust: Coarse-grained Granulites or Magnesian Anorthosites **[#1572]**
Dhofar 489 is a possible sample from the farside crust of the Moon, and its major clast types are not granulitic breccias. Two magnesian anorthosite clasts and one coarse-crystalline granulite were recognized by mineralogical study of new PTSs.

Nishiizumi K. Hillegonds D. J. Welten K. C.
Exposure and Terrestrial Histories of Lunar Meteorites LAP 02205/02224/02226/02436, MET 01210, and PCA 02007 **[#2369]**
We measured the cosmogenic radionuclide concentrations in new lunar meteorites, LAP 02205/02224/02226/02436, MET 01210, and PCA 02007. All meteorites contain solar cosmic ray produced ^{26}Al indicating a small preatmospheric radius.

Irving A. J. Kuehner S. M. Korotev R. L. Rumble D. III Hupé G. M.
Mafic Granulitic Impactite Northwest Africa 3163: A Unique Meteorite from the Deep Lunar Crust **[#1365]**
This large lunar meteorite from Northwest Africa ia a fresh, recrystallized granulitic breccia similar to clasts within some Apollo highlands samples.

Karouji Y. Arai T. Ebihara M.
Chemical Composition of Another KREEP-rich Lunar Regolith Breccia Yamato 983885 **[#1919]**
We analyzed recently found lunar meteorite Yamato 983885, which contains various lithic clasts, which are associated with KREEP, such as Mg-rich rocks and KREEPy basalt. We propose its possible source region of this meteorite on the Moon.

Braden S. E. Robinson M. S.
Lunar Mineral Modal Abundances from Digital Petrographic Thin Sections **[#2237]**
We have developed a fast and accurate technique to derive mineral modal abundances from digital scans of lunar petrographic thin sections. From the mineral modal abundances we can estimate TiO_2 wt% to a typical accuracy of 1 wt% for samples with opaque grain sizes greater than ~60 μm.

Hudgins J. A. Spray J. G.
Lunar Impact-fluidized Dikes: Evidence from Apollo 17 Station 7, Taurus-Littrow Valley **[#1176]**
3–5 cm wide dikes intruding noritic breccia at the Apollo 17 station 7 boulder comprise angular mineral and lithic clasts. The dikes are not igneous. They were generated by vapour-fluidized comminuted material and lithified by condensing silicate vapours and/or by subsequent shock welding.

Cohen B. A. Symes S. J. Swindle T. D.
Petrography and Chemistry of Impact-Melt Clasts in Apollo 16 Breccias **[#1379]**
Impact-melt clasts and glass fragments in ancient Apollo 16 breccias represent samples of pre-Imbrium lunar impacts. The major-element composition of these samples spans a wide range, suggesting that these samples represent multiple impact events.

Levine J. Muller R. A. Renne P. R. Rohde R. A.
Potassium and Calcium in Lunar Impact Spherules **[#1192]**
We use argon isotopic data from lunar impact spherules to determine relative abudances and distributions of potassium and calcium. Our observations constrain models of spherule formation.

Edmunson J. Gaffney A. M. Borg L. E.
Disturbance of U-Pb Isotopic Systematics in Lunar Samples: Mare Basalt 10017 and Norite 78238 **[#1506]**
Interpretation of lunar U-Pb isotopic systematics must be made in the context of more robust isotopic systems such as Sm-Nd or Rb-Sr. There is no single U-Pb system isochron that reliably provides the crystallization age for all samples.

Puchtel I. S. Walker R. J. James O. B.
Further Study of $^{187}Os/^{188}Os$ and Highly Siderophile Element Systematics of Apollo 14 and 17 Impact Melt Rocks **[#1428]**
New $^{187}Os/^{188}Os$ and HSE data for lunar impact melt rocks indicate that 73215 and 73255 aphanites plot in the middle of the chondrite range, whereas 72395 poikilitic rocks and 14321 microbreccias plot beyond the highest end of the range for ordinary and enstatite chondrites.

Dikov Yu. P. Gerasimov M. V. Yakovlev O. I.
High-Temperature Reduction of Slightly Siderophile Elements (V, Cr, and Mn) in Impact Process **[#1087]**
Experiments show that high-temperature processing of silicates results in sufficient reduction of iron and slightly siderophile elements (V, Cr, and Mn) into metallic states.

LUNAR BASALTIC VOLCANISM

Zeigler R. A Korotev R. L. Irving A. J. Jolliff B. L. Kuehner S. M. Hupé A. C.
Petrography and Composition of Lunar Basaltic Meteorite NWA 3160 **[#1804]**
NWA 3160 is a dilithologic lunar meteorite consisting of basalt and basaltic fragmental breccia lithologies. NWA 3160 is paired with other basaltic lunar meteorites collectively known as NWA 2727, and may have a petrogenic relationship with NWA 773.

Bunch T. E. Wittke J. H. Korotev R. L. Irving A. J.
Lunar Meteorites NWA 2700, NWA 2727 and NWA 2977: Mare Basalt/Gabbro Breccias with Affinities to NWA 773 **[#1375]**
Three new lunar meteorites from Northwest Africa are either paired with or related to NWA 773 found in 2000.

Koizumi E. Mikouchi T. Chokai J. Miyamoto M.
Crystallization of Lunar Basaltic Meteorites Northwest Africa 032 and 479: Preservation of the Parent Melt Composition and Relationship to LAP 02205 **[#1586]**
The crystallization experiments with the bulk composition of NWA 032 suggest that the NWA bulk composition represents its parent melt composition, and the difference of cooling rate made the differences between NWA and LAP 02205.

Haloda J. Korotev R. L. Tycova P. Jakeš P. Gabzdyl P.
Lunar Meteorite Northeast Africa 003-A: A New Lunar Mare Basalt **[#2269]**
Northeast Africa 003-A is a 124 g new lunar meteorite (low-Ti mare basalt) found in northern Libya in the wadi Zam Zam area. NEA 003-A represents a previously unsampled lithology with no exact match to any lunar basaltic meteorite described so far.

Haloda J. Tycova P. Jakes P. Gabzdyl P. Kosler J.
Lunar Meteorite Northeast Africa 003-B: A New Lunar Mare Basaltic Breccia **[#2311]**
Northeast Africa 003-B is the brecciated lithology of a new, 124 g lunar meteorite Northeast Africa 003 found in northern Libya in the wadi Zam Zam area. The presence of low-Ti basaltic rocks in NEA 003 meteorite could be related to the progressive fractionation of single parent low-Ti melt.

Hill E. Day J. M. D. Davidson J. Taylor L. A.
Petrogenesis of Apollo 17 Mare Basalts — Revisited **[#2067]**
Our study of six Apollo 17 mare basalts reveal complex, shallow-level processes, superimposed on long-lived, relatively homogeneous mantle-derived magmatism.

Schnare D. W. Norman M. D. Day J. M. D. Taylor L. A.
Origin of Apollo 15 Olivine- and Quartz-normative Basalts **[#2212]**
This study addresses the relationship of Apollo 15 olivine- and quartz-normative basalts using whole-rock data, and an *in-situ* mineralogic approach (EMP + LA-ICP-MS), to understand the causes of chemical dispersion and the relationships between these two groups.

Day J. M. D. Nowell G. M. Norman M. D. Pearson D. G. Chertkoff D. G. Taylor L. A.
Evidence for Age-Progressive Melting of Increasingly Incompatible-Element-enriched Mantle Reservoirs on the Moon? **[#2235]**
There are age-progressive variations in incompatible-element and Sr-Nd-Hf isotope data for lunar basalts. These variations indicate an increased role for KREEP in lunar mantle sources with time.

Langenhorst F.   Smyth J. R.   Kroll H.
On the Nature of Guninier-Preston Zones in Meteoritic and Lunar Orthopyroxene **[#2104]**
The question of the structure of GP zones in orthopyroxene has been addressed by transmission electron microscopy. Electron diffraction data reveals that the GP zones are metrically orthorhombic but possess monoclinic symmetry.

Shearer C. K.   Papike J. J.   Karner J.
Pyroxene Europium Valence Oxybarometer. Effects of Pyroxene Composition, Melt Composition and Crystallization Kinetics **[#1289]**
The behavior of multivalent elements in magmatic systems reflects the fO_2 of the environment. Here, we evaluate the effect of pyroxene and melt composition, crystallization sequence, and crystallization kinetics on the behavior of Eu in natural basalts from similar, reducing environments (IW-1).

Neal C. R.   Shearer C. K.
High-Ti Volcanic Glasses: Derivation from a Garnet-bearing Source Coupled with Assimilation of Late-Stage LMO Cumulates **[#2086]**
Compositions of volcanic glasses are modeled to investigate the presence of garnet in their source regions.

Nicholis M. G.   Rutherford M. J.
Vapor/Melt Partitioning Behavior of S and Cl in a C-O Gas Mixture **[#2061]**
The partitioning of S and Cl between a CO-rich gas-phase and a mafic melt composition have been investigated. Results have been applied to both lunar fire-fountain and terrestrial volcanism.

LUNAR GEOPHYSICS

Bulow R. C.   Johnson C. L.   Bills B. G.
Tidal Stress and Deep Moonquakes **[#1183]**
Using our recent discovery of additional moonquakes, an improved model of the gravitational tidal potential, and a suite of internal structure models, we analyze tidal stress at deep moonquake occurrence times to search for a failure criterion.

Stubbs T. J.   Halekas J. S.   Farrell W. M.   Vondrak R. R.   Delory G. T.
Global Modeling of the Electrostatic Lunar Surface Potential **[#2217]**
This is a study of the global-scale variation of electrostatic potentials and electric fields on the surface of the Moon in both the solar wind and magnetosphere environments. Data is used from the Lunar Prospector Electron Reflectometer (LP/ER).

Nakamura Y.   Frohlich C.
Possible Extra-Solar-System Cause for Certain Lunar Seismic Events **[#1048]**
All but a few of a rare class of events detected by the Apollo lunar seismic network occurred when the Moon faced a fixed direction on the celestial sphere. This suggests that a source outside the solar system may be responsible for causing them.

Khan A.   Connolly J. A. D.   Olsen N.   Mosegaard K.
Constraining the Composition and Thermal State of the Moon from an Inversion of Electromagnetic Lunar Day-Side Transfer Functions **[#1166]**
Inversion of the lunar electromagnetic inductive response to directly constrain its composition and thermal state. Our results show that the bulk mantle composition of the Moon is dissimilar to that of the Earth, in agreement with recent giant impact models for lunar origin.

Garrick-Bethell I.   Zuber M. T.
Long-Wavelength Lunar Geology and the Fossil Bulge **[#2429]**
We examine the effect of large geologic units on the low-order shape and gravity of the Moon.

Wieczorek M. A.   Huang S.
A Reanalysis of Apollo 15 and 17 Surface and Subsurface Temperature Series **[#1682]**
We show that the 18.6 year precession of the lunar orbit has a substantial influence on the lunar surface temperature. The neglect of this signal in previous publications will act to bias the heat flow estimates that have been made at the Apollo 15 and 17 sites.

Williams J. G. Boggs D. H. Ratcliff J. T.
Lunar Interior Results and Possibilities **[#1229]**
Solutions for lunar science parameters continue to improve. A fluid core and strong tidal dissipation are inferred from the effects of dissipation on rotation. Detection of core-mantle boundary flattening provides additional evidence for a fluid core.

LUNAR IMPACT STUDIES

Gallant J. Gladman B.
Lunar Cratering Asymmetries **[#2336]**
We seek to numerically determine the magnitude of cratering asymmetries on the lunar surface (nearside/farside and leading/trailing). We find no nearside to farside asymmetry, and a small (12%) enhancement on the leading hemisphere.

Morota T. Haruyama J. Furumoto M.
Lunar Apex-Antapex Cratering Asymmetry and Origin of Impactors in the Earth-Moon System **[#1554]**
In this paper, we purpose to derive the lunar apex-antapex cratering asymmetry as functions of the mean encounter velocity of impactors and time, considering the temporal variation in the lunar orbital velocity last 4.0 Gyr.

Ivanov B. A.
Earth/Moon Impact Rate Comparison: Possible Constraints for Lunar Secondary/Primary Cratering Proportion **[#1262]**
Impact rate of bolides are compared with the cratering rate on the moon in the past 100 Ma. The current meteoroid flux fits observed cratering rate, provided most of the small craters on the young lunar surface are primary, not secondary craters.

TERRESTRIAL IMPACT CRATERS

Gohn G. S. Koeberl C. Miller K. G. Reimold W. U. Browning J. V. Cockell C. S. Dypvik H. Edwards L. E. Horton J. W. Jr. McLaughlin P. P. Ormö J. Plescia J. B. Powars D. S. Sanford W. E. Self-Trail J. M. Voytek M. A.
Preliminary Site Report for the 2005 ICDP-USGS Deep Corehole in the Chesapeake Bay Impact Crater **[#1713]**
First report for the ICDP-USGS 1.7-km-deep corehole drilled into the central part of the Chesapeake Bay impact crater during 2005.

Le Feuvre M. Wieczorek M. A.
The Asymmetric Cratering History of the Terrestrial Planets: Latitudinal Effect **[#1841]**
As the population of asteroids and comets that strike a planet is not isotropic in space, we have found that a latitudinal dependency of the cratering rate is to be expected.

Gucsik A. Bérczi Sz. Kereszturi Á. Hargitai H. Nagy Sz.
Shock Metamorphism of Zircon in Nature and Experiment: A Review **[#1544]**
Zircon is a highly refractory and weathering-resistant mineral that has proven useful as an indicator of shock metamorphism in the study of impact structures and formations that are old, deeply eroded, and metamorphically overprinted.

Gucsik A. Nishido H. Ninagawa K. Okumura T. Wilcox J. Z. Urguiles E. Götze J. Bérczi Sz. Kereszturi Á. Hargitai H. Polgári M. Nagy Sz.
Cathodoluminescence and Its Application in the Planetary Sciences: A Review **[#1543]**
The purpose of this study is to summarize the cathodoluminescence and its application in the planetary sciences emphasizing the astrobiological aspects, too.

Rajmon D.
Suspected Earth Impact Sites **[#2372]**
Suspected Earth Impact Sites is a new database aspiring to provide reliable basic data and references on proposed but not confirmed impact structures.

Dypvik H. Krøgli S. O. Etzelmüller B. Sørbel L. Thoresen T. A. A.
The Hunt for Impact Structures in Norway **[#1013]**
A systematic search for topographic impact structures in Norway has started. In a first stage, based on an automatic scan of digital elevation models (DEM), about 1201 circular structures have been picked out matching the topographic pre-described structure.

Paillou Ph. Reynard B. Malezieux J.-M. Dejax J. Heggy E. Rochette P. Reimold W. U. Michel P. Baratoux D.
An Extended Field of Crater Structures in Egypt: Observations and Hypotheses **[#1286]**
We detected more than 1000 crater structures in the Western Egyptian Desert, distributed over 40000 km^2, among which 62 were studied on the field. Two hypotheses are proposed for their origin: hydrothermal vent complexes or impact craters generated by a rubble-pile asteroid.

Morgan J. Smith A. Styles E. Surendra A. Barton P.
Chicxulub Revealed with New Seismic and Gravity Data **[#1626]**
We will present results from new seismic and gravity data acquired across the Chicxulub impact crater in 2005. These data provide a more detailed image of crater structure, and allow more accurate mapping of features from offshore to onshore.

Pinto J. A. Warme J. E.
Alamo Impact Crater Documented **[#2453]**
Recent investigations on the Late Devonian Alamo Impact Event at Tempiute Mountain, Nevada, reveal that pervasive deformation in bedrock, breccia types, and the presence of high-pressure, shock-metamorphism in minerals and rocks suggest a scenario produced by impact-cratering processes.

Albin E. F. King D. T. Jr. Harris R. S. Petruny L. W. Jaret S. J. Gibson J. C.
Cosmic Impact in the Piedmont of Georgia? The Woodbury Structure **[#2375]**
The Woodbury structure is a 7 km diameter circular basin with an elevated quartzite rim situated in west-central Georgia. The morphology and setting are discussed with regard to an impact hypothesis. Preliminary results of fieldwork and petrography are presented.

Deane B. Milam K. A. Stockstill K. R. Lee P. C.
The Dycus Disturbance, a Second Impact Crater in Jackson County, Tennessee? **[#1358]**
The Dycus Disturbance, a small, suspected impact structure in Jackson County, TN, is all but unknown to the impact community. We review the previous research which was conducted over a half century ago, and present the preliminary results from the current field work.

Tagle R. Claeys Ph. Grieve R. A. F. Schmitt R. T. Erzinger J.
Evidence for a Second L Chondrite Impact in the Late Eocene: Preliminary Results from the Wanapitei Crater, Canada **[#1278]**
Wanapitei crater, Canada, is a second L chondrite impact in the Late Eocene. Results for Popigai and Wanapitei combined with cosmic ray exposure ages of L chondrites suggest that the asteroid shower in the Late Eocene was triggered by a major disruption of the L chondrite parent body.

Tagle R. Claeys Ph. Öhman T. Schmitt R. T. Erzinger J.
Traces of an H Chondrite in the Impactites from Lappajärvi Crater, Finland **[#1277]**
Traces of an H chondrite in the impactites from Lappajärvi crater, Finland support the hypothesis that ordinary chondrites represent a major component of the projectiles impacting Earth.

Huson S. A. Foit F. F. Watkinson A. J. Pope M. C.
X-Ray Diffraction Powder Patterns and Thin Section Observations from the Sierra Madera Impact Structure **[#2377]**
X-Ray powder diffraction analysis and thin section observations of carbonate and siliciclastic samples from the Sierra Madera impact structure indicate moderate shock pressures (8 to 30 GPa) were generated during the formation of this crater.

Gerard-Little P. Abbott D. Breger D. Burckle L.
Evidence for a Possible Late Pliocene Impact in the Ross Sea, Antarctica **[#1399]**
Based on the discovery of possible tektites, impact glass, and other grains that may be impact markers, there is the possibility of a Late Pliocene impact in the Ross Sea, Antarctica.

Abbott D.   Mazumder R.   Breger D.
Native Iron in the Chaibasa Shales: Result of a Pre 1.6 Ga Impact? **[#1889]**
We have found bulbous droplets and broken fragments of native Fe in the pre-1.6 Ga Chaibasa shales. The native Fe is primary and is not detrital. We infer that the native Fe grains must have come from melting and reduction of Fe rich material during a nearby impact event.

Miura Y.
Corona Texture of Quartz and K-Feldspar at Impact Crater Structure of Takamatsu-Kagawa District in Japan **[#1239]**
Complicated corona textures of quartz and K-feldspar are found at drilled breccias at the Takamatsu-Kagawa district in Japan. The corona texture contains anomalous composition and carbon during impact event at granite.

Misra S.   Srivastava P. K.   Dube A.
Lonar Impact Crater, India: Did It Form by Oblique Impact? **[#1085]**
Studies of Landsat 7 ETM+ image and DEM data of the 52,000 year old Lonar Crater (~1.8 km diameter), India, along with field studies and comparison with experimental results, suggest that the impactor of the crater came from east and hit the pre-impact surface at an angle between 30° and 45°.

Larionova Y.   Samsonov A.   Sizova E.
Tagamites of the Yanis-Yarvi Crater (Karelia, Russia): An Example of Non-Equilibrated Impact Melt? **[#1373]**
Although a number of studies have shown that impact melt products are rather homogeneous, there is growing evidence for a certain geochemical and isotopic heterogeneity of impact melts.

Salminen J.   Donadini F.   Pesonen L. J.   Masaitis V. L.
Paleomagnetism of the Lake Jänisjärvi Impact Structure and Its Implication to Baltica's Neoproterozoic Paleoreconstructions **[#1160]**
Paleomagnetic, rock magnetic and petrophysical results are presented for rocks from the Janisjarvi impact structure, Russian Karelia. We will also discuss about the paleomagnetic results implications to Baltica's apparent polar wander path.

Schönian F.   Salge T.   Kenkmann T.   Stöffler D.   Soler Arechalde A. M.   Urrutia Fucugauchi J.
Chicxulub Ejecta Blanket: The Suevite of the UNAM 5 and 7 Drill Cores **[#2229]**
The suevites of the Chicxulub ejecta blanket from the UNAM 5 and 7 cores have been described in detail. The units defined do allow a correlation with impactites in the crater and help to reconstruct the emplacement of the ejecta plume material.

Wittmann A.   Kenkmann T.   Hecht L.   Stöffler D.
Composition and Characteristics of the Chicxulub Ejecta Plume **[#1590]**
Quantitative analyses of ejecta components at Chicxulub yield implications for oxidizing conditions in the ejecta plume and the depositional sequence of the continuous suevite-like deposits.

Nagy Sz.   Gucsik A.   Kubovics I.   Jozsa S.   Berczi Sz.   Galne G. S.
Shock-induced Microdeformations of Garnet from the Ries Impact Structure **[#1993]**
Garnet and its shock stages can play an important role as a indicator mineral of shock metamorphism at impact structures that have crystalline target rocks.

Kyte F. T.   Gersonde R.   Kuhn G.
Sedimentation Patterns of Meteoritic Ejecta in Eltanin Impact Deposits at Site PS58/281 **[#2305]**
Site PS58/281 was close to the Eltanin impact site. Some meltrock was injected into the water column, and settled into the top of the chaotic sediment fragments, and included as traces during subsequent deposition. Early ballistic ejecta is mainly meteorites, followed by vesicular meltrock.

Rajmon D.   Reid A. M.   Copeland P.
Petrography and Geochemistry of Upper Eocene Spherules from 709C (Indian Ocean) and DSDP 612 (NW Atlantic) **[#2201]**
Spherules from ODP 709c (Indian ocean) diplay petrographic and geochemical characteristics similar to spherules from ODP 216 and 292 (SE Asia). The data, however, neither strongly support nor reject the hypothesis of a third Upper Eocene ejecta layer in SE Asia.

Petaev M. I. Jacobsen S. B. Becker L.
Search for Extraterrestrial and Impact Materials in the P-T Boundary Samples from Graphite Peak, Antarctica **[#2309]**
We report on the discovery of meteoritic grains in magnetic separates of new P-T boundary samples from Graphite Peak, Antarctica. A search for these materials *in situ* is underway, with results to be reported at the conference.

Miura Y.
Carbon-rich and Ni-Fe-rich Spherules at the End of the Permian: Application to Materials of Space Explorations **[#2441]**
1) The Meishan PTB spherules contain C-rich (up to ~90% C) and Ni-Fe rich spherules (31% Ni and 29% Fe). 2) Akiyoshi drilled limestone breccias contains C-rich grains with Ca from limestone target rocks.

Nishido H. Ninagawa K. Sakamoto M. Gucsik A. Okumura T. Toyoda S. Bérczi Sz. Nagy Sz.
3D Raman Spectroscopical Study of Quartz from Mt. Oikeyama, Japan, Emphasizing the Shock-induced Microdeformations **[#1651]**
This comparison study of the Raman properties of Ries quartz and a Oikeyama sample indicates that the Oikeyama structure was formed by an impact event.

Serefiddin F. Herzog G. F. Koeberl C.
Terrestrial Cosmic-Ray Exposure History of a 23-gram Moldavite and Evidence for the Presence of Meteoric Beryllium-10 **[#1300]**
The presence of a meteoric component of ^{10}Be in a 23-g moldavite indicates that the precursor material was near the Earth's surface and loosely consolidated at the time of formation.

Badjukov D. D. Raitala J.
Ni in Impactite Sulphides in the Lappajärvi, Sääksjärvi, Suvasvesi S, and Paasselkä Impact Craters in Finland **[#1676]**
The melt rocks of the meteorite craters in central Finland are enriched in siderophile elements and other meteoritic components. Sulphides in the impact melt rocks are main carriers of siderophile elements, especially for Ni and Co.

Lindgren P. Parnell J. Bowden S. A. Taylor C. Osinski G. R. Lee P.
Preservation of Biological Signature Within Impact Melt Breccias, Haughton Impact Structure **[#1028]**
Our study shows preservation of biological signatures in clasts of the target carbonate bedrock embedded in melt breccias, Haughton impact crater. The results also indicate that an increase in heating can be detected from the centre to the edge of a clast.

Horton J. W. Jr. Vanko D. A. Naeser C. W. Naeser N. D. Larsen D. Jackson J. C. Belkin H. E.
Postimpact Hydrothermal Conditions at the Central Uplift, Chesapeake Bay Impact Structure, Virginia, USA **[#1842]**
Studies of petrography, mineralogy, fission-track ages of zircon and apatite, and fluid inclusions in calcite reveal postimpact hydrothermal conditions near the center of the Chesapeake Bay impact structure.

Kirkland L. E. Herr K. C. Adams P. M.
Craters as Drills on Mars: Results from a Manmade, 260 Meter Diameter Crater in Layered Terrain **[#1864]**
The manmade explosion crater "Schooner" is a unique Mars analog asset in layered terrain at the Nevada Test Site. We explore using infrared, hyperspectral imaging analogs to current instruments, with a focus on material uncovered by recent craters.

Johnson R. C. King D. T. Jr.
Abrasive (Sand) Blasting as a Means of Cleaning Weakly Lithified Impact-related Drill Core from the Wetumpka Impact Structure, Elmore County, Alabama **[#1866]**
Abrasive (sand) blasting has been a very successful and essential method for cleaning dried but otherwise poorly consolidated drill core from Wetumkpa impact structure, Alabama.

IMPACTS: MODELING AND STRUCTURES

Shuvalov V. Trubetskaya I.
Numerical Modeling of Impact Induced Aerial Bursts **[#1075]**
The purpose of this paper is to study numerically an influence of impact angle and projectile velocity on the processes accompaning aerial bursts.

Shuvalov V. V. Artemieva N. A.
Impact Ejecta Escaping the Moon **[#1168]**
We calculate the mass of escaping ejecta on the Moon as a function of projectile type and impact angle to address the questions: 1) Does the Moon gain or lose its mass? 2) Are solid escaping ejecta a source of lunar meteorites? 3) How much vapor is in escaping plume?

Artemieva N. A.
Fluidized Impact Ejecta and Volcanic Blast Surge — Numerical Modeling **[#1525]**
3D numerical simulations of a volcanic eruption similar to Mount St. Helens lateral blast is presented. Modelled distribution of pyroclastics is compared with geological data. Perspectives for impact ejecta modeling (Chicxulub, rampart craters) are discussed.

Ormö J. Lepinette A.
Numerical Simulation of Heating of Target at Crater-Field-forming Impact Events **[#1351]**
We show that small (10–100 m) meteorite craters may have significant amount of target material heated to several hundred degrees. Some meteoritic and heated material are spread as ejecta, but the majority remains within the crater, most likely at great depth near the center.

Kenkmann T. Jahn A. Wünnemann K.
"Block Size" in a Complex Impact Crater Inferred from the Upheaval Dome Structure, Utah **[#1540]**
To better define acoustic fluidization parameters for numerical models of impact crater formation, the block size distribution was determined in a 7 km crater. We found a trend of increasing block size with increasing distance from the center.

Hiraoka K. Arakawa M. Seto M. Nakamura A. M.
Measurement of Compressive and Tensile Strength of Ice-Silicate Mixtures **[#1602]**
We measured the compressive and tensile strength of the ice-silicate mixture at low strain rate. Using these strengths, we discuss the results of impact cratering on ice-silicate mixture targets.

Anderson J. L. B. Schultz P. H.
Flow-Field Center Migration During Oblique Impacts: Implications for Curved Uprange Ejecta Rays **[#1726]**
Ejecta dynamics measured using 3D PIV during experimental oblique impacts constrain the three-dimensional migration of uprange, downrange, and lateral flow-field centers. These data are used to model uprange ejecta deposits at planetary scales.

Nazarova K. Bland P. A.
Numerical Modelling for Strength Estimation of Fragmenting Meteoroids **[#1825]**
We used the model of separate fragments (SF) to model the crater fields. The comparison of the measured and estimated values of material strength of meteoroids was performed. The separate fragments model application was shown for the Morasko iron shower.

Baldwin E. C. Vocadlo L. Crawford I. A.
Influence of Target Yield Stress on Crater Dimensions: A Numerical Approach Based on Chicxulub **[#1887]**
AUTODYN is used to consider the influence of target yield stress on crater dimensions, based on parameters appropriate for Chicxulub.

Senft L. E. Stewart S. T.
Modeling Impact Cratering into Layered Targets **[#2210]**
We (i) implement a new strength model into the shock physics code CTH to more accurately describe impacts into rocks, and (ii) begin to study the outcome of impacts into layered targets, including modeling selected terrestrial craters.

Byrne C. J.
Radial Profiles of Lunar Basins **[#1900]**
Radial profiles of selected lunar basins were generated from Clementine elevation data. An empirical model represents the entire profile of the inner basin, rim, and ejecta. New data is provided on isostatic adjustment.

King D. T. Jr.   Ormö J.   Petruny L. W.   Morrow J. R.   Neathery T. L.
Excavation and Modification of the Late Cretaceous Wetumpka Impact Structure (Alabama), a Shallow Marine Impact Feature **[#2019]**
Wetumpka impact structure, a 7.6 km diameter feature of the inner coastal plain, has a distinctive breached rim morphology, interior crater fill of broken sedimentary formation, and an exterior disturbed terrain that show the effects of excavation and modification within a shallow sea.

METEORITES: EXPERIMENTS AND NEW TECHNIQUES

Mendybaev R. A.   Richter F. M.   Davis A. M.
Reevaluation of the Åkermanite-Gehlenite Binary System **[#2268]**
Experiments were conducted to reevaluate 65+ years old data for the Åk-Ge binary system. The liquidus position from our experiments is consistent with the previous results, while the solidus is shifted by up to 20°C to lower temperatures for gehlenitic compositions.

Faure F.
Oswald Ripening of Ca-rich Pyroxene. Implication on the Very Late Cooling History of Chondrule Mesostasis **[#1624]**
New experimental method of Oswald ripening established on the segmentation of dendritic pyroxene previously crystallized can be used to precise the very late cooling history of chondrule mesostasis.

Zega T. J.   Stroud R. M.
In Situ Lift-Out with a Focused-Ion-Beam/Scanning-Electron Microscope: A New Technique for Creating Transmission-Electron-Microscope Samples of Earth and Planetary Materials **[#1441]**
Here we describe a new technique for creating transmission-electron-microscope samples of earth and planetary materials.

Rumble D.   Miller M. F.   Franchi I. A.   Greenwood R. C.
Variations in the Oxygen Three-Isotope Terrestrial Fractionation Line Revealed by an Inter-Laboratory Comparison of Silicate Mineral Analyses **[#1416]**
An inter-laboratory comparison of analytical results for the slopes of Terrestrial Fractionation Lines (TFL) measured on a group of quartz and a separate group of garnet samples shows good agreement between laboratories. However, the slopes of the TFL's for each mineral group differ slightly.

Wilson T. L.   Mittlefehldt D. W.
Is Q for Quantum? From Quantum Mechanics to Formation of the Solar System **[#1386]**
The Q-phase carrier of entrapped planetary noble gases has not been identified. Endohedral carbon cages are viable candidates, and we argue that quantum effects have now become relevant to an ultimate understanding of Q-phase in cosmochemistry.

Yasuda S.   Nakamoto T.
Possible Size of Porphyritic Chondrules in Shock-Wave Heating Model **[#1674]**
We examined that the possible size of porphyritic chondrules due to the stripping of the liquid surface by solving the heat conduction equation with the viscosity variation, and found that the shock-wave heating model is consistent with observations.

Chen J. H.   Papanastassiou D. A.
Nickel Isotope Investigation by MC-ICP-MS and PTIMS **[#1997]**
We present high precision data for Ni isotopes in meteorites, by both MC-ICP-MS and TIMS.

Papanastassiou D. A.   Chen J. H.
Comparison of MC-ICP-MS and NTIMS Ru Endemic Isotope Anomalies in Meteorites **[#1976]**
We obtained MC-ICP-MS data for Ru and compare with TIMS results. There is complete agreement for the endemic Ru effects, at ^{100}Ru.

DeCarli P. S. Xie Z. Sharp T. G.
Modeling the Impact Histories of Veined Chondrites **[#1950]**
Studies of the mineralogy of melt veins in chondrites constrain the pressure range of the vein-forming shock event. Heat flow calculations constrain the minimum shock pressure duration. The Autodyn(TM) wave propagation code was used to model impacts on a chondrite parent body.

McCanta M. C. Dyar M. D. Hörz F. P.
Shock Oxidation of Pyroxene: Effects on Redox Ratio **[#1903]**
In this study we investigate the effects of shock on pyroxene redox ratio. Shock has the potential to increase pyroxene Fe^{3+} content, requiring caution to be exercised when applying redox dependent oxybarometers to shocked samples.

Karner J. M. Papike J. J. Shearer C. K.
V Systematics in Planetary Pyroxenes and the Potential for a Quantitative Pyroxene Vanadium Valence Oxybarometer **[#1116]**
V partitioning into pyroxene is only partly controlled by fO_2.

Miura H. Nakamoto T.
Shock-Wave Heating Model for Chondrule Formation: Hydrodynamics of Rotating Droplets Exposed to High-Velocity Gas Flows **[#1765]**
We perform hydrodynamic simulations of molten silicate dust particles in the framework of the shock-wave heating model for chondrule formation. We simulate the deformation of rapidly rotating molten droplets exposed to the high-velocity gas flow.

Hezel D. C.
Is the 2D Information of Objects in Thin Sections Representative of the 3D-Object? — Determining the Bulk Compositions of Chondrules from Meteorite Thin Sections **[#1668]**
Only few chondrule bulk compositions exist. I use a computer model to verify whether 2D bulk data obtained from thin sections are representative for the 3D bulk. Results of the model are verified by serial sectioning of meteorite thick sections.

Uesugi M. Sekiya M.
Separation of Melted Iron Spheres in Chondrules During the Chondrule Formation **[#1502]**
We propose a new viewpoint for the study of the depletion of siderophile elements in natural chondrules, based on the theoretical calculation of the separation of melted chondrules and iron spheres at the time of chondrule formation.

DIFFERENTIATED METEORITES

Amelin Y. Wadhwa M. Lugmair G.
Pb-Isotopic Dating of Meteorites Using ^{202}Pb-^{205}Pb Double-Spike: Comparison with Other High-Resolution Chronometers **[#1970]**
We report high-precision Pb isotopic dates for achondrites A-881394, Ibitira and Acapulco, and discuss their implications for the early solar system timescale and homogeneous vs. heterogeneous distribution of short-lived radioactive isotopes.

Burbine T. H. Dyar M. D. Seaman S. J. McCoy T. J.
Water Content of Nominally Anhydrous Minerals in the Ibitira Eucrite **[#2220]**
We have used Fourier transform infrared (FTIR) spectroscopy to quantify the possible presence of CO, CO_2, and H_2O in nominally anhydrous minerals in the vesicle-rich eucrite Ibitira.

Warren P. H. Huber H.
Chromium-Silicates, Feldspars and Highly Silicic Glasses Formed from Felsic Melts in Post-Depressurization Ferroan Ureilites, Especially LEW 88774 **[#2400]**
We describe the diverse suite of post-depressurization redox phases in the LEW 88774 ureilite, and discuss the origin of these materials, including the highly silicic (typically ~70 wt% SiO_2) glasses that are associated with Cr-spinels.

Goodrich C. A.
Composition of Ureilite Precursors Materials **[#1194]**
Reexamination of constraints on ureilite precursors in MAGPOX and MELTS indicates that they had Ca/Al ~2.5 × CI but were otherwise CV-like. The ureilite parent body likely accreted with an Fe-rich CV-like composition.

Welten K. C. Nishiizumi K. Caffee M. W. Hillegonds D. J.
Cosmogenic Radionuclides in Ureilites from Frontier Mountain, Antarctica: Evidence for a Polymict Breccia **[#2391]**
Cosmogenic radionuclides in 11 Antarctic ureilites provide evidence that 9 fragments represent a polymict ureilite breccia. The results are discussed in terms of target element composition, exposure history and terrestrial age of these ureilites.

Wright A. Parnell J. Tsikos H.
Interpreting the Carbon Isotopic Composition of Ureilites **[#1056]**
The carbon isotopic shift between carbonaceous chondrites and ureilites is of similar magnitude and direction as the shift observed between country rock and mobilized graphite in a case study, removing a problem in this widely inferred relationship.

Danielson L. R. Humayun M. Righter K.
Highly Siderophile Elements in Pallasites and Diogenites, Including the New Pallasite, CMS 04071 **[#2304]**
Trace element LA-ICP-MS analyses were conducted on individual phases in four pallasites and three metal bearing diogenites in order to understand pallasite formation and possible magmatic processes which may link pallasites to IIIAB irons and HEDs.

Sadilenko D. A. Borisovskiy S. E. Korochantsev A. V. Abdrakhimov A. M. Ivanova M. A. Zhuravlev D. I.
Discovery, Petrography, Mineralogy, and Chemistry of Pallasovka, a New Pallasite from Russia **[#1623]**
Pallasovka, a new stony-iron meteorite, was found recently in the Volgograd region of Russia. It belongs to the main group of pallasites, though its chromite is different in composition from other pallasites.

Tomiyama T. Huss G. R.
Minor and Trace Element Zoning in Pallasite Olivine: Modeling Pallasite Thermal History **[#2132]**
Minor and trace element profiles of pallasite olivine were obtained by ion microprobe analysis. Cooling history of pallasite was discussed based on diffusion calculations.

McCausland P. J. A. Flemming R. L.
Preliminary Bulk and Grain Density Measurements of Martian, HED and Other Achondrites **[#1574]**
We report preliminary bulk and/or grain density measurements for ten achondrites (including two martian, six HED, a ureilite and a winonaite), mostly from North West Africa

Maruoka T. Varela M. E. Kurat G. Zinner E.
Isotopically Heavy and Heterogeneous C in Graphite of the Vaca Muerta Mesosiderite **[#1449]**
We report on C-bearing Fe-Ni metal objects of Vaca Muerta and C isotopic ratios of graphite associated with the metal. Our results severely constrain the conditions prevailing during formation of the Vaca Muerta mesosiderite.

Cook D. L. Wadhwa M. Davis A. M. Clayton R. N.
Heterogeneity of the Hoba IVB Iron Meteorite: Implications for Its Use as an Analytical Standard **[#2116]**
Electron probe and scanning electron microscope analyses of a polished section of the Hoba IVB iron meteorite reveal fine-scale textural and compositional heterogeneities.

Markowski A. Quitté G. Kleine T. Bizzarro M. Leya I. Wieler R. Ammon K. Halliday A. N.
Early and Rapid Differentiation of Planetesimals Inferred from Isotope Data in Iron Meteorites and Angrites **[#2000]**
We will be presenting Hf-W data in some iron meteorites and angrite (SAH99555) in order to refine the chronology of the early solar system.

Johanesen K. J. Watson H. C. Fei Y.
Compositional Dependence of Au Diffusion in Fe-Ni Alloys: Implications for Meteorite Cooling Rate Models **[#2392]**
An experimental study to determine the effect of Ni concentration on diffusion of siderophile elements in Fe-Ni alloys relevant to iron meteorites. The implications that this has on current meteorite cooling rate models is also discussed.

ASTEROIDS, COMETS, METEORITES

Clark C. S. Clark P. E.
Using Boundary-based Mapping Projections to Reveal Patterns in Depositional and Erosional Features on 433 Eros **[#1189]**
Asteroid CSNB maps reveal morphological feature distribution patterns. On Eros, ponds are associated with local topographic maxima, particularly "noses" acting as "dust collectors". Eroded craters surround ponds perhaps provide a source of dust.

Wyrick D. Y. Buczkowski D. L.
Understanding Regolith Distribution on 433 Eros Using Analyses of Pit Chains and Grooves **[#1195]**
The distribution of pit chains and grooves on Eros provides clues to the internal structure and the spatial distribution of regolith. Additional analyses of pit slopes and volumes provide information on regolith thickness and mechanical properties.

Haseltine J. D. Franzen M. A. Sears D. W. G.
Fluidization from Continuous Outgassing as a Cause of Geological Structures on 433 Eros **[#1103]**
We have performed experiments in a large environmental chamber to explore the possibility of subsurface volatiles emerging from the inside of 433 Eros, causing continuous fluidization processes that create various visible geological structures.

Haugsjaa A. L. Colwell J. E.
Modelling Electrostatic Dust Transport on Eros **[#1225]**
Images of the surface of Eros reveal a multitude of smooth dust ponds located within Eros craters. We present preliminary results from 3D modeling of electrostatic dust transport as a mechanism to explain these pond formations.

Prettyman T. H. Barraclough B. L. Feldman W. C. Baldonado J. R. Bernardin J. D. Dingler R. D. Enemark D. C. Little C. K. Miller E. A. Patrick D. E. Pavri B. Raymond C. A. Russell C. T. Storms S. A. Sweet M. R. Williford R. L. Wong-Swanson B.
Gamma Ray and Neutron Spectrometer for Dawn **[#2231]**
The gamma ray and neutron spectrometer for the Dawn mission to asteroids Vesta and Ceres is described.

Usui T. McSween H. Y. Jr.
Characterizing the Surface Elemental Composition of 4 Vesta Based on HED Meteorites: Prospective Study of Gamma-Ray and Neutron Spectrometer for the DAWN Mission **[#1407]**
The DAWN mission will explore two of the largest main-belt asteroids, Ceres and Vesta. We compile 42 whole-rock compositions of HED meteorites and present two diagnostic compositional diagrams to characterize the surface type of Vesta from GR/NS data.

Nishihara S. Abe M. Kitazato K. Sarugaku Y. Kuroda D. Hasegawa S. Kinoshita D.
Ground Based Observation for Asteroid Sample Return Mission Target **[#2352]**
We have observed 23 NEAs during 2003–2005, using the 1.05-m Kiso Schmidt telescope and the Lulin 1-m telescope. As the taxonomic types of 238 candidates are unknown, we performed the BVRI photometry. I present the results of multicolor photometry.

Hiroi T. Ueda Y. Nimura T. Abe M. Ishiguro M. Sasaki S.
A New Scheme for Estimating the Degree of Space Weathering Through Visible Multiband Spectroscopy Using an ECAS-type Filter System Such as Hayabusa AMICA **[#1396]**
We have newly developed a scheme for estimating the degree of space weathering which is more free from effects of grain size and viewing geometry, utilizing the spectral inflections at around 0.4 and 0.55 μm. It is very useful for planetary remote sensing including spacecraft missions.

Trigo-Rodríguez J. M. Castro-Tirado A. J. Jelínek M. Vitek S. Llorca J. Fabregat J.
Two Likely Meteorite-dropping Bolides Recorded by a New High-Res All-Sky CCD Camera **[#1559]**
During 2005 all-sky CCD observations were carried out by two stations of the Spanish Meteor Network. As a result of this continuous monitoring two extraordinary bolides were recorded. Preliminary results obtained in studying both events are presented.

Binzel R. P.   Thomas C. A.   DeMeo F. E.   Tokunaga A.   Rivkin A. S.   Bus S. J.
The MIT-Hawaii-IRTF Joint Campaign for NEO Spectral Reconnaissance **[#1491]**
Near-infrared spectra for ~80 near-Earth objects are publicly available via http://smass.mit.edu, where these data are obtained through a collaborative program on the NASA Infrared Telescope Facility.

Kaletzke L.   Cloutis E.   Craig M.   McCormack K.   Stewart L.
Possible Explanations for the 506 nm Feature in Telescopic Spectra of Vesta, Vestoids, and HED Meteorites **[#2174]**
On the basis of new high-resolution laboratory reflectance spectra, variations in the wavelength position of the 506 nm feature seen in reflectance spectra of Vesta, vestoids, and HED meteorites may be due to variations in plagioclase feldspar abundances rather than changes in pyroxene composition.

Milliken R. E.   Mustard J. F.
Estimating Absolute H_2O Content of Low-Albedo Materials Using Reflectance Spectroscopy **[#1954]**
Physical and numerical experiments of minerals mixed with darkening agents were studied under various hydration states in an attempt to find a correlation between the 3 μm water band and absolute H_2O content for low-albedo materials.

Dameron S. N.   Burbine T. H.
Analysis of Meteorite Spectra in the Mid-Infrared **[#1828]**
To try to determine how well meteorites can be differentiated in the mid-infrared wavelength region, we are analyzing the spectral properties of meteorites from 0.3 to 25 μm.

Reddy V.   Dyvig R. R.   Pravec P.   Kusnirak P.   Kornos L.   Vilagi J.   Galad A.   Gajdos S.   Pray D. P.   Benner L. A. M.   Nolan M. C.   Giorgini J. D.   Ostro S. J.   Abell P. A.
Photometric and Radar Observations of 2005 AB: A New Binary Near-Earth Asteroid **[#1755]**
An estimated 15% of the NEA population are binaries. To better understand asynchronous binaries, a photometric survey was launched in 2004. We present photometric and radar observations of 2005 AB, the first binary discovered as part of the survey.

Kumar S.   Hardersen P. S.   Gaffey M. J.
Albedo Estimates and Near-Infrared Reflectance Spectroscopy of Near Earth Asteroids 1999 HF1 and 2005 AB **[#1113]**
Reflectance spectra and albedo estimates for NEAs 1999 HF1 and 2005 AB will be presented.

Nimura T.   Hiroi T.   Ohtake M.   Ueda Y.   Abe M.   Fujiwara A.
An Attempt of Restricting Olivine Bands in the Modified Gaussian Model **[#1600]**
As an attempt of improving the capability of MGM in deconvolving olivine absorption bands from a mixture spectrum, a new set of constraints are proposed and tested for for its applicability. This preliminary study has shown its potential usefulness.

Hoffman E. J.   Hart C.   Hatcher S.
Anomalous NIR and Mössbauer Spectra of High-Ca Pyroxenes: The Effect of Minor Phases **[#1215]**
High-Ca pyroxenes are common surface minerals, but some produce Type B NIR spectra, with anomalous 2-μm absorption. For one, PYX018, SEM shows minute amounts of andradite, which we are mixing into PYX020, a compositionally-matched Type A sample.

Marsh C. A.   Della-Giustina D. N.   Giacalone J.   Lauretta D. S.
Experimental Tests of the Induction Heating Hypothesis for Planetesimals **[#2078]**
Induction heating has been proposed to explain thermal processing of asteroidal materials. With our induction furnace we are unable to melt Fe metal alone, and mixtures of metal and olivine are more resistant to induction heating.

Wilson L.   Goodrich C. A.   Van Orman J.
Thermal History and Physics of Melt Extraction on the Ureilite Parent Body **[#1177]**
We show that melt extraction from the ureilite parent asteroid was very efficient, consistent with the preservation of oxygen isotopic heterogeneity despite high-T igneous processing, and with perfect fractional melting.

Conrad A. R. Dumas C. Merline W. J. Campbell R. D. Goodrich R. W. Le Mignant D. Chaffee F. H. Fusco T. Kwok S. Knight R. I.
Rotation and Morphology of Asteroid 511 Davida **[#1955]**
We present spatially resolved images of asteroid 511 Davida, one of ten large main belt asteroids imaged during the course of our Resolved Asteroid Program. We compare the shape, pole orientation, and size to measurements obtained by other methods.

García-Martínez J. L. Ortega-Gutiérrez F.
Four NEAs Associated with Meteroid Streams **[#2038]**
Four NEAs apparently associated with meteoroid streams have been detected. The objects are thought to be asteroids of C-, D-, or P-types. The dimensions of these objects suggest they would be the top end of the meteoroid size distribution.

Cheng A. F. Dombard A. J.
Viscous Relaxation on Comets **[#1986]**
Observations suggest viscous relaxation of cometary ice might modify both the shapes and cratering records of Jupiter family comets. Model parameters and predictions are consistent with plausible values for comets.

Bottke W. F. Chapman C. R.
Determining the Main Belt Size Distribution Using Asteroid Crater Records and Crater Saturation Models **[#1349]**
Craters on Eros, Ida and Mathilde were formed by a shallow main belt size distribution (SD) w/differential $q \sim -3.5$. The steep crater SD on Gaspra was the by-product of a recent event and does not represent time-averaged main belt conditions.

Izenberg N. R. Barnouin-Jha O. S.
Laboratory Simulation of Surface Seismic Effects on Low Gravity Bodies **[#2017]**
The effects of seismic shaking on low gravity bodies are being explored via laboratory modeling using a Seismic Simulation Mockup containing regolith simulant, mounted on a vibration table. Pilot test data and results will be presented.

Korycansky D. G. Asphaug E.
Rigid-Body Dynamics and Secondary Impact Ejecta on Asteroids **[#1465]**
We report results of modeling rigid-body dynamics applied to asteroids, in particular, the dynamics of ejecta from impacts onto asteroids.

STARDUST: MISSION ACCOMPLISHED

Glavin D. P. Doty J. H. III Matrajt G. Dworkin J. P.
Protocol for Future Amino Acid Analyses of Samples Returned by the Stardust Mission **[#1031]**
We have optimized a new liquid chromatography-time of flight-mass spectrometry technique with UV fluorescence detection for the analysis of amino acids in Stardust analog materials. Preliminary results from these analyses are reported.

Jones S. M. Flynn G. J.
Non-Silicate Aerogel as a Hypervelocity Particle Capture Material **[#1852]**
The Stardust mission used silica aerogel for the sample capture and return material. By using non-silicate aerogel the science return for future particle capture and return missions can be expanded.

Sandford S. A. McNamara K. Zolensky M.
The Recovery of the Stardust Sample Return Capsule **[#1123]**
The details of the recovery of the Stardust sample return capsule in Utah on January 15, 2006, will be discussed.

Spencer M. K. Zare R. N.
μL^2MS Analysis of Standards in Preparation for the Return of NASA Stardust **[#1432]**
Laser desorption/ionization mass spectrometry (μL^2MS) will be used to study PAHs in samples returned by Stardust. Investigations have been pursued to assess PAH background levels in aerogel and optimize μL^2MS for the study of particles in aerogel.

INTERPLANETARY DUST PARTICLES

Landgraf M. Grün E. Srama R. Helfert S. Kempf S. Morgas-Klostermeyer G. Rachev M. Srowig A. Auer S. Horànyi M. Sternovsky Z. Harris D.
The Sky in Dust — Methods and Prospects of Dust Astronomy **[#1084]**
Dust particles, like photons, carry information from remote sites in space and time. We show that with a large-area (1 square metre) dust telescope substantial new results can be obtained regarding the evolution of interstellar matter.

Djouadi Z. Davoisne C. Leroux H. d'Hendecourt L. Jones A. P. Deboffle D.
Micro-Structural Evolution of Amorphous Silicates with Annealing: Clues for Understanding the Origin of GEMS in IDPs **[#1296]**
In this work, we propose a possible scheme for the formation of the GEMS (glass embedded with metal and sulfides) present in the anhydrous IDPs (interplanetary dust particles). It requires amorphous silicates heated in the presence of carbon atmosphere.

Pitman K. M. Hofmeister A. M.
Thin Film Absorbance Spectra of Forsterite and Fayalite Dust Grains **[#1338]**
Forsterite and fayalite dust grains exist in a variety of astrophysical and planetary environments. We present mid- and far-IR laboratory DAC thin film absorbance spectra and peak positions for ~20 compositions along the Fo/Fa binary, including intermediate values absent in recent studies.

Ipatov S. I. Kutyrev A. S. Madsen G. J. Mather J. C. Moseley S. H. Reynolds R. J.
Dynamical Zodiacal Cloud Models **[#1471]**
Asteroidal dust particles alone cannot explain observations of velocities of zodiacal dust particles, and particles produced by high-eccentricity comets are needed for such explanation.

Gounelle M. Bleuet P. Bonal L. Borg J. Chaussidon M. d'Hendecourt L. Djouadi Z. Duprat J. Engrand C. Ferroir T. Gillet P. Grossemy F. Le Guillou C. Lemelle L. Leroux H. Marty B. Meibom A. Montagnac G. Mostefaoui S. Quirico E. Reynard B. Robert F. Rouzaud J.-N. Simionovici A. van de Moortèle B.
Coordinated Studies of Pristine Concordia Micrometeorites **[#1613]**
We have set up a consortium of French scientists specialized in the microanalysis of extraterrestrial matter. We have tested our ability to generate reliable data, using a great diversity of techniques on submillimeter-sized samples within one month.

Nagahara H. Ozawa K. Ikeda Y. Tachibana S.
Condensation of Forsterite and Metallic Iron Around Evolved and Young Stars **[#1636]**
Growth of metallic iron and forsterite grains around evolved and young stars are studied by using experimentally obtained condensation coefficients, which results in smaller grain size of forsterite than metallic iron due to smaller coefficients.

Herzog G. F. Gallien J.-P. Khodja H. Flynn G. J. Taylor S.
Preparation for Cometary Sample Return: Nuclear Microprobe Analysis of C and N in NaOCN, KOCN, $K_3Fe(CN)_6$, Tagish Lake, Murchison, and Two Cosmic Spherules **[#1694]**
A (d,p) method giving N/C atom ratios for grains as small as 15 μm pressed into In foils can be applied to samples from comet Wild-2. To illustrate, we show results for Murchison, Tagish Lake and two cosmic spherules.

Durda D. D. Flynn G. J. Sandel L. E. Strait M. M.
Size/Mass-Frequency Distributions of Dust-Size Debris from the Impact Disruption of Chondritic Meteorites **[#1801]**
We report results of impact disruption experiments involving chondritic meteorites where size/mass-frequency distributions of dust-size ejecta were determined from foil penetration data.

Chizmadia L. J. Nuth J. A. III Rietmeijer F. J. M.
Experimental Aqueous Alteration of Amorphous Silicate Smokes **[#2187]**
Hydration experiments were conducted on amorphous silicate smokes. The Mg-smokes contain serpentine crystalites after 3 days at 25°C and 5 days at 5°C. The Fe-smokes do not react with water after 28 days.

Ishii H. A. Luening K. Brennan S. Pianetta P. Ignatyev K. Matrajt G. Bradley J. P.
Micro-SXRF on Interplanetary and Cometary Dust Particles: Technical Considerations for Trace Element Analysis **[#2198]**
We present technical requirements for obtaining high quality trace element data from micron-sized dust particles by micro-synchrotron X-ray fluorescence analysis. Challenges include contamination, stability, damage and data processing.

Ishii H. A. Bradley J. P.
Macroscopic Cutting of Aerogel Collectors for Stardust and Future Sample Return Missions **[#2240]**
We report an "ultrasonic macroblade" technique for making large-scale cuts in silica aerogel collector tiles for the Stardust mission. The technique produces smooth cut surfaces with high optical clarity and can be used to subdivide tiles and extract large impacts.

Westphal A. J. Von Korff J. Anderson D. Alexander A. Betts B. Brownlee D. Butterworth A. Craig N. Gainsforth Z. Mendez B. See T. Snead C. J. Srama R. Tsitrin S. Warren J. Zolensky M.
Stardust@home: Virtual Microscope Validation and First Results **[#2225]**
We describe Stardust@home (S@H), a project with the goal of identifying interstellar dust in the Stardust Interstellar Tray using volunteers. We present measurements of the performance the S@H Virtual Microscope using inexperienced volunteers.

Bonal L. Quirico E. Montagnac G. Reynard B.
Interplanetary Dust Particles: Organic Matter Studied by Raman Spectroscopy and Laser Induced Fluorescence **[#2271]**
Preliminary results obtained on IDPs by multiwavelength Raman spectroscopy (including the 244 nm UV excitation), and by laser-induced fluorescence (LIF).

Graham G. A. Kearsley A. T. Chater R. J. Teslich N. Moberlychan W. Dai Z. R. Burchell M. J. Cole M. J. McPhail D. S. Grant P. G. Bradley J. P. Hörz F.
Experimental Impact Craters in Aluminum Foils: Insights for Cometary Sample Return **[#2280]**
We summarize the sample recovery methods and analysis of experimental impact residues generated in the laboratory to support the Stardust cratering preliminary examination.

Rashev M. V. Ahrens T. J.
Modeling of Micrometeoroid Impact Upon a Solid Target of the Impact Ionization Detector **[#2292]**
This work deals with a simulation of micro-meteoroid impacting onto the impact ionization detector. The goal is to get a visualization of an impact event and estimation of an ion number and atomic mass numbers released during an impact.

Huwig K. A. Harvey R. P. Henkel T.
A Comparison of "Identical" Antarctic Micrometeorites from Glacial Ice and Aeolian Sediments **[#2403]**
We compare two "identical" looking micrometeorites using TOFSIMS and TEM to determine whether glacial and aeolian micrometeorites differ due to their collection methods.

Ogawa R. Nagahara H. Ozawa K. Tachibana S.
Experimental Condensation of Crystalline Magnesium-rich Silicates **[#2415]**
Kinetic condensation experiments of Mg-rich silicates were perfomed to investigate phase and crystallinity of condensates as a function of temperature and supersaturation under astrophysical conditions.

Robert F. Mostefaoui S. Aléon J. Derenne S. Remusat L. Meibom A.
NanoSIMS H, C, N, and O-Isotopic Study of Insoluble Organic Matter in Murchison **[#1301]**
Murchison insoluble residue was analyzed using NanoSIMS. A molecular interpretation is proposed to account for observed D/H hot-spots.

PLANET FORMATION AND DIFFERENTIATION

Bond J. C. Lauretta D. S.
Chemical Models of the Protoplanetary Disks for Extrasolar Planetary Systems **[#1857]**
Chemical models of protoplanetary disks for three known planetary host stars are obtained using stellar spectroscopic abundances.

Scott E. R. D.
Constraints on Jupiter's Age and Formation Mechanism and the Nebula Lifetime from Chondrites and Asteroids **[#2367]**
Chondrule ages and models for the accretion and evolution of the asteroid belt require a period of 3–5 Myr after CAIs formed before Jupiter approached its current size and position. Jupiter formed by core formation — not gravitational instabilities.

Coradini A. Magni G.
Jupiter and Saturn Evolution by Gas Accretion onto a Solid Core **[#1591]**
New results are presented from the development of a complex hydrodynamic code able to model the process of Jupiter and Saturn formation, starting from a solid core able to collect the surrounding gas.

Yuki T. Abe Y.
Core Formation Condition that Satisfies the Ni Abundance and W Isotopic Ratio **[#1638]**
We investigated the core formation condition considering the multiple giant impacts. Ni abundance and W isotopic ratio are satisfied when at least half of impactor's iron equilibrates in a shallow magma ocean. The formation age ranges 30–70 Myr.

Mann U. Frost D. J. Rubie D. C. Shearer C. K. Agee C. B.
Is Silicon a Light Component in the Earth's Core? — Constraints from Liquid Metal-Liquid Silicate Partitioning of Some Lithophile Elements **[#1161]**
Metal-silicate partitioning of the lithophile elements Ta, Ga, In and Zn at 6–20 GPa and 2100°–2400°C show that they become more siderophile than Si at low oxygen fugacities. Si is therefore unlikely to be a major light element in the Earth's core.

Chabot N. L. Righter K.
Sulfur in Earth's Mantle and Its Behavior During Core Formation **[#1062]**
The sulfur content of Earth's mantle is consistent with metal-silicate equilibrium in a high pressure, high temperature magma ocean, providing constraints on the conditions of core formation as well as the contribution of a late veneer.

Campbell A. J. Danielson L. Righter K. Wang Y. Davidson G.
Oxygen Fugacity at High Pressure: Equations of State of Metal-Oxide Pairs **[#1977]**
The Re-ReO_2 oxygen fugacity buffer is precisely evaluated at high pressures, based on new equation of state data.

Malavergne V. Tarrida M. Siebert J. Combes R. Bureau H. Berthet S.
Partitioning of Trace Elements Between Silicate, Sulfide and Metal at High Pressure and High Temperature: Investigation of Dopant Influence on Partition Behavior **[#1951]**
The partition coefficients of (Cr, Mn, Fe, Co, Ni) and W between liquid metal, sulfides and silicates is investigated between 1.5 GPa–25 GPa up to 2200°C, at different oxygen fugacity and with different light elements present in the metallic phases.

Malavergne V. Jones J. Campbell A. J. Perronet M.
Pt, Au, Pd and Ru Partitioning Between Olivine and Silicate Liquid **[#1974]**
In the present study, we have tried to determine the abundances of Pt, Au, Ru and Pd in olivine and quenched silicate melt from high temperature experiments with variable redox conditions.

GENESIS MISSION

Allton J. H. Calaway M. J. Rodriguez M. C. Hittle J. D. Wentworth S. J. Stansbery E. K. McNamara K. M.
Genesis Solar Wind Sample Curation: A Progress Report **[#1611]**
Basic characterization of Genesis solar wind array collector fragments consists of solar regime identification, whole fragment surface condition imaging, particle density imaging, and molecular film thickness. Fragment catalogs are in work.

Allton J. H. Calaway M. J. Hittle J. D. Rodriguez M. C. Stansbery E. K. McNamara K. M.
Cleaning Surface Particle Contamination with Ultrapure Water (UPW) Megasonic Flow on Genesis Array Collectors **[#2324]**
UPW/Megasonic cleaning appears to be a rapid, simple way to remove larger particles from Genesis array collector fragments.

Brennan S.   Ishii H. A.   Luening K.   Pianetta P.   Burnett D. S.
Synchrotron Total-Reflection X-Ray Fluorescence (SR-TXRF) of Genesis Return Samples **[#2029]**
Synchrotron-based Total-Reflection X-Ray Fluorescence (SR-TXRF) has been used to measure the surface cleanliness of flown Genesis sapphire sample pieces. Megasonic UPW cleaning does not increase surface roughness. Brown stain was found on some, but not all, of the flown sapphire pieces.

Burnard P.   Zimmermann L.   Marty B.
Vacuum UV Laser Ablation of Genesis Target Materials: Results from Gold-on-Sapphire Analogs **[#1695]**
An excimer laser system has been developed that ablates between <5 nm and ~100 nm of material per pulse; this will be used for extracting N and noble gases from Genesis targets.

Burnett D. S.
Genesis Mission: Overview and Status **[#1848]**
The Genesis Project is making slow, but steady, progress in meeting science objectives following the crash of the return capsule.

Calaway M. J.   Stansbery E. K.   McNamara K. M.
Modeling Ellipsometry Measurements of Molecular Thin-Film Contamination on Genesis Flown Array Samples **[#1420]**
Spectroscopic ellipsometry models are discussed that determine accurate thickness measurements of thin-film contamination on Genesis mission flown collector array materials.

Hittle J. D.   Calaway M. J.   Allton J. H.   Warren J. L.   Schwarz C. M.   Stansbery E. K.
Genesis Spacecraft Science Canister Preliminary Inspection and Cleaning **[#1411]**
Inspection of the Genesis Science Canister revealed a micrometeorite impact, white paint discoloration, and black residue adhering to the structure. Loose particles were removed with a fine-haired brush and filter-trap vacuum.

Huang S.   Humayun M.   King S.   Goddard B.   Burnett D.
Step-Cleaning Experiment on the Genesis Wafers **[#2440]**
Step-cleaning of the Genesis wafers.

Kitts K.   Sutton S.   Eng P.   Ghose S.   Burnett D.
Discrimination and Quantification of Contamination and Implanted Solar Wind in Genesis Collector Shards Using Grazing Incidence Synchrotron X-Ray Techniques: Initial Results **[#1451]**
Grazing incidence X-ray fluorescence is a non-destructive technique that can differentiate the embedded solar wind component from surface contamination and collector background in the Genesis shards. Initial solar Fe abundance in D30554 is $8 \times 10^{12}/cm^2$.

Kuhlman K. R.   Jurewicz A. J. G.   Grimberg A.   Heber V.   Sridharan K.
Progress Toward Low-Energy Genesis Simulants **[#2443]**
Description of fabrication of Genesis simulants.

Mao P. H.   Kunihiro T.   McKeegan K. D.   Coath C. D.   Jarzebinski G.   Burnett D.
MegaSIMS Update: Oxygen Transmission, Destruction of OH Molecular Ions, and Stability of Three-Isotope Measurements **[#2153]**
We will present calibration results from MegaSIMS: oxygen charge state and transmission measurements, destruction efficiency of OH molecular ions by the accelerator and instrument stability with respect to oxygen three-isotope measurements.

Meshik A. P.   Marrocchi Y.   Hohenberg C. M.   Pravdivtseva O. V.   Mabry J. C.   Olinger C.   Burnett D. S.   Allton J. H.   Bastien R.   McNamara K. M.   Stansbery E. K.
Measurements of Light Noble Gases in the Genesis Polished Aluminum Collector **[#2433]**
Fragment of the Genesis polished aluminum collector was degased using incrementally increased laser power, resolving the Ne depth profiles. The weighted average of the three extractions can be considered as our current best estimate for bulk solar wind Ne.

Reedy R. C.
Solar-Proton Event-Integrated Fluences During the Current Solar Cycle **[#1419]**
The event-integrated fluences of energetic solar protons from 1996 up through 2005 at the Earth have been compiled and compared to previous data. The current solar cycle has been very active with the highest proton fluxes since about 1976.

Sestak S. Franchi I. A. Verchovsky A. B. Al-Kuzee J. Braithwaite N. St. J. Burnett D. S.
Application of Semiconductor Industry Cleaning Technologies for Genesis Sample Collectors **[#1878]**
Genesis array collectors recovered after the sub-nominal landing have been exposed to particulate and molecular contamination. In this study, semiconductor industry based cleaning technologies are being evaluated for their efficacy in contaminant removal.

Sisterson J. M.
New Cross Section Measurement for Neutron-induced Reactions in Elements Found in Extraterrestrial Materials **[#1667]**
New cross section measurements for neutron-induced reactions producing relatively short-lived radionuclides in Ti, Fe and Ni will be reported as well as the status of the cross section measurements for the production of long-lived radionuclides.

Veryovkin I. V. Calaway W. F. Tripa C. E. Pellin M. J.
Advanced Analytical Instrument Facility for Analysis of Return Samples from NASA Space Exploration Missions **[#1849]**
A new mass spectrometer with laser post-ionization of neutral species constructed at Argonne National Lab is well suited for analyses of return samples from NASA space exploration missions because of its high useful yield and analytical resolutions.

ASTROBIOLOGY: MISSIONS

Starke V. Maule J. Monaco L. Flores G. Steele A.
Microarray Technology for Space Exploration **[#2124]**
We discuss the use of microarrays in several areas of planetary exploration interest. We detail a protoype microarray for the simultaneous detection of over 120 microorganisms of interest to space exploration.

Vasavada A. R. MSL Science Team
NASA's 2009 Mars Science Laboratory: An Update **[#1940]**
The Mars Science Laboratory will launch in fall 2009. Its overall scientific goal is to explore and quantitatively assess a local region on Mars' surface as a potential habitat for life, past or present.

Schmidt T. J. Beegle L. W. Wilson M. G. Wilson G. R.
A Concept for the 2016 Mars Astrobiology Field Laboratory **[#2337]**
An overview of the 2016 Mars Astrobiology Field Laboratory.

Zent A. P. Quinn R. C. Lambert J. L. Kounaves S. Young S. Bell J. Hecht M. Taylor C.
Measurement of Total Organic and Total Inorganic Carbon on Mars **[#2184]**
A wet-chemistry spectroscopic system for total carbon and C isotope analysis.

Beegle L. W. Guerrero J. Douglas S. Kidd R. Lane A. L. Pelletier M. Feldman S. Mungas G. S. Blake D. Dissly R. Waite J. H. Young D. T. Sun H. Wells S. MSE Team
The Mars Subsurface Explorer **[#1467]**
We have developed a terrestrial field campaign to explore two subsurface biological habitats under the Mojave Desert to a depth of 20 meters. This will be done by combining four instruments of high TRL with a field demonstrated drilling platform.

Schulze-Makuch D. Dohm J. M. Fairen A. G. Baker V. R. Fink W. Strom R. G.
Sample Return Missions to Mars, Venus, and the Ices on Mercury and the Moon **[#1324]**
Missions to our neighboring planets Venus and Mars should be planned to explore potentially life-containing refuges and return samples for analysis. Sample return missions should also include ice samples from Mercury and the Moon.

Fink W. Dohm J. M. Tarbell M. A. Hare T. M. Baker V. R. Schulze-Makuch D. Furfaro R. Fairén A. G. Ferré T. P. A. Miyamoto H. Komatsu G. Mahaney W. C.
Multi-Tier Multi-Agent Autonomous Robotic Planetary Surface/Subsurface Reconnaissance for Life **[#1433]**
Tier-scalable autonomous reconnaissance enables intelligent, unconstrained, and distributed science-driven exploration of prime locations on Venus, Mars, Io, Europa, Titan, and elsewhere, allowing for increased science return and the search for life.

Schuerger A. C.   Berry B.   Nicholson W. L.
Terrestrial Bacteria Typically Recovered from Mars Spacecraft Do Not Appear Able to Grow Under Simulated Martian Conditions **[#1397]**
Bacteria typically recovered from spacecraft were tested for growth at low pressures. Results indicated that most species were strongly inhibited at low pressues, and that there may be a direct pressure effect on bacterial growth.

Weinstein S.   Pane D.   Warren-Rhodes K.   Cockell C.   Ernst L. A.   Minkley E.   Fisher G.   Emani S.   Wettergreen D. S.   Wagner M.   Cabrol N.   Grim E.   Waggoner A. S.
Implementation of a Daylight Fluorescence Imaging System to Autonomously Detect Biomarkers of Extant Life in the Atacama Desert **[#2456]**
We have integrated a biomarker detection system with a rover for the search for sparse life in extreme environments. The system incorporated a pulsed fluorescence imager, a reagent sprayer, and a surface scraping device for remote detection of fluorescence signals.

Thompson D. R.   Smith T.   Wettergreen D.
Autonomous Detection of Novel Biologic and Geologic Features in Atacama Desert Rover Imagery **[#2085]**
Novelty detection helps planetary rovers perform adaptive sampling and return to maximize the value of transmitted data. We investigate context-sensitive novelty detection using images collected during rover traverse in the Atacama desert.

Parnell J.   Lindgren P.   Osinski G. R.   Cockell C. S.   Lee P.
Simple Devices for Concentration of Microbial Life: Experiments in Haughton Impact Structure **[#1050]**
Simple devices that create environments with high levels of light and moisture could attract extant microbial life on a planetary surface and hence enhance the detection of it. Experience in the Haughton crater shows that this can occur readily.

Van Houten K. A.   Strauch L. R.   Murray G. M.   Izenberg N. R.
Molecularly Imprinted Polymers for Astrobiology **[#1381]**
Molecular Imprinted Polymer (MIP)-based sensors are promising candidates for a variety of *in-situ* planetary astrobiological and geochemical mission profiles, and are currently being developed under NASA Grant #NNG05GM90G.

Izenberg N. R.   Murray G. M.   Van Houten K.   Strauch L.   Hofstra A.   Uy O. M.
Development of Astrobiological Molecularly Imprinted Polymer Sensors **[#1372]**
Molecular Imprinted Polymer-based sensors are promising candidates for a variety of *in-situ* planetary astrobiological and geochemical mission profiles. We have begun developing and testing them through the NASA ASTID Program.

Kim H. I.   Kim H.   Beegle L. W.   Johnson P. V.   Beauchamp J. L.   Kanik I.
Theoretical Ion Mobility Studies of Amino Acids **[#2127]**
ESI/IMS is a potential onboard instrument for searching organic molecules on future missions to Mars. DFT calculated geometries of amino acids yield predicted mobilities in good agreement with previous amino acid mobility experiments.

Duong T. A.   Liu D.   Kanik I.
Neural Network Prediction of Reduced Ion Mobility of Amino Acid Based on Molecular Structure **[#1474]**
We present a new input feature mapping technique which is based on Riemannian metric tensor to enhance the neural network learning capability for predicting the reduced ion mobility based on the molecular structure for NASA remote applications.

MARS EXPRESS: PROBING THE DEPTHS

Thompson T. W.   Horttor R. L.   Acton C. H. Jr.   Zamani P.   Johnson W. T. K.   Plaut J. J.   Holmes D. P.   No S.   Asmar S.   Goltz G.
The Mars Express/NASA Project at JPL **[#1083]**
The Mars Express/NASA Project at JPL supports much of the U.S. involvement in ESA's Mars Express mission. Mars Express has just completed its prime mission in late 2005 and has embarked on its first extended mission cycle.

Pischel R. Zegers T. Jansen F. Chicarro A. Martin P. Walker H. Denis M. Moorhouse A. Rabenau E. Peschke S. Schulster J. McCarthy C.
One Martian Year of Mars Express Science Operations Planning **[#1734]**
Europe's Mars Express mission has achieved the milestone of 1 martian year in orbit. This paper describes the science operations for Mars Express throughout the nominal mission, including special operations such as the MEX-MER link demo tests.

Zender J. Heather D. Diaz del Rio J. Ortiz I. Dowson J. Arviset C. Zegers T. E.
Mars Express Scientific Data Distribution Via ESA's Planetary Science Archive **[#1631]**
This poster explains the use of ESA's Planetary Science Archive for Mars Express data.

Safaeinili A. Kofman W. Herique A. Gim Y. Hagfors T. Kirchner D. Gurnett D. Nilesen E. Plaut J. J. Picardi G.
Estimation of Mars Ionosphere Total Electron Content Using MARSIS Radar Surface Echo **[#1736]**
We use MARSIS subsurface data to derive Mars ionosphere's total electron content (TEC). Our estimation technique provides a high resolution behavior of TEC versus solar zenith angle and shows potential dependence of the TEC on local Mars magnetic field.

Carley R. A. Heggy E.
Characterization of the Density Dependent Dielectric Properties of Mars-like Soils: Implications for Mars Radar Studies **[#1261]**
We present laboratory measurements of the complex dielectric permittivity of a variety of synthesized and Mars analog soils with varying iron oxide content, over the frequency range 1 MHz–1 GHz and density range 0.8–2.4 gcm^{-3}.

Nunes D. C. Phillips R. J. Picardi G. Plaut J. J. Safaeinili A. Seu R. Egan A.
Resolving Stratigraphy of the Polar Layered Deposits with MARSIS and SHARAD **[#1450]**
We contrast radar sounding profiles of the Martian polar caps obtained by MARSIS with wave propagation models in order to understand how both MARSIS and SHARAD responses define our ability to map the internal stratigraphy of the Martian polar caps.

Murray J. B. Balme M. R. Muller J.-P. Kim J-R. Morley J. Neukum G. HRSC Co-Investigator Team
Preliminary Observations on New Images of the Elysium Frozen Sea Deposits from HRSC Mars Express **[#2293]**
A series of new HRSC Mars Express images have provided new information on the extent, age, development and formation of the equatorial frozen sea deposits in Elysium.

Murray J. B. Iliffe J. C. Muller J.-P. A. L. Neukum G. Werner S. Balme M.
New Evidence on the Origin of Phobos' Parallel Grooves from HRSC Mars Express **[#2195]**
New HRSC images of Phobos indicate that the groove pattern is independent of Stickney crater, and favour an origin for the grooves quite unconnected with it: that they are chains of secondary impact craters from primary impacts on Mars.

Kreslavsky M. A. Bondarenko N. V. Pinet P. C. Raitala J. Foing B. H. Neukum G.
Mars Express HRSC Co-Investigator Team
Mapping of Photometric Anomaly of Martian Surface with HRSC Data **[#2211]**
We propose a practical method for mapping photometric anomaly of Mars surface from five panchromatic HRSC channels. The method tolerates atmospheric effect and calibration errors. We show examples of interpretation in terms of the surface structure.

Balme M. Mangold N. Baratoux D. Costard F. Gosselin M. Masson P. Pinet P. Neukum G. HRSC Co-I Team
Orientation and Distribution of Recent Gullies in the Southern Hemisphere of Mars: Observations from HRSC/MEX and MOC/MGS Data **[#1610]**
MOC and HRSC data reveal martian gullies form most commonly on pole facing slopes in the mid latitudes. Impact crater walls are the most common setting for gullies but many are found on isolated knobs and hills. Lengths up to ~7 km have been observed.

Kirk R. L. Howington-Kraus E. Galuszka D. Redding B. Hare T. M. Heipke C. Oberst J.
Neukum G. HRSC Co-Investigator Team
Mapping Mars with HRSC, ISIS, and SOCET SET **[#2050]**
HRSC images of Mars can be processed in ISIS, and used to make digital topographic models (DTMs) in commercial software. The HRSC team will evaluate and compare our DTMs and those of other team members who use a variety of software and techniques.

Quantin C. Gendrin A. Mangold N. Bibring J. -P. Hauber E. Allemand P. OMEGA Team
Stratigraphy and Elevation Distribution of Sulfate Deposits in Valles Marineris **[#2046]**
Sulfates have been detected by OMEGA in Valles Marineris in association with layered deposits. We studied the repartition and the elevation distribution of sulfate signatures for each canyon of Valles Marineris.

Loizeau D. Mangold N. Poulet F. Bibring J.-P. Gendrin A. Gomez C. Langevin Y. Gondet B. Ansan V. Masson P. Neukum G. OMEGA Team HRSC Team
Phyllosilicates Rich Terrains in Mawrth Vallis Region, Mars, as Seen by OMEGA and HRSC/Mars Epress **[#1658]**
Phyllosilicates have been detected by OMEGA on bright outcrops of a massive layered unit in the Mawrth Vallis region. Theses minerals are due to a specific alteration of rocks during the Noachian, indicating a different environment than today.

Zhu M. Xie H. Guan G. Smith R. K.
Mineral and Lithologic Mapping of Martian Low Albedo Regions Using OMEGA Data **[#2173]**
This paper used the OMEGA data to produce a geologic endmember map, and to estimate possible minerals and lithology for each endmember for three selected low albedo areas: Meridiani Planum, Ophir-Candor Chasma, and Syrtis Major.

Le Mouélic S. Sotin C. Combe J.-P. Ledeit L. Gendrin A. Mustard J. Bibring J-P Langevin Y. Gondet B. Pinet P.
Composition of the Dust on Mars Derived from OMEGA Hyperspectral Images **[#1409]**
The spectral signatures of bright units of Mars are investigated with OMEGA/Mars Express in order to study the composition of the dust. Spectra are consistent with ferric oxides, and possibly a very minor orthopyroxene component.

Gendrin A. Bibring J.-P. Mustard J. Kanner L. Mangold N. Gondet B. Langevin Y. Poulet F. Baratoux D. Sotin C. Le Mouelic S.
Strong Pyroxene Absorption Bands on Mars Identified by OMEGA: Geological Counterpart **[#1858]**
We describe the global high and low calcium pyroxene distribution on Mars as seen by OMEGA and their geological counterpart.

Costard F. Poulet F. Bibring J.-P. Baratoux D. Mangold N. Meresse S. Pinet P. OMEGA Team
Detection of Hydrated Minerals on Fluidized Ejecta Lobes from Omega Observations: Implications in the History of Mars **[#1288]**
The Omega data acquired during the first two years of the Mars Express mission already reveal a few examples of lobate ejecta with hydrated minerals. Here we discuss their geological context and their implications for Martian climate and subsurface volatiles.

Combe J.-Ph. Le Mouélic S. Sotin C. Gendrin A. Le Deit L. Mustard J. F. Bibring J.-P. Gondet B. Langevin Y. OMEGA Science Team
Analysis of OMEGA/Mars Express Hyperspectral Data Using a Linear Unmixing Model: Methods and Preliminary Results **[#2010]**
The mineralogy of the Martian surface is analysed with the OMEGA hyperspectral data set. An iterative linear spectral unmixing algorithm provides maps that are consistent with previous studies. Further investigations will be performed by this way.

Brown A. J.
Spectral Absorption Band Mapping at Cerberus Fossae Using Mars Express OMEGA Data **[#1477]**
A spectral absorption band mapping algorithm is applied to a set of data produced by the hyperspectral Mars orbiting OMEGA instrument. Weak absorption bands are detected in the Cerberus Fossae region that may be indicative of hydrothermal alteration minerals in this region.

Gondet B. Bibring J.-P. Langevin Y. Poulet F.
Composition of White Rock Formation Within Pollack Crater as Inferred from the OMEGA/MEX Data **[#1592]**
The surface composition of White Rock (Pollack crater, Arabia, Mars) will be presented from OMEGA/MEX observations.

Mangold N. Poulet F. Mustard J. F. Bibring J.-P. Langevin Y. Gondet B. Ansan V. Masson P. Hoffman H. Neukum G. HRSC Co-I Team OMEGA Co-I Team
Correlation Between Phyllosilicates, Olivine and Landforms in Nili Fossae Region, Mars **[#1791]**
Clay minerals are found in Nili Fossae region in connection with Noachian bedrock exposures, impact crater ejectas and, locally, olivine rich deposits. This suggests the alteration of the primitive crust by liquid water including the olivine rich rocks.

Jouglet D. Poulet F. Mustard J. F. Milliken R. E. Bibring J.-P. Langevin Y. Gondet B.
Observation of 3 μm Hydration Feature on Mars from OMEGA-MEx Data **[#1741]**
OMEGA data has been used to study Mars surface hydration through the 3 μm absorption band. The results will be presented and discussed.

Vincendon M. Langevin Y. Poulet F. Bibring J.-P. Gondet B. Schmitt B. Douté S.
Surface Water Ice and Aerosols Evolution of 77°N, 90°E Mars Crater During Early Summer by OMEGA/MEx **[#1769]**
OMEGA spectral data have been used to study aerosols and surface ice properties changes of a water ice rich northern crater during early 2004 summer.

Schmidt F. Douté S. Schmitt B. Bibring J.-P. Langevin Y.
Automatic Detection of H_2O and CO_2 Ices in OMEGA/MEX Images for the Monitoring of the South Polar Cap Recession **[#1979]**
The martian seasonal polar ice deposit is a major annual climatic signal observed by OMEGA/MEX. We will use an algorithm, wavanglet, for the automatic detection of the spectral signatures of H_2O and CO_2 ices during martian spring and summer of 2005.

Guan H. Xie H. Zhu M.
Development of an Alternative Martian Atmospheric Correction Algorithm for OMEGA/Mars Express Imagery **[#1934]**
A new martian atmospheric correction algorithm for hyperspectral imaginary is presented. This algorithm directly removes CO_2 absorptions based on the target image. It does not require reference spectra at the Olympus Mons.

ODYSSEY: A NEW VIEW OF THE SURFACE

Winfree K. W. Titus T. N.
Estimation of CO_2 Coverage on Mars' South Pole: An Interannual Assessment **[#2283]**
We present preliminary results taken from calibrated THEMIS images in Mars years 25, 26, and 27, showing that the south polar CO_2 residual cap is not shrinking. These results will be compared to OMEGA and MOC imaging.

Piatek J. L. Moersch J. E.
A Strategy for Atmospheric Correction of THEMIS Infrared Data **[#1158]**
A method for deriving the multiplicative atmospheric absorption correction from the additive radiance offset correction has been tested over a variety of THEMIS images with different surface temperatures and topography.

Burger P. Shearer C. K. Newsom H. E. Reedy R. C. Taylor G. J.
Microscale Distribution and Behavior of Th and K in Late-Stage Melts and Shock Melts in Olivine-Phyric Shergottites: Implications for the Interpretation of Remote Sensing and In Situ Measurements of the Martian Surface **[#2317]**
Th and K in many of the Mars surface lithologies are not reflected in the martian meteorite collection. In this study, we examine the variation in Sm, Th, K, and major elements in both late stage-melt and shock-melt assemblages in martian meteorites.

AEOLIAN PROCESSES ON MARS: WAR OF THE WHIRLS

Mullins K. F. Hayward R. K. Tanaka K. L.
Dune Forms and Ages and Associated Oblate Depressions in the Chasma Boreale Region of Planum Boreum, Mars **[#1998]**
THEMIS and MOC images acquired over the Chasma Boreale contain key geologic and stratigraphic information relating to aeolian deposition and the PLD. Preliminary analyses of these images show a clear progression of morphologic change of dark albedo dune deposits along the chasma axis.

Williams K. K.
Are Martian Dunes Migrating? A Planet-wide Search for Dune Movement **[#2322]**
Overlapping MOC images containging dunes have been used to search for dune movement across the planet.

De Hon R. A.
Transitional Dune Forms on Mars **[#1361]**
A morphological progression from simple dome to intermediate, incipient dune-forms (fortune cookie and wedge dunes) to barchan and linear dunes suggests that dune development in a unidirectional wind regime is controlled by dune width and height of the growing dunes.

Dressing C. D.   Andros J. L.   Kashdan H. E.   Zimbelman J. R.   Hennig L. A.
Transverse Aeolian Ridges Observed at Pressure Extremes Within the Martian Atmosphere **[#1740]**
Transverse aeolian ridges are documented in MOC NA images of the summit of Ascraeus Mons and floor of the Hellas basin, which covers the pressure extremes within the Martian atmosphere.

Neakrase L. D. V.   Greeley R.   Haan F. L. Jr.   Sarkar P.   Iversen J. D.   Balme M. R.   Eddlemon E. E.
Dust Devils on Earth and Mars: Extension of Particle Threshold Laboratory Simulations **[#1196]**
Laboratory simulations were conducted for vortices approaching the size of natural dust devils to determine the threshold for sand-sized particles. Applications of this study pertain to scaling of field cases of martian and terrestrial dust devils.

Michaels T. I.
Numerical Modeling of Particle Transport by Mars Dust Devils **[#2027]**
Mars dust devils (DD) are thought to be an important part of the global dust cycle. What sizes of DD-lifted dust accomplish this, and which are quickly redeposited? How exactly does a DD create a "track" that can be seen from orbit? A 3D, DD-resolving model is used to investigate these questions.

Desch S. J.   Wilson G. R.   Perret B.   Neakrase L. D. V.   Greeley R.
Investigations into Dust Charging and Transport in Martian and Terrestrial Dust Devils **[#1983]**
Electrical discharges may occur in martian dust devils, but it is uncertain if they do. We plan wind-tunnel experiments using the Particle Charge Spectrometer to determine how dust grains charge, and numerical modeling of dust charging and transport in dust devils.

Abel M. F.   Foley D. J.   Neakrase L. D. V.   Greeley R.   Eddlemon E. E.   Shakkottai P.
Aeolian Particle Transport as a Function of Spacecraft Design: An Experimental Study of Potential Forward Contamination **[#1385]**
Experimental results of aeolian particle transport as a function of spacecraft design. To mitigate potential forward contamination of planetary bodies, a method for predicting flow patterns, distribution zones, and static thresholds were devised.

LAYERED DEPOSITS ON MARS

Hauber E.   Gwinner K.   Gendrin A.   Fueten F.   Stesky R.   Pelkey S.   Wulf H.   Reiss D.   Zegers T.   MacKinnon P.   Michael G.   Jaumann R.   Bibring J.-P.   Neukum G.   HRSC Co-Investigator Team
An Integrated Study of Interior Layered Deposits in Hebes Chasma, Valles Marineris, Mars, Using MGS, MO, and MEX Data **[#2022]**
We use recent data from several missions to constrain the geometry and composition of layered deposits in Hebes Chasma. We find that a lacustrine origin is unlikely, and that groundwater might be responsible for alteration products like sulfates.

Stesky R.   Fueten F.   MacKinnon P.   Hauber E.   Gwinner K.   Scholten F.   Zegers T. E.   Neukum G.   HRSC Co-Investigator Team
Layering Attitudes in Southwestern Candor Chasma from HRSC Image Data and Stereo-derived DTM **[#2013]**
The ILD layering shows low dips generally in the direction of the local topographic slope, suggesting draping over an irregular basement, either by subaerial or deep water deposition. The presence of an unconformity indicates a complex history.

Ansan V.   Mangold N.   Lucas A.
Layered Deposits in Terby Crater (Hellas Region, Mars) from Multi-Datasets (MOLA, THEMIS and MOC): Geologic Implications **[#1877]**
Terby impact crater is located at the northeastern part of Hellas region (75°E, 30°S) on the cratered highlands. Using multi-dataset available on this area, we show that Terby was filled by rhythmical layered deposits interpreted as sedimentary deposits.

Fassett C. I. Head J. W.
Layered Mantle Deposits in Northeast Arabia Terra, Mars: I. Observations of Noachian-Hesperian Sedimentation, Erosion and Terrain Inversion **[#1722]**
In northeast Arabia Terra, an extensive mantle was deposited and subsequently eroded. We describe new observations of this mantle, which provide constraints its evolution and suggest that the erosion took place in a relatively short amount of time.

Fassett C. I. Head J. W.
Layered Mantle Deposits in Northeast Arabia Terra, Mars: II. Models for Noachian-Hesperian Sedimentation, Erosion and Terrain Inversion **[#1728]**
In northeast Arabia Terra, an extensive mantle was deposited and subsequently eroded. We describe hypotheses for its evolution and emphasize the potential role that volatile-dust mixtures might have played in its deposition and subsequent erosion.

Jaumann R. Stephan K. Poulet F. Tirsch D. Wagner R. Hoffmann H. Reiss D. Hauber E. Bibring J.-P. Neukum G. HRSC Co-Investigator Team
Dark Materials in Martian Craters **[#1735]**
Dark materials are chemically unaltered and probably the result of mechanical erosion and global distribution by aeolian processes. This could indicate recent erosion and redistribution without enough time for chemical weathering.

MAPPING MARS

Chamberlain S. Bailey J. Crisp D. Walter M.
Topographic and Atmospheric Pressure Mapping of Mars **[#1357]**
Ground-based near-infrared images and spectral observations of Mars are shown to provide relatively detailed topographic images of the martian surface and may be used to obtain martian atmospheric pressure system information.

Werner S. C. Ivanov B. A. Neukum G.
Secondary Cratering and Age Determination on Mars **[#1595]**
Detailed investigations of the crater distributions of the Zunil (and other) secondary crater strewn field(s) are performed and compared to measured and predicted crater distributions to test different approaches and the applicability of crater counts for age determination.

Quantin C. Mangold N. Hartmann W. K. Allemand P.
Time Dependence of Geological Processes on Mars and Consequences on the Impact Chronology **[#2024]**
Our work on the time-dependence of geological processes on Mars shows an apparent increasing trend of geological processes over the Amazonian period. It may support a decline in inner solar system of the cratering rates since 3 Gy ago.

Dohm J. M. Anderson R. C. Baker V. R. Barlow N. G. Miyamoto H. Davies A. G. Taylor G. J. Boynton W. V. Keller J. Kerry K. Janes D. Fairén A. G. Schulze-Makuch D. Glamoclija M. Marinangeli L. Ori G. G. Strom R. G. Williams P. Ferris J. C. Rodriguez J. A. P. de Pablo Hdez M. A. Karunatillake S.
Tharsis/Elysium Corridor: A Marker for an Internally Active Mars? **[#1131]**
An internally active Mars is supported by geologic, hydrologic, geomorphic, impact cratering, and elemental information, highlighted in a region that straddles parts of Tharsis and Elysium, referred to as the Tharsis/Elysium corridor.

Thaisen K. Schieber J.
Mapping Stratigraphic Discontinuities in West Candor Layered Deposits and the Potential for Sequence Stratigraphic Analysis **[#2393]**
Stratigraphic discontinuities are common in West Candor layered deposits. Mapping these surfaces on MOC images in combination with MOLA data for development of stratigraphic architecture.

Chuang F. C. Crown D. A.
Geologic Mapping of MTM Quadrangles 35337, 40337 and 45337: Deuteronilus Mensae Region, Mars **[#1332]**
To assess the geologic evolution of martian highland terrains and the modification of these terrains by volatile-driven degradation, we are currently mapping three MTM quads in the Deuteronilus Mensae region that extend across the dichotomy boundary.

Bleamaster L. F. III Crown D. A.
Geology of MTM Quadrangles -40277, -45277, and -45272, Eastern Hellas Planitia, Mars **[#1798]**
Geologic mapping, at 1:1M scale, in eastern Hellas Planitia is being used to characterize geologic processes that have shaped the rim and and floor of the Hellas impact basin.

MARS VOLCANISM

Dalton H. A. Christensen P. R.
Investigation of the Extent of the Apollinaris Patera Ash Deposits: Implications for the Origin of the Columbia Hills **[#2430]**
The deposits from Apollinaris Patera on Mars were mapped to determine if they extended far enough to be the source of the Columbia Hills ash deposits in Gusev Crater.

Bulmer M. H. Zimmerman B. Finnegan D. Glaze L.
An Examination of the Rheology of Martian Debris Aprons **[#2275]**
In this study, MOC, THEMIS and MOLA data have been used to derive apron topography, thickness, and where possible travel speeds. These data have been combined with a Chezy modeling approach to examine their dynamics and to determine to first order their rheologies,

Monders A. G. Médard E. Grove T. L.
Basaltic Lavas at Gusev Crater Revisited **[#1834]**
Experimental study of the recalibrated basalt composition confirms previous findings that they are high-degree shallow melts of the primitive Martian mantle. However, they cannot be related to surface types or SNCs by low-pressure crystallization.

Patiño-Douce A. E. Roden M. F.
Fluorine, Chlorine and Water Fugacities in Planetary Basalts Recorded by Phosphate Equilibria **[#2037]**
We use apatite-merrillite equilibria to compare the relative values of halogen (F, Cl) and water fugacities in martian, lunar, eucritic and terrestrial basalts and conclude that the martian mantle is depleted in Cl and water compared to the terrestrial mantle.

Jacques N. M. Lescinsky D. T. Stooke P. J.
Interaction of Martian Ground Ice with Magmatic Intrusions **[#2394]**
We employ a numerical finite difference method to examine the non-explosive interaction of magma and ground ice and propose several potential sites for where such interactions may now be exposed on the martian surface.

Bargery A. S. Mège D. LeMouélic S. Combe J. P.
Near-Infrared Analysis of Tempe Terra, Olympica Fossae and Nili Fossae from OMEGA Data **[#1684]**
We calibrate and analyse raw OMEGA data from Tempe Terra, Olympica Fossae and Nili Fossae. We interpret our observations to identify the presence of localised orthopyroxene, water ice and extensive olivine in the respective regions.

Schupack B. B. Sakimoto S. E. H.
Eruption Styles of Small Martian Shield Volcanoes and Indications of Post-Flow Tectonic Deformation on Syria Planum, from MOLA, TES, and THEMIS Data **[#1157]**
In this study we look at the eruption styles of shield volcanoes in an area of plains volcanism, we measure similar volumes between volcanic shields and lava flows, and we successfully determine an approximate axis of post-flow tectonic deformation.

Garry W. B. Zimbelman J. R. Gregg T. K. P.
Emplacement of a Long Lava Flow near Ascraeus Mons Volcano, Mars **[#1508]**
Analysis of the morphology for a ~365 km long lava flow near Ascraeus Mons.

Bjonnes E. E. Zimbelman J. R.
Comparison of Lava Flows from Hawaii and Ascraeus Mons **[#1733]**
Topographic data from a 1907 lava flow on Mauna Loa and a pre-historic lava flow on Mauna Kea, along with MOLA data for a long lava flow on Mars, are used to calculate rheologic parameters for all three flows.

Somerville J. R.   Gregg T. K. P.
Amphitrites and Peneus Paterae, Mars: Characteristics and Possible Origins **[#2197]**
Morphologic characteristics of Amphitrites and Peneus Paterae, Mars, suggest that they are unlike any other central-vent martian volcano, and may represent a distinct style of volcanism on Mars.

Williams D. A.   Greeley R.   Werner S.   Neukum G.   Crown D. A.   Gregg T. K. P.   Gwinner K.
Raitala J.   HRSC Co-Investigator Team
Tyrrhena Patera: Volcanic History Derived from HRSC-based Crater Counts **[#1306]**
We will discuss the results of applying the Hartmann and Neukum crater counting methods to map-based units on Tyrrhena Patera using new HRSC images.

Warner N. H.   Farmer J. D.
Morphologic Observations of Chasma Boreale, Mars Using MOC, THEMIS, and MOLA: Origins Revisted **[#1363]**
The current models of formation for Chasma Boreale involve wind or catastrophic fluvial erosion. We provide new evidence from THEMIS and MOC data suggesting basal north polar ice melting, possibly induced by youthful volcanic activity.

Baloga S. M.   Glaze L. S.
Volatile Losses from Lava Flows Revisited: Implications for Large Sheet Flows on Mars **[#1961]**
Degassing may be an important process for explaining why long lava flows on Mars show modest increases in thickness with distance. A new formulation for the rate of degassing sets the stage for deriving exsolution velocities and extending the model to include bubble growth during emplacement.

MARS TECTONICS

McGowan E.   McGill G. E.
The Southwest Tilt of Isidis Planitia, Mars **[#1170]**
The southwest tilt of Isidis Planitia, Mars can be explained by a peripheral bulge created by a load located in Utopia basin. We use a lithospheric flexure model to calculate the amount and location of a load that would create the current topography.

Wolfe E. M.   Vidal A.   Mueller K. J.
Interpreting Mascon Wrinkle Ridges on Isidis Planitia, Mars Using Axial Surface Mapping Techniques: Reconstructing Structural Development and Stress Environments **[#1430]**
Isidis Planitia on Mars is a mascon containing radial and concentric wrinkle ridges, surrounded by concentric graben. Using axial surface mapping techniques, we analyze the wrinkle ridges to constrain their blind thrust geometry at depth in order to constrain the nature of basin rheology.

Smart K. J.   Ferrill D. A.   Colton S. L.
En Echelon Segmentation of Wrinkle Ridges in Solis Planum, Mars, and Implications for Counter-Clockwise Rotation of Shortening Direction **[#1966]**
We hypothesize a 20° rotation in shortening direction and fault reactivation as the cause of the consistent en echelon right-stepping arrangement of wrinkle ridge fold axes mapped from new high-resolution imagery of Solis Planum, Mars.

Colton S. L.   Smart K. J.   Ferrill D. A.
Wrinkle Ridge Detachment Depth and Undetected Shortening at Solis Planum, Mars **[#1729]**
Martian wrinkle ridges have estimated detachment depths of 0.25 to 60 km. Our alternative method for determining detachment depth reveals differences and has implications for the predominant scale of deformation at Solis Planum.

Öhman T.   Aittola M.   Kostama V.-P.   Raitala J.
Preliminary Geological Analysis of Polygonal Impact Crater Data from Argyre Region, Mars **[#1236]**
Argyre region's polygonal craters reveal that fresh craters have straight rim segments parallel to ridges, hinting to a common tectonic origin. Older craters might depict same stresses as graben. Geologic units and polygonality may have no relation.

Grott M.   Hauber E.   Werner S. C.   Kronberg P.
Thrust Faulting in the Thaumasia Region and Implications for the Structure of the Early Martian Lithosphere **[#1051]**
We use forward mechanical modelling of lobate scarps in the Thaumasia region to gain insight into the thermal state of the early Martian lithosphere.

Knapmeyer M.   Oberst J.   Hauber E.   Waehlisch M.   Deuchler C.   Wagner R.
Martian Seismicity: Implications of the Global Surface Fault Distribution and of Lithospheric Cooling **[#1059]**
We present a catalog of visible surface faults and use it to simulate marsquake catalogs with realistic moment-frequency and spatial distribution, as tool for seismological experiment development.

Allemand P.   Baratoux D.   Mondoux M.
Elliptical Craters in Thaumasia, Mars: Consequences on Fault Behavior **[#2031]**
We demonstrate that some elliptical craters in Thaumasia result from tectonic deformation. The amount of extension per fault is discussed given the strain measurement from these craters.

Dimitrova L. L.   Holt W. E.   Haines A. J.   Schultz R. A.
Towards Understanding the History and Mechanisms of Martian Faulting **[#1838]**
Stresses associated with gradients of GPE provide an excellent fit to most of the normal faults and many wrinkle ridges in Tharsis. The remaining misfit can be removed by adding membrane stresses associated with modest deflections of the lithosphere.

Kiefer W. S.
Gravity Observations of Structure in Valles Marineris, Mars **[#1458]**
Spatial domain gravity modeling of Valles Marineris provides new constraints on the structure of this system, including possible dike systems and sedimentary deposits.

Fueten F.   MacKinnon P.   Stesky R.   Hauber E.   Gwinner K.   Scholten F.   Zegers T.
Neukum G.   HRSC Co-Investigator Team
Structural Attitudes of Large Scale Layering Within Coprates Chasma in Valles Marineris, Mars, Using High Resolution Stereo Camera Data from Mars Express **[#1439]**
Measurements of attitudes of layering within the northern canyon wall of Coprates Chasma indicate gentle dips into the chasma. In the pit-chains south of Coprates, layer attitudes are more complex.

Zegers T. E.   Dabekaussen W.   Hauber E.   Gwinner K.   Scholten F.   Fueten F.   Stesky R.   MacKinnon P.   Neukum G.
HRSC Co-Investigator Team
3D Structural Analysis of Ophir Chasma Based on HRSC Image Data and Stereo-derived DTM **[#1605]**
Layer attitude measurements in Ophir Chasma ILD and wall rock show angular unconformities.

Kronberg P.   Hauber E.   Schäfer T.   Grott M.   Gwinner K.   Giese B.   Masson Ph.
Neukum G.   HRSC Co-Investigator Team
Rifting in Acheron Fossae, Mars, Observed by the High Resolution Stereo Camera (HRSC) **[#1661]**
We use HRSC-imagery as well as HRSC- and MOLA-derived topographical data for detailed photogeological mapping and structural evaluation of extensional structures in Acheron Fossea, following earlier studies of the Tempe and Claritas Fossae.

PHOENIX LANDING SITE

Guinn J.   Bonfiglio G.   Craig L.   Desai P.   Garcia M.   Grover R.   Parker T. J.   Prince J.   Seelos K.
Shotwell R.   Slimko E.
The Engineering Behind Mars Exploration Program 2007 Phoenix Mission Landing Site Selection **[#2051]**
This abstract details the engineering processes used in the overall landing site selection process. The performance of the landing RADAR, IMU, thrusters and robustness of the lander structure to slopes and rocks drive safety concerns.

Golombek M. Grant J. Lorenzoni L. Steltzner A. Vasavada A. R. Voorhees C. Watkins M.
Preliminary Constraints and Plans for Mars Science Laboratory Landing Site Selection **[#2172]**
Mars Science Laboratory science objectives, preliminary constraints (planetary protection and engineering) and the plans for selection of a landing site via a series of landing site workshops open to the science community are discussed.

Seelos K. D. Arvidson R. E. Golombek M. Parker T. Tamppari L. Smith P.
Geomorphology and Terrain Characterization of the 2007 Phoenix Mission Landing Sites in the Northern Plains of Mars **[#2166]**
Geomorphology is described for the regions under consideration for Phoenix landing site selection. Patterned ground is ubiquitous and suggestive of widespread and long-term influence of subsurface ice.

Putzig N. E. Mellon M. T. Golombek M. P. Arvidson R. E.
Thermophysical Properties of the Phoenix Mars Landing Site Study Regions **[#2426]**
Analysis of Phoenix Mars study regions places 4 of 5 in a previously-identified duricrust-dominated thermophysical unit which also contains the Viking and Spirit landing sites. Extrapolation of lander-observed properties to the study regions may be complicated by surface heterogeneity.

Marlow J. J. Klein C. R. Martinez M. M. McGrane B. S. Golombek M. P.
Boulder Hazard Assessment of Potential Phoenix Landing Sites **[#1094]**
In the search for a safe landing site for the Phoenix Mars Lander, the threat posed by boulders visible from orbit was evaluated. Intensive analysis indicated that such boulders represent a minimal hazard and will most likely not significantly constrain landing site selection.

Beyer R. A.
Meter-scale Slopes from Point Photoclinometry for the Potential Phoenix Landing Sites **[#1923]**
A point photoclinometry technique is used to evaluate the meter-scale slope statistics of MOC images within the three potential Phoenix landing site boxes.

Barge L. M. Parker T. J.
Landing Site Map Compilation and Hazard Assessment for Phoenix **[#2341]**
Compilation of image base maps and hazard maps of the Phoenix B landing site region for: science team's final landing site selection; nav team's assessment of need for course corrections; assess surface hazards to EDL; localization after landing.

Kirk R. L. Rosiek M. R. Galuszka D. Redding B. Hare T. Parker T. J.
Topography of Candidate Phoenix Landing Sites from MOC Images **[#2033]**
Stereo and photoclinometry applied to MOC narrow angle images show that candidate landing sites for Phoenix are relatively smooth. Slopes over baselines $\geq$3 m are 0.8°–4.5°, comparable to the MER landing sites. HiRISE will address smaller hazards.

Gunnarsdottir H. M. Linscott I. R. Callas J. L. Cousins M. D.
Surface Properties of the 2007 Phoenix Landing Site B Using Bistatic UHF Radar **[#2421]**
During December 2005, several 70-cm bistatic radar experiments were conducted using the SRI 150-ft (46-m) diameter dish and the Mars Odyssey spacecraft, with the objective of recovering surface dielectric properties and roughness of landing site B.

Simpson R. A. Tyler G. L. Pätzold M. Häusler B.
Mars Express Bistatic Radar Observations in Northern Mars Plains with Possible Application to Phoenix Landing Site Characterization **[#1862]**
MEX bistatic radar data have been collected in northern plains (including two experiments near VL-2) and may be useful in characterizing the general environment for Phoenix.

Poulet F. Mustard J. Arvidson R. Bibring J.-P. Langevin Y. Gondet B. Milliken R. Pelkey S.
Mineralogy of the PHOENIX Landing Sites from the OMEGA-MEX Imaging Spectrometer **[#1706]**
OMEGA-MEx has targeted the three PHOENIX landing sites during the early 2004 summer (Ls=90°–110°). The surface composition of the three landing sites will be presented.

Titus T. N.   Prettyman T. P.   Colaprete A.
Thermal Characterization of the Three Proposed Phoenix Landing Sites **[#2161]**
We use Mars Global Surveyor (MGS) Thermal Emission Spectrometer (TES) temperature observations immediately following the springtime disappearance of seasonal CO_2 to estimate the thermal inertia and soil depth at the three proposed Phoenix landing sites.

Sizemore H. G.   Mellon M. T.
Multi-Scale Variability in the Ice-Table Depth at Potential Phoenix Landing Sites **[#2141]**
We employ numerical simulations of subsurface thermal behavior on Mars to address questions of ice-table depth and variability on all scales relevant to Phoenix, with particular emphasis on scales relevant to excavation.

Boynton W. V.   Janes D. M.   Finch M. J.   Williams R. M. S.
Simultaneous Determination of Dry-Layer Thickness and Sub-Surface Ice Content in the Polar Regions of Mars: Implications for the Phoenix Landing Site Selection **[#2376]**
By combining data from Si and H gamma rays from the polar regions, we can determine both the ice content of a sub-surface ice-rich layer and the thickness of an ice-free overlying layer. The dry layer is very thin at the Phoenix landing sites.

Tamppari L. K.   Smith M. D.   Bass D. S.   Hale A. S.
Water-Ice, Water Vapor and Dust at the Phoenix Landing Latitudes and Seasons **[#2055]**
The Phoenix mission will carry two experiments that will observe water-ice, water-vapor, and dust in the martian atmosphere. As background and context, MGS TES observations of water-ice, water vapor and dust in the Phoenix landing zone and season have been examined and will be presented.

Tyler D.   Barnes J. R.
Mesoscale and LES Model Simulations of the Meteorological Environment Expected During the Phoenix Mission **[#2466]**
The OSU Mars MM5 developed and described by Tyler et al. (2002) was adapted to simulate the meteorological environment that will be experienced by Phoenix during EDL and when on the surface of Mars.

Drube L.   Madsen M. B.   Olsen M.   Jørgensen J.   Britt D.   Lemmon M.   Shinohara C.   Smith P.
Simulation of Dust Sedimentation on the Calibration Targets for the Surface Stereo Imager Onboard the Phoenix Mars Lander 2007 **[#1149]**
The Phoenix SSI calibration target contains six ring-magnets, each of which protects their inner area from dust (each inner area is a different color). This poster contains results from testing of the target in a dust sedimentation chamber.

MARS MISSIONS MRO

Slavney S.   Arvidson R. E.   Bennett K.   Guinness E. A.   Stein T. C.
Recent and Planned Planetary Data System Geosciences Node Activities **[#2232]**
The PDS Geosciences Node works with missions to help them generate quality archives and with users to help them obtain and use the archives. The node is planning new services that will benefit both the producers and the users of the data.

Schaller C. J.
Automated HiRISE Data Processing: Conductor in Action **[#2134]**
The MRO/HiRISE ground data system is using Conductor to manage the processing pipelines that will handle the ~280,000 image data files acquired by the HiRISE instrument during its primary operation. Conductor, a software tool for managing processing pipelines, has performed admirably thus far.

McGuire P. C.   Wolff M. J.   Arvidson R. E.   Smith M. D.   Clancy R. T.   Murchie S. L.   Mustard J. F.   Pelkey S. M.   Martin T. Z.
Retrieval of Surface Lambert Albedos from the Mars Reconnaissance Orbiter CRISM Data **[#1529]**
By November 2006, the CRISM hyperspectral imager on the Mars Reconnaissance Orbiter (MRO) will begin acquiring hyperspectral image cubes of the martian surface and atmosphere. We outline an approach for extracting surface Lambert albedos from multispectral and targeted mode observations.

Castalia B.
Conductor: Managing Processing Pipelines **[#2159]**
Conductor is a Java application for managing queues of source files to be processed by sequences of procedures.

MARS ANALOG STUDIES

Wan Bun Tseung J-M. Wainstein P. A. Moorman B. J. Stevens C. W. Hugenholtz C. H.
Integrating GPR and CCRI Techniques: Implications for Identifying and Mapping Near-Surface Ground Ice on Mars **[#1410]**
Preliminary results using GPR and CCRI techniques in a proglacial environment show that both techniques complement each other by resolving different characteristics of the ground, thus proving beneficial to the continuing exploration of Mars.

Chemtob S. M. Arvidson R. E. Fernández-Remolar D. C. Amils R. Morris R. V. Ming D. W. Prieto-Ballesteros O. Mustard J. F. Hutchison L. Stein T. C. Donovan C. E. Fairchild G. M. Friedlander L. R. Karas N. M. Klasen M. N. Mendenhall M. P. Robinson E. M. Steinhardt S. E. Weber L. R.
Identification of Hydrated Sulfates Collected in the Northern Rio Tinto Valley by Reflectance and Raman Spectroscopy **[#1941]**
This abstract reports results of VNIR and Raman spectroscopic analyses of sulfate efflorescents from the northern Rio Tinto Valley, a martian analog terrain. Phases identified include copiapite-group minerals, gypsum, jarosite and schwertmannite.

Carlisle O. Lucey P. G. Sherman S. B.
Thermal Infrared Weathering Trajectories in Hawaiian Basalts: Results from Airborne, Field and Laboratory Observations **[#2063]**
TIR spectra of weathered basaltic rocks are used to better understand the relationship between weathering and TIR data. Results suggest complex relation between heavy and light wetting events and spectral shape.

Velbel M. A.
Early Stages of Olivine Weathering in Hawai'i **[#1807]**
Olivine corrosion is similar in slightly weathered rocks from several Hawai'ian volcanic centers and regolith/outcrop settings. Etch pits are devoid of products; weathering takes place by dissolution-reprecipitation as well as by replacement.

Rossi A. P. Huvenne V. A. I. Henriet J. P. Wagner R. Hauber E. Chicarro A. Di Lorenzo S. Neukum G. HRSC Co-Investigator Team
A Buried Earth Analogue to Martian Chaotic Terrains **[#1573]**
We are comparing martian chaotic terrains with a recently discovered ancient submarine slope failure, which shows great resemblance to the polygonal pattern of chaos on Mars.

Komatsu G. Ori G. G. Arzhannikov S. G. Arzhannikova A. V.
The Azas Plateau in Southern Siberia: A Proposed Terrestrial Analogue Site for Ice-Magma-Flood Processes on Mars **[#1065]**
The Azas Plateau in southern Siberia is rich in examples of landforms that resulted from glaciation and ice-magma interactions. Understanding these processes will deepen our knowledge that would be applicable to studies of similar processes on Mars.

MARS MISCELLANEOUS

Bills B. G.
Non-Chaotic Obliquity Variations of Mars **[#2093]**
In the absence of energy dissipation, obliquity variations of Mars would likely be chaotic. However, relatively small amounts of dissipation suffice to suppress chaotic variations. Spin pole estimates from a fully damped model agree well with observation.

Rainey E. S. G. Aharonson O.
Estimate of Tidal Q of Mars Using MOC Observations of the Shadow of Phobos **[#2138]**
Phobos's secular acceleration can give us information about tidal dissipation in Mars. We used MOC images to indirectly observe Phobos using its shadow. We calculate the secular acceleration of Phobos, and use this to estimate the tidal Q of Mars.

Espley J. R. Connerney J. E. P. Acuña M. H. Delory G. T.
Low Frequency Ionospheric Plasma Waves at Mars and the Implications for Subsurface Sounding **[#2380]**
Observations of low frequency plasma waves in the Martian ionosphere using Mars Global Surveyor pre-mapping data are presented.

Yingst R. A. Haldemann A. F. C. Biedermann K. L. Monhead A. M.
Comparing Quantitative Morphology of Clasts at Three Landing Sites on Mars: Mars Pathfinder, Viking 1 and Viking 2 **[#1617]**
Rock morphologies can be assessed quantitatively to classify rock types. Here we compare quantitative values for sphericity, elongation and roundness for rocks in the Mars Pathfinder Rock Garden to those for the Viking 1 and 2 landing sites.

SATURNIAN SYSTEM

Moses J. I. Vervack R. J. Jr.
The Structure of the Upper Atmosphere of Saturn **[#1803]**
We compare synthetic light curves generated from a photochemical model with a reanalysis of the Voyager UVS occultation light curves to place constraints on Saturn's upper atmospheric structure and chemistry.

Greathouse T. K. Strong S. B. Richter M. J.
Saturn: The Observed Seasonal Variations of Stratospheric Temperature and Hydrocarbon Abundances Since 2002 **[#1737]**
We present results from a Saturn seasonal monitoring program. Observations from Sept. 2002, Oct. 2004, and Dec. 2005 will be shown. The meridional and temporal variations of stratospheric temperature and hydrocarbon abundances will be inferred from the data.

Strong S. B. Greathouse T. Moses J.
A Radiative Seasonal Climate Model for the Saturnian Atmosphere **[#1742]**
We have constructed a complete radiative seasonal climate model for Saturn's atmosphere that extends from the ultraviolet through the mid-infrared, and includes hydrocarbon abundance variations. The first seasonal results for at least one saturnian latitude will be presented at this time.

Weiss J. W. Porco C. C. Richardson D. C. Dones L.
Photometric Examination of Saturn's Rings as Seen in Cassini ISS Images **[#2371]**
We present our latest results comparing measurements of brightnesses of Saturn's rings from Cassini ISS images to numerical models based on ray-tracing output of N-body simulations.

Nelson R. M. Hapke B. W. Brown R. H. Spilker L. J. Smythe W. D. Kamp L. Boryta M. Leader F. Matson D. L. Edgington S. Nicholson P. D. Filacchione G. Clark R. N. Bibring J.-P. Baines K. H. Buratti B. Bellucci G. Capaccioni F. Cerroni P. Combes M. Coradini A. Cruikshank D. P. Drossart P. Formisano V. Jaumann R. Langevin Y. McCord T. B. Mennella V. Sicardy B. Sotin C.
Cassini Observations of the Opposition Effect of Saturn's Rings-1 **[#1461]**
Pronounced opposition surges are found for the first time in individual ringlets of the Saturnian ring system using Cassini Visual Infrared Mapping Spectrometer (VIMS). Analysis of these data permits the size of the ring scatterers to be determined.

Schenk P. M.
Impact Crater Morphology on Saturnian Satellites — First Results **[#2339]**
First results from mapping and measuring of impact crater shapes and morphology on Saturn satellites will be presented.

Castillo J. C. Matson D. L. Sotin C. Johnson T. V. Lunine J. I. Thomas P. C.
A New Understanding of the Internal Evolution of Saturnian Icy Satellites from Cassini Observations **[#2200]**
The Cassini spacecraft has provided us with a wealth of data likely to revolutionize our understanding of medium-sized icy satellites. We address some aspects of the geophysical concepts arising from the new observations.

Prieto-Ballesteros O. Kargel J. S.
Clathration as a Process for the Cryomagmatic Differentiation of Icy Satellites. Application to Enceladus and Europa **[#1971]**
We suggest that the formation of clathrates from an aqueous magmatic chamber enriched in gasses and dissolved ions will result in the cryomagmatic differentiation into the icy satellites. Then, magmas could ascend, decompress, and erupt explosively.

Jaumann R. Stephan K. Wagner R. Hansen G. B. Brown R. H. Baines K. H. Belucci G. Bibring J.-P. Buratti B. J. Capaccioni F. Cerroni P. Clark R. N. Combes M. Coradini A. Cruikshank D. P. Drossart P. Filacchione G. Formisano V. Hibbitts C. A. Langevin Y. Matson D. L. McCord T. B. Menella V. Nelson R. M. Nicholson P. D. Sicardy B. Sotin C.
Distribution of Icy Particles Across Enceladus' Surface **[#1766]**
Variations in particle size of water ice across the surface of Enceladus which strongly correlate to surface features of this satellite will be presented.

Bogdán Á. Illés-Almár E. Varga P.
On the Crust Thickness of Enceladus **[#1171]**
If the tidal stress could fracture the icy crust of Enceladus at the vicinity of the South Pole but not at that of the North Pole, then the thickness of the icy crust must be different. The derived thickness from our simple two-layer model is maximum 25 km at south and minimum 45 km at north.

Giese B. Wagner R. Neukum G. Helfenstein P. Porco C. C.
Topographic Features of Ithaca Chasma, Tethys **[#1749]**
Cassini-ISS stereo images have been used to derive the topography of Tethys' Ithaca Chasma. The topographic data reveal large rift flank uplift of Ithaca Chasma that allowed us to determine the effective elastic thickness of the lithosphere.

Palmer E. E. Brown R. H.
Carbon Dioxide Transport on Iapetus **[#2215]**
We created computer simulation to track the distribution of free CO_2 on Iapetus. Movement was calculated via suborbital ballistic flight and included mass loss due to gravitational escape. We calculated flux required to have CO_2 poles.

Mastrapa R. M. Bernstein M. P. Sandford S. A.
Near Infrared Spectra of H_2O/HCN Mixtures **[#1378]**
We present near IR spectra of H_2O/HCN ice mixtures and review the differences between mixtures and pure solids: the creation of new features, weakening and shifting of bands, dependence on concentration, and changes with temperature.

Tosi F. Coradini A. Capaccioni F. Cerroni P. Filacchione G. Bellucci G. Adriani A. Moriconi M. D'Aversa E. Brown R. H. Baines K. H. Bibring J.-P. Buratti B. J. Clark R. N. Combes M. Cruikshank D. P. Drossart P. Formisano V. Jaumann R. Langevin Y. Matson D. L. McCord T. B. Mennella V. Nelson R. M. Nicholson P. D. Sicardy B. Sotin C.
Iapetus, Phoebe and Hyperion: Are They Related? **[#1582]**
In this work, an automatic spectral correlation between Iapetus, Phoebe and Hyperion is attempted through the G-mode clustering method. A closer spectral correlation between Iapetus and Phoebe is suggested on the basis of 256 IR bands measured by VIMS.

Hendrix A. R. Hansen C. J.
Cassini UVIS: A Year of Icy Satellites **[#2349]**
Cassini Ultraviolet Imaging Spectrograph measurements of Saturn's icy moons are investigated to understand surface composition.

Lopes R. M. Stofan E. R. Paganelli F. Mitchell K. L. Kirk R. Lorenz R. Lunine J. Soderblom L. A. Wall S. D. Wood C. Radebaugh J. Robshaw L. E. Elachi C. Cassini Radar Team
Geologic Features on Titan's Surface as Revealed by the Cassini Titan Radar Mapper **[#1347]**
Results from four Titan fly-bys using SAR are summarized and show that Titan has a complex and relatively young surface, with features formed by cryovolcanism, fluvial and aeolian activity, cratering, and possibly tectonism.

Paillou Ph.   Crapeau M.   Elachi Ch.   Wall S.   Encrenaz P.
Modeling SAR Backscattering of Bright Flows and Dark Spots on Titan **[#1285]**
We present first analysis of radar-bright and radar-dark features on Titan obtained from the Cassini Radar Ta flyby, based on the use of two-layer SAR backscattering models.

Paganelli F.   Janssen M. A.   Lopes R. M.   Stofan E.   Stiles B.   West R.   Roth L.   Wall S. D.   Lorenz R. D.   Lunine J. I.   Kirk R. L.   Soderblom L.   Elachi C.   RADAR Team
A Look at Titan Surface from the Cassini RADAR SAR and Radiometry Data **[#1497]**
The Cassini RADAR SAR and radiometry data are reviewed with emphasis on the correlation and comparison of surface features and physical characteristics. Inverse correlation between SAR and radiometric data has been observed extensively in association with diverse geological features.

Towner M. C.   Garry J. R. C.   Svedhem H.   Hagermann A.   Clark B. C.   Lorenz R. D.   Leese M. R.   Hathi B.   Zarnecki J. C.
Constraints on the Huygens Landing Site Topography from the Surface Science Package Acoustic Properties Instrument **[#1567]**
We present analysis of the results from the Huygens acoustic sounder instrument. The sounder sees a relatively smooth terrain, with specular reflectance characteristics.

Neish C. D.   Lorenz R. D.   Kirk R. L.
Radar Topography of Dome Volcanoes on Venus and Titan **[#2151]**
We forward-modeled the radar appearance of different volcanic dome morphologies, and compared them to observed SAR images of domes on Venus and Titan.

Perry J. E.   McEwen A. S.   Turtle E. P.   Fussner S.   Cassini ISS Team
Equatorial Faculae on Titan: Distribution and Orientation **[#2170]**
Bright features within Titan's dark equatorial regions are examined using Cassini ISS images. The size and orientation distributions and faculae morphology are also compared between the various regions.

Mitchell K. L.   Lopes R. M. C.   Robshaw L. E.   Kargel J. S.   Lunine J.   Lorenz R.   Petford N.   Stofan E.   Wilson L.   Cassini Radar Science Team
Eruption of Ammonia-Water Cryomagmas on Titan 2: Eruption Styles and Landforms **[#2425]**
We are developing a semi-analytical model for the ascent of methane-expansion driven ammonia-water cryomagmas on Titan, and discuss how our initial findings relate to observed cryovolcanic landforms.

Mitri G.   Showman A. P.   Lunine J. I.   Lopes R.
Resurfacing of Titan by Ammonia-Water Cryomagma **[#1994]**
We propose mechanism for cryovolcanic processes on Titan involving bottom crevasse formation in an ice shell floating on an ammonia-water ocean, transport of ammonia-water pockets to the base of the stagnant lid by convective motions in the ice, and refreezing of chambers of ammonia-water.

Fortes A. D.   Grindrod P. M.
A Sulfate-rich Model of Titan's Interior 1: Implications for the Composition of Cryomagmas **[#1293]**
An alternative model of Titan's interior is presented in which primordial ammonia is consumed by sulfate-bearing solutions from the core. Implications of this structure for the composition of igneous materials are discussed.

Grindrod P. M.   Fortes A. D.
A Sulfate-rich Model of Titan's Interior 2: Implications for Possible Explosive Cryovolcanism **[#1294]**
We use a revised sulfate-rich model of Titan's interior to assess the role of magmatic volatiles in generating explosive cryovolcanism, and consider the consequences for the state of Titan's surface and atmosphere.

Choukroun M.   Tobie G.   Grasset O.
Ammonia, a Methane Hydrate Inhibitor — Implications for Titan's Atmospheric Methane **[#1640]**
As methane is dissociated in Titan's atmosphere, cryovolcanism is required to explain its current abundance. This work provide experimental constraints on methane hydrate stability in the system H_2O-CH_4-NH_3 for describing cryovolcanic processes.

Smythe W. D. Nelson R. M. Shirley J. H. Boryta M. C.
Ammonia Ice — Detectability Through Titan's Atmospheric Windows **[#2136]**
Spectra and optical constants of ammonia frost are used to assess the detectability of ammonia frost viewed through Titan's atmospheric windows in the spectral range 1–5 μm.

Quirico E. Bernard J.-M. Montagnac G. Rouzaud J.-N. Szopa C. Cernogora G. Reynard B. McMillan P. Fray N. Schmitt B. Coll P. Raulin F.
Chemical Structure and Optical Properties of Titan's Tholins and HCN Polymer. Implications for the Analysis of Cassini-Huygens Observations and Refractory Organics in Cometary Grains **[#2105]**
Tholins and HCN polymers were studied by UV Raman spectroscopy and High Resolution Transmission Electron Microscopy. Both have very close chemical structure. HCN polymer could be easily identified in cometary grains by UV Raman spectroscopy.

TERRESTRIAL FIELD ANALOGS

Burt D. M.
Using an Inexpensive Digital Camera to Take Mars-Analog Photographs at Near-Infrared Wavelengths **[#2326]**
With a filter costing less than $50, an ordinary digital camera can take near-infrared photos of Mars-analog subjects, at wavelengths appoximating those used by the commonly used Filter 2 on the MER PanCams (about 750 nm). An otherworldly appearance may result.

Ciarletti V. Le Gall A. Berthelier J. J. Corbel C. Dolon F. Ney R.
Bistatic Soundings with the HF GPR TAPIR in the Egyptian White Desert **[#2238]**
The TAPIR HF GPR has been initially developed to perform deep soundings on Mars in the frame of the NETLANDER mission. In November 2006, an updated version of the instrument working either in monostatic or in bistatic mode was tested in the Egytian White Desert. Preliminary results are presented.

Heggy E. Paillou P.
Sounding Cratonic Fill in Small Buried Craters Using Ground Penetrating Radar: Analog Study to the Martian Case **[#1264]**
We report results from a 270 MHz GPR survey performed on a recently discovered impact field in the southwestern Egyptian desert. The investigation suggests the ability of radar techniques to detect small-buried craters and probe their filling.

Hardgrove C. Moersch J. Drake D. Piatek J. Wettergreen D. Cabrol N.
Field Tests and Ground Truthing of a Surface-based Neutron Detector in the Atacama Desert, Chile **[#2320]**
Summary of prototype neutron detector field tests in the Atacama Desert, as part of the Life in the Atacama Project. Ground truth experiments are also discussed.

Misra A. K. Sharma S. K. Chio C. H. Lucey P. G.
Detection of Water and Water Bearing Minerals from 10 m Distance Under Bright Condition Using Remote Raman System **[#2155]**
The ability of a portable remote Raman system to detect water, ice and water bearing minerals from a distance of 10 m in a well illuminated background is promising for detecting water molecules in minerals lying in the dry environment.

TERRESTRIAL LABORATORY ANALOG STUDIES

McCormack K. Cloutis E. Bell J. F. III Stewart L. Kaletzke L. Craig M.
Determining Mineral Composition in the Ultraviolet Spectral Region from 200 to 400 Nanometres **[#2158]**
Ultraviolet (200–400 nm) reflectance spectra of major rock-forming minerals (e.g., olivine, pyroxene, plagioclase feldspar, ilmenite) exhibit measurable differences in their spectral properties. This suggests that these minerals can be discriminated in the UV.

Kuebler K. Wang A. Freeman J. J. Jolliff B. L.
Database of Raman Mineral Spectra for Planetary Surface Exploration **[#1907]**
A database of Raman mineral spectra is presented, which will be posted on line. It includes representatives of the most important mineral groups, especially those for the *in-situ* mineralogical investigation of planetary materials.

Clegg S. M. Wiens R. C. Sharma S. K. Lucey P. Misra A. Barefield J.
LIBS — Raman Spectroscopy of Minerals Using Remote Surface Modification Techniques **[#2069]**
LIBS and Raman Spectroscopy are highly complementary remote analytical tools developed to explore lunar and planetary geological samples. Here, LIBS was used to remove dust or other coatings that interfere with mineral analysis by Raman spectroscopy.

Sallé B. Mauchien P. Lacour J.-L. Maurice S. Manhès G.
Quantitative Rock Analysis by Laser-induced Breakdown Spectroscopy at the Surface of Mars **[#1560]**
We develop an analytical methodology enabling quantitative analysis of rocks in the context of Remote Laser-Induced Breakdown Spectroscopy, selected as part of the ChemCam instrument package for the MSL rover scheduled to be launched in 2009.

Anderson R. C. Buehler M. G. Keymeulen D. Chin K. B. Seshadri S.
Detecting Water/Ice in Lunar and Martian Regoliths Using Impedance Spectroscopy **[#2073]**
Detecting the presence of water/ice within planetary regoliths is crucial for future manned exploration as well as understanding the geologic history of the surface. This project is directed at fabricating a simple apparatus that can quickly measure water/ice on lunar and planetary surfaces.

Elphic R. C. Lawrence D. J. Feldman W. C.
Mars Airborne Neutron Spectrometry, Relict Ice and Recent Climate Change **[#2460]**
An airborne neutron spectrometer at Mars offers the possibility of achieving a much higher spatial resolution for detection of near surface water ice and hydrous minerals, while achieving greater range than with a rover.

Baratoux D. Pinet P. C. Kaydash V. G. Shkuratov Y. Daydou Y. Besse S. Jehl A. Chevrel S.
The Derivation of Hapke Parameters Using Multi-Angular Observations from Orbit and Laboratory: An Ill-posed Problem **[#1340]**
The derivation of Hapke parameters from multi-angular observations can be an ill-posed inverse problem. We present a direct approach to optimize future and present observations aimed at the derivation of scattering properties of planetary surfaces.

Lauer H. V. Jr. Ming D. W. Golden D. C. Boynton W. V.
Thermal and Evolved Gas Analysis of Geologic Samples Containing Organic Materials: Implications for the 2007 Mars Phoenix Scout Mission **[#1780]**
The Thermal and Evolved Gas Analyzer instrument scheduled to fly onboard the 2007 Mars Phoenix Scout Mission will perform DSC and EGA of soil samples. In this study, we examine two possible modes of detecting organics, namely, pyrolysis and combustion.

Rakocevic L. Dixon J. C. Cothren J. D. Dixon J. B.
Digitization and Web Access of a Historic Collection of Remotely-sensed Imagery **[#1017]**
The goal is to preset a method for digitizing and improving analog remotely-sensed imagery collected using five different platforms during the periods of 60s until 80s to the research community.

Kalchgruber R. McKeever S. W. S. Blair M. W. Deo S. Reust D. K. Gupta S. Strecker B. N.
Development of a Luminescence Dating Device for In Situ Dating of Geomorphological Features on Mars **[#1718]**
We address some of the challenges associated with developing an optically stimulated luminescence (OSL) device for *in situ* dating of sediments on Mars. Results of experiments, using martian simulant materials, as well as the design of an OSL instrument will be described.

Carmona J. A. Cook M. Schmoke J. Hyde T. W.
Low-Velocity Impacts on Targets Containing Embedded Carbon Nanotubes **[#1394]**
A one stage Light Gas Gun at CASPER was employed to test the shielding capabilities of tiles composed of four different laminated nanotube combinations.

ROVERS AND ROVER INSTRUMENTS

Curtis S. A. Clark P. E. Rilee M. L. Cheung C. Y. Wesenberg R. Dorband J. Lunsford A.
TET Rovers: An Approach for Exploring Rugged Terrains with Addressable Reconfigurable Technology **[#1129]**
We are in the process of developing extremely mobile TET Rovers with the reconfigurable architecture essential in the crossing or exploration of rugged terrains of great potential interest, including volcanic terrains which could harbor life on Mars.

Kanik I. Beegle L. W. Kounaves S. Cooks R. G. Hecht M. Johnson P. V.
Wet Chemistry Experiment at Mars (WETCHEM) **[#2154]**
We describe a novel field experiment utilizing wet chemistry combined with mass spectroscopy called "Wet Chemistry Experiment at Mars (WetChem)."

Lognonne Ph. Spohn T. Mimoun D. Ulamec S. Biele J.
GEP-ExoMars: A Geophysics and Environment Observatory on Mars **[#1982]**
The Geophysics Package (GEP) onboard the ESA's ExoMars 2011 mission intends to initiate the setup of a permanent network of geophysics stations on Mars, for several years of operation. We review scientific objectives and main characteristics of the GEP.

Herman J. Zacny K. Morris R. Davis K.
Development of Crushing and Sieving Technologies for Use in Sample Preparation in Mars Exploration **[#2332]**
This paper investigates potential crushing and sieving technologies for Mars exploration. The use of these technologies can increase the amount of data that can be extracted from surface and subsurface samples.

Glass B. Cannon H. Hanagud S. Lee P. Paulsen G.
Drilling Automation Tests at a Lunar/Mars Analog Site **[#2300]**
The Drilling Automation for Mars Exploration (DAME) project is developing drilling automation and robotics for use in 2011–16 lunar/martian missions. This has been tested recently, drilling in permafrost at a lunar/martian analog site (Haughton Crater, Devon Island, Canada).

Paulsen G. L. Mumm E. Kennedy T. Chu P. Davis K. Frader-Thompson S. Petrich K. Glass B.
Development of Autonomous Drills for Planetary Exploration **[#2358]**
Honeybee Robotics has developed science driven drill systems to allow scientific instruments direct access to the subsurface. Embedded drill segment electronics accommodate sensors and actuators for high rate data transmission to the surface.

Stoker C. R. Lemke L. G. Gonzales A. A.
Applications of Burrowing Moles for Planetary and Lunar Subsurface Access **[#1542]**
The Mars Underground Mole (MUM) can efficiently provide methods for planetary and lunar subsurface access in regolith using compact, light-weight, low-power devices while addressing objectives such as mineralogy assaying, water content determination, definition of engineering properties, and others.

Chen A. Meyer J. Carlos C. I. Linell B. Buhler C. R. Clements S. Mazumder M. K.
Numerical and Analytical Model of an Electrodynamic Dust Shield for Solar Panels on Mars **[#1873]**
Analytical and numerical calculations are presented for a multi-phase Voltage and Electric Field over the electrodynamic dust shield parallel electrodes under Mars environment.

Johnson P. V. Tang K. Beegle L. W. Smith R. D.
Laser Ablation-Electrodynamic Ion Funnel for In Situ Mass Spectrometry on Mars **[#1429]**
The laser ablation-ion funnel (LAIF) is being developed to ionize rock samples in the ambient Martian environment. The LAIF will then efficiently capture, transport and inject the product ions into a mass spectrometer for *in situ* analysis.

Brinckerhoff W. B. Corrigan C. M. Cornish T. J. Ganesan A. L. Ecelberger S. A.
Progress in Laser Desorption Mass Spectrometry for In Situ Analysis **[#2015]**
We present details of our ongoing development of laser desorption time-of-flight mass spectrometers for *in situ* analysis on planetary missions.

Castano R. Estlin T. Gaines D. Castano A. Bornstein B. Chouinard C. Anderson R. C. Judd M.
Automated Target Selection for Opportunistic Rover Science **[#2434]**
A number of rover remote sensing instruments require selection of specific focused targets for sampling. In this work we describe a system that can identify opportunistic targets and collect data on these targets.

Bergstralh J. T. Zawodny J. M. Tolson R. H.
Landing Massive Payloads, Accurately, on Mars: A 25-Year Roadmap **[#1040]**
Progress in exploring Mars's surface demands precise delivery of massive payloads to locations anywhere on the planet. This requires new entry/descent/landing (EDL) technologies. Characterization of Mars' atmospheric dynamics are needed to support development of these technologies.

FLIGHT INSTRUMENTS AND CONCEPTS

Zakharov A. V. Ozorovich Yu. R. Linkin V. M. Lukomsky A. K. Skalsky A. A. Klimov S. I. Vaisberg O. L. Manukin A. B. Khavroshkin O. B. Smirnov V. M. Armand N. A.
Project "Phobos-Soil": A Complex Sounding of the Phobos Moon **[#1276]**
The primary goal of the "Phobos Soil" mission is an investigation of the Phobos moon and particularly its internal structure.

Schibler P. Mimoun D. Lognonne P. Giardini D. Pike W. T. Mars SEIS Team
The Mars SEIS Experiment: First Tests **[#1549]**
The objective of the Mars SEIS experiment is the determination of the deep internal structure of Mars. The instrument integrates a Very Broad Band 2 axis seismometer, completed by a 3rd axis short period seismometer.

Campbell B. A. Eagle Science Team
Eagle: A Synthetic Aperture Radar Mapper for the Mars Scout Program **[#2188]**
Many aspects of the geologic and climate history of Mars are hidden beneath surficial sediments. A radar imaging system can penetrate these sediments to reveal buried fluvial, volcanic, impact, and perhaps glacial features. Eagle is an orbiting radar mapper for the Mars Scout program.

Levine J. S. ARES Science and Engineering Teams
The Aerial Regional-scale Environmental Survey (ARES): A New Tool for the Exploration of Mars **[#1311]**
The Mars Aerial Regional-scale Environmental Survey (ARES) is a robotic, powered airplane that will obtain measurements of the atmosphere, surface and sub-surface from an altitude of 1–2 km over hundreds to thousands of kilometers distance.

Coradini A. Adriani A. Filacchione G. Lunine J. I. Magni G. Cosi M. Tommasi L.
The JIRAM (Jovian InfraRed Auroral Mapper) Experiment **[#1564]**
JIRAM is an imager spectrometer proposed for the Juno mission to Jupiter. JIRAM would add the capability of imaging and making spectra of the Jovian aurora, the hot spots and exploring the troposphere between 1 and 10 bars.

Murchie S. Cooper K. Darlington E. H. Domingue D. Morgan F. Greeley R. Paranicas C. Prockter L. Roth D. Roush T. Strohbehn K. Thompson P. Wirzburger M.
ISIS: Imaging Spectrometer for Icy Satellites **[#1821]**
The Imaging Spectrometer for Icy Satellites (ISIS) is an instrument design adapted from the Compact Reconnaissance Imaging Spectrometer for Mars (CRISM) on the Mars Reconnaissance Orbiter (MRO).

Nehéz I. Bérczi Sz. Varga T. Darányi I. Cseh R.
Long Life and Light Gas Balloons with Active Isolation Envelope for Martian Applications **[#1719]**
Instead of one envelope layer, at least two separating envelope layers are applied in our balloons. The gases penetrating through the inner and outer material layers are removed and after selection they are sent back to their source space.

Nehéz I. Bérczi Sz. Varga T. Darányi I. Cseh R.
Theoretical Questions of the Application of the Light and Long Life Gas Balloons in Martian and Planetary Atmospheres **[#1703]**
Diffusion of gas from gas balloons can be returned by active separation of gases in the multiple layer spaces of balloon envelopes of several layers. Balloons created this way are of long life for research or storage gases in martian environment.

Andrews D. J. Barber S. J. Morse A. D. Sheridan S. Wright I. P. Morgan G. H.
Ptolemy: An Instrument Aboard the Rosetta Lander Philae, to Unlock the Secrets of the Solar System **[#1937]**
Ptolemy is a miniature chemical analysis suite currently on board the ESA Rosetta comet lander Philae. This poster describes the operation of the instrument, and presents data generated thus far during a comprehensive ground testing programme.

Urgiles E. Wilcox J. Z. Toda R. Crisp J. George T.
Elemental Composition Analyses in Thick Atmosphere Using the Atmopsheric Electron-induced X-Ray Spectrometer (AEXS) Instrument **[#2178]**
The results of the analyses of the XRF spectra excited by using the recently assembled stand-alone AEXS microprobe to determine surface elemental composition of NIST and USGS metal and mineral standards in ambient atmosphere pressure is described.

Wilcox J. Z. Urgiles E. Toda R. Crisp J.
Atmospheric Electron-Induced X-Ray Spectrometer (AEXS) Instrument Development **[#2126]**
The status of the AEXS instrument for elemental analysis of samples in planetary ambient atmosphere is described, with emphasis on describing the stand-alone 20keV electron microprobe vacuum-sealed with a SiN membrane that requires no active pumping.

Mungas G. S. Johnson K. R. Pelletier M. J. Sepulveda C. A. Feldman J. Lebow C. Boynton J. E. Deans M. Pain B. Beegle L.
Raman/CHAMP — Camera, Handlens, and Microscope with Integrated Raman Laser Probe **[#2451]**
Raman/CHAMP (Camera, Handlens and Microscope Probe) is a novel field imager/microscope with an internal scanning Raman laser probe. We summarize recent integration development efforts for this remote sensing instrument suite.

INSTRUMENT FACILITIES

Cloutis E. Craig M. Kaletzke L. McCormack K. Stewart L.
HOSERLab: A New Planetary Spectrophotometer Facility **[#2121]**
A newly constructed spectrophotometer facility at the University of Winnipeg enables us to conduct spectroscopic studies of planetary materials and terrestrial analogues and environments from the micro to the macro scale.

Huss G. R. Nagashima K. Keil K. Krot A. N. Taylor G. J. Scott E. R. D.
The University of Hawaii ims 1280 Ion Microprobe **[#1208]**
In March, 2006, the Hawaii Institute of Geophysics and Planetology will take delivery of a new Cameca ims 1280 ion microprobe. This presentation describes this state-of-the-art instrument and the research that we will do with it.

Kohout T. Elbra T. Pesonen L. J. Schnabl P. Slechta S.
Study of the Physical Properties of Meteorites Using Mobile Laboratory Facility **[#1607]**
We present the mobile laboratory facility used for studies of physical properties of meteorites directly in museums and collections. The physical properties of meteorites can be used in rapid classification of meteorites and in planetary studies.

MISSION AND SPACECRAFT CONCEPTS

Trigwell S. Schuerger A. C. Buhler C. R. Calle C. I.
Use of Atmospheric Glow Discharge Plasma to Modify Spaceport Materials **[#2257]**
Atmospheric pressure glow discharge plasma was used to modify spaceport materials to render them compliant with KSC ESD standards. The plasma treatment both inhibited and enhanced the recovery of adhered bacteria depending upon the material.

Prockter L. M. Rivkin A. S. McNutt R. L. Jr. Gold R. E. Ostdiek P. H. Leary J. C. Fiehler D. I.
Oleson S. R. Witzberger K. E.
Enabling Decadal Survey Science Goals for Primitive Bodies Using Radioisotope Electric Propulsion **[#1922]**
We show how Radioisotope-Electric Propulsion (REP) spacecraft could orbit one or more Trojan asteroids with reasonable trip times and payloads, enabling many of the Decadal Survey primitive bodies' science goals, within a New Frontiers-scale budget.

Manian D. P. Barney R. B. Legge R. S. Lind A. H. Sisco G. J.
FLASH — First Lunar Appulsion Spacecraft at Hypervelocity **[#2404]**
Mission statement: Impact a selected target area on the Moon with three consecutive impacts at a hypervelocity of 10 km/sec using a small, low cost spacecraft by leveraging available, low cost, excess launch capacity.

Abakians H. Bothwell M. Chmielewski A. B. Nelson R. M. Stevens C. M. Ku J. McEachen M. E. White S.
Samson J. R. Jr. Zsoldos J. McDermott T.
NASA's New Millennium ST8 Project **[#1475]**
NASA's ST8 project is a subsystem demonstration mission that will qualify, on a single spacecraft, four technologies deemed necessary to enable future NASA space science missions.

Stocky J. F. Stevens C. M. Nelson R. M.
NASA's New Millennium ST9 Mission **[#1469]**
NASA's ST-9 mission is an integrated system validation project and part of an effort to identify the technological capabilities needed for future space science missions and the technology advances that require validation in deep space to provide those capabilities.

EDUCATION AND PUBLIC OUTREACH: TRAINING TEACHERS, ENGAGING STUDENTS, INVOLVING THE PUBLIC

Holden P. N. Faszewski E. E.
The Clear Sky Experience: NASA Jumpstarts an Elementary Science Teaching Program **[#1641]**
Wheelock College has moved forward with a new program to produce scientifically skilled and knowledgeable pre-service elementary teachers. A science design team consisting of science and education faculty has planned and begun implementation of the program working through NASA's NOVA Program.

Fauerbach M. Couch T.
Introductory Space Science — An Inquiry-based Approach **[#1112]**
This poster is an overview of a novel course, which utilizes "space science" as the overarching theme to provide inquiry-based, hands-on activities, which combine mathematics and science content. Student responses to this class will be reported.

Aubele J. C. Stanley J. Grochowski A. Jones K. Aragon J.
K–12 Science Education Linked to Mars and the MER Mission: A New Curriculum Entitled Making Tracks on Mars Teacher Resource and Activity Guide **[#1730]**
Students' interest in Mars can be used as a "hook" to teach a wide range of topics. Mars-related science is used as the basis of a new K–12 integrated curriculum created by the New Mexico Museum of Natural History and classroom educators.

Lebofsky L. A. Lebofsky N. R. Sears D. Schmitt B.
STORI and ORION: Bringing Inquiry into the Classroom **[#1107]**
We have developed two hands-on observing programs for teachers in Arizona, Arkansas, and Ohio. STORI and ORION have created standards-driven and inquiry-based investigations for developing significant understanding of Space Science content.

Grier J. A. Ruberg L. Perrow K.
Balloon Science: Towards Building a Strong Community of Scientists, Administrators and Educators to Promote Partnerships for Suborbital Research and Learning **[#2142]**
The Balloon Science Program is an ideal venue for development of robust research programs as well as learning opportunities. We are facilitating partnerships, old and new, between parties interested in the Balloon Science and suborbital programs.

Kuhlman K. R.
Student Nanoexperiments for Outreach and Observational Planetary Inquiry (SNOOPY): An Update **[#2333]**
Proposed potential instrument payload for student participation in missions to the Moon and Mars.

Croft S. K. Pompea S. M.
Braving the Wilderness of Rocks: Educational Outreach Among the Asteroids **[#2208]**
A new middle school educational outreach program involving the classification and characterization of NEOs and asteroids is being developed at the NOAO in anticipation of the flood of new asteroid discoveries that is being produced by professional search programs.

Flanagan C. de Villiers G. Tlaka C.
Involving Learners in Planning TNO Observations with SALT **[#1812]**
We present a "real science project" at the Johannesburg Planetarium in which learners from less-well-resourced schools helped plan observations at SALT by "observing" home-made "minor planets" using cellphone cameras and photo-software.

Pennypacker C. R. Miller J. P. Canaday M.
Search for Asteroids and Kuiper Belt Objects: A National Research Program for High School and College Students **[#1010]**
Global Hands-On Universe (Lawrence Halls of Science, UC Berkeley) conducts national astronomy research programs for high school and college students. Using Collaboratory (Northwestern University), students work with professional researchers via the Internet.

Hardersen P. S. de Silva S. Reddy V. Cui P. Kumar S. Gaffey M. J.
An Internet Observatory for Solar System Astronomy at the University of North Dakota **[#1074]**
The University of North Dakota has recently begun operating a renovated remote Internet observatory for planetary science research and education. Besides education, the observatory is also being used for asteroid astrometry and photometry studies.

Prabhat Forsberg A. Morgan G. Petro N. Levy J. Head J. W.
Virtual Field Trip to Mars: Experiences with a Virtual Reality Lab for Undergraduate Students **[#1319]**
We present experiences with conducting a Virtual Reality Lab for undergraduate students. Students choose an area of their interest, pose some questions and try to answer them during the lab. Our positive experience indicates that VR might be a useful medium for conducting such educational exercises.

Elkshoulder A. Franklin J. Yawea O. Gchachu K. Simmons J. Cohen B. A. Newsom H. E.
Meteorite Identification and Classification Using Magnetic Susceptibility **[#1485]**
Magnetic susceptibility measurements of eight meteorites in the collection of the Institute of Meteoritics are consistent with literature data and confirm the usefulness of this technique for meteorite identification and classification.

Speyerer E. J. Ferrari K. A. Lowes L. L. Raad P. E. Cuevas T. Purdy J. A.
Virtual Space Camp Video Game **[#2228]**
With advances in computers, graphics, and especially video games, manned space exploration can become real, by creating a safe, fun learning environment that allows players to explore the solar system from the comfort of their personal computers.

Wood C. A.
MOONWORLD: A MMORPG Needs Your Input **[#2213]**
Schoolwork is boring. Videogames exciting. Vid-game learning now?

Hutson M. L. Pugh R. N. Ruzicka A. M.
Public Outreach and Education with Meteorites Involving a Museum Exhibit, Website, and Teacher Workshops **[#1095]**
In 2003, members of the Cascadia Meteorite Laboratory were awarded an E/PO grant to increase knowledge about meteorites among the public, K–12 teachers, and students. Here we pass on some of the lessons we learned.

King D. T. Jr. Petruny L. W. Johnson R. C. Gilomen A. T. Gibson J. C. de Villiers G.
Wetumpka's Annual "Crater Tours" — An Unusual Educational Outreach Activity in Planetary Science **[#1905]**
Scientific discoveries confirming that the Wetumpka structure is of impact origin have affected city and county planning for tourism. One unique aspect of this public outreach is the annual "crater tour" organized by the city and county and conducted by graduate students in planetary geology.

Klug S. L. Sharp T. Jackson C.
Teaching, Modeling and Mentoring Graduate and Undergraduate NASA Space Grant Students on How to be Effective in STEM Outreach Using Immersive Experience, Personal Storytelling, and Focused Educational Opportunities **[#2405]**
The ASU/NASA Space Grant Program has created a teaching, modeling, and mentoring program for its graduate and undergraduate students to help train them in best practice methodologies and approaches so they can become more proficient at STEM outreach.

Mörtl M. Homonnay Z. Lukács B. Weidinger T. Bérczi Sz.
Planetary Science and Chemistry: New Concise Atlas in the Solar System Series of Textbooks at Eötvös University, Hungary **[#1618]**
The *8th Concise Atlas of the Solar System* deals with planetary chemistry: (a) igneous rocks, (b) Mössbauer spectra, (c) weathering of the martian rocks, (d) photochemistry, (e) terrestrial circulation of elements, (f) water-ammonia mirror for amino acids.

Hargitai H. I. Bérczi Sz. Gucsik A. Horvai F. Illés E. Kereszturi A. Nagy Sz. J.
Impacts: Its Processes, Traces and Effects — A Textbook **[#1282]**
A textbook about impacts in Hungarian, is the first such publication dealing with impacts in detail, with emphasis on morphology.

Eichhorn G. Kurtz M. J. Accomazzi A. Grant C. S. Henneken E. Bohlen E. H. Thompson D. M. Murray S. S.
New Capabilities of the ADS Abstract Service **[#1691]**
The ADS Abstract Service provides a sophisticated search capability for the literature in astronomy and physics. The ADS is free to anybody world-wide. New features have added significant new functionality to the ADS.

Bigwood D. P.
Enhancing Access to Space Science Literature **[#1880]**
By participating in the Name Authority Program Component and Subject Authority Cooperative Program of the Program for Cooperative Cataloging of the Library of Congress even the smallest libraries can enhance access to the space science literature.

MARS: VOLATILES AND INTERIOR
Wednesday, 8:30 a.m., Crystal Ballroom A

Chairs: E. M. Parmentier and J. S. Kargel

8:30 a.m. Kargel J. S. * Rodruiguez J. A. P. Baker V. R.
Volatile-rich Upper Crust of Mars Constructed During the Impact Cataclysm **[#2052]**
A global Noachian crustal unit, several kilometers thick, consists of intercalated sedimentary rocks, impact breccia, volcanic rocks, and volatile condensation deposits produced during the impact cataclysm 3.8–3.9 billion years ago.

8:45 a.m. McGovern P. J. * Morgan J. K. Higbie M. A.
Structure and Evolution of the Olympus Mons Volcanic Edifice and Basal Escarpment, Mars **[#2329]**
Topographic profiles of Olympus Mons are compared to Distinct Element Method models of volcanic spreading, to evaluate the effects of spreading on the volcano's structure and to infer the spatially varying boundary conditions (i.e., high- or low-friction) at the base of the edifice.

9:00 a.m. Elkins-Tanton L. T. * Parmentier E. M.
Water and Carbon Dioxide in the Martian Magma Ocean: Early Atmospheric Growth, Subsequent Mantle Compositions, and Planetary Cooling Rates **[#2007]**
The volatile content of a magma ocean has significant effects on planetary evolution. Calculations are presented for water and carbon dioxide degassing to form a planetary atmosphere, cooling of the magma ocean, and subsequent mantle composition.

9:15 a.m. Johnson S. S. * Zuber M. T. Grove T. L. Mischna M. A.
Sulfur-related Greenhouse Warming on Early Mars **[#2094]**
We present a model for sulfur delivery to the early martian atmosphere and its potential warming effects. We obtain a high sulfur solubility in martian melts, ~1400 ppm, and find an up to 20K greenhouse effect due to sulfur-related absorption following large, discrete volcanic events.

9:30 a.m. Médard E. * Grove T. L.
Andesites in the Primitive Martian Crust: Products of Hydrous Melting? **[#1762]**
Experiments show that basaltic-andesitic and andesitic surface-types 1 and 2 could be explained by hydrous melting of the primitive martian mantle and/or by hydrous fractional crystallization, but not by anhydrous magmatic processes.

9:45 a.m. Agee C. B. *
Static Compression of Hydrous Fe-rich Ultrabasic Liquid and Density Crossovers in the Martian Mantle **[#2147]**
High pressure sink/float experiments have been performed on a komatiite/fayalite liquid mixture with 5 wt% added H_2O in order to investigate the effect of water on magma density at high pressure and to determine if density crossovers can exist in a FeO-rich martian mantle.

10:00 a.m. Parmentier E. M. * Elkins-Tanton L. Hess P. C.
Melt-Solid Segregation and Fractional Magma Ocean Solidification with Implications for the Evolution of Mars **[#1995]**
Fractional solidification of magma oceans which can occur with efficient separation of solid and its residual liquid may significant influence longterm planetary evolution. We examine the retained melt fraction and how this depends on the rate of magma ocean solidification.

MER: SPIRIT AND OPPORTUNITY I
Wednesday, 10:30 a.m., Crystal Ballroom A

Chairs: J. R. Johnson and T. D. Glotch

10:30 a.m. Bell J. F. III* Arneson H. M. Dean E. C. Farrand W. H. Herkenhoff K. Johnson M. J. Johnson J. R. Joseph J. Kinch K. M. Lemmon M. T. McCartney E. Proton J. Savransky D. Soderblom J. Sohl-Dickstein J. N. Sullivan R. J. Wolff M. J. Athena Science Team
A Martian Year of High Resolution Multispectral Imaging from the Pancam Instruments on the Mars Exploration Rovers Spirit and Opportunity **[#1747]**
This presentation summarizes the last Earth year of Mars Exploration Rover Pancam multispectral imaging observations and results from Gusev crater and Meridiani Planum.

10:45 a.m. Herkenhoff K. * Squyres S. Arvidson R. Bell J. III Cabrol N. Chapman M. Ehlmann B. Franklin B. Gaddis L. Geissler P. Greeley R. Grotzinger J. Johnson J. Jolliff B. Keszthelyi L. Knoll A. Lanagan P. Lee E. Maki J. McLennan S. Ming D. Mullins K. Rice J. Richter L. Sims M. Soderblom L. Spanovich N. Springer R. Sucharski R. Sullivan R. Weitz C. Athena Science Team
Overview of Athena Microscopic Imager Results **[#1816]**
Recent observations by the Microscopic Imagers on the Mars Exploration Rovers will be presented.

11:00 a.m. Lemmon M. T. * Athena Science Team
Mars Exploration Rover Atmospheric Imaging: Dust Storms, Dust Devils, Dust Everywhere **[#2181]**
The Spirit and Opportunity rovers have been used for a campaign to study dust in Mars' atmosphere via imaging. Results include the record of dust optical depth including dust storms, the time frame when dust devils were commonly observed, and constraints on the vertical extent of the dust.

11:15 a.m. Morris R. V. Klingelhoefer G. * Ming D. W. Schroeder C. Rodionov D. Yen A. Gellert R. Athena Science Team
Fe-bearing Phases Identified by the Mössbauer Spectrometers on the Mars Exploration Rovers: An Overview **[#2087]**
The Mössbauer spectrometers on the Mars Exploration Rovers have identified 15 Fe-bearing phases, including jarosite and goethite, which are marker minerals for aqueous processes because they contain structural hydroxide anions.

11:30 a.m. Greenwood J. P. * Blake R. E.
Phosphorus Geochemistry of Martian Rocks and Soils: Evidence for Acidic Weathering at Gusev and Meridiani **[#2196]**
Phosphorus correlations with sulfur in martian soils and sulfur-rich rocks are indicative of acidic weathering.

TITAN
Wednesday, 8:30 a.m., Crystal Ballroom B

Chairs: J. I. Lunine and D. L. Matson

8:30 a.m. Elachi C. Wall S. D. Allison M. D. Anderson Y. Boehmer R. Callahan P. Encrenaz P. Flamini E. Franceschetti G. Gim Y. Hamilton G. Hensley S. Janssen M. A. Johnson W. T. K. Kelleher K. Kirk R. L. Lopes R. M. Lorenz R. Lunine J. I. * Muhleman D. O. Orosei R. Ostro S. J. Paganelli F. Picardi G. Posa F. Roth L. E. Seu R. Shaffer S. Soderblom L. A. Stiles B. Stofan E. Vetrella S. West R. Wood C. A. Wye L. Zebker H. Rizk B. McFarlane L.
Cassini RADAR's Third and Fourth Looks at Titan **[#1252]**
The Cassini Titan RADAR Mapper has made two close passes of Titan's southern hemisphere in 2005, discovering extensive drainage channels, embayments, and broad areas of dark dunes. Together these emphasize the relative youthfulness of the surface.

8:45 a.m. Lorenz R. D. * Wall S. D. Reffet E. Boubin G. Radebaugh J. Elachi C. Allison M. D. Anderson Y. Boehmer R. Callahan P. Encrenaz P. Flamini E. Francescetti G. Gim Y. Hamilton G. Hensley S. Janssen M. A. Johnson W. T. K. Kelleher K. Kirk R. L. Lopes R. M. Lunine J. I. Mitchell K. Muhleman D. O. Ori G. Orosei R. Ostro S. J. Paganelli F. Picardi G. Posa F. Roth L. E. Seu R. Schaffer S. Soderblom L. A. Stiles B. Stofan E. R. Vetrella S. West R. Wood C. A. Wye L. Zebker H.
RADAR Imaging of Giant Longitudinal Dunes: Namib Desert (Earth) and the Belet Sand Sea (Titan) **[#1249]**
Titan's dark regions. Long dunes, like Zen rock garden. Seas of sand, not oil.

9:00 a.m. Wood C. A. * Lunine J. I. Lopes R. M. Stofan E. R. Mitchell K. Radebaugh J.
Crateriform Structures on Titan **[#1659]**
Impact craters, two. Ambiguous, many. Titan mystery.

9:15 a.m. Radebaugh J. * Lorenz R. Kirk R. Lunine J. Cassini Radar Team
Mountains on Titan Observed by Cassini Radar **[#1007]**
Cassini Radar has found isolated blocks and chains demonstrating high topography. These have slopes of 10–15 degrees and elevations of 300–500 m above surrounding blankets. These could have formed by tectonics, impact ejecta, or layer erosion.

9:30 a.m. Mitri G. * Lunine J. I. Showman A. P.
Hydrocarbons Lakes on Titan **[#1962]**
We address two questions: Are the observations of atmospheric methane relative humidity and thunderstorms/cloud frequency consistent with a desert planet containing tiny fractional lake coverage? Are hydrocarbon lakes stable on the surface of Titan?

9:45 a.m. Paganelli F. * van Zyl J. Janssen M. A. Stiles B. West R. Lopes R. M. Stofan E. Callahan P. Roth L. Wall S. D. Farr T. G. Elachi C. Lorenz R. D. Soderblom L. RADAR Team
Titan Electromagnetic Response and Surface Roughness Imaged by Cassini RADAR **[#1501]**
Cassini RADAR SAR data have been used to estimate the electromagnetic response and surface roughness as Root Mean Square (RMS). Estimates are derived using a modified empirical model developed from data of the LCX POLARSCAT, and RASAM systems of Earth observations.

10:00 a.m. Wye L. C. * Zebker H. A. Lorenz R. D. Cassini Radar Team
Modeling Titan's Surface from Cassini RADAR's Scatterometer and Radiometer Measurements **[#1473]**
We present separate model solutions obtained from the active and passive data in terms of electrical and physical properties. We are beginning to reconcile the implications of the two using a unified surface model.

10:15 a.m. Sotin C. * Rodriguez S. Le Mouélic S. Tobie G. Buratti B. J. Brown R. H. Jaumann R. Clark R. N. Baines K. H. McCord T. B. Nelson R. M. VIMS Science Team
Cassini/VIMS Observations of Titan: Geological Implications **[#1598]**
This paper describes the surface features of Titan revealed by the Visual and Infrared Mapping Spectrometer onboard the Cassini spacecraft. The observations are used to constrain models of Titan's geological history.

10:30 a.m. Barnes J. W. * Brown R. H. Turtle E. P. Perry J. Buratti B. J. Baines K. H. Sotin C. Clark R. N. Nicholson P. D.
Titan's Enigmatic 5-Micron-Bright Terrain **[#2319]**
We present data from the Visual and Infrared Mapping Spectrometer (VIMS) instrument on-board the Cassini Spacecraft identifying three regions on Titan that show anomalous 5-μm reflectivity.

10:45 a.m. McCord T. B. * Hansen G. B. Buratti B. J. Clark R. N. Cruikshank D. P. D'Aversa E. Griffith C. A. Baines K. H. Brown R. H. Dalle Ore C. M. Filacchione G. Formisano V. Hibbitts C. A. Jaumann R. Lunine J. I. Nelson R. M. Sotin C. Cassini VIMS Team
Titan: Surface Composition from Cassini VIMS **[#1398]**
The surface composition of Titan was explored using Cassini VIMS data. Surface compositional units appear. Dirty water ice is consistent with the visually dark units but no compositional match for the visually bright units was found.

11:00 a.m. Rodriguez S. * Le Mouélic S. Sotin C. Clénet H. Clark R. N. Buratti B. Brown R. H. McCord T. B. VIMS Team
Possible Detection of Local Enrichment in Water Ice in the VIMS Observations of the Huygens Landing Site **[#1326]**
We report here on the VIMS images of the Huygens landing site acquired during the first Titan flyby. We discovered in these images a peculiar area which could be interpreted as a local enrichment in water ice, consistent with DISR images and spectra results.

11:15 a.m. Tobie G. * Choblet G. Sotin C. Mitri G. Lunine J. I. Showman A. P.
Numerical Simulations of Plume Cryovolcanism: Implication for Methane Outgassing on Titan **[#1797]**
In the present study, we perform numerical simulations of thermal convection to quantify how thermal icy plumes can destabilize a subsurfacic clathrate reservoir and thus induce methane outgassing on Titan.

11:30 a.m. Mitchell K. L. * Kargel J. S. Lopes R. M. C. Lunine J. Mitri G. Lorenz R. Petford N. Wilson L.
Eruption of Ammonia-Water Cryomagmas on Titan 1: Crystallisation and Cooling During Ascent **[#2355]**
We are developing a semi-analytical model for the ascent of methane-expansion driven ammonia-water cryomagmas on Titan. The range of different crystal fractions resulting from decompression may help to explain the range of apparent rheological properties inferred for surface features.

ALL KINDS OF ACHONDRITES
Wednesday, 8:30 a.m., Marina Plaza Ballroom

Chairs: **G. K. Benedix and H. Downes**

8:30 a.m. Kuehner S. M. * Irving A. J. Bunch T. E. Wittke J. H. Hupé G. M. Hupé A. C.
Coronas and Symplectites in Plutonic Angrite NWA 2999 and Implications for Mercury as the Angrite Parent Body **[#1344]**
Disequilibrium metamorphic textures in this new plutonic angrite imply decompression and cooling in the angrite parent body, which might be Mercury.

8:45 a.m. Zartman R. E. * Jagoutz E. Bowring S. A.
Pb-Pb Dating of the D'Orbigny and Asuka 881371 Angrites and a Second Absolute Time Calibration of the Mn-Cr Chronometer **[#1580]**
Lead ages of D'Orbigny and Asuka 881371 pyroxenes are used for additional calibration of Mn-Cr chronometer.

9:00 a.m. Benedix G. K. * Lauretta D. S.
Thermodynamic Constraints on the Formation History of Acapulcoites **[#2129]**
We present thermodynamic properties (closure temperature and oxygen fugacity) of acapulcoites. The data indicate acapulcoites likely experienced some reduction during cooling.

9:15 a.m. Herrin J. S. * Mittlefehldt D. W. Humayun M.
Thermal Constraints from Siderophile Trace Elements in Acapulcoite-Lodranite Metals **[#2297]**
Acapulcoite-lodranites experienced temperatures of thermal metamorphism relevant to the onset of metal segregation. Siderophiles in metals record temperature and extent of metallic melt extraction and movement of metals en masse.

9:30 a.m. Rubin A. E. *
Shock Features in Acapulcoites and Lodranites: Implications for the Origin of Primitive Achondrites **[#1090]**
Many acapulcoites contain relict shock features; five contain relict chondrules. These rocks formed from CR-like chondrites by shock heating, reduction and annealing. Some rocks were later shocked again. Lodranites formed in a similar manner, but suffered more extensive heating than acapulcoites.

9:45 a.m. Mayne R. G. * Sunshine J. M. McCoy T. J. McSween H. Y. Jr.
Substantial Lithologic Diversity on 4 Vesta: Evidence from the Petrology and Spectra of Antarctic Eucrites **[#1796]**
In this abstract we describe preliminary results of a combined spectral and petrologic study of the unbrecciated eucrites, concentrating solely on those samples recovered from Antarctica.

10:00 a.m. Greenwood R. C. * Franchi I. A. Jambon A.
New Oxygen Isotope Evidence for the Origin of Mesosiderites and Main Group Pallasites **[#1768]**
High precision oxygen isotope analyses reveal that the silicate portion of mesosiderites are indistinguishable from the HEDs and suggest a common origin. However, the main group pallasites have a distinct signature, and therefore different source.

10:15 a.m. Yamaguchi A. * Okamoto C. Ebihara M.
The Origin of FeNi-Metals in Eucrites and Implication for Impact History of the HED Parent Body **[#1678]**
We performed a geochemical and petrologic study of brecciated eucrites and anomalous eucrites (Dhofar 007 and EET92023) to understand impact history of the parent body. It seems that these eucrites have genetic relationships with mesosiderites.

10:30 a.m. Gardner K. G. * Lauretta D. S. Hill D. H. Goreva J. S. Domanik K. J. Franchi I. A. Drake M. J.
Petrology and Geochemistry of the NWA 3368 Eucrite **[#2389]**
We report the petrology and geochemistry of NWA 3368, a new non-cumulate, monomict eucrite breccia with a variety of clast sizes and a pink-tinted matrix. Analytical techniques include electron microprobe, INAA, and ICP-MS.

10:45 a.m. Srinivasan G. * Whitehouse M. J. Weber I. Yamaguchi A.
Crystallization Ages of Zircons on Eucrite Parent Body from Hf-W Systematics **[#2042]**
Here we report the new ^{182}Hf-^{182}W evolution systematics composition of several zircons from A881388 and A881467 eucrite and use this to construct relative crystallization ages and model Pb ages for these zircons.

11:00 a.m. Shukolyukov A. * Lugmair G. W.
The Mn-Cr Isotope Systematics in the Ureilites Kenna and LEW 85440 **[#1478]**
The ureilite parent body is characterized by an anomalous ^{54}Cr/^{52}Cr ratio that is deficient in ^{54}Cr. Thus, its precursor material was different from the known carbonaceous chondrite classes. The Mn-Cr system in Kenna and LEW85440 closed late.

11:15 a.m. Downes H. * Mittlefehldt D. W.
Evidence for a Single Ureilite Parent Asteroid from a Petrologic Study of Polymict Ureilites **[#1150]**
Olivine core compositions in polymict ureilites cover the entire range found in monomict ureilites and show a similar compositional distribution. Such similarity is unlikely to have arisen if monomict ureilites represent separate parent asteroids.

11:30 a.m. Goodrich C. A. * Van Orman J. Wilson L.
Disequilibrium Fractional Melting on the Ureilite Parent Body **[#1191]**
REE patterns of ureilites are successfully modelled by disequilibrium fractional melting. Because melt extraction was extremely efficient, REE partitioning was diffusion-limited.

SPECIAL SESSION: BOSUMTWI METEORITE IMPACT CRATER DRILLING PROJECT
Wednesday, 8:30 a.m., Amphitheater

Chairs: C. Koeberl and B. Milkereit

8:30 a.m. Koeberl C. * Milkereit B. Overpeck J. T. Scholz C. A. Reimold W. U. Amoako P. Y. O. Boamah D. Claeys P. Danuor S. Deutsch A. Hecky R. E. King J. Newsom H. Peck J. Schmitt D. R.
An International and Multidisciplinary Drilling Project into a Young Complex Impact Structure: The 2004 ICDP Bosumtwi Impact Crater, Ghana, Drilling Project — An Overview **[#1859]**
First results from the study of two drillcores into the impactite rocks at the Bosumtwi crater, Ghana, obtained within an ICDP project, are summarized.

8:45 a.m. Milkereit B. * Ugalde H. Karp T. Scholz C. A. Schmitt D. Danuor S. Artemieva N. Kück J. Qian W. L'Heureux E.
Exploring the Lake Bosumtwi Crater — Geophysical Surveys, Predictions and Drilling Results **[#1687]**
Deep drilling of the Bosumtwi impact crater confirmed its gross structure as imaged by seismic surveys. The analysis of sonic and resistivity logs, in conjunction with petrophysical data, revealed that the impactites have extremely high porosities.

9:00 a.m. Reimold W. U. * Coney L. Koeberl C. Gibson R. L.
ICDP Borehole LB-07A (Bosumtwi Impact Structure, Ghana): An Overview and First Multidisciplinary Results **[#1350]**
As part of the 2004 ICDP drilling of the Bosumtwi impact structure, Ghana, a drillcore through a thick package of impact breccia was obtained within the crater moat. This contribution provides first multidisciplinary (stratigraphic, petrographic, and geochemical) results on these impact breccias.

9:15 a.m. Deutsch A. * Heinrich V. Luetke S.
The Lake Bosumtwi Impact Crater Drilling Project (BCDP): Lithological Profile of Wellhole BCDP-8A **[#1292]**
Core BCDP-8A into the central uplift of L. Bosumtwi crater consists of carbonaceous greywackes, finely laminated shales/slates (upper greenschist facies; 60% of the core), and allochthonous and autochthonous impact breccias; impact melt lithologies have not been found.

9:30 a.m. Coney L. * Reimold W. U. Koeberl C. Gibson R. L.
Mineralogical and Geochemical Investigations of Impact Breccias in the ICDP Borehole LB-07A, Bosumtwi Impact Crater, Ghana **[#1279]**
Mineralogical and geochemical studies of the impact breccias and target rocks intersected in borehole LB-07A, Bosumtwi impact structure, Ghana, have been undertaken to characterize the impact breccias and contribute to the understanding of their formation.

9:45 a.m. Ferrière L. * Koeberl C. Reimold W. U. Gibson R. L.
First Mineralogical Observations and Chemical Analyses of Core LB-08A from the Central Uplift of the Bosumtwi Impact Structure, Ghana: Comparison with Suevite from Outside the Crater **[#1845]**
We present lithostratigraphy, mineralogy, shock petrography, and geochemical analyses of core LB-O8A at the Bosumtwi crater, representing the first material from the central uplift. Suevites from this borehole and from outside the crater rim have different petrographic characteristics.

10:00 a.m. Morrow J. R. *
Petrographic Characteristics of Quartz in Suevitic Impact Breccia, Drillcore LB07A, Bosumtwi Crater, Ghana **[#1258]**
Quartz grain populations in suevitic breccia from the Bosumtwi impact crater drillcore LB07A were examined petrographically to evaluate the occurrence, abundance, and characteristics of unshocked and shock-metamorphosed quartz.

10:15 a.m. Luetke S. * Deutsch A. Langenhorst F. Kreher-Hartmann B.
Lake Bosumtwi Impact Structure, Ghana: First Geochemical and Sr Isotope Results for Target Lithologies **[#1811]**
Carbonaceous greywackes from core BCPD-8A show wide spread in Sr isotopic composition. Whole rock analyses for these, and target rocks from the N crater rim, extend the range of known target lithologies towards Ca- and Al-rich varieties.

10:30 a.m. Schleifer N. H. * Elster D. Schell C. M.
Petrophysical Characterization of the Core Samples of the Bosumtwi Meteorite Impact Crater (Ghana) **[#1273]**
Comparing available log and field data with laboratory measurements on core samples from boreholes B07 and B08, centered in the Bosumtwi Meteorite Impact Crater, the question was, if and how differences in petrophysics relate to specific characteristics of the impact event.

10:45 a.m. Kontny A. * Just J.
Magnetic Mineralogy and Rock Magnetic Properties of Impact Breccias and Crystalline Basement Rocks from the BCDP-Drillings 7A and 8A **[#1343]**
The Bosumtwi crater drilling project provides impact and crystalline basement lithologies. Our study contributes rock magnetic and magnetic mineralogy data of the drilled rocks, which will help to understand the aeromagnetic anomaly pattern.

11:00 a.m. Ugalde H. * Danuor S. K. Milkereit B.
A 3D Gravity Model of the Bosumtwi Impact Structure **[#1063]**
New gravity data was acquired at Lake Bosumtwi between 1999–2001. It allowed the creation of an updated Bouguer gravity anomaly map. A 3D model was constructed from the integration of gravity, petrophysics and seismic data.

11:15 a.m. Goderis S. * Tagle R. Claeys Ph. Schmitt R. T. Erzinger J.
Platinum Group Elements in the ICDP Cores from the Bosumtwi Crater, Ghana **[#1305]**
This abstract presents the results of the platinum group element analyses carried out on the impactites recovered from the two cores recently drilled by ICDP in Lake Bosumtwi. No meteoritic component was detected.

11:30 a.m. Koeberl C. * Brandstätter F. Hecht L. Reimold W. U. Peck J. King J.
Uppermost Impact Fallout Layer in a Drillcore at the Bosumtwi Impact Crater (Ghana): A Preliminary Study **[#1552]**
A fine-grained impact fallout layer was preserved in a drill core from the Bosumtwi crater, with accretionary lapilli, microtektite-like glass spherules, and shocked quartz grains.

MER: SPIRIT AND OPPORTUNITY II
Wednesday, 1:30 p.m., Crystal Ballroom A

Chairs: **B. C. Clark and S. W. Ruff**

1:30 p.m. Squyres S. W. * Arvidson R. E. Athena Science Team
Recent Results from the Spirit Rover at Gusev Crater **[#1472]**
The Mars Exploration Rover Spirit has now completed two years of operations on Mars, traversing more than 5.5 km in Gusev crater. The talk will provide an overview of the most recent science findings from the rover.

1:45 p.m. Golombek M. P. * Crumpler L. S. Grant J. A. Greeley R. Cabrol N. A. Parker T. J. Rice J. W. Jr. Ward J. G. Arvidson R. E. Moersch J. E. Fergason R. L. Christensen P. R. Castaño A. Castaño R. Haldemann A. F. C. Li R. Bell J. F. III Squyres S. W.
Geology of the Gusev Cratered Plains from the Spirit Rover Traverse **[#1424]**
Spirit's investigation of the Gusev cratered plains reveals an impact regolith that likely formed in basalt lava flows. A dry and desiccating environment since the Hesperian is indicated by eolian trapping of fines within craters on the surface.

2:00 p.m. Gellert R. * Brückner J. Clark B. C. Dreibus G. d'Uston C. Economou T. Klingelhöfer G. Lugmair G. Ming D. W. Morris R. V. Rieder R. Squyres S. W. Wänke H. Yen A. Zipfel J.
Chemical Diversity Along the Traverse of the Rover Spirit at Gusev Crater **[#2176]**
The paper gives an updated overview of the chemical analyses with the APXS at Gusev Crater. The Rover Spirit has characterized new rock classes and soil types along its nearly 6 km traverse.

2:15 p.m. Ruff S. W. * Athena Science Team
The Absence and Presence of Olivine in the Columbia Hills of Gusev Crater, Mars: The Latest Results from Mini-TES **[#1989]**
The variation in mineralogy that most distinguishes the different rock units in the Columbia Hills is that of olivine. If olivine is a telltale mineral for the interaction of water, the role of water in the Columbia Hills has been highly variable.

2:30 p.m. Clark B. C. * Gellert R. Ming D. W. Morris R. V. Mittlefeldt D. W. Squyres S. W. Yen A. Athena Science Team
PYTi-NiCr Signatures in Columbia Hills are Present in Certain Martian Meteorites **[#1509]**
The elements P, Ti and Y are enriched in certain samples in Columbia Hills, Gusev crater, Mars. Similarly, the elements Ni and Cr are lower than typical. This overall signature also occurs in the igneous martian meteorites QUE 94201, EETA79001-B, and Los Angeles.

2:45 p.m. King P. L. * McSween H. Y. Jr.
New Approaches to Interpreting the Geochemistry of the Columbia Hills Rocks, Gusev Crater, Mars **[#2108]**
We use the bulk chemical (APXS) data from the Columbia Hills to evaluate the following models: acid fog addition; mineral mixing; acidic or neutral-basic aqueous weathering; and, precipitation from a brine.

3:00 p.m. Kuzmin R. O. Christensen P. R. * Ruff S. W. Graff T. G. Knudson A. T. Zolotov M. Yu. Athena Science Team
Spatial and Temporal Variations of Bound Water Content in the Martian Soil Within the Gusev Crater: Preliminary Results of the TES and Mini-TES Data Analysis **[#1673]**
We presents the preliminary study results of spatial and temporal variations of bound water content in the martian soil within Gusev crater based on the TES and the Mini-TES data analysis.

3:15 p.m. Grotzinger J. P. * Arvidson R. E. Bell J. F. III Clark B. C. Farrand W. H. Herkenhoff K. Johnson J. R. Knoll A. H. McCartney E. McLennan S. M. Metz J. Parker T. Soderblom J. Squyres S. W. Sullivan R. Tosca N. Athena Science Team
Sedimentary Facies, Subaqueous Sediment Transport, and Depositional Environment of the Burns Formation, Meridiani Planum **[#2254]**
The bedrock stratigraphy at the Opportunity Landing Site defines a "wetting-upward" succession which records a progressive increase in the influence of groundwater and, ultimately, surface water in controlling primary depositional processes.

3:30 p.m. Brückner J. * Gellert R. Clark B. C. Dreibus G. d'Uston C. Economou T. Klingelhöfer G. Lugmair G. Ming D. W. Rieder R. Squyres S. W. Wänke H. Yen A. Zipfel J. Athena Science Team
Two Years of Chemical Sampling on Meridiani Planum by the Alpha Particle X-Ray Spectrometer Onboard the Mars Exploration Rover Opportunity **[#1882]**
The MER rover Opportunity has been exploring Meridiani Planum using besides other instruments the Alpha Particle X-Ray Spectrometer. We report on chemical composition of soils, spherules, and outcrops determined along the traverse by the APXS.

3:45 p.m. McLennan S. M. * Arvidson R. E. Clark B. C. Golombek M. P. Grotzinger J. P. Jolliff B. L. Knoll A. H. Squyres S. W. Tosca N. J. Athena Science Team
Constraints on the Extent and Timing of Groundwater Diagenesis in the Burns Formation, Meridiani Planum **[#1926]**
Evaporitic sandstones of the Burns formation have experienced an extended history of groundwater fluctuation and diagenesis. As Opportunity moves south to Erebus crater and beyond, the diagenetic character of the rocks appears to be changing.

4:00 p.m. Dyar M. D. * Schaefer M. W. Agresti D.
Mössbauer Spectroscopy of Outcrop at the Meridiani Planum Site **[#2382]**
Mössbauer data from outcrops at the Meridiani Planum site are studied, and possible interpretations of the parameters of two sextets and three doublets are presented.

4:15 p.m. Thompson S. D. * Calvin W. M. Farrand W. H. Johnson J. R. Bell J. F. III Athena Science Team
Fine Scale Multispectral Features of Sedimentary Bedrock Structures of Meridiani Planum, Mars **[#1938]**
Pancam data from Opportunity have been analyzed for multispectral differences and relationships among the fine scale sedimentary features of the Meridiani Planum outcrop.

4:30 p.m. Yen A. S. * Grotzinger J. Gellert R. Clark B. C. McLennan S. M. Morris R. V. Schröder C. Klingelhöfer G. Herkenhoff K. E. Johnson J. R. Athena Science Team
Evidence for Halite at Meridiani Planum **[#2128]**
The presence of halite, an aqueous precipitate, is indicated by MER analyses of rinds and certain rock coatings at Meridiani Planum.

SATURN'S COMPANIONS: SATELLITES AND RINGS
Wednesday, 1:30 p.m., Crystal Ballroom B

Chairs: T. V. Johnson and C. Sotin

1:30 p.m. Dougherty M. K. * Khurana K. K. Neubauer F. M. Russell C. T. Saur J. Leisner J. S. Burton M. E.
Discovery of a Dynamic Atmosphere at Enceladus from Cassini Magnetometer Observations **[#1585]**
This paper describes Cassini magnetometer observations which identified a dynamic atmosphere at Enceladus.

1:45 p.m. Helfenstein P. * Thomas P. C. Veverka J. Rathbun J. Perry J. Turtle E. Denk T. Neukum G. Roatsch T. Wagner R. Giese B. Squyres S. Burns J. McEwen A. Porco C. Johnson T. V. Cassini Imaging Team
Patterns of Fracture and Tectonic Convergence near the South Pole of Enceladus **[#2182]**
We use recent Cassini ISS coverage of Enceladus to investigate the extent to which the morphology, placement, and orientations of recent tectonic patterns are consistent with a global change in Enceladus' rotational figure.

2:00 p.m. Spencer J. R. * Pearl J. C. Segura M. Flasar F. M. Mamoutkine A. Romani P.
The South Polar Hot Spot on Enceladus **[#2252]**
In July 2005, Cassini's Composite Infrared Spectrometer (CIRS) detected 3–7 GW of thermal emission emanating from troughs in the south polar region of Enceladus, at temperatures up to 145 K or higher. These warm troughs are presumably the source of the plume seen by multiple Cassini instruments.

2:15 p.m. Matson D. L. * Castillo J. C. Sotin C. Johnson T. V. Lunine J. I. Davies A. G. McCord T. B. Thomas P. C. Turtle E. P.
Enceladus' Interior and Geysers — Possibility for Hydrothermal Geochemistry and N_2 Production **[#2219]**
Enceladus' thermal evolution modeling and associated hydrothermal activity and geochemistry.

2:30 p.m. Pappalardo R. T. * Nimmo F.
Diapir-Induced Reorientation of Enceladus **[#2113]**
The pole-centered location of the warm, active area of Enceladus can be explained by reorientation induced by a large, low-density diapir within a relatively thick ice mantle.

2:45 p.m. Wagner R. * Neukum G. Giese B. Roatsch T. Wolf U. Denk T. Cassini ISS Team
Geology, Ages and Topography of Saturn's Satellite Dione Observed by the Cassini ISS Camera **[#1805]**
Geologic units and topographic features of the surface of Saturn's satellite Dione are examined. Ages of geologic units are obtained from crater size-frequency measurements.

3:00 p.m. Castillo J. C. * Matson D. L. Johnson T. V.
Can There be Dissipation Without Heat? Constraints on Tidal Dissipation in the Medium-sized Saturnian Satellites **[#2351]**
Constraints on tidal dissipation in the saturnian medium-sized satellites.

3:15 p.m. Thomas P. C. * Veverka J. Helfenstein P. Porco C. Burns J. Denk T. Turtle E. Jacobson R. A.
Shapes of the Saturnian Icy Satellites **[#1639]**
Shapes of six icy saturnian satellites have been measured from Cassini ISS images. Possible interior models are evaluated on the basis of observed shapes and mean densities.

3:30 p.m. Porco C. C. * Weiss J. W. Thomas P. C. Richardson D. C. Jacobson R. A. Spitale J.
Physical Characteristics and Possible Accretionary Origins for Saturn's Small Satellites **[#2289]**
From high quality Cassini images yielding the physical characteristics of Saturn's small satellites, as well as numerical simulations of accretion around a monolithic small "core" in a planetary ring, we have found that the small saturnian satellites have likely formed by accretion.

3:45 p.m. Colwell J. E. * Esposito L. W. Stewart G. R.
Density Waves Observed by Cassini Stellar Occultations as Probes of Saturn's Rings **[#1221]**
Observations of stellar occultations by Saturn's rings from the Cassini spacecraft provide a high resolution view of density waves. We report on analysis of these waves to determine the ring surface mass density and vertical thickness.

4:00 p.m. Spitale J. N. * Porco C. C.
Kinematic Models of Non-Circular Features in Saturn's Rings **[#2242]**
Using high-resolution movie frames and azimuthal imaging scans with radial scales as fine as a few km and longitudinal resolutions as fine as a fraction of a degree, we examine the shapes and kinematics of the B-ring outer edge and the Huygens ringlet.

4:15 p.m. Spilker L. J. * Pilorz S. H. Ferrari C. Leyrat C. Wallis B. D. Brooks S. M. Edgington S. G. Altobelli N. Flasar F. M. Pearl J. C. Showalter M. R. Achterberg R. K. Nixon C. A. Romani P. N. Cassini CIRS Investigation Team
Cassini CIRS Observations of Thermal Differences in Saturn's Main Rings with Increasing Phase Angle **[#2299]**
Cassini CIRS obtained spatially resolved thermal scans of Saturn's main rings that show temperatures decreasing with increasing solar phase angle. These temperature differences indicate that Saturn's rings contain slowly rotating ring particles.

4:30 p.m. Hapke B. W. * Nelson R. M. Brown R. H. Spilker L. J. Smythe W. D. Kamp L. Boryta M. Leader F. Matson D. L. Edgington S. Nicholson P. D. Filacchione G. Clark R. N. Bibring J.-P. Baines K. H. Buratti B. Bellucci G. Capaccioni F. Cerroni P. Combes M. Coradini A. Cruikshank D. P. Drossart P. Formisano V. Jaumann R. Langevin Y. McCord T. B. Mennella V. Sicardy B. Sotin C.
Cassini Observations of the Opposition Effect of Saturn's Rings 2. Interpretation: Plaster of Paris as an Analog of Ring Particles **[#1466]**
Cassini VIMS data of the opposition effect of Saturn's rings finds that ring particles are porous aggregates of interlocking grains ~10 μm in size of water frost plus impurities.

SPECIAL SESSION: RESULTS FROM THE DEEP IMPACT MISSION
Wednesday, 1:30 p.m., Marina Plaza Ballroom

Chairs: P. H. Schultz and H. J. Melosh

1:30 p.m. A'Hearn M. F. * Deep Impact Team
Deep Impact: Excavating Comet Tempel 1 **[#1978]**
This talk will provide an overview of the results from Deep Impact, including brief summaries of results presented in subsequent talks and more detailed discussions of results not being presented individually.

2:00 p.m. Schultz P. H. * Ernst C. A'Hearn M. F. Eberhardy C. Sunshine J. M. Deep Impact Team
The Deep Impact Collision: A Large-Scale Oblique Impact Experiment **[#2294]**
The Deep Impact collision produced a distinctive pattern of evolving ejecta to very late time, indicative of a layered, high porosity surface.

2:15 p.m. Belton M. J. S. * Deep Impact Science Team
A Deep Impact Mission Contribution to the Internal Structure of Jupiter Family Cometary Nuclei: The TALPS or "Layered Pile" Model **[#1232]**
We propose that the widespread layering now seen on 9P, 19P and 81P is an essential element of the internal structure of JFC nuclei. This leads to a new model for cometary interiors called the TALPS or "layered pile" model. We argue that these layers are primordial.

2:30 p.m. Melosh H. J. * Deep Impact Team
Deep Impact: The First Second **[#1165]**
During the first second after Deep Impact struck Tempel 1, the flyby spacecraft observed a bright arc-shaped plume that expanded rapidly away from the impact site. This plume was probably composed of about 4000 kg of incandescent silicate melt droplets.

2:45 p.m. Richardson J. E. * Melosh H. J.
Modeling the Ballistic Behavior of Solid Ejecta from the Deep Impact Cratering Event **[#1836]**
We describe results from a forward model of the first-order, solid ejecta particle behavior from the impact produced by the Deep Impact mission. The expansion rate of the plume places constraints on the gravity field, mass, and density of Tempel 1.

3:00 p.m. Veverka J. * Thomas P. Hidy A.
Tempel 1: Surface Processes and the Origin of Smooth Terrains **[#1364]**
Deep Impact images reveal the nucleus of comet Tempel 1 to be a geologically complex body with prominent layering and extensive smooth terrains suggestive of flow deposits.

3:15 p.m. Groussin O. * A'Hearn M. F. Li J.-Y. Thomas P. C. Sunshine J. M. Lisse C. M. Delamere A. Deep Impact Science Team
Temperature of the Nucleus of Comet Tempel 1 **[#1297]**
Deep Impact successfully encountered comet 9P on July 4th. From the IR spectra of the nucleus, we derived its temperature map. Here, we present the resulting temperature map and its implications for the surface thermal properties of the nucleus.

3:30 p.m. Ernst C. M. * Schultz P. H. A'Hearn M. F. Deep Impact Science Team
Photometric Evolution of the Deep Impact Flash **[#2192]**
On July 4, 2005, the Deep Impact mission performed a planetary-scale impact experiment into comet 9P/Tempel 1. We report on the characteristics and photometric evolution of the impact flash in the context of laboratory-scale impact experiments.

3:45 p.m. Sugita S. * Kadono T. Ootusbo T. Honda M. Sako S. Miyata T. Sakon I. Yamashita T. Kawakita H. Fujiwara H. Fujiyoshi T. Takato N. Fuse T. SUBARU/COMICS Deep Impact Observation Team
A High-Resolution Mid-IR Observation of the Collision Between Deep Impact Projectile and Comet 9P/Tempel 1 **[#2431]**
We present results of our detailed analysis of the mid-infrared observation of the collision between Deep Impact projectile and comet 9/P Tempel 1, which provides crucial information on both the style of the cratering and the origin of the comet.

4:00 p.m. Lisse C. M. * Deep Impact Spitzer Science Team
Spitzer Space Telescope Observations of the Nucleus and Dust of Deep Impact Target Comet 9P/Tempel 1 **[#1960]**
Comet 9P/Tempel 1 was observed before, during, and after the Deep Impact encounter using the Spitzer Space Telescope IR Spectrometer. We report here on the results of the SST observations, the new materials found in the ejecta, and the resulting implications for the proto-solar nebula.

4:15 p.m. Sunshine J. M. * A'Hearn M. F. Groussin O. Feaga L. M. Li J.-Y. Schultz P. H. Deep Impact Science Team
Water Ice on Tempel 1: Before, During, and After the Impact Event **[#1890]**
We present the identification, spatial distribution, and particle size of water ice on the surface of comet 9/P Tempel 1 and trace its path during impact and in relation to the comet's structure.

4:30 p.m. Feaga L. M. * A'Hearn M. F. Sunshine J. M. Groussin O. Deep Impact Science Team
Asymmetry of Gaseous CO_2 and H_2O in the Inner Coma of Comet Tempel 1 **[#2149]**
Gaseous emission bands of CO_2 and H_2O are detected in the spectra of the inner coma of comet 9P/Tempel 1. Asymmetries are found in the distribution of the gas with CO_2 more prevalent in the southern coma and H_2O more prevalent in the sunward direction.

4:45 p.m. Holsapple K. A. * Housen K. R.
Gravity or Strength? An Interpretation of the Deep Impact Experiment **[#1068]**
A study of the deep impact event using current results and scaling laws for cratering ejecta. Within the uncertainties, whether the cratering was dominated by strength or gravity cannot be distinguished. As a consequence, the mechanical nature of the surface of Tempel 1 remains uncertain.

IRON METEORITES AND PALLASITES
Wednesday, 1:30 p.m., Amphitheater

Chairs: R. J. Walker and D. S. Lauretta

1:30 p.m. Wasson J. T. * Huber H.
Compositional Trends Among IID Irons; Their Possible Formation from the P-rich Lower Magma in a Two-Layer Core **[#2119]**
Magmatic iron-meteorite group IID has a low S content but high contents of other volatiles. We suggest that the S was extracted in an early metallic magma. A second metallic magma formed at much higher-temperatures was parental to the IID irons.

1:45 p.m. Gangopadhyay A. * Humayun M. Goddard R. E.
The Partitioning of Siderophile Elements Between Kamacite and Cohenite **[#1456]**
Determination of partition coefficients for siderophile elements between cohenite and kamacite in IAB iron meteorites.

2:00 p.m. Corrigan C. M. * McCoy T. J. Chabot N. L. McDonough W.
Trace Element Partitioning in the Fe-Ni-P System: Applications to P-rich Iron Meteorites **[#2314]**
Experiments to determine the partitioning behavior of trace elements in the Fe-Ni-P system have been completed. Results will be presented with implications as to their effects on the formation of iron meteorites.

2:15 p.m. Vogel I. A. * Pack A. Spettel B. Palme H.
Constraints on Iron Meteorite Formation from Lithophile Element Abundances **[#2150]**
Activity coefficients of Si and Cr in FeNi were experimentally determined. This and the low Si contents of 15 analysed iron meteorites (<0.3 ppm) and low Cr indicate equilibration of FeNi with silicates at temperatures below 1250°C.

2:30 p.m. Ammon K. * Leya I.
Noble Gas Measurements in the Grant IIIAB Iron Meteorite **[#1556]**
The preatmospheric center of Grant IIIAB has been recalibrated. The goal of this study is to establish a purely physical model to calculate the cosmogenic nuclide production in iron meteorites.

2:45 p.m. Schulz T. * Münker C. Mezger K. Palme H.
Age and Origin of IAB Iron Meteorites and Their Silicate Inclusions Inferred from Hf/W Chronometry **[#1401]**
The Hf/W systematics of metal and silicate inclusions of IAB iron meteorites were studied. Silicates have larger excesses in ^{182}W. A two point isochron for Copiapo inclusions gives an age of 4571.0 ± 2.6 million years before CAI formation.

3:00 p.m. Qin L. * Dauphas N. Wadhwa M. Janney P. E. Davis A. M. Mazarik J.
Evidence of Correlated Cosmogenic Effects in Iron Meteorites: Implications for the Timing of Metal-Silicate Differentiation in Asteroids **[#1771]**
Iron meteorites with low exposure ages show no GCR effect in ε^{184}W and have ε^{182}W values similar to initial CAI value. We report the first evidence for correlated cosmogenic effects in W isotopes for the high exposure age iron meteorites. ε^{184}W can potentially be used to correct for GCR effects

3:15 p.m. Markowski A. * Leya I. Quitté G. Wieler R. Ammon K. Halliday A. N.
Tungsten Isotopic Composition Corrected for Cosmic Ray Effects and the Hf-W Age of Iron Meteorites **[#1984]**
We report a method to correct W isotopic compositions in iron meteorites for cosmic-ray induced variations. This allows us to deduce that at least some magmatic irons segregated within less than 1 Myr of CAI formation.

3:30 p.m. Honesto J. * McDonough W. F. Walker R. J. Corrigan C. M. McCoy T. J. Chabot N. L. Ash R. D.
^{187}Re-^{187}Os Isotopic and Highly Siderophile Element Systematics of Group IVB Irons, and Ungrouped Irons Chinga, Tishomingo and Willow Grove **[#1374]**
IVB irons and the ungrouped irons Chinga, Tishomingo and Willow Grove were analyzed for HSE abundances and ^{187}Re-^{187}Os systematics. Chinga and Willow Grove cannot be related to the IVBs by igneous fractionation. Tishomingo is more ambiguous.

3:45 p.m. Lee S. R. Walker R. J. * McCoy T. J. McDonough W. F.
^{187}Re-^{187}Os Isotopic and Highly Siderophile Element Systematics of Pallasites **[#1167]**
Abundances of highly siderophile elements (HSE) and the Re-Os isotopic systematics of main group pallasites have been examined. If all main group pallasites are cogenetic, variations in HSE patterns are difficult to explain via single stage crystal-liquid fractionation models.

4:00 p.m. Lauretta D. S. * Hill D. H. Della-Giustina D. N. Killgore M.
The Fukang Pallasite: Evidence for Non-Equilibrium Shock Processing **[#2250]**
We report the results of our initial investigation of the Fukang pallasite, an ~1000 kg mass recently recovered from the Gobi desert. Evidence of shock and annealing on a subset of the Fukang olivine grains is exhibited by two texturally distinct populations.

4:15 p.m. Yang J. * Goldstein J. I. Sherman B. Corrigan C. M. McCoy T. J. Walker R. J. Chabot N. L. McDonough W. F.
How the Fuzzy Creek IVA Iron Got So Fuzzy **[#1308]**
We observed an unique microstructure in Fuzzy Creek among all IVA irons. The microstructure resulted from multiple reheating and impacts.

4:30 p.m. Bottke W. F. * Nesvorny D. Grimm R. E. Morbidelli A. O'Brien D. P.
Iron Meteorites as Remnants of Planetesimals Formed in the Terrestrial Planet Region **[#1388]**
Most iron meteorites are core fragments from differentiated planetesimals that formed and fragmented in the terrestrial planet region. Their precursors were then scattered into the main asteroid belt by interactions with planetary embryos.

SPECIAL MEETING ON RETURN TO THE MOON
Wednesday, 5:30 p.m., Marina Plaza Ballroom

Chairs: P. Lee and C. P. McKay

MARS: SEDIMENTS AND GEOCHEMISTRY
Thursday, 8:30 a.m., Crystal Ballroom A

Chairs: N. J. Tosca and H. E. Newsom

8:30 a.m. Knauth L. P. * Burt D. M. Wohletz K. H.
Impact Surge as the Simplest of the Proposed Hypotheses for the Origin of Sediments at the Opportunity Landing Site on Mars **[#1869]**
The MER Athena Team interpretation that sediments at the Opportunity Landing Site on Mars are altered eolian sands derived from a wet playa is complex and has difficulties. Newly published data further support sedimentation from an impact surge followed by normal martian weathering.

8:45 a.m. Tosca N. J. * McLennan S. M.
Constraints on Evaporation Processes at Meridiani Planum: Combining Theoretical and Experimental Data **[#2278]**
New experimental data on evaporation processes related to Meridiani Planum are combined with theoretical modeling to provide an in depth analysis of evaporite mineral formation at the martian surface.

9:00 a.m. Rothstein Y. R. * Dyar M. D. Bishop J. L.
Mössbauer and Reflectance Spectroscopy of Synthetic Jarosite with Variable Compositions and Temperatures **[#1727]**
A suite of synthetic jarosites was studied using Mössbauer and reflectance spectroscopy in order to better understand the change in parameters as a function of composition.

9:15 a.m. Bish D. L. * Scanlan M. K.
The Hydration and Dehydration of Hydrous Mixed-Cation Sulfates **[#1011]**
Based on X-ray diffraction and thermogravimetric data, the mixed-cation sulfate-chloride minerals kainite, blödite, and polyhalite are more stable than hydrated ferric sulfates and are reasonable combined reservoirs of S, Cl, and H_2O on Mars.

9:30 a.m. Harvey R. P. * Bish D. L. Socki R. Tonui E.
Cryogenic Evaporite Formation at the Lewis Cliff, Antarctica: A Mars Analog Study **[#1044]**
Large layered evaporite deposits near the Lewis Cliff Ice Tongue in Antarctica appear to have formed through periodic short-term cycling of very small volumes of water. These cryogenic, low water/rock ratio processes offer possible analogs for Martian evaporite formation events.

9:45 a.m. Chan M. A. * Parry W. T. Park A. J.
"Microberries": Nucleation Heterogeneity in Concretion Formation **[#1377]**
Terrestrial concretion comparisons with Mars "microberries" suggest an abundant and reactive iron source with varying conditions of diffusion with supersaturated solutions and temperature/pressure regimes favorable for hematite formation on Mars.

10:00 a.m. Chevrier V. *
Thermodynamics of Clay Minerals on Mars: Insight into the Geochemical Environment of Early Mars **[#1038]**
Following the recent discovery of clays on Mars by the Mars Express OMEGA spectrometer, thermodynamics of these phases are used to infer the weathering conditions in the primitive water rich Noachian environment of Mars.

10:15 a.m. Park A. J. * Chan M. A. Parry W. T.
Diagenesis of Mars Sediments: Coupled Water-Rock Interaction and Mass-Transfer Model **[#1826]**
The model proposed in this study addresses diagenesis of Mars volcanic rocks and sediments by combining volcanic gas, water, and basalt interaction with evaporation-induced reactions in a continuous column of sediments.

10:30 a.m. Niles P. B. * Zolotov M. Yu. Leshin L. A.
The Role of CO_2 in Aqueous Alteration of Ultra-Mafic Rocks and the Formation of Mg-, Fe-rich Aqueous Solutions on Early Mars **[#1440]**
We use data from thermodynamic modeling and studies of martian meteorites to show that high partial pressures of CO_2 were likely present during the formation of the Mg-, Fe-rich fluids that precipitated secondary minerals on early Mars.

10:45 a.m. Hurowitz J. A. * McLennan S. M. Athena Science Team
Geochemcial Mixing Relationships Between Bedrock Lithologies on Husband Hill, Gusev Crater, Mars **[#1621]**
The chemistry of rocks analyzed by Spirit on Husband Hill is consistent with two component mixing, complicated by superimposed weathering processes unique to Mars. Two component mixing implies an impact/volcaniclastic origin for the Columbia Hills.

11:00 a.m. McAdam A. C. * Zolotov M. Yu. Mironenko M. V. Leshin L. A. Sharp T. G.
Aqueous Chemical Weathering of a Mars Analog Lithology: Kinetic Modeling for a Ferrar Dolerite Composition **[#2363]**
Kinetic modeling is applied to explore weathering of a basaltic rock at 0°C in an open system. The results are interpreted in terms of temporal changes in the pyroxene/plagioclase ratio, with application to Antarctic soils and martian materials.

11:15 a.m. Zent A. P. * Ichimura A. I. Quinn R. C.
Superoxide Radical Formation and Stability Under Mars-like Conditions **[#2162]**
Oxygen radical chemistry under Mars-like conditions is complex; the superoxide radical has a number of formation and destruction mechanisms that affect its stability.

11:30 a.m. Newsom H. E. * Crumpler L. S. Reedy R. C. Peterson M. T. Newsom G. C. Evans L. G. Taylor G. J.
Geochemistry of Martian Soil and Bedrock in Mantled and Less Mantled Terrains with Gamma Ray Data from Mars Odyssey **[#1427]**
A study of mantled and less mantled areas with GRS data do not support a homogeneous surface soil composition. Variations among less mantled areas, however, may reflect an enrichment of soils in K and Th compared to bedrock.

LUNAR BASALTS AND BASINS
Thursday, 8:30 a.m., Crystal Ballroom B

Chairs: C. R. Neal and J. Longhi

8:30 a.m. Joy K. H. * Crawford I. A. Russell S. S. Swinyard B. Kellett B. Grande M.
Lunar Regolith Breccias MET 01210, PCA 02007 and DaG 400: Their Importance in Understanding the Lunar Surface and Implications for the Scientific Analysis of D-CIXS Data **[#1274]**
A discussion of the petrography and geochemistry of three lunar regolith breccias: MET 01210, PCA 02007 and DaG 400. These complicated samples represent the varied nature of the lunar surface and help to understand and interpret remotely sensed data from planetary instruments like D-CIXS.

8:45 a.m. Arai T. * Takeda H. Miyamoto M. Kojima H.
Apollo 14 Oldest Mare Basalt Revisited: Possible Petrogenetic Connection Between Mg Gabbronorite and VHK Basalt **[#2387]**
Mineralogical study of the Apollo 14 oldest mare basalt clasts in the multiple thin section showed the possible petrogenetic connection between Mg gabbronorite and VHK basalt.

9:00 a.m. Neal C. R. * Shih C.-Y. Reese Y. Nyquist L. E. Kramer G. Y.
Derivation of Apollo 14 High-Al Basalts from Distinct Source Regions at Discrete Times: New Constraints **[#2003]**
The Apollo 14 high-Al basalts represent the earliest lunar volcanism recorded in the Apollo sample collection. We report an Rb-Sr age from basalt 14321,1353 and integrate the new data with those previously published to investigate the petrogenesis of these basalts.

9:15 a.m. Boesenberg J. S. * Delaney J. S.
Elephant Moraine 87521: Two Pyroxenes, Two Chromites, and Two Ilmenites, but Only One Fractionation Series **[#1680]**
Detailed correlation of chromite, ulvospinel, and ilmenite compositions with Cr-Ti-Fe-Mg variation in pyroxene suggest fractionation of a single magma and render a two magma hypothesis unnecessary for the EET87521 lunar VLT basalts.

9:30 a.m. Grove T. L. * Chatterjee N. Singletary S. J. Delano J. W.
Experiments on the Apollo 15 Red Glass: New Constraints on Melting Depth and TiO_2 Melt Contents of Ilmenite Saturated Residues **[#1758]**
Differences in phase relations of the Apollo 15R and 14B glasses are a consequence of slow dissolution of metastable olivine. New experiments lower the multiple saturation pressure to ~1.5 GPa and raise the TiO_2 content of ilmenite-saturated liquids.

9:45 a.m. Liang Y. * Hess P. C.
Preferential Assimilation Due to Melt-Rock Reaction in the Lunar Mantle: A Laboratory and Ophiolite Field Perspective **[#1943]**
The compositional diversity of low to high Ti picritic magmas is discussed in the context of magma transport and melt-rock reaction in the lunar mantle and crust.

10:00 a.m. Hiesinger H. * Head J. W. III Wolf U. Jaumann R. Neukum G.
New Ages for Basalts in Mare Fecunditatis Based on Crater Size-Frequency Measurements **[#1151]**
We performed crater counts in order to date mare basalts in the Fecunditatis Basin. We find that all units dated in Mare Fecunditatis are Imbrian in age. There are some differences in crater size-frequency ages compared to ages in the geologic maps.

10:15 a.m. Longhi J. * Walker D.
Fickle Nickel: Compositional Systematics of Lunar Rocks Appear to be a Magma Ocean Signature **[#2452]**
A quantitative model of magma ocean fractional crystallization predicts that Ni-ol/liq partitioning starts out slightly incompatible near the liquidus of the MO that eventually changes to the more familiar compatible behavior as the MO fractionally crystallizes.

10:30 a.m. Pidgeon R. T. * Nemchin A. A. Meyer C.
Complex Histories of Two Lunar Zircons as Evidenced by Their Internal Structures and U-Pb Ages **[#1548]**
We present two examples of lunar zircons that preserve their primary U-Pb age and the age of a later thermal event. This, combined with zircon structure and radiation damage, provides a comprehensive history of lunar events.

10:45 a.m. Norman M. D. * Bennett V. C.
Impactor Populations and Lunar Crustal Compositions Inferred from Highly Siderophile Element Compositions of Apollo 16 and 17 Melt Breccias **[#1526]**
Siderophile element compositions of lunar breccias demonstrate multiple impact events and a source for the impactors in the inner solar system rather than comets. Siderophile elements can be fractionated during emplacement of impact breccias.

11:00 a.m. Hood L. L. * Artemieva N. A.
Formation of Magnetic Anomalies Antipodal to Lunar Impact Basins: Improved Numerical and Analytic Analysis **[#2137]**
More detailed numerical and analytic calculations are reported of the antipodal effects of lunar basin forming impacts, including ejecta distribution, magnetic field amplification, and possible magnetization acquisition mechanisms.

11:15 a.m. Garrick-Bethell I. * Weiss B. P.
Blocking Temperature Relations for Iron and the Origins of Lunar Rock Magnetism **[#2413]**
New time-temperature relations for remagnetization of the mineral kamacite show that much of the magnetization observed in ancient lunar rocks is stable over billions of years and almost certainly originated on the Moon.

11:30 a.m. Purucker M. E. * Sabaka T. J. Halekas J. Olsen N. Tsyganenko N. Hood L. L.
The Lunar Magnetic Field Environment: Interpretation of New Maps of the Internal and External Fields **[#1933]**
Long, arcuate magnetic field features whose origin may lie deep within the Moon's crust have been isolated from Lunar Prospector magnetic field observations from the South Pole-Aitken (SPA) basin region. These features may reflect compositional variations or tectonic responses to the SPA impact.

CHONDRITES: PARENT BODY ALTERATION AND ORGANICS
Thursday, 8:30 a.m., Marina Plaza Ballroom

Chairs: **A. J. Brearley and T. J. Zega**

8:30 a.m. Brearley A. J. *
The Role of Microchemical Environments in the Alteration of CM Carbonaceous Chondrites **[#2074]**
Microscale differences in fluid pH played an important role in the dissolution and precipitation of minerals during the aqueous alteration of CM carbonaceous chondrites.

8:45 a.m. Dyl K. A. * Manning C. E. Young E. D.
Modeling Aqueous Alteration of CM Carbonaceous Chondrites: Implications for Cronstedtite Formation by Water-Rock Reaction **[#2060]**
We explore the implications of cronstedtite as a major component of CM matrix. We find that increased CO_2 content in the fluid has implications for the production of cronstedtite, lowering the range of water-rock ratios at which the phase is a dominant alteration product.

9:00 a.m. Trigo-Rodríguez J. M. * Rubin A. E.
Evidence for Parent-Body Aqueous Flow in the MET 01070 CM Carbonaceous Chondrite **[#1104]**
MET 01070 contains a lens produced by aqueous flow. Its mineralogy suggests that it was produced by precipitation of soluble minerals from a water-rich fluid. Such a feature can only be produced in the parent body and not in the solar nebula.

9:15 a.m. Goreva J. G. * Lauretta D. S.
Early Oxidation of Phosphorus Associated with Sulfides in CM Chondrites **[#2422]**
Analyses of sulfides in Murchison meteorite show presence of Ca-phosphate exsolved within Fe, Ni-rich phase. This indicates very early alteration of sulfides in CM chondrites.

9:30 a.m. Guo W. * Eiler J. M.
Temperatures of Aqueous Alteration on CM Chondrite Parent Bodies Based on Carbonate 'Clumped-Isotope' Thermometry **[#2288]**
Temperatures of aqueous alteration on CM chondrite parent bodies were determined to be between 19 to 23°C(±10°C) based on carbonate 'clumped-isotope' thermometry. Implications of the results were discussed in the context of thermal models.

9:45 a.m. Nakamura T. * Okazaki R. Huss G. R.
Thermal Metamorphism of CM Carbonaceous Chondrites: Effects on Phyllosilicate Mineralogy and Presolar Grain Abundances **[#1633]**
Thermal metamorphism of CM chondrites results in phyllosilicate decomposition, presolar grain destruction, and radiogenic noble gas depletion. The depletion of ^{129}Xe and ^{40}Ar suggests that heating occurred later in the meteorite history.

10:00 a.m. Kita N. T. * Nagahara H. Tomomura S. Tachibana S. Valley J. W.
Systematic Oxygen Isotopic Variations Among Chondrules from the Least Equilibrated Ordinary Chondrites: Improved Ion Microprobe Precision **[#1496]**
We report subpermil oxygen isotope analyses on olivine and pyroxene in 26 chondrules from LL3.0–3.1 chondrites. Data show several permil mass dependent fractionation among type I, small variation among type II, and localized % level ^{16}O enrichments.

10:15 a.m. McDonough W. F. * Teng F.-Z. Rudnick R. L. Ash R. D.
Lithium Isotopic Analyses of Chondrites and Chondrules **[#2416]**
The lithium isotopic composition of chondrites and chondrules are reported along with data which demonstrate the accuracy and precision of our methodology. The average δ^7Li value for all of the chondrites is 1.3 ± 1.3 (1σ).

10:30 a.m. Cody G. D. * Alexander C. M. O'D. Yabuta H. Araki T. Kilcoyne A. L. D.
Complexity in the Early Solar System as Recorded in Meteoritic Organic Matter **[#1795]**
The analysis of insoluble organic matter isolated from 23 meteorites spanning CM, CI, CR, CV, CO, ordinary, and enstatite chondrites reveals startling chemical complexity possibly disconnected from processes recorded by meteorite matrix mineralogy.

10:45 a.m. Zega T. J. * Stroud R. M. Nittler L. R. Busemann H. Alexander C. M. O'D.
Correlated Analytical Studies of Organic Material from the Tagish Lake Carbonaceous Chondrite **[#1444]**
We report on correlated studies of organic material using SIMS, FIB-SEM, and TEM.

11:00 a.m. Remusat L. Palhol F. Robert F. Derenne S. *
Enrichment of Deuterium in Insoluble Organic Matter from Primitive Meteorites: A Solar System Origin? **[#1250]**
Molecular hydrogen isotope composition of pyrolysis and oxidation products from the insoluble organic matter of the Orgueil meteorite provides explanation on deuterium enrichment in the solar system.

11:15 a.m. Glavin D. P. * Dworkin J. P. Aubrey A. Botta O. Doty J. H. III Bada J. L.
Amino Acid Analyses of the Antarctic CM2 Meteorites ALH 83100 and LEW 90500 Using Liquid Chromatography-Time of Flight-Mass Spectrometry **[#1021]**
Amino acids and their enantiomeric abundances were measured in the CM meteorites ALH 83100, LEW 90500 and Murchison using a new liquid chromatography-time of flight-mass spectrometry technique. ALH 83100 has an amino acid distribution that is distinct from other CM2 meteorites.

11:30 a.m. Garvie L. A. J. * Buseck P. R.
Carbonaceous Nanospheres in Chondrites **[#1455]**
Carbonaceous nanospheres are widespread in carbonaceous chondrites including CI1, CM2, Tagish Lake, CR2 and CH meteorites.

THE GALILEAN SATELLITES
Thursday, 8:30 a.m., Amphitheater

Chairs: **R. M. Nelson and J. R. Spencer**

8:30 a.m. Geissler P. E. * McMillan M.
Galileo Observations of Volcanic Plumes on Io **[#1913]**
Galileo images of the gas and dust components of Io's plumes show that Prometheus-type plumes deposit pyroclastic particles entrained with the gas flow. Pele-type plumes, in contrast, may deposit material condensed from the gas phase.

8:45 a.m. Rathbun J. A. * Spencer J. R.
Loki, Io: Groundbased Observations and a Model for the Change from Periodic Overturn **[#2365]**
Loki is the most powerful volcano on Io. Here we present new groundbased observations of Loki's brightness and a model for the observed change from periodic to constant behavior.

9:00 a.m. Davies A. G. * Keszthelyi L. P. Wilson L.
Estimation of Maximum Effusion Rate for the Pillan 1997 Eruption on Io: Implications for Massive Basaltic Flow Emplacement on Earth and Mars **[#1155]**
We estimate maximum effusion rate for the 1997 Pillan eruption to be 18000 to 59000 m^3/s, in the range proposed for rubbly pahoehoe flood lava flows on Mars and Earth. Modelled thermal emission compares favourably with observations.

9:15 a.m. Jaeger W. L. * Davies A. G.
Models for the Crustal Structure of Io: Implications for Magma Dynamics **[#2274]**
We present a robust model for the crustal density structure of Io, which we use to constrain magma dynamics with emphasis on the Prometheus volcanic center. Preliminary results indicate that magma will pond at shallow depths under a volatile layer.

9:30 a.m. Hurford T. A. * Bills B. G. Sarid A. R. Greenberg R.
Unraveling Europa's Tectonic History: Evidence for a Finite Obliquity? **[#1303]**
It has been shown that Europa should have a forced obliquity of ~ 0.1 degrees, which must be accounted for when computing Europa's diurnal stress field. Using this fact, we produce maps of hypothetical cycloids on Europa that give better fits to observed cycloid patterns.

9:45 a.m. Tobie G. * Duval P. Sotin C.
Grain Size Controlling Processes Within Europa's Ice Shell **[#2125]**
On the basis of a physical model of grain size evolution, we determine the grain size distribution within a convective ice shell on Europa. Our simulations demonstrate that the grain size distribution is strongly heterogeneous with values ranging from 1 mm to several centimeters.

10:00 a.m. Barr A. C. * McKinnon W. B.
Convection in Icy Satellites with Self-Consistent Grain Size **[#2130]**
Ice grain size controls the evolution of ice I shells of large to midsized icy satellites. Measurements of recrystallized ice grain size observed in terrestrial ice sheets are used to determine the likelihood of convection in the satellites and to constrain grain size in convecting shells.

10:15 a.m. McCarthy C. * Cooper R. F. Kirby S. H. Durham W. B.
Ice/Hydrate Eutectics: The Implications of Microstructure and Rheology on a Multiphase Europan Crust **[#2467]**
Water-ice/salt-hydrate aggregates (of composition of interest to tectonics on Europa), prepared by eutectic solidification, are evaluated for their microstructures and mechanical (creep) responses. Eutectic microstructures affect strength to first order, increasing it significantly over that for pure ice I, for appropriate phase volume fraction.

10:30 a.m. Han L. * Tobie G. Showman A. P.
Thermal Convection in Europa's Silicate Mantle **[#2302]**
We perform numerical simulations in 3D spherical geometry to study the properties of convection in Europa's silicate mantle using the finite-element code CitcomS including temperature-dependent viscosity.

10:45 a.m. Zolotov M. Yu. * Krieg M. L. Shock E. L. McKinnon W. B.
Chemistry of a Primordial Ocean on Europa **[#1435]**
Physical-chemical modeling shows that ocean-forming fluids and a primordial ocean were cold, reduced, alkaline, Na-, Cl-rich but not saline, depleted in Mg, sulfides and sulfates, and departed from redox equilibria because of H_2 separation and escape.

11:00 a.m. Bland M. T. * Showman A. P.
Tectonic Resurfacing of Icy Satellites by Periodic Necking Instabilities: Application to Ganymede and Enceladus **[#1417]**
We present two-dimensional finite element models of the formation of Ganymede's grooved terrain. These models provide significant insight into tectonic resurfacing processes on both Ganymede and smaller icy satellites such as Enceladus.

11:15 a.m. McKinnon W. B. *
Formation Time of the Galilean Satellites from Callisto's State of Partial Differentiation **[#2444]**
Simple energy arguments imply that Callisto cannot have finished accretion any earlier than 2.5 Myr after CAI condensation. Such a limit has important implications for the formation of Jupiter and other giant planet satellites.

11:30 a.m. Johnson T. V. * Clark K. B. Greeley R. Pappalardo R. T.
Europa Exploration: Challenges and Solutions **[#1459]**
Post-Galileo exploration of Europa presents a number of major technical challenges. We conclude that a flagship class Europa mission can now be developed relying on existing technologies, having significantly more capability and returning more science than the previous Europa Orbiter concept.

MARS: IMPACT CRATERING
Thursday, 1:30 p.m., Crystal Ballroom A

Chairs: J. A. Skinner Jr. and N. G. Barlow

1:30 p.m. Barlow N. G. * Hillman E.
Distributions and Characteristics of Martian Central Pit Craters **[#1253]**
An analysis of ~1500 central pit craters on Mars finds that floor pits are more common and larger than summit pits. Pit craters are commonly associated with multiple layer ejecta morphologies. Regional variations in pit crater distribution are seen.

1:45 p.m. Osinski G. R. *
Role of Volatiles in the Emplacement of Ejecta Deposits Around Martian Impact Craters **[#1060]**
A new mechanism for the emplacement of fluidized ejecta deposits is presented, based on considerations of the terrestrial impact cratering record and observations of martian impact craters.

2:00 p.m. Baloga S. M. * Barnouin-Jha O. S.
Formation of Mars Impact Crater Ramparts by Volatile Degassing of the Overland Ejecta Flow **[#1309]**
We present a two component crater ejecta flow model where solids are conserved and volatiles are released. The presence of a gaseous component that is lost during emplacement may uniquely distinguish Mars rampart deposits from those of impact-generated deposits on other planetary surfaces.

2:15 p.m. Berman D. C. * Crown D. A. Bleamaster L. F. III
Survey of Mid-Latitude Martian Craters: Volatile-driven Degradational Morphologies **[#1781]**
We have identified 16 craters in the southern mid-latitudes of Mars with lobate flow features on their walls. These craters typically contain several such lobes, typically on the pole-facing side, with a dependence on latitude and crater diameter.

2:30 p.m. Thomson B. J. *
Cut Craters on Mars: A Study of Impact Craters Exposed in Cross Section **[#1906]**
This study presents reconstructed cross sections of craters that have been exposed along the edges of Valles Marineris. Such craters permit direct observation of crater substructure and can provide mechanical constraints on wall rock layering.

2:45 p.m. Fristad K. E. * Frey H. V.
Age Variations in the Martian Lowlands **[#1406]**
Areas in Utopia and Vastitas Borealis have identical cratering and resurfacing histories, with a total N(100) crater retention age of 10. Amazonis appears to be much younger with N(100) = 5 (west) and 2 (east). The eastern side appears more buried.

3:00 p.m. Frey H. V. * Fristad K. E.
Martian Lowland Basement Ages: Is Amazonis Really Younger? **[#1391]**
Amazonis appears to be much younger than other Mars lowlands, but crustal thickness data suggests there is a population of very deeply buried basins. The basement of Amazonis may be just as old as that elsewhere in the martian lowlands.

3:15 p.m. Buczkowski D. L. *
Surface Relief and Geographic Distribution of QCDs on the Northern Plains of Mars and Implications Towards Lowland Material Thickness **[#1333]**
QCDs in the northern lowlands are mapped. QCD locations are compared to geologic units and materials and are identified only in units where differential compaction is possible. Relative thicknesses of cover for lowlands regions are evaluated.

3:30 p.m. Skinner J. A. Jr.* Hare T. M. Tanaka K. L.
Northern Plains Craterforms: Evidence for the Accumulation and Degradation of Paleo-Mantles **[#1476]**
An inventory of lowland craterforms may be remnants of a ~35-m-thick, Amazonian-age paleo-mantle at mid- to high-latitude. Our observations suggest most lowland craterforms are not volcanic in origin but rather impact craters that were modified due to cyclic mantling and exhumation.

3:45 p.m. Boyce J. M. * Mouginis-Mark P. J. Garbeil H. Soderblom L. A.
History of Major Crater Degradational Events on Mars: Preliminary Results from Carter Depth and Diameter Maeasurements **[#2354]**
Crater depth and diameter measurements have been made for 4355 craters planetwide on Mars to investigate degradational history of Mars.

4:00 p.m. Wrobel K. E. * Schultz P. H.
The Generation and Distribution of Martian Impact Melt/Glass: A Computational Study with Implications for the Nature of Dark Surface Materials **[#2386]**
Estimates of the accumulation and distribution of distal impact melt across the surface of Mars since the Hesperian support the proposal of an impact glass-based origin for the concentrated regions of dark material found on the present-day surface.

4:15 p.m. Ivanov B. A. *
Giant Martian Impact Basins — Numerical Modeling **[#1263]**
The reconnaissance study of giant basin formation on Mars with the numerical modeling is presented. The model shows the giant melt pools formation. Solidification of the melt pool may result in new crust/mantle boundary formation under impact basins.

4:30 p.m. Mohit P. S. * Phillips R. J.
Mid-sized Martian Basins: A Window into Early Martian History **[#1975]**
We investigate the importance of viscous relaxation of impact basins on early Mars. Our results show that this is likely to have been an important process and has significant implications for early martian thermal history.

MARTIAN MINERALOGY
Thursday, 1:30 p.m., Crystal Ballroom B

Chairs: M. E. Minitti and W. C. Koeppen

1:30 p.m. Gomez C. * Poulet F. Bibring J.-P. Langevin Y. Gondet B. Pelkey S. M. Mustard J. F. Bellucci G. C. OMEGA Science Team
Global Mineral Maps on Mars **[#1405]**
Global mineral maps are realized from spectral parameters using the Visible/NIR domains of the OMEGA imaging spectrometer on-board Mars Express. These maps highlight unique as well as familiar processes that have occurred during Mars' history.

1:45 p.m. Koeppen W. C. * Hamilton V. E.
The Distribution and Composition of Olivine on Mars **[#1964]**
We use spectral index mapping and deconvolution to analyze the distribution of multiple compositions of olivine on Mars.

2:00 p.m. Tornabene L. L. * Moersch J. E. McSween H. Y. Jr. Hamilton V. E. Piatek J. L. Milam K. A. Christensen P. R.
The Subsurface Geology of Mars: Remote Sensing of Impact Craters Using THEMIS, TES, MOC and MOLA **[#1739]**
Impact craters provide natural exposures of subsurface composition, stratigraphy and, in some cases, geologic features that are not otherwise exposed at the surface. Here we present results from a THEMIS-based remote sensing study of martian impact craters that expose subsurface materials.

2:15 p.m. Baratoux D. * Gendrin A. Pinet P. Mustard J. Kanner L. Heuripeau F. Clenet H. Daydou Y. Vaucher J. Chevrel S. Bibring J.-P. OMEGA Co-Investigator Team
Toward a 3-D View of the Mineralogy of Syrtis Major Through Impact Cratering from OMEGA Data **[#1376]**
Impact ejecta at Syrtis Major are enriched in high-calcium pyroxene. Using a model of excavation flow we interpret this observation as an enrichment in high-calcium pyroxene at a few hundred meters depth.

2:30 p.m. Kanner L. C. * Mustard J. F. Gendrin A. Bibring J.-P.
Joint OMEGA-THEMIS Investigation of TES Type II Deposits and Local Terrain, Nili Patera, Syrtis Major, Mars **[#1648]**
An integrated OMEGA-THEMIS dataset offers enhanced understanding of TES Type II deposits in the context of local spectral diversity. The spectral similarity of Type II to the surrounding terrain at OMEGA wavelengths presents new interpretations.

2:45 p.m. Dunn T. L. * McSween H. Y. Jr.
New Linear Deconvolutions of Martian Surface Types 1 and 2 Using Alkalic Mineral Endmembers **[#1291]**
An overview of deconvolutions of surface types 1 and 2 using endmember sets tailored for alkalic rocks.

3:00 p.m. Milliken R. E. * Mustard J. F. Poulet F. Bibring J.-P. Langevin Y. Gondet B. Pelkey S.
The H_2O Content of the Martian Surface as Seen by Mars Express OMEGA **[#1987]**
The absolute H_2O content of the Martian surface is derived from MEX OMEGA data by comparing several methods. Hydration increases poleward of 60 degrees latitude in both hemispheres, up to 12 wt% H_2O, whereas equatorial regions have 2–4 wt% H_2O.

3:15 p.m. Wang A. * Freeman J. F. Jolliff B. L. Arvidson R. E.
Conversion of Crystalline $MgSO_4.XH_2O$ to the Hydrated Amorphous Phase — A Raman, NIR, and XRD Study **[#2168]**
Amorphous $MgSO_4$•$2H_2O$ was made by vacuum dehydration of epsomite/hexahydrite. Kieserite and starkeyite were unaffected under the same conditions. Kieserite shows the best match to OMEGA NIR spectra obtained from dark etched terrain at Meridiani Planum.

3:30 p.m. Mustard J. F. * Poulet F. Head J. W. Mangold N. Bibring J.-P. Fassett C. Langevin Y. Neukum G.
Ancient Crust, Aqueous Alteration, and Impact Melt Preserved in the Isidis Basin, Mars **[#1683]**
The Nili Fossae region preserves a critical record of early Mars: Noachian basement enriched in low-Ca pyroxene, a deep and pervasive aqueous alteration, on which rests olivine-rich deposits interpreted to be impact melt from the Isidis event.

3:45 p.m. Wright S. P. * Christensen P. R. Sharp T. G.
Thermal Emission Spectroscopy of Shocked Basalt from the Earth and Mars: A Review Plus New Insights **[#1786]**
Thermal emission spectra of shocked minerals and martian basalts are reviewed for constraints on laboratory spectra of shocked basalt from Lonar Crater, India and Mini-TES data of Bounce Rock.

4:00 p.m. Minitti M. E. * Hamilton V. E. Wyatt M. B.
Investigation of the Role of New Glass Compositions in Remotely-sensed Martian Lithologies **[#2101]**
We investigated the role of a new suite of glasses with basaltic to dacitic compositions in deconvolutions of martian thermal emission spectra. Our results suggest an andesitic glass might be an important component of martian surface lithologies.

4:15 p.m. Schaefer M. W. * Dyar M. D. Agresti D. G.
Comparison of Mössbauer Spectra of Soils from Gusev Crater and Meridiani Planum **[#2111]**
Mössbauer spectra of selected soils from Gusev Crater and Meridiani Planum are analyzed and compared. Variations in ferrous/total Fe ratio are found, and evidence for variations in Fe^{3+} mineralogy.

4:30 p.m. Bishop J. L. * Schiffman P. Dyar M. D. Lane M. D. Murad E. Drief A.
Soil-forming Processes on Mars as Determined by Mineralogy: Analysis of Recent Martian Spectral, Chemical and Magnetic Data and Comparison with Altered Tephra from Haleakala, Maui **[#1423]**
Integrated analyses of recent mission data and Haleakala tephra is applied to soil formation processes on Mars. This altered tephra contains silica, jarosite, FeOx, clays, magnetic phases, and a mid-IR doublet like that observed for the Martian soil.

TOWARD UNDERSTANDING REFRACTORY INCLUSIONS
Thursday, 1:30 p.m., Marina Plaza Ballroom

Chairs: F. M. Richter and H. C. Connolly Jr.

1:30 p.m. Richter F. M. * Janney P. E. Mendybaev R. A. Davis A. M. Wadhwa M.
Recondensation Reconsidered: Effects in Evaporation Experiments and in Natural Settings **[#2353]**
Theory and experiments show that recondensation of previously evaporated species can, depending on conditions (e.g., into an unconfined or confined surrounding gas), reduce or enhance the isotopic fractionation of residues.

1:45 p.m. Thrane K. * Bizzarro M. Baker J.
Brief Formation Interval for Calcium-Aluminum-rich Inclusions in the Early Solar System **[#1973]**
We report an isochron for bulk CAIs from four CV chondrites, which yields an initial $^{26}Al/^{27}Al$ of $(5.85 \pm 0.05) \times 10^{-5}$, and intercept of $-0.0317 \pm 0.00038‰$, suggesting that primary CAI formation may have occurred within an interval as brief as 20,000 years.

2:00 p.m. Simon J. I. * Russel S. S. Tonui E. Young E. D.
Reconstructing Changing Conditions in the Solar Nebula: Model Constraints and Evidence from Magnesium Isotopes in CAIs **[#2160]**
We fit the isotope record obtained by *in situ* measurements of $^{27}Al/^{24}Mg$, $^{25}Mg/^{24}Mg$, and $^{26}Mg/^{24}Mg$ isotope ratios by LA-MC-ICPMS comprising core-to-rim traverses across five CV3 CAIs with numerical models that consider mass dependent isotope fractionation processes.

2:15 p.m. Liu M.-C. * McKeegan K. D. Davis A. M.
Magnesium Isotopic Compositions of CM Hibonite Grains **[#2428]**
Hibonite is thought to be one of the earliest solids in the solar system, therefore the Mg isotope compositions of hibonite grains can help elucidate the initial abundance and distribution of ^{26}Al in the early solar system.

2:30 p.m. Simon S. B. * Sutton S. R. Grossman L.
Measurement of Ti^{3+}/Ti^{4+} Ratios in Pyroxene in Wark-Lovering Rims: Evidence for Formation in a Reducing Solar Nebula **[#1772]**
The pyroxene rim layers on CAIs are important recorders of nebular conditions, including oxygen fugacity. Using XANES, we have directly measured the Ti^{3+}/Ti^{tot} of pyroxene in the rim of an Allende fluffy Type A inclusion.

2:45 p.m. Toppani A. * Paque J. M. Burnett D. S. Teslich N. Moberlychan W. Dai Z. R. Bradley J. P.
Wark-Lovering Rims at the Nanometer Scale: A Transmission Electron Microscopy Study **[#2030]**
We report the first transmission electron microscopy study of the Wark Lovering rim of a coarse-grained igneous CAI. First observations argue for crystallization from a liquid.

3:00 p.m. Fagan T. J. * Guan Y. MacPherson G. J.
Al-Mg Isotopic Constraints on Alteration of Allende Ca-Al-rich Inclusions **[#1213]**
Multiple stages of alteration of Allende CAIs are implied from SIMS analyses of Al-Mg isotopes in secondary minerals from one B2 and one FTA CAI. ^{26}Mg-excesses are absent from most B2 analyses, but present in one B2 grossular and most FTA analyses.

3:15 p.m. Connolly H. C. Jr.* Ebel D. S. Weisberg M. K. Beckett J. R. Paque J. M.
The Petrography and Geochemistry of an Allende Type B CAI: V Depletion, Relict Regions and Remelting **[#1521]**
We describe an unusual type B2 CAI from Allende that contain regions that are potentially relict, small (~20–40-μm-sized) euhedral to anhedral melilites with fassaite and spinels that are highly depleted in V. This CAI may have experienced multiple melting episodes.

3:30 p.m. Beckett J. R. *
Phase Relations of Grossite-bearing Ca-, Al-rich Inclusions **[#1775]**
A diagram useful for interpreting the liquidus phase relations and crystallization sequences of melilite + grossite-bearing inclusions in carbonaceous chondrites is presented. In general, grossite is on the liquidus for these CAIs only if significant amounts of melilite are also present.

3:45 p.m. Nehru C. E. * Ebel D. S. Friedrich J. M. Weisberg M. K.
Petrologic and Trace Element Study of Seven Type A Inclusions from Lance (CO3) **[#2044]**
We report petrology and LA-ICPMS REE analyses of six type A inclusions and one hibonite-bearing inclusion from Lance CO 3.4. The inclusions show group III and V REE patterns. We compare the Lance inclusions to those in other chondrites.

4:00 p.m. Cosarinsky M. * Taylor D. J. McKeegan K. D.
Aluminum-26 Model Ages of Hibonite and Spinel from Type A Inclusions in CV Chondrites **[#2357]**
We studied Al-Mg isotopes on spinel, hibonite, and melilite from type A CAIs in CV chondrites to constrain chronological events early in the solar system by analyzing samples with varying degrees of secondary mineral alteration and isotopic resetting.

4:15 p.m. Ushikubo T. * Guan Y. Hiyagon H. Sugiura N. Leshin L. A.
^{36}Cl, ^{26}Al and Oxygen Isotopes in an Allende CAI: Implications for Secondary Alteration in the Early Solar System **[#2082]**
^{36}S and ^{26}Mg excesses were observed in secondary phases of an Allende type B2 CAI. This suggests that some alteration processes of CAIs occurred while ^{36}Cl and ^{26}Al were alive.

4:30 p.m. Hsu W. * Guan Y. Leshin L. A. Ushikubo T. Wasserburg G. J.
A Late Episode of Irradiation in the Early Solar System: Evidence from Extinct ^{36}Cl and ^{26}Al in Meteorites **[#2028]**
We provide strong evidence in support of the existence of ^{36}Cl in CAIs and chondrules of CV3 chondrites. ^{36}Cl is not correlated with ^{26}Al. These results indicate that intense late irradiation processes occurred in the early solar system.

ASTROBIOLOGY
Thursday, 1:30 p.m., Amphitheater

Chairs: C. C. Allen and B. Gladman

1:30 p.m. Banerjee N. R. * Furnes H. Simonetti A. Muehlenbachs K. Staudigel H. de Wit M. van Kranendonk M.
Ancient Microbial Alteration of Oceanic Crust on Two Early Archean Cratons and the Search for Extraterrestrial Life **[#2156]**
We demonstrate that biosignatures are preserved in basaltic glass from *in situ* oceanic crust and ophiolites as far back as the early Archean and show how our methods could be applied to the search for life on Mars and other extraterrestrial bodies.

1:45 p.m. Cates N. L. * Mojzsis S. J.
Geochronology and Geochemistry of a Newly Identified Pre-3760 Ma Supracrustal Sequence in the Nuvvuagittuq Belt, Québec, Canada **[#1948]**
We report geochronology, geochemistry and mapping of a newly discovered pre-3760 Ma supracrustal (volcanosedimentary) locality from northern Québec, Canada.

2:00 p.m. Dauphas N. * Cates N. L. Mojzsis S. J. van Zuilen M. Wadhwa M. Janney P. E. Busigny V. Davis A. M.
The Iron Isotopic Composition of 3.7–3.8 Ga Chemical Sediments: Comparison Between Isua (Greenland) and Nuvvuagittuq (Northen Quebec) **[#1053]**
The BIFs in the 3.7–3.8 Ga Nuvvuagittuq Belt have heavy Fe isotopic compositions, similar to those measured in the better-characterized Isua Supracrustal Belt. This is the first time in 40 years that an early Archean supracrustal belt has been opened up for study.

2:15 p.m. Lindsay J. F. * Bennett V.
The Late Archean Biospheric Explosion **[#1174]**
Concretionary structures are abundant in late Archean rocks. They provide evidence for a rapid expansion of the biosphere in the late Archean. This expansion coincides with the assembly of the first continents and the initiation of plate tectonics.

2:30 p.m. Oehler D. Z. * Mostefaoui S. Meibom A. Selo M. McKay D. S. Robert F.
"Nano" Morphology and Element Signatures of Early Life on Earth: A New Tool for Assessing Biogenicity **[#1067]**
NanoSIMS reveals new structural and elemental markers of early life on Earth. These biosignatures may aid in assessments of problematic organic materials, such as those in early Archean sediments and any that may occur in Martian samples.

2:45 p.m. Grimm R. E. * Bullock M. Dec S. Jepsen S. Olhoeft G. Painter S. Priscu J.
Unfrozen Groundwater in the Martian Cryosphere **[#2090]**
Thin films of unfrozen water at subfreezing temperatures may provide permanent microbial habitats in the deep cryosphere of Mars or transiently at the surface.

3:00 p.m. Allen C. C. * Oehler D. Z. Venechuk E. M.
Prospecting for Methane in Arabia Terra, Mars — First Results **[#1193]**
We are using orbital data and methodologies derived from petroleum exploration in an attempt to locate the release points of methane on Mars. Southwest Arabia Terra, particularly in the area of 2 to 12 N, 5 to 12 W, is a prime area for detailed exploration.

3:15 p.m. Basilevsky A. T. * Werner S. Neukum G. van Gasselt S. Head J. W. Ivanov B. A.
Potential Life Habitat at the Eastern Flank of the Olympus Mons as Seen in MEX HRSC and MGS MOC Images of Mars **[#1179]**
East of Olympus Mons there are channel networks carved by water and/or lava and postdating them wrinkle ridges and volcanic ridges/chains of cones. Such channels and wrinkle ridges are typically Hesperian, but here they are very young (<26 Myr).

3:30 p.m. Lefticariu L. * Pratt L. M. LaVerne J. A. Ripley E. M.
Experimental Study of Radiolytic Oxidation of Pyrite: Implications for Mars-relevant Crustal Processes **[#1953]**
Crustal radiolysis is an efficient mechanism in the production of oxidizing species in geologically long-lived oxidizing systems that has profound implications for assessing microbial metabolism in the deep subsurface on Earth and Mars.

3:45 p.m. Nicholson W. L. * Fajardo-Cavazos P. Langenhorst F. Melosh H. J.
Bacterial Spores Survive Hypervelocity Launch by Spallation: Implications for Lithopanspermia **[#1808]**
Spores of Bacillus subtilis were demonstrated to survive launch by spallation from a granite target initiatied by a high-speed (5.4 km/s) impact using the NASA Ames Vertical Gas Gun.

4:00 p.m. Stöffler D. * Meyer C. Fritz J. Horneck G. Möller R. Cockell C. Ott S. de Vera J. P. Hornemann U. Artemieva N. A.
Impact Experiments in Support of "Lithopanspermia": The Route from Mars to Earth **[#1551]**
Shock recovery experiments on a Martian analogue rock (gabbro) loaded with three types of microorganisms reveal that these organisms survive the impact and ejection phase on Mars at shock pressures up to about 50 GPa with exponentially decreasing survival rates.

4:15 p.m. Gladman B. * Dones L. Levison H. Burns J. Gallant J.
Meteoroid Transfer to Europa and Titan **[#2165]**
Via extensive numerical simulations, we calculate the delivery efficiency of terrestrial impact ejecta to Europa and Titan. We show that (perhaps surprisingly) in an averaged large-scale impact (KT-level) a few to a hundred terrene meteoroids reach Europa and Titan.

4:30 p.m. McKay D. S. * Clemett S. J. Thomas-Keprta K. L. Wentworth S. J. Gibson E. K. Jr. Robert F. Verchovsky A. B. Pillinger C. T. Rice T. Van Leer B.
Observation and Analysis of In Situ Carbonaceous Matter in Nakhla: Part I **[#2251]**
New analyses of indigenous secondary material in the martian meteorite Nakhla reveal amorphous carbon-rich veins and dendrites. The texture and chemistry of this material resembles that of biogenically altered sub-ocean basaltic glasses.

SPECIAL SESSION: PLANETARY CARTOGRAPHY
Thursday, 5:30 p.m., Marina Plaza Ballroom

Chair: T. K. P. Gregg

5:30 p.m. Gaddis L. R. * Archinal B. Kirk R. NASA Planetary Cartography/Geologic Mapping Working Group
The NASA Planetary Cartography Program
NASA planetary research is supported by an ongoing mapping program, directed by the PCGMWG and executed largely by the USGS. A document outlining the strategy for cartography over the coming decade is in preparation and community input is solicited.

5:45 p.m. Kirk R. L. * Archinal B. A. Gaddis L. R. Rosiek M. Howington-Kraus E. Hare T. M.
What Is Planetary Cartography And Why Does It Matter?
Planetary data of ever-increasing volume and resolution must be integrated into a precise, consistent cartographic reference system if their research/mission-planning value is to be realized. Examples of the challenges and benefits will be presented.

6:00 p.m. Gehrke S. * Wählisch M. Lehmann H. Albertz J. Neukum G. HRSC Co-Investigator Team
Generation of Topographic and Thematic Planetary Maps Using the Software System "PIMap" **[#1322]**
PIMap (Planetary Image Mapper) is a software system for producing topographic image maps and thematic maps. The entire topographic content, grids, frame line, titles, sheet designation, and marginal elements are automatically generated "all in one."

6:15 p.m. Williams D. A. * Keszthelyi L. P. Geissler P. E. Jaeger W. L. Becker T. L. Crown D. A.
Global Geologic Mapping of Io: First Steps **[#1143]**
We will discuss the methodology required to produce a global geologic map of Io using new mosaics that combine Galileo and Voyager data.

LUNAR REMOTE SENSING

Chevrel S. D. Pinet P. C. Jehl A. Besse S. Cord A. Daydou Y. Baratoux D. Kaydash V. G. Shkuratov Y.
Surface Physical Properties of the Lunar Regolith at Reiner Gamma: Characterization and Distribution Using Hapke Model Inversion **[#1173]**
Inversion of the Hapke model using Clementine multi-angular observations of the Reiner Gamma formation permits us to characterize and map physical properties of surface materials of lunar swirls.

Hawke B. R. Gaddis L. R. Blewett D. T. Boyce J. M. Campbell B. A. Giguere T. A. Gillis-Davis J. J. Lucey P. G. Peterson C. A. Robinson M. S. Smith G. A.
The Composition and Origin of Lunar Crater Rays: Implications for the Copernican-Eratosthenian Boundary **[#1133]**
Since compositional rays can persist for 3 Ga or more, the mere presence of bright rays is not a reliable indicator that a crater was formed during the Copernican Period. The OMAT parameter could be used to define the C-E boundary.

Hawke B. R. Giguere T. A. Blewett D. T. Gillis-Davis J. J. Hagerty J. J. Lawrence D. J. Lucey P. G. Peterson C. A. Smith G. A. Spudis P. D. Taylor G. J.
Ancient Volcanism in the Schiller-Schickard Region of the Moon **[#1516]**
Lunar Prospector elemental abundance data and Clementine multispectral images were used to identify and investigate a major cryptomare deposit in the Schiller-Schickard region near the southwestern limb of the Moon.

Thompson T. W. Campbell B. A. Ghent R. R. Hawke B. R. Leverington D. W.
Unusual Radar Backscatter Along the Northern Rim of Imbrium Basin **[#1140]**
The enigmatic low radar backscatter associated with the Montes Jura on the northern rim of the Imbrium basin is attributed to rock-poor distal ejecta of the Sinus Iridum and Plato impacts.

Clark P. E. Clark C. S. De Hon R. A.
Using Boundary-based Maps to Illustrate the Palimpsest Effect of Early Impacts on Lunar Surface Formation **[#1153]**
We apply CSNB approach to Moon mapping for insight on its surface morphology unavailable from standard maps. The Moon, typically mapped in an Earth-like projection but more asteroid-like in terms of surface modification, reveals impact palimpsests.

Isaacson P. J. Pieters C. M.
Variations Within the Northern Imbrium Noritic Deposits **[#1867]**
The NIN deposits have a heterogeneous noritic surface overlying an anorthositic substrate. Further variations of the NIN deposits were seen both with depth and with longitude, suggesting that multiple processes contributed to their evolution.

Petro N. E. Pieters C. M.
The Effects of Basin Formation on the Lunar Geochemical Terranes **[#1868]**
Investigation of the basin history of lunar geochemical terranes reveals added differences between the near and farside. The FHT and SPAT cover areas that received little post-SPA basin modification, while the PKT was significantly modified by basins.

Korokhin V. V. Shkuratov Yu. G. Stankevich D. G. Pieters C. Mall U.
Artificial Neural Networks as a Tool for Prognosis of Chemical and Mineral Composition of Lunar Soils from Spectral Measurements **[#1280]**
We compared two statistical techniques (Multiple Linear Regression and Artificial Neural Networks) for prognosis of lunar surface composition using the LSCC data. The results may be a useful for analysis of data obtained from SMART-1 and Chandrayaan missions.

Staid M. I.
Lunar Mineralogy from Spectral Merging of ROLO Telescopic Data with Clementine Images **[#1874]**
ROLO telescopic observations are mathematically combined with higher spatial, but lower spectral resolution Clementine images to obtain the average reflectance properties of small craters from several near side mare deposits.

Arai T. Ohtake M. Nimura T.
Visible/Near Infrared Spectral Characterization of Brecciated Mare Basalt Flow and Surface Mare Basalt **[#1895]**
The Fe-rich surface basalts and more Mg-rich brecciated basalts which likely represent the average compositions of basalt flow can be spectroscopically distinguished by the lateral shift of reflectance spectra and associated individual absorption bands to the shorter wavelength.

Mimura M. Kobayashi S. Tezuka C. Hosojima T. Yamashita N. Miyajima M. Miyachi T. Hasebe N.
New Approach to Planetary Surface Imager Based on Gamma-Ray High Pressure Xenon Time Projection Chamber **[#1563]**
New approach to planetary surface imager based on HPXe-TPC is proposed. By introducing a new method of gamma-ray measurement, the possibility of high resolution gamma-ray imager is discussed for a global mapping of planetary surface.

Lawrence S. J. Hawke B. R. Lawrence D. J. Gillis-Davis J. J. Lucey P. G. Taylor G. J. Cahill J. Smith G. A. Hagerty J. Keil K.
The Composition and Origin of the Dewar Geochemical Anomaly: Final Results **[#1581]**
We report the final results of our remote sensing investigation of the thorium anomaly located near Dewar crater on the lunar farside. The elevated thorium values correlate with FeO and TiO_2 enhancements. Possible origin mechanisms are discussed.

Yamamoto H. Sakurai K. Miyachi T. Hasebe N.
Lunar Mare Volcanism Based on Chemical Composition of Titanium, Iron, Calcium and Magnesium as Observed by Lunar Prospector Gamma-Ray Spectrometer **[#1604]**
By using the data from Lunar Prospector gamma-ray spectrometer, good correlations of TiO_2 with FeO, CaO and MgO in five mare regions were found to exist, suggesting that the age and period are closely related to the composition.

Weller L. Redding B. Becker T. Gaddis L. Sucharski R. Soltesz D. Cook D. Archinal B. Bennett A. McDaniel T.
Lunar Orbiter Revived: Very High Resolution Views of the Moon **[#2143]**
U.S. Geological Survey Astrogeology Program report on the progress of the Lunar Orbiter filmstrip scanning, archiving and processing efforts. We describe the status of the global mosaic and describe additional work on very high resolution data of the Moon's near side acquired at low altitude.

Kramer G. Y. Jolliff B. L. Neal C. R.
Searching for High-Al Mare Basalts: Mare Fecunditatis and Luna 16 **[#2227]**
Clementine and Lunar Prospector data are used to search for high-Al basaltic units in Mare Fecunditatis that may be related to the Luna 16 high-Al mare basalts.

Kaydash V. G. Pinet P. C. Baratoux D. Besse S. Jehl A. Chevrel S.
Lunar Photometry from Clementine Multiangular Data: Analysis of Hapke Parameters Estimate and Implication for Upcoming Smart-1 Spot-Pointing Data **[#1692]**
We explore how well constrained is the determination of photometric function parameters using: 1) the widely used Hapke photometric model and 2) extensive set of spot-pointing observations provided by Clementine over the Reiner-Gamma region.

Rosiek M. R. Archinal B. A. Kirk R. L. Becker T. L. Weller L. Redding B. Howington-Kraus E. Galuszka D.
Utilization of Digitized Apollo and Lunar Orbiter Imagery for Mapping the Moon **[#2171]**
This abstract presents the results of using modern "softcopy" digital mapping techniques for extracting digital elevation models (DEMs) from Lunar Orbiter (LO) and Apollo imagery.

Lawrence D. J. Elphic R. C. Feldman W. C. Hagerty J. J. Prettyman T. H.
Spatial Deconvolution Studies of Nearside Lunar Prospector Thorium Abundances **[#1915]**
We have carried out spatial deconvolution studies of Lunar Prospector thorium abundances. We show that these techniques can be useful in improving interpretations of low-spatial resolution datasets such as orbital gamma-ray data.

WATER ON THE MOON

Lawrence D. J. Feldman W. C. Elphic R. C. Hagerty J. J. Maurice S. McKinney G. W. Prettyman T. H.
Improved Modeling of Lunar Prospector Neutron Spectrometer Data: Implications for Hydrogen Content at Lunar Poles **[#1893]**
New transport modeling has been carried out for lunar neutron data to understand the variation of epithermal neutrons for all lunar soils. We find that enhanced hydrogen deposits are still the best explanation for the polar neutron signals.

Head J. N.
Earthshine at the Lunar Poles and Volatile Stability **[#1886]**
Earthshine is too weak to devolatilize lunar regolith in permanently shadowed craters. Therefore ice validation missions may be landed in areas with direct line-of-sight to Earth, eliminating the need for and cost of a dedicated relay satellite.

Schorghofer N. Taylor G. J.
Subsurface Migration of H_2O at Lunar Cold Traps **[#1197]**
Water molecules can slowly diffuse into the lunar regolith and can remain there longer than on the surface. We develop a physical model for molecular subsurface diffusion in lunar environments and study its consequences.

Campbell D. B. Campbell B. A. Carter L. M. Margot J. L. Stacy N. J. S.
High Resolution Radar Polarimetric Observations of the Lunar South Pole **[#1408]**
New high resolution radar observations of the lunar south pole have provided images of the circular polarization ratio that support the hypothesis that any water ice present must be widely disseminated in the lunar regolith.

Ong L. Asphaug E. Plesko C.
Water Delivered to the Moon by Comet Impacts **[#2450]**
We calculate the fate of cometary water impacting the Moon. We use the hydrocode RAGE to model impacts of water-ice spheres with diameters of 10 m to 10 km. Velocities vary from 2 to 3 km/s, and impact angles include 15, 30, 45, and 90 degrees.

LUNAR REGOLITH

Levine J. Muller R. A. Renne P. R.
Implanted and Cosmogenic ^{38}Ar and ^{36}Ar in Lunar Impact Spherules **[#1190]**
We present argon isotopic data from lunar impact spherules, and discuss exposure histories of the spherules to the solar wind, to solar energetic particles, and to cosmic rays.

Starukhina L. V.
Impact Melting of Regolith Particles by Micrometeorites as a Mechanism of Soil Maturation **[#1147]**
Impact melting by micrometeorites can provide formation of reduced nanophase Fe grains in regolith particles. This enables regolith maturation on Mercury shielded from solar wind and on asteroids with projectile velocities sufficient for impact melting only.

Burger P. Shearer C. K. Vaniman D.
Microscale Distribution and Behavior of Th, REE, and K During Regolith Formation Processes on the Moon: Implications for Remote Sensing of the Surfaces of Airless Planetary Bodies **[#2097]**
Electron and ion microprobe analyses of Sm, Th, K and major elements in lunar regolith glasses are used to examine the effect of impact melting on primary crustal signatures to more accurately interpret planetary data obtained through remote sensing.

Noble S. K. Keller L. P. Christoffersen R.
Nanometer-Scale Chemical Mapping of Space Weathered Lunar Soil: A New View **[#1819]**
Quantitative X-Ray mapping with a new generation FE-STEM reveals incredible complexity within lunar space weathering products. Rims are found to be heterogeneous at the nm-scale and differences are observed between products on silicates vs. oxides.

Abbas M. M. Tankosic D. Craven P. D. Hoover R. B. Taylor L. A. Spann J. F. LeClair A. West E. A.
Photoelectric Emission Measurements on Apollo 17 Lunar Dust Grains **[#1415]**
We present the first measurements of the photoelectric yields of micron-size dust grains, selected from sample returns of the Apollo 17 mission. The measured yields of individual dust grains are determined to be more than an order of magnitude larger than the bulk values reported in the literature.

Basu A.
A Mass-Balance Perspective on the Origin of Agglutinitic Glass **[#1679]**
Glass composition of individual lunar agglutinate grains is determined largely by the composition of a few soil grains, heterogeneous with respect to the bulk soil, impacted by a micrometeorite.

Liu Y. Thompson J. R. Taylor L. A. Park J.
Magnetic Properties of Unique Apollo 17 Soil 70051 **[#1945]**
The magnetic properties of unique Apollo 17 soil 70051, and comparison with several lunar soil simulants.

Mellin M. J. Taylor L. A. Patchen A. D.
Characterization of a Unique Soil Sample from the Apollo 17 Site, 70051 **[#2334]**
70051 has great potential as a ground truth for remote-sensing data of the Apollo 17 site. This soil is also important for in-situ resource utilization studies. Such significance has prompted us to perform a detailed characterization of this unique soil.

LUNAR EXPLORATION AND RESOURCE UTILIZATION

Park J. S. Liu Y. Kihm K. D. Taylor L. A.
Micro-Morphology and Toxicological Effects of Lunar Dust **[#2193]**
We shall briefly describe about the possible toxicity and particle size and shape of lunar dust, and explain the detailed experimental methods of particle-size measurement, and report on the particle-size distribution (PSD) and reactivation surface areas.

Boldoghy B. Kummert J. Szilágyi I. Varga T. Bérczi Sz.
Construction of a Lunar Architectural Environment with Joint Constraints of Thermal Balance, Economic Technologies, Local Material Using: Strategy, Design and On Site Assembly **[#1152]**
We studied the strategies, technologies, designs of the lunar base architectural construction in the lunar geological environment from the viewpoint of physical, energetic, local materials use and allocation constraints.

Elphic R. C. Hahn S. Lawrence D. J. Feldman W. C. Johnson J. B.
Neutron Probes for the Construction and Resource Utilization Explorer (CRUX) **[#1677]**
Neutron probes are tools for *in situ* prospecting, detection, and assay of hydrogenous resources in lunar polar cold traps. The Surface Neutron Probe is designed to be rover-borne, while the Borehole Neutron Probe assesses stratigraphy.

Zacny K. Glaser D. Bartlett P. Davis K. Wilson J.
Drilling Results in Ice-bound Simulated Lunar Regolith (FJS-1) as Part of the Construction and Resource Utilization Explorer Project (CRUX) **[#2226]**
As part of the development of a lunar drill, a preliminary study was performed using custom designed drill bits and augers in simulated ice-bound lunar soil under a variety of conditions. Colder drilling temperatures demonstrated beneficial results.

Sibille L. Carpenter P. K.
Standard Lunar Regolith Simulants for Space Resource Utilization Technologies Development: Effects of Materials Choices **[#1789]**
The recommendation of the recently held 2005 Workshop on Lunar Regolith Simulant Materials at Marshall Space Flight Center of establishing standard simulant materials to be used in lunar technology development and testing will be discussed here with an emphasis on space resource utilization.

Clark P. E. Keller J. W. Farrell W. M. Stubbs T. J. Nuth J. A. Curtis S. A.
Electrostatic Dust Control and Collection on Planetary Surfaces **[#1128]**
Strategies initially implemented to deal with abrasive velcro-like lunar dust failed. The successful mission-critical strategy we are attempting will deal with dynamics resulting from interaction between mechanical and electrostatic forces.

Immer C. Starnes J. Michalenko M. Calle C. I. Mazumder M. K.
Electrostatic Screen for Transport of Martian and Lunar Regolith **[#2265]**
The martian and lunar soil contains fine particulate that contaminate all surfaces. With the electrostatic screen, alternating waveforms of voltage applied to patterned grids of electrodes will transport dust. Experiments have been performed in ambient, martian, and lunar conditions.

Sternovsky Z. Horanyi M. Colwell J. Robertson S. Wang X.
Near-Surface Dusty Environments of Planetary Objects **[#1460]**
An overview will be given on recent and planned laboratory studies of dust charging near surfaces, and the characterization of near-surface plasma environments relevant to the Mars, Moon, asteroids, and the dense ring system of Saturn.

MOON MISSIONS: PAST, PRESENT, FUTURE

Haruyama J. H. Ohtake M. O. Matsunaga T. M. Morota T. M. Yoshizawa A. M. LISM Working Group
Planned Digital Terrain Model Products from SELENE Terrain Camera Data **[#1132]**
The Terrain Camera (TC) is a stereo imager that will be launched on SELENE in 2007. The DTM from TC data will cover the entire surface of the Moon with 10 m spatial resolution. In this paper, we will introduce the planned TC DTM products.

Kato M. Takizawa Y. Sasaki S. SELENE Project Team
SELENE, the Japanese Lunar Orbiting Satellites Mission: Present Status and Science Goals **[#1233]**
Present status and science goals of the SELENE project will be reported. Final integration test will be started in April 2006 to target a launch of 2007 summer.

Ohtake M. Haruyama J. Mastunaga S. Morota T. Kodama S. LISM Team
Observation and Data Analyses Plan of the SELENE Multiband Imager **[#1536]**
MI is a high-resolution multiband imaging camera being developed for the SELENE project that will be launched in 2007. Manufacturing and integration of MI flight model have been completed and pre-flight test as SELENE satellite is underway.

Ogawa K. Okada T. Shirai K. Yamamoto Y. Arai T. Shiraishi H. Hosono K. Inoue T. Inoue T. Maruyama Y. Arakawa M. Kato M.
Development of X-Ray Fluorescence Spectrometer Onboard SELENE **[#2244]**
An X-ray fluorescence spectrometer (XRS) onboard SELENE, a Japanese lunar polar orbiter that will be launched in 2007, is being developed for lunar X-ray exploration. We would like to present instruments and current development status of XRS.

Foing B. H. Grande M. Huovelin J. Josset J. L. Keller H. U. Nathues A. Malkki A. Noci G. Kellett B. Beauvivre S. Almeida M. Frew D. Volp J. Heather D. Schwehm G. Koschny D. Zender J. McMannamon P. Camino O. Racca G. D.
ESA's SMART-1 Mission: Lunar Science Results After One Year **[#1920]**
We summarise one year of SMART-1 lunar science results with the optical camera (polar and colour high res imaging), infrared spectrometer (mineralogy), and X-ray spectrometer (elemental composition). We describe the plan for operations until end of mission impact in August 2006.

Kellett B. J. Grande M.
X-Ray Fluorescence Observations of the Moon — Highlights from the First Year of Observations from D-CIXS on SMART-1 **[#1897]**
Highlights from the first year of D-CIXS observations of the Moon include a big flare over Mare Crisium, seven smaller flares across the nearside southern highlands (including Apollo 12 site) and a big flare on the farside including the South-Pole Aitken basin.

Josset J. L. Beauvivre S. Cerroni P. De Sanctis M. C. Pinet P. Chevrel S. Langevin Y. Barucci M. A. Plancke P. Koschny D. Almeida M. Sodnik Z. Mancuso S. Hofmann B. A. Muinonen K. Shevchenko V. Shkuratov Y. Ehrenfreund P. Foing B. H.
SMART-1/AMIE Camera System **[#1847]**
The Advanced Moon micro-Imager Experiment (AMIE), on board ESA SMART-1, the first European mission to the Moon (launched on 27th September 2003), is a camera system with scientific, technical and public outreach oriented objectives.

Cerroni P. De Sanctis M. C. Josset J.-L. Beauvivre S. Koschny D. Pinet P. Chevrel S. Langevin Y. Barucci M. A. Plancke P. Almeida M. Hofmann B. A. Muinonen K. Shevchenko V. Shkuratov Yu. Ehrenfreund P. Foing B. H.
Preliminary Analysis of Colour Information from AMIE on Smart-1 **[#1831]**
The Advanced Moon micro-Imager Experiment (AMIE) is the imaging system on board the ESA mission to the Moon SMART-1. We present a preliminary assessment of push-broom data acquired during the first push-broom orbital phase of Smart-1 mission.

Heldmann J. L. Moore J. M. Lee P. C. Girten B. McKay C. P.
Return to the Moon: Site Selection Process and Considerations for NASA's Robotic Lunar Exploration Program (RLEP) **[#2066]**
Site selection drives the lunar program in terms of both near-term and long-term planning. We consider site selection criteria for both robotic and human landings to determine optimal landing sites and implications for lunar architecture.

Chin G. Bartels A. Brylow S. Foote M. Garvin J. Kaspar J. Keller J. Mitrofanov I. Raney K. Robinson M. Smith D. Spence H. Spudis P. Stern S. A. Zuber M.
Lunar Reconnaissance Orbiter Overview: The Instrument Suite and Mission **[#1949]**
The Lunar Reconnaissance Orbiter (LRO) is first in this series of missions under NASA's Robotic Lunar Exploration Program. This presentation will give an introduction to the instruments and objectives of the LRO mission.

Sanin A. B. Mitrofanov I. M. Sagdeev R. Z. Boynton W. Evans L. Harshman K. Litvak M. L. Kozyrev A. S. Milikh G. Mokrousov M. Schvetsov V. Shevchenko V. Starr R. Tret'yakov V. I. Trombka J.
Searching for Water Ice in the Moon Cold Traps by LEND Instrument Onboard the NASA LRO Mission **[#1690]**
In this paper we focus on identification of prospective lunar polar cold traps, as targets for LEND investigation onboard LRO mission. We also present the results of numerical studies of the LEND detection limits of hydrogen deposits for these traps.

Greenhagen B. T. Paige D. A.
Mapping Lunar Surface Petrology Using the Mid-Infrared Emissivity Maximum with the LRO Diviner Radiometer **[#2406]**
Diviner is scheduled to launch in 2008 on LRO. Diviner will map petrologic variations in the lunar surface by determining the location of the mid-infrared emissivity maximum (Christiansen feature), which is a good compositional identifier.

Carpenter P. Sibille L. Wilson S.
Development of Standardized Lunar Regolith Simulant Materials **[#2279]**
Lunar exploration requires standardized testing procedures that ultimately support flight certification of technologies and hardware. We discuss standardized lunar regolith simulant (SLRS) materials that are traceable interlaboratory standards for technology development.

Battler M. M. Richard J. Boucher D. Spray J. G.
Developing an Anorthositic Lunar Regolith Simulant **[#1622]**
The Moon's bedrock is dominated by anorthosite-norite-troctolite rocks. We report the results of developing an anorthositic regolith simulant so as to better understand regolith evolution and assist industry with drilling and excavation protocols.

Martirosyan K. S. Luss D.
Combustion Synthesis of Ceramic Composites from Lunar Soil Simulant **[#1896]**
The process for rapid production of dense ceramics from lunar soil simulant by using combustion synthesis is presented. A reaction between Ti, B, JSC-1 generates a temperature front that propagates through reactants converting it to a solid product.

Pieters C. Boardman J. Buratti B. Clark R. Green R. Head J. W. III McCord T. B. Mustard J. Runyon C. Staid M. Sunshine J. Taylor L. Tompkins S.
Global Mineralogy of the Moon: A Cornerstone to Science and Exploration **[#1630]**
The Moon Mineralogy Mapper (M3) will fly on the Chandrayaan-1 mission to the Moon and will return unprecedented compositional information at high resolution, providing a foundation for decades of scientific exploration.

Gaddis L. R. Skinner J. A. Jr. Hare T. Tanaka K. Hawke B. R. Spudis P. Bussey B. Pieters C. Lawrence D.
The Lunar Geologic Mapping Program and Status of Copernicus Quadrangle Mapping **[#2135]**
We are mapping a lunar quadrangle at 1:2.5M scale that centers on Copernicus crater.

Williams D. R. Grayzeck E. J. Jr.
The Lunar Data Project — Restoration of Apollo Data for Future Lunar Exploration **[#1187]**
The Lunar Data Project is an effort to restore Apollo data sets and make them available for use by the lunar scientific and exploration communities. This poster will outline the project and show some examples of data being restored.

MER — SPIRIT

Li R. Arvidson R. E. Agarwal S. Bell J. Brodyagina E. Crumpler L. Des Marais D. J. Di K. Golombek M. Grant J. Kirk R. L. Maimone M. Matthies L. H. Malin M. Parker T. Soderblom L. A. Squyres S. W. Wang J. Yan L. Athena Science Team
New Topographic Products and Rover Localization Results for the 2003 Mars Exploration Rover Mission **[#2118]**
For over two years of MER surface operations, topographic maps, rover traverse maps, and updated rover locations of Spirit and Opportunity have supported tactical and strategic mission operations. Here we present the recent topographic products and the latest localization results.

Leer K. Basso B. Binau C. Goetz W. Gorevan S. Hviid S. F. Kusack A. Madsen M. B. Squyres S. W. Wilson J.
Simulating Collection of Dust on the RAT Magnets Onboard the Mars Exploration Rovers **[#1784]**
RAT magnet experiments with the aim to examine the dust collected on the RAT magnets during grinding. Tell the difference between bulk rock and collected dust by Mössbauer spectroscopy.

Moller L. E. Tuller M. Baker L. Kuhlman K.
Mars Dust Micromechanics: MER Marsdial and Laboratory Observations **[#2407]**
Small spheres yield micromechanics data for Mars dust surrogate deposition in laboratory trials. We use images of the MER Marsdial gnomon sphere to examine Mars dust angle of repose. Lab trials using spheres similarly treated in a Mars dust environmental chamber confirm an angle >50°.

Johnson J. B. Haldemann A. F. C. Hopkins M. A. Moore J. Peters J. Sullivan R. J. Athena Science Team
Preliminary Report on the Development of Analysis Methods to Determine Mars Soil Mechanical Properties from Laboratory Tests, Discrete Particle Modeling, and Mars Trenching Experiments **[#1528]**
Laboratory tests and discrete element methods (DEM) are being developed to determine soil mechanical properties from Mars Exploration Rover wheel trenching, Mössbauer contact plate indentation, and other soils tests. DEM simulations reduce uncertainties caused by test geometry.

Soderblom J. M. Bell J. F. III Johnson J. R. Maki J. N. Wolff M. J. Athena Science Team
Photometry of the Martian Surface Using Data from the Navigation Cameras on the Mars Exploration Rovers Spirit and Opportunity **[#1935]**
We model the broadband photometric properties of the surface materials at the Mars Exploration Rovers (MER) landing sites using data from the MER navigation cameras and a radiative transfer model based on that described by Hapke.

Landis G. A. Herkenhoff K. Greeley R. Thompson S. Whelley P. MER Athena Science Team
Dust and Sand Deposition on the MER Solar Arrays as Viewed by the Microscopic Imager **[#1932]**
To characterize atmospheric dust which has deposited on the deck of the Mars Exploration Rovers, we used the Microscopic Imager (MI) to examine the surface of the solar array.

Castano A. Fukunaga A. Castano R. Chien S. Greeley R. Whelley P. Neakrase L. Lemmon M.
Feature Detection Onboard Mars Rovers: Automated Cloud and Dust Devil Detection **[#2059]**
To improve the effectiveness of rover atmospheric imaging campaigns, we have developed an approach to screen images for the science features of interest (i.e., clouds and dust devils) onboard the rovers.

Crumpler L. S. McCoy T. Athena Science Team
MER Surface Geologic Transect Mapping in the Plains and Hills, Gusev Crater **[#1685]**
Sufficient traverse distance and outcrop characterization has occurred by the Spirit rover in the Gusev plains and Columbia Hills of Mars that "field maps" may now be prepared showing the distribution of the bedrock geology from surface observation along the entire traverse.

Haldemann A. F. C. Crumpler L. Grant J. A. Golombek M. P. Cohen B. A. Rice J. W. Jr.
Mapping and Interpreting the Cratering Record in the Columbian Hills with Spirit **[#1231]**
MOC images of the Columbia Hills show a mystery: the plains, which appear superposed on the CH, have more craters than do the hills. Addressing this mystery stems from our desire to provide a proper structural geologic context for the many rock types, and bedrock exposures, being found by Spirit.

Grant J. A. Wilson S. A. Koestler D. L.
The Distribution of Rocks on the Gusev Plains and on Husband Hill **[#1184]**
The size and number of rocks measured from images obtained by the Spirit Mars Rover at over 30 sites along its traverse in Gusev crater indicate a minimal role of non-impact processes in modification of surfaces in this area since the Hesperian.

Stone A. S. Bridges N. T. Thomson B. J.
A Catalog of Rock Abrasion Features at the MER Landing Sites: Preliminary Results from Spirit and Comparisons with Orbital Wind Direction Indicators **[#2080]**
We provide a record and interpretation of results, so far, of ventifacts and related features at the Spirit landing sites using Pancam data. The use of MOC NA and THEMIS VIS images are also used to observe and interpret relevant wind direction features.

Sullivan R. Bell J. F. III Farrand W. Grotzinger J. Herkenhoff K. Johnson J. Richter L. Weitz C. Whelley P.
Mars Exploration Rover Spirit Investigation of the "El Dorado" Sand Deposit **[#1829]**
MER Spirit investigated an unusual 170 m-wide dark patch that MOC images show remains relatively free of dust. Spirit found a rippled, cohesionless, basaltic sand deposit that likely is subject to regular wind mobilization.

McSween H. Y. Ruff S. W. Morris R. V. Bell J. F. Herkenhoff K. E. Gellert R.
Backstay and Irvine: Alkaline Volcanic Rocks from Gusev Crater, Mars **[#1120]**
Unweathered alkaline lava samples found on Husband Hill appear to have formed by low-pressure fractionation of olivine-rich basaltic magmas like those on the Gusev plains. Their mode of occurrence may suggest a local magmatic source under the crater.

Mittlefehldt D. W. Gellert R. McCoy T. McSween H. Y. Jr. Li R. Athena Science Team
Possible Ni-rich Mafic-Ultramafic Magmatic Sequence in the Columbia Hills: Evidence from the Spirit Rover **[#1505]**
Spirit has recently descended the southeast slope of the Columbia Hills doing detailed measurements of a series of outcrops. The mineralogical and compositional data on these rocks are consistent with an interpretation as a magmatic sequence becoming increasingly olivine-rich down slope.

Blaney D. L. Christensen P. Ruff S. Athena Science Team
Minealogical Units in the Columbia Hills from Mini-TES **[#2057]**
Outcrops in the Columbia Hills have distinctive spectral signatures permitting their extent and variability to be mapped. There is variability between outcrops and within one outcrop indicating a complex history and localized alteration processes.

Tréguier E. d'Uston C. Gellert R.
Principal Component Analysis of Geochemical Data at Gusev Crater **[#1956]**
Multivariate analysis of the elemental abundances for the rock samples encountered by the Spirit rover at the Gusev Crater site.

MER — OPPORTUNITY

Arvidson R. E. Squyres S. W. Clark B. Grotzinger J. Knoll A. H. McLennan S. M. Tosca N.
Regional Setting and Model for the Meridiani Planum Deposits Investigated by the Opportunity Mars Exploration Rover **[#1400]**
The results from the Opportunity rover mission are placed in a regional geologic setting, and a rising ground water table model is presented for the formation of the wide-spread plains and underlying etched terrain materials in Terra Meridiani.

Parker T. J. Grotzinger J. P. Athena Science Team
Relative Ages of Geomorphic Features Visited by the Opportunity Rover **[#2312]**
The Opportunity Rover is currently investigating the largest contiguous expanse of *in situ* outcrop ever been visited by a landed spacecraft on Mars. It lies just inside the degraded west rim of Erebus Crater — 4 kilometers from where the exploratory mission began in Eagle Crater.

Wiseman S. M. Arvidson R. E. Guinness E. A. Fergason R. Athena Science Team
Coordinated Analysis of Orbital and Ground Remote Sensing Data Along the Opportunity Rover Traverse from Endurance to Erebus Crater **[#2207]**
Surface and orbital observations acquired over the Opportunity rover's traverse south are consistent with the incorporation of an increased amount of locally derived nanophase Fe oxide dust into the hematite bearing plains material.

Griffes J. L. Arvidson R. E. Poulet F. Bibring J.-P. OMEGA Team
Geomorphic and Spectral Mapping of Northern Meridiani Planum **[#1756]**
Presented here is a geomorphic and spectral analysis of a several hundred meter vertical section of plains, etched, and cratered units in the northern portion of Meridiani Planum using various orbital data.

Clark B. C. Squyres S. W. Ming D. W. Morris R. V. Yen A. Gellert R. Knoll A. H.
Arvidson R. E. Athena Science Team
Chemistry of Meridiani Outcrops **[#1711]**
The MER Opportunity Rover has measured additional outcrop at Meridiani Planum, including the most sulfate-rich sample to date. A single basaltic source material reacted with SO_3-rich acid brine may account for the observed chemistries.

Perl S. M. McLennan S. M. Grotzinger J. P. Johnson J. R. Clark B. C. Athena Science Team
Secondary Porosity Classification and Analysis of the Burns Formation, Meridiani Planum, Mars **[#2164]**
This research and abstract is intended to summarize the attempts to quantify the classifications and volumes of the three types of secondary porosity found at the Burns formation, Meridiani Planum, Mars.

Chavdarian G. V. Sumner D. Y.
Cracks and Fins in Sulfate Sand: Evidence for Recent Mineral-Atmospheric Water Cycling in Meridiani Planum Outcrops? **[#1888]**
The MER rover Opportunity catalogued polygonal cracks and fins on Meridiani. Similar cracks and fins are documented at White Sands National Monument, NM, providing evidence for recent water cycling between sulfate outcrops and the martian atmosphere.

Watters W. A.
Structure of Polygonal Craters at Meridiani Planum, Mars, and a Model Relating Target Structure to Crater Shape **[#2163]**
In this study we characterize the structure of a polygonal simple crater visited by MER-Opportunity, as well as the local fracture network. We present a simple model relating fracture network structure to the distribution of polygonal crater shapes.

Jolliff B. L. Farrand W. H. Johnson J. R. Schröder C. Weitz C. M. Athena Science Team
Origin of Rocks and Cobbles on the Meridiani Plains as Seen by Opportunity **[#2401]**
Cobbles and stand-alone rocks at Meridiani have been analyzed by the Opportunity rover. To date these include fragments of outcrop ejected from local craters, meteorites, basalt delivered as far-flung crater ejecta, and possibly impact breccias.

Calvin W. M. Glotch T. D. Arvidson R. E. Wiseman S. Johnson J. R. Ruff S. W. Knudson A. T. Christensen P. R.
Directional Emissivity Effects on the Meridiani Plains **[#1481]**
Over the course of nearly two Earth years and several kilometers of traverse a series of observations have been acquired that allow systematic exploration of the emission angle dependence of the hematite signature across the Meridiani plains and on dune slope faces.

Learner Z. A. Bell J. F. III Farmer J. Farrand W. H. Grotzinger J. P. Johnson J. R. Jolliff B. L. Knoll A. H. McLennan S. M. Squyres S. W. Watters W. A.
Surface Coatings at Meridiani Planum, Mars **[#2040]**
This is an investigation into rock surfaces observed by the MER Opportunity rover at Meridiani Planum. The elemental composition of the rock surfaces is studied using data from the rover's Alpha X-ray Spectrometer and Rock Abrasion Tool.

Rogers A. D. Aharonson O. Glotch T. D. Christensen P. R.
Mineralogy of Basaltic Sands at Meridiani Planum from the Miniature Thermal Emission Spectrometer and Comparison to Orbital Observations **[#2273]**
Modal mineralogy of Meridiani Planum basaltic soils is derived from Mini-TES observations and compared with TES-derived mineralogy and emissivity of the landing site and vicinity. Mineralogy of low-albedo surfaces peripheral to the hematite unit and etched terrain is also derived and presented.

Greenwood J. P. Gilmore M. S. Blake R. E. Martini A. M. Gomes M. Tracy S. Dyar M. D. Gilmore J. A. Varekamp J.
Nascent Jarosite Mineralization of Sulphur Springs, St. Lucia, W.I.: Implications for Meridiani Jarosite Formation **[#2230]**
We have discovered newly formed jarosite (<1 year) in the acid-sulfate environment of the Sulphur Springs, St. Lucia, W.I.

Farrand W. H. Joliff B. L. Bell J. F. III Johnson J. R.
Visible/Near Infrared Spectral Trends Between Meridiani Planum Surface Materials: Comparisons Between Spherules, Basaltic Sands, Outcrop, Rinds, and Cobbles **[#1707]**
Trends in VNIR spectral parameter plots of Meridiani surface materials observed by Opportunity are examined for clues to the nature of unusual surface materials such as rinds, fracture fills, and cobbles.

Johnson J. R. Arvidson R. E. Bell J. F. III Deen R. Farrand W. Grundy W. Guinness E. Johnson M. Herkenhoff K. E. Lemmon M. Seelos F. IV Soderblom J. Squyres S. Athena Science Team
Spectrophotometric Modeling of Soils and Rocks at the Opportunity Landing Site **[#1480]**
The Pancam on Opportunity acquired multispectral reflectance observations of outcrop rocks and spherule-rich soils at different incidence, emission, and phase angles (0°–155°) that were used for photometric modeling to constrain the albedo and physical properties of the surface materials.

Glotch T. D. Bandfield J. L. Christensen P. R. Calvin W. M. McLennan S. M. Clark B. C. Athena Science Team
Mineralogy of the Light-Toned Outcrop Rock at Meridiani Planum as Seen by Mini-TES **[#2021]**
We expand on the initial Mini-TES analyses of the light-toned outcrop rock, using the results of the APXS and Mössbauer instruments to constrain mineral deconvolution models. The outcrop rock is composed largely of amorphous silica and Mg-, Ca-, and Fe-sulfates.

McCollom T. M. Hynek B. M.
Is the Chemistry of the Bedrocks at Meridiani Planum Indicative of a Volcanic or Sedimentary/Evaporite Origin? **[#2023]**
The chemical composition of bedrocks is evaluated in the context of possible volcanic and sedimentary/evaporite origins. Although either model can be consistent with the bulk chemistry of the rocks, the volcanic model provides a more simple and straightforward interpretation.

MARS FLOWING AND STANDING WATER

Bargery A. S. Wilson L.
Modelling Water Flow with Bedload on the Surface of Mars **[#1218]**
We theorise the thermodynamical effects of entrainment of eroded cold rock and ice on proposed aqueous flow on the surface of Mars, at temperatures well below the triple point, with an upper surface exposed to the Martian atmosphere.

Keszthelyi L. O'Connell D. R. H. Denlinger R. P. Burr D.
A 2.5D Hydraulic Model for Floods in Athabasca Valles, Mars **[#2245]**
We present initial results from the application of a new numerical model to floods in Athabasca Valles, Mars. Issues with the sparseness of MOLA data are of concern.

Collier A. Sakimoto S. E. H. Grossman J. A. Silliman S. E.
Parametric Study of Martian Floods at Cerberus Fossae **[#2313]**
Recent studies of Athabasca Valles use values that may be artificially constrained. A set of Earth-derived values are proposed to be used when calculating flow rates. This will allow for the determination of the formation events of Athabasca Valles with greater accuracy.

Gregoire-Mazzocco H. Stepinski T. F. McGovern P. J. Lanzoni S. Frascati A. Rinaldo A.
Martian Meanders: Wavelength-Width Scaling and Flow Duration **[#1185]**
Martian meanders reveals linear wavelength/width scaling with a coef. k~10, that can be used to estimate discharges. Simulations of channel evolution are used to determine flow duration from sinuosity. Application to Nirgal Vallis yields 200 yrs.

Howard A. D. Matsubara Y.
Flow Routing in a Cratered Landscape: 1. Background and Application to Mars **[#1209]**
A model is presented which routes runoff through enclosed depressions, balancing lake evaporation with runoff. As evaporation relative to precipitation decreases, flow integration increases. Global and regional Martian simulations are presented.

Matsubara Y. Howard A. D.
Flow Routing in a Cratered Landscape: 2. Model Calibration for Pleistocene and Modern Lakes and Rivers of the U.S. Great Basin **[#1210]**
A hydrologic routing model for cratered is applied to the U.S. Great Basin, a strong analog to the Martian highlands. Estimates of areally distributed runoff and evaporation closely match both present and Pleistocene lake distribution.

Molloy I. Stepinski T. F.
Automated Mapping of Valley Networks on Mars **[#1743]**
An automated channel mapping algorithm is developed and applied to map valley networks on Mars. Results in eight test sites reveal an excellent agreement with accurate manual maps.

Grant J. A. Fortezzo C.
The Evolution of Martian Drainage Basin Hypsometry **[#1393]**
Basin hypsometry on Mars may be created predominately by impact cratering. The resulting topography may be predisposed to relatively efficient discharge of water and sediment along later forming valleys.

Raitala J. Korteniemi J. Aittola M. Kostama V.-P. Hauber E. Kronberg P.
Neukum G. HRSC Co-Investigator Team
Fluvial Activity Resulted in Alluvial Fan in Icaria Planum, Mars **[#1299]**
The channel out of the Claritas paleolake led out water and deposited particles. Dust was washed away, particles were sorted and re-oriented. The alluvial fan can be identified by four-channel HRSC classification.

Di Achille G. Ori G. G. Reiss D. Hauber E. Gwinner K. Michael G. Neukum G. HRSC Co-Investigator Team
A Steep Fan at Coprates Catena, Valles Marineris, Mars as Seen by High Resolution Stereo Camera (HRSC) **[#1672]**
Using the new HRSC data, we present a sedimentological and morphometric analysis of an unusually steep and high fan-shaped deposit found into one of the secondary troughs associated to Coprates Catena, Valles Marineris, Mars.

Weitz C. M. Irwin R. P. III Chuang F. C. Bourke M. C. Crown D. A.
Formation of a Terraced Fan Deposit in Coprates Catena, Mars **[#1362]**
We favor a deltaic origin for the fan deposit, with the terraces representing erosion and re-distribution of material during each drop in lake level.

Kraal E. R. Moore J. M. Howard A. D. Asphaug E.
Martian Alluvial Fans: Prelimary Results from Southern Hemisphere Survey **[#1342]**
Preliminary results confirm that there is a distinctive grouping of three alluvial fan clusters originating from the rims of impact craters. We have also found several 'outlier' fans including geographically isolated fans and one in Capris Chasm.

Plescia J. B.
Acheron Fossae, Mars: Evidence of Fluvial Activity and Mass Flow **[#1488]**
Acheron Fossae is an arcuate block north of Olympus Mons. The Noachian surface displays fluvial, aeolian and mass flow modification. Mass flow features are suggested to be glacial or periglacial. Faulting and fluvial activity were contemporaneous.

Mangold N. Ansan V. Baratoux D. Masson P. Neukum G. HRSC Co-I Team
Identification of a New Outflow in the Syrtis Major Region, Mars **[#1802]**
HRSC images display erosional features such as valleys, grooves and tear-dropped islands suggesting a megaflood was once flowing over the lavas of Syrtis Major Planum, a location previously considered as composed by volcanic and eolian landforms only.

Lucchitta B. K.
Possible Secondary Aqueous Deposits in West Candor Chasma, Mars **[#1952]**
Possible channels with inverted relief on Ceti Mensa merge with a lobe of rounded, blocky deposits, suggesting that aqueous processes formed lobes on this ILD mound. Younger, finely layered materials in troughs below the mound may be secondary and eroded from the mensa.

Gaddis L. R. Skinner J. Hare T. Kirk R Titus T. Weller L. Neukum G.
Morphology and Morphometry of Ceti Mensa, West Candor Chasma, Mars **[#2076]**
We use high-resolution topographic data to examine the morphology and morphometry of Ceti Mensa (CM), a feature comprised of layered units on the floor of West Candor Chasma in the Valles Marineris (VM), Mars.

Wilson S. A. Howard A. D. Moore J. M.
The Geologic History of Terby Crater: Evidence for Lacustrine Deposition and Dissection by Ice **[#1863]**
The landforms in Terby Crater were likely deposited in a lacustrine environment when the circum-Hellas region may have been occupied by a body of water up to 3.6 km deep. The interior deposits were then subsequently dissected and modified by ice.

Ghatan G. J. Zimbelman J. R. Irwin R. P.
Oceans on Mars: A Search for Coastal Constructional Landforms Using THEMIS, MOC and MOLA Data **[#1916]**
We use THEMIS, MOC and MOLA data to search for coastal constructional landforms on Mars, possibly formed in association with a northern lowlands-filling ocean.

Lu X. Kieffer S. W.
A Comparison of Terrestrial and Martian Gravity Conditions on the Behavior of CO_2-driven Aqueous Flow **[#2011]**
Exsolution of small amounts of volatiles from discharging water can cause pulsing flow (geysering) on Mars (forming streamlined mesas in the Cerberus Plains). Martian gravity changes the properties of the pulses from terrestrial conditions.

Smith Z. E. Tullis J. A. Steele K. F. Malfavon L.
Martian Sinkholes: Implications for Large Scale Evaporite Deposits **[#1071]**
We believe that sinkholes can form on Mars and be used as evidence for regional deposition of limestone rather than the calcite cemented sandstone that is thought to be the dominant form of calcite deposition.

Bart G. D.
Comparison of Martian Gullies and Lunar Crater-Wall Landslides **[#1345]**
I present lunar landslides that resemble martian gullies, despite the lack of water on the Moon. Thus, gully features can be formed via dry landslides. On Mars, morphology alone is insufficient to determine the gully formation mechanism.

Ishii T. Miyamoto H. Sasaki S. Tajika E.
Constraints on the Formation of Gullies on Mars: A Possibility of the Formation of Gullies by Avalanches of Granular CO_2 Ice Particles **[#1646]**
Martian gullies are formed on the slopes with high inclination and their distribution seems to be consistent with distribution of seasonal condensation of CO_2 at high obliquity. This may suggest that gullies have been formed by avalanches of CO_2 ice.

Lanza N. L. Gilmore M. S.
Depths, Orientation and Slopes of Martian Hillside Gullies in the Northern Hemisphere **[#2412]**
Basic measurements of northern hemisphere gullies will be presented.

MARS SURFACE ICE

Gánti T. Bérczi Sz. Horváth A. Kereszturi A. Pócs T. Sik A. Szathmáry E.
Hypothetical Time Sequence of the Morphological Changes in Global and Local Levels of the Dark Dune Spots in Polar Region of Mars **[#1918]**
Our time sequence of DDS transformations was interpreted as phenomenon resulting from interaction of soil material participants, frosted cover of CO_2, soil grains, water ice, water adsorbed layer, and possible formations of martian surface organisms.

Rodriguez J. A. P. Tanaka K. L. Sasaki S.
Sources, Sinks and Migration Patterns of Dark Veneers in the North Polar Deposits of Mars **[#1437]**
We report on the geology of veneers of dark materials that commonly mantle the surfaces of layered deposits in the Martian north polar plateau. These features may help explain polar trough formation.

Lu R. Byrne S. Zuber M. T.
Seasonal Albedo Changes on Mars from MOLA Radiometry and TES: Seeking an Explanation for Apparent "Summer Snow" **[#1482]**
Radiometry data from the MOLA have identified an anomalous late summer brightening of the northern hemisphere of Mars. We investigate possible causes of this brightening and our results indicate water frost is the most likely brightening agent.

Chittenden J. D. Sears D. W. G. Chevrier V. Hanley J. Roe L. A.
Soil Effect on the Evaporation Rate of Pure Water Ice Under Martian Conditions **[#1054]**
In order to understand the possibility of increasing the likelihood of liquid water on the surface of ice on Mars, we have measured the effect of a 0–10 cm dust layer. We find that such a layer decreases the evaporation rate by a factor of 5.

Piqueux S. Christensen P. R.
Mapping the Exposed Water Ice and CO_2 Perenial Cap Around the South Pole of Mars with THEMIS Visible and Infrared Data **[#1163]**
The water and CO_2 ices and the material composing the polar layered deposits have different albedo and thermal characteristics. THEMIS visible and infrared data is also powerful for mapping polar material around the South Pole of Mars.

Zuber M. T.
Changes in the Masses of the Seasonal Polar Icecaps over 3 Mars Years **[#2083]**
The seasonal mass of carbon dioxide on Mars' polar ice caps has been derived from the Doppler and range tracking of the MGS spacecraft for a period of nearly 6 Earth-years.

Jian J. J. Ip W. H.
The Annual Cycle of CO_2 Snow Depth at Martian Polar Caps from MOLA Data **[#1777]**
North and south polar regions of Mars are affected by the CO_2 that stored in the atmosphere. In a seasonal cycle, 25% of the mass of the atmosphere has been estimated to exchange with the surface.

Jian J. J. Ip W. H.
Observation of the Martian Cryptic Region from Mars Orbiter Camera **[#1313]**
The distribution of the Martian south pole is not symmetric during the springtime retreat. On the opposite side of the residual cap a so-called cryptic region is found between latitudes 75° and 85° and longitude 150°W and 310°W.

Milkovich S. M. Plaut J. J.
Initial Results of Stratigraphic and Signal Analysis of the Mars South Polar Layered Deposits **[#1947]**
Fourier analysis and matching algorithms are applied to the south polar layered deposits using DN-depth profiles constructed from MOC, MOLA, and THEMIS data. Preliminary results include evidence for multiple climate signals recorded in the layers.

Pais D. Murray B. C. Pathare A. V. Byrne S. Chomko R. F.
The Peculiar Stratigraphy of Offset Troughs Within the Martian North Polar Layered Deposits — Evidence for Deformation? **[#1042]**
We present observations of curvilinear "wrinkle"-like layering exposed near the junctions of some offset troughs in the Martian North Polar Layered Deposits (NPLD). This may represent evidence of localized ductile deformation within the NPLD.

Fortezzo C. M. Tanaka K. L.
Unconformity Orientations in Planum Boreum, Mars: Preliminary Results and Interpretation **[#2277]**
Measuring the orientations of unconformities and mapping their locations in the PLD of Planum Boreum, Mars with the goal of understanding the relationship between unconformities and their adjacent layers and troughs in which they lie.

Xie H. Zhu M. Guan H. Smith R. K.
Isolated Water Ice in an Unnamed Crater Away from the Residual North Polar Cap of Mars: The Only One? **[#1764]**
This paper examined water ice patches in craters at high latitude regions of Mars but outside the residual polar caps using THEMIS time series visible and brightness temperature images.

Durham W. B. Pathare A. V. Stern L. A.
The Brittle-Ductile Transition in Mixtures of Rock and Ice: Experiments at Planetary Conditions **[#2036]**
The brittle-ductile transition in mixtures of rock and ice: Experiments at planetary conditions.

McGraw M. A. Light A. S. Travis B. J.
The Effect of Experimentally Determined Salt Viscosity on Convective Plumes in the Subsurface of Mars **[#2224]**
We examine how brines alter hydrothermal convection in the subsurface of Mars. The viscosity of the fluid was experimentally determined and then used for simulations. Results indicate that the two brines influence convection differently.

Pathare A. V. Koutnik M. Murray B. C. Marshall S.
Glacial Flow Modeling of the Martian North Polar Layered Deposits **[#2290]**
After adapting a three-dimensional terrestrial flow model to martian conditions, the effects of various surface mass balance scenarios upon present day flow patterns in the north polar layered deposits will be assessed.

Barnhart C. J. Asphaug E. Tulaczyk S.
Properties of Large Water-filled Crater Basins on Mars **[#2437]**
In this work we apply a critical examination to the possibility that the MARSIS detected subsurface feature in Chryse Planitia is a buried ice filled crater and explore its thermodynamic and gravitational properties.

MARS PERIGLACIAL AND GLACIAL PROCESSES

Levy J. S. Head J. W.
Evidence of Low Northern Midlatitude (~33°N) Valley Glacier Deposits Along the Dichotomy Boundary: Nilosyrtis Mensae, Mars **[#1244]**
New observations in the Nilosyrtis Mensae region of Mars detail: the transition from LDA to LVF in small alcove valleys, the processes involved LVF tributary confluence, and the development of LDA and LVF at low latitudes.

Levy J. S. Head J. W.
Lineated Valley Fill Surface Textures, Nilosyrtis Mensae, Mars: Comparison with Analagous Glacier Surface Textures in the Antarctic Dry Valleys **[#1245]**
We compare the lobate LVF feature observed in Nilosyrtis Mensae with the Mullins Valley debris-covered glacier, located in the Antarctic Dry Valleys. Cold-based glaciers in the hyper-arid, cold environments of the ADV are considered to be physical analogs for martian valley-glacial processes.

Head J. W. III Marchant D. R.
Modification of the Walls of a Noachian Crater in Northern Arabia Terra (24°E, 39°N) During Northern Mid-Latitude Amazonian Glacial Epochs on Mars: Nature and Evolution of Lobate Debris Aprons and Their Relationships to Lineated Valley Fill and Glacial Systems **[#1126]**
Modification of the walls of a Noachian-aged crater in northern Arabia Terra shows that lobate debris aprons and lineated valley fill form in intimate association as deposits of debris-covered glaciers during the Amazonian.

Marchant D. R. Head J. W. III
Glacial Landsystems on Mars: Integrating Landform Assemblages, Glaciations, and Climate Cycles **[#1422]**
The distribution of glaciers and deposits formed during build up, maturation, and sublimation of Miocene-age cold-based glaciers (Antarctic Dry Valleys) provides insight into the nature and origin of deposits thought to be of glacial origin on Mars.

Marchant D. R. Head J. W. III Kreslavsky M. A.
Mid-Latitude Glacial Modification of Moreux Crater (44°E, 42°N; 135 km): Evidence for Polythermal Glaciation Related to Impact-induced Enhanced Thermal Gradients **[#1425]**
Most northern mid-latitude glacial deposits are cold based. Wet-based glacial features are observed in Moreux crater, interpreted as a local thermal anomaly in the northern mid-latitude Amazonian cold polar desert thermal environment.

Head J. W. III Marchant D. R.
Evidence for Global-Scale Northern Mid-Latitude Glaciation in the Amazonian Period of Mars: Debris-covered Glacier and Valley Glacier Deposits in the 30°–50° N Latitude Band **[#1127]**
Analysis of the northern mid-latitudes (30°–50°N) reveals widespread lobate debris aprons and lineated valley fill that form as deposits of debris-covered glaciers and valley glaciers in the Amazonian during high-obliquity conditions.

Aittola M. Korteniemi J. Öhman T. Törmänen T. Raitala J.
Geology of Central Noachis Terra, Mars **[#1654]**
According to the preliminary study, Noachis Terra has been modified by several processes, which have characterized the unforeseeably varied geological history of the region.

Williams K. E. Toon O. B.
Stability of Mid-Latitude Snowpacks on Mars **[#1201]**
Mid-latitude snowpacks on Mars would have difficulty surviving from the last obliquity cycle. We have modeled the lifetime of a mid-latitude snowpack on a poleward slope and found that it will completely sublime in 5–20 years without melting.

Edlund S. J. Heldmann J. L.
Correlation of Subsurface Ice Content and Gully Locations on Mars: Testing the Shallow Aquifer Theory of Gully Formation **[#2049]**
We test the shallow aquifer theory of gully formation by calculating the temperature and pressure of the martian subsurface at the measured alcove base depths using measured GRS ice contents to determine if liquid water can exist at these locations.

Dickson J. L. Head J. W. Kreslavsky M. A. Marchant D. R.
Linear Lobate Debris Aprons, Piedmont-like Lobes, and Crater Fill in the Acheron Fossae Graben Region, Mars: Evidence for Debris-covered Glacier Formation and Flow **[#1321]**
The graben of Acheron Fossae contain linear lobate debris aprons (LDA) where slopes are low and lineated valley fill (LVF) and piedmont-like lobes on steeper slopes; post-graben craters host LDAs on pole-facing slopes.

Dickson J. Head J. W. Marchant D. R.
Modification of Graben Along the Dichotomy Boundary in Eastern Arabia Terra (Coloe Fossae; 53–59°E, 37–41°N): Nature and Evolution of Lobate Debris Aprons and Their Relationships to Lineated Valley Fill and Glacial Systems **[#1317]**
Linear lobate debris aprons (LDAs) form in Coloe Fossae, creating central breached folds; LDA/LVF transitions are common at the dichotomy boundary, supporting the presence of an integrated Amazonian glacial landsystem for this area.

Johnston J. G. Boston P. J. Stafford K. W.
Assessment of Karst Landform Potential on Mars **[#1980]**
A variety of possible Earth analogs are considered in the development of a new model of martian speleogenesis, and the conditions under which martian karst landforms might occur are discussed.

Wan Bun Tseung J-M. Soare R. J.
Thermokarst and Related Landforms in Western Utopia Planitia, Mars: Implications for Near-Surface Excess Ice **[#1414]**
We have identified polygon pits in western Utopia Planitia suggestive of terrestrial thermokarst landforms. We argue that the polygon pits are the result of periglacial processes and imply the presence of excess near-surface ice on Mars.

Williams R. M. E.
Latitude-dependence of Meter-Scale Surface Textures in Deuteronilus Mensae, Mars **[#1445]**
Meter-scale surface textures on lobate aprons and valley floors within the study region exhibit latitude dependence: knobby transitions to pitted terrain at higher latitudes. Observations suggest recent surface mantle degradation via ice sublimation.

Li H. Robinson M. S. Jurdy D. M.
Martian Southern Hemisphere Debris Aprons **[#2390]**
We surveyed the southern debris aprons near eastern Hellas region to understand their topographic and morphometric nature. By comparing the topographic characteristics of the southern and northern aprons, we seek to understand their development mechanisms.

van Gasselt S. Hauber E. Neukum G. HRSC Co-Investigator Team
Origin and Nature of a Debris-Tongue in Hellas Montes, Mars **[#2417]**
We here report on an investigation and new interpretation of a landform in Hellas Montes formerly described as avalanche deposit which has a more complex history than thought before and is connected to a newly discovered volcanic feature in the Hellas vicinity.

MARS GEOCHEMISTRY

Chevrier V. Chittenden J. D. Sears D. W. G.
The Stability of Sulfate-bearing Waters on Mars **[#1039]**
The evaporation process of sulfate-bearing brines is experimentally investigated. It is shown that when the solutions become highly concentrated, their evaporation rate slows down, which could stabilize them as a liquid form on Mars.

Vaniman D. T. Chipera S. J. Carey J. W.
Hydration Experiments and Physical Observations at 193 K and 243 K for Mg-Sulfates Relevant to Mars **[#1442]**
Hydration of kieserite and amorphous Mg-sulfate at 243 K progresses along simple pathways involving only hexahydrite and kieserite. Kieserite forms a duricrust-like cement, but the anhydrous precursor does not.

Chipera S. J. Vaniman D. T. Carey J. W.
Dehydration and Metastable States of Mg-Sulfate Hydrates that May be Present on Mars **[#1457]**
Mg-Sulfate-6H_2O was placed over 2, 11, 17, and 27% RH solutions at 75°C and the dehydration products were monitored with time. Hexahydrite dehydrates by recrystallizing sequentially through lesser-hydrated states before reaching the final monohydrate.

Tosca N. J. McLennan S. M.
Experimental Constraints on Evaporation Processes at Meridiani Planum **[#2260]**
A new experimental approach to evaporation processes on Mars is described. Solid and solution analyses from evaporation experiments related to Meridiani Planum are discussed.

Marion G. M. Kargel J. S. Catling D. C.
Modeling Ferrous/Ferric Iron Chemistry with Application to Martian Surface Geochemistry **[#1898]**
The objectives of this work were to (1) add ferric iron chemistry to an existing ferrous iron model (FREZCHEM), (2) extend ferrous/ferric iron geochemical models to lower temperatures (< 0°C), and (3) use the reformulated model to explore ferrous/ferric iron geochemistries on Mars.

Longhi J. Takahashi T.
Oceans on Mars: Whither Carbonate? **[#2455]**
Carbonate sediments are not necessary consequences of a martian water ocean under a CO_2 atmosphere.

Hintze P. E. Buhler C. R. Calle L. M. Calle C. I. Trigwell S. Starnes J. W. Schuerger A. C.
Degradation of Organics in a Glow Discharge Under Martian Conditions **[#2098]**
We present initial results on the degradation of organic material in a Mars gas glow discharge plasma. The plasma simulates the discharges that are likely to occur in Martian dust storms and may be a factor in the degradation of organic material.

Lefticariu L. Pratt L. M. Eng P. J. Gose S. K. Bish D. L.
Interaction of Radiolytically Produced Oxidants with the Pyrite Surface: A Crystal Truncation Rod (CTR) Study **[#2167]**
The interaction of radiolytically produced oxidants with pyrite surfaces could be one of the most significant chemical reactions occurring on Mars subsurface.

Archer P. D. Jr. Smith P. H.
The Effect of Impact Gardening and Impact-induced Pyrolysis on the Concentration of Organic Molecules on Mars **[#2262]**
The current concentration of organic material on Mars is a result of the rate of accumulation vs. the rate of destruction. This work investigates how impacts influence organic concentration.

Fernández-Remolar D. C. Prieto-Ballesteros O. Chemtob S. M. Morris R. V. Ming D. Knoll A. H. Hutchison L. Mustard J. F. Amils R. Arvidson R.
Geochemical Processes Driving the Rio Tinto Acidic Sedimentation: Insights into Sedimentary Sequences on Early Mars **[#1809]**
Geochemical and sedimentary processes observed in the Rio Tinto fluvial basin are used to elucidate those sedimentation mechanisms that originated the sulfate and silicate deposits of ancient Mars basins.

Fairén A. G.
Does Olivine Indicates Dry Conditions on Mars? **[#1645]**
The existence of liquid water on Mars has been debated following the discovery of olivine, as olivine readily alters in the presence of water. But this interpretation finds problems when is confronted to detailed analyses of olivine locations.

Fairén A. G. Amils R. Leandro F. Dohm J. M. Schulze-Makuch D. Rodríguez J. A. P.
Spherical Hematite Concretions in Meridiani Planum, Mars, and Monterde, Northeast Spain: An Analogue Aqueous Origin **[#1650]**
Hematite-enriched spherules, similar to those observed in Meridiani, have been found in Monterde, Spain. Their formation process involved subsurface and/or surface water transport and precipitation of iron in an ocean/land transitional environment.

Busigny V. Dauphas N.
Iron Isotopes in Spherical Hematite and Goethite Concretions from the Navajo Sandstone (Utah, USA): A Prospective Study for "Martian Blueberries" **[#1200]**
Iron isotopes of terrestrial hematite and goethite concretions provide clues on fluid transport, reservoir sizes, redox variations and biotic versus abiotic processes. This opens several avenues of research for future work on Martian blueberries.

Mahaney W. C. Milner M. W. Netoff D. I. Dohm J. Sodhi R. N. S. Aufreiter S. Hancock R. G. V. Bezada M. Kalm V. Malloch D.
Blueberries on Earth and Mars: Some Correlations Between Andean Paleosols, Geothermal Pipes in Navajo Sandstone and Terra Meridiani on Mars **[#1101]**
The origin of "blueberries" on Mars and their relationship to similar concretionary forms on Earth invokes a process of variable redox conditions in underground fluids. The possible role of microorganisms in the origin of bluberries opens an avenue for biological investigations.

Ormö J.   Souza-Egipsy V.   Chan M. A.   Park A. J.   Stich M.   Komatsu G.
Laboratory Experiments to Study Spherical, Iron Oxide Concretion Growth Without Solid Nuclei: Implications for Understanding Meridiani "Blueberries" **[#1356]**
Spherical hematite concretions can form without a nucleus. Self-organized zones of super-saturated solution cause spherical precipitates of amorphous iron-hydroxide. Diffusion of Fe ions towards the outer perimeter of the amorphous sphere forms a rind, which then grows inwards.

MARTIAN MINERALOGY

Sklute E. C.   Dyar M. D.   Schaefer M. W.
Mössbauer Spectroscopy of Olivines Across the Mg-Fe Solid Solution **[#2109]**
Variations in Mössbauer spectra of synthetic olivines across the compositional range from fayalite to forsterite are studied.

Lineberger D. H.   King D.   Shepard C.   Serafin S.   Moersch J. E.   Bandfield J. L.
Determination of Olivine Composition from Thermal Infrared Spectra **[#2091]**
Using the relationship between position of thermal IR absorption features and Fo content of terrestrial olivine samples, a quantitative model has been derived that predicts olivine compositions in Martian rocks.

Nicholis M.   Milliken R. E.   Mustard J. F.   Rutherford M.
VIS-NIR Spectral Properties of Olivine in a Basaltic Glass: Implications for Olivine-rich Terrains on Mars **[#2378]**
Basaltic glasses with varying amounts of olivine crystals are examined using NIR spectroscopy to study the effects of a glassy matrix on olivine identification.

Chemtob S. M.   Jolliff B. L.   Arvidson R. E.
Si- and Ti-rich Surface Coatings on Hawaiian Basalt and Implications for Remote Sensing on Mars **[#1443]**
This abstract reports on the composition, mineralogy and morphology of coatings on Kilauean basalt, as determined by Raman spectroscopy and electron microprobe methods. Implications for remote sensing of coated volcanic surfaces are also discussed.

Le Mouélic S.   Chevrier V.   Roy R.
Spectral Characterization of Weathering Products of Elemental Iron in a Martian Atmosphere: Implications for Mars Hyperspectral Studies **[#1172]**
We describe the evolution of visible and near-infrared spectra of metal iron alteration products obtained during a two-year weathering experiment in a H_2O-CO_2 simulated atmosphere.

Arlauckas S. A.   McLennan S. M.   Lindsley D. H.
The Effect of Low-Temperature Acidic Weathering on the Magnetic Signature of Primary Fe-Ti Oxides on Mars **[#1609]**
Low-T, pH alteration of Fe-Ti oxides readily yields magnetite and maghemite. Such ferrimagnetic minerals can be produced quickly and would have enhanced the magnetic signature on Mars however their presence may be veiled by homogenization.

Sharma S. K.   Misra A. K.   Ismail S.   Singh U. N.
Remote Raman Spectroscopy of Various Mixed and Composite Mineral Phases at 7.2 m Distance **[#2285]**
The remote Raman spectra of mixed and composite minerals show the ability of a portable remote Raman system to detect mixed mineral phases and the minerals underlying the transparent minerals from a distance of 7.2 m.

Schneider R. D.   Hamilton V. E.
Spectral and Compositional Variations Among Dark-toned Intracrater Features in Amazonis Planitia **[#1929]**
Spectral and compositional variations among dark-toned intracrater features in Amazonis Planitia are examined using data from MGS TES. We find that the features can be classified into two groups, a basaltic lithology similar to surface type I and a mafic-rich lithology.

Elteto A.   Toon O. B.
Using Sensitivity Matrix for Parameter Retrieval from Mars Global Surveyor Thermal Emission Spectrometer Data **[#1495]**
We use knowledge of first-order spectral response to variation of parameters for parameter retrieval from MGS TES data.

Michalski J. R. Ruff S. W. Christensen P. R. Cloutis E.
Thermal Emission Spectroscopy of Zeolite Minerals **[#1146]**
In this abstract, we discuss the infrared emission spectral characteristics of zeolite minerals — a potentially important group of minerals in chemical weathering environments on Mars.

Kraft M. D. Rampe E. Sharp T. G. Michalski J. R.
Thermal Emission Spectroscopy of Mixtures of Primary and Secondary Minerals Mixed in Controlled Experiments **[#2457]**
We are performing mineral mixing experiments to better understand the effects of thermal emission spectral mixing for spectra from weathered surfaces.

Kraft M. D. Michalski J. R. Sharp T. G.
Thermal Emission Spectral Modeling of Weathered Basalt Surfaces **[#2449]**
Mineral spectra from lightly weathered basalt surfaces mix nonlinearly, making it challenging to model primary and secondary mineralogy.

Presley M. A. Craddock R. A.
Thermal Conductivity Measurements of Natural Eolian and Fluvial Materials **[#2327]**
The results of thermal conductivity measurements of natural fluvial and eolian samples are presented. The larger particle sizes appear to control the thermal conductivity.

Presley M. A. Christensen P. R.
The Effect of Bulk Density on the Thermal Conductivity of Particulate Materials Under Martian Atmospheric Pressures **[#2383]**
The results of thermal conductivity measurements from several samples of various particle sizes and shapes over several different bulk densities will be presented. Under martian atmospheric pressures bulk density is a significant but minor effect.

Kuzmin R. O. Cristensen P. R. Zolotov M. Yu. Anwar S.
Mapping of Seasonal Bound Water Content Variations on the Martian Surface Based on the TES Data **[#1846]**
We presented the results of the global mapping of the seasonal bound water content variations on the surface of Mars based on the TES data collected during three martian years.

Kirkland L. E. Herr K. C. Adams P. M.
The Primary Uncertainties in Infrared Spectral Studies of Mars **[#1885]**
Currently, the same infrared remote sensing data sets are interpreted as pointing both to a "cold/dry Mars" and a "watery past." Here we explain the primary uncertainties in these data sets, and what work would reduce the current state of confusion.

McDowell M. L. Hamilton V. E. Riley D.
Effects of Weathering on TIR Spectra and Rock Classification **[#2016]**
Changes in mineralogy due to weathering are detectable in the TIR and cause misclassification of rock types. We survey samples over a range of lithologies and attempt to provide a method of correction for rock identification from weathered spectra.

Milam K. A. McSween H. Y. Jr. Moersch J. E. Christensen P. R.
The Accuracy of Derived Plagioclase Compositions from Multi-Component, Multi-Phase Sand Mixtures: Implications for Determining Martian Plagioclase Compositions **[#1156]**
Here we report the accuracy of derived plagioclase feldspar compositions from multi-phase mixtures analogous to typical martian lithologies.

Craig M. Cloutis E. A. Kaletzke L. McCormack K. Stewart L.
Alteration of Hydration Absorption Features in Reflectance Spectra of Selected Sulfates in a Low Pressure Environment: 0.45–4.3 μM **[#2112]**
Exposure of sulfates to a low pressure (0.01 Torr) carbon dioxide-rich atmosphere, and intense UV irradiation, results in significant and wide-ranging spectral changes. This has implications for the stability of sulfates on Mars.

Stewart L. Cloutis E. Bishop J. Craig M. Kaletzke L. McCormack K.
Classification of Iron Bearing Phyllosilicates Based on Ferric and Ferrous Iron Absorption Bands in the 400–1300 nm Region **[#2185]**
Iron-associated absorption features in a range of phyllosilicates show differences associated with the oxidation state of iron, in the 400–1300 nm range. However, no systematic variations are seen in the positions of these bands as a function of phyllosilicate structural type.

Lane M. D. Dyar M. D. Bishop J. L. King P. L. Cloutis E.
Laboratory Emission, Visible-near Infrared, and Mössbauer Spectroscopy of Iron Sulfates: Application to the Bright Paso Robles Soils in Gusev Crater, Mars **[#1799]**
The MER in Gusev crater has exposed in its tracks an unusual soil containing Fe(III)-sulfates at Paso Robles. Here we present a suite of Fe(III)-sulfate spectra measured using many spectroscopic techniques to identify the iron sulfate mineralogy.

Roush T. L. Esposito F. Rossman G. R. Colangeli L.
Gypsum Optical Constants in the Visible and Near-Infrared: Real and Imagined **[#1188]**
We compare gypsum optical constants (n and k), derived via two radiative transfer models (rtms), to independent and previously reported values. The rtms provide estimates of n and k in regions of weak absorptions, where previous models are insensitive.

Bishop J. L. Dyar M. D. Parente M. Drief A. Mancinelli R. L. Lane M. D. Murad E.
Understanding Surface Processes on Mars Through Study of Iron Oxides/Oxyhydroxides: Clues to Surface Alteration and Aqueous Processes **[#1438]**
Low-temperature oxidation and reduction reactions are being performed on hydrated ferric oxide minerals to investigate alteration under a variety of conditions on Mars. Samples are characterized with Mössbauer and visible-infrared spectroscopies.

Agresti D. G. Dyar M. D. Schaefer M. W.
Derivation of Velocity Scales for Mars Mössbauer Data **[#1517]**
An automated Windows-based procedure is introduced to calibrate the velocity of MER Mössbauer data, including correcting for velocity non-linearity and deriving the mm/s scale, which, along with spectral data, may be exported to file for later use.

Wang A. Freeman J. F. Jolliff B. L. Chou I. M.
Sulfates on Mars, a Systematic Raman Spectroscopic Study of Hydration States of Magnesium Sulfates **[#2191]**
The unique Raman spectral patterns and the systematic Raman peak shift permit accurate identification of the individual hydration states of Mg-sulfates from mixtures. These features were used to study the stability field and the pathway in de-/re-hydration processes of Mg-sulfates.

Sharma S. K. Chio C. H. Muenow D. W.
Raman Spectroscopic Investigation of Ferrous Sulfate Hydrates **[#1078]**
Our objective is to unambiguously distinguish between the mono-, tetra-, and heptahydrates of $FeSO_4$ that may be present on Martian surface. We have investigated these $FeSO_4$ hydrates with micro-Raman spectroscopy.

Jehl A. Pinet P. C. Cord A. Daydou Y. D. Baratoux D. Chevrel S. C. Manaud N. Greeley R. Kreslavsky M. A. Raitala J. Hoffmann H. Gwinner K. Scholten F. Roatsch T. Jaumann R. Neukum G. Mars Express HRSC Co-Investigator Team
Improved Surface Photometric Mapping Across Gusev and Apollinaris from an HRSC/Mars Express Integrated Multi-Orbit Dataset: Implication on Hapke Parameters Determination **[#1219]**
Surface physical properties derived from HRSC multi-angular observations are determined and mapped for different units (volcanic plains, wrinkled terrains and dark wind streaks) present on the northern part of Gusev and to the north, toward Apollinaris Patera.

Le Deit L. Le Mouélic S. Combe J.-Ph. Hauber E. Gendrin A. Sotin C. Mège D. Bourgeois O. Bibring J.-P. OMEGA Science Team
Geology of East Candor Chasma, Mars Inferred from Analysis of OMEGA and HRSC Data **[#2115]**
The analysis of the imaging spectrometer OMEGA data shows spectral signatures of ferric oxides in East Candor Chasma, Valles Marineris. The HRSC images are used to characterise the geomorphological context of the detected signatures.

Farrand W. H.   Lane M. D.
Multi-Dataset Analysis of Surface Units and Landforms on the Northern Plains of Mars **[#1499]**
Multiple orbital datasets are combined to constrain the origin of unusual surface units and small scale landforms on the northern plains of Mars. Relevance of these features to the action of water on the northern plains is considered.

Pinet P. C.   Clenet H.   Rosemberg C.   Ceuleneer G.   Heuripeau F.   Harris E.   Daydou Y.   Baratoux D.   Chevrel S. C.   Launeau P.   Combes J.-P.   LeMouélic S.   Sotin C.
Mantle Rock Surface Mineralogy Mapping in Arid Environment from Imaging Spectroscopy: The Case of Maqsad Peridotitic Massif in Oman and Implications for the Spectroscopic Study of Exposed Mafic Units on Mars **[#1346]**
We present an assessment of the derivation of the mafic mineralogy using MGM technique and orbital data on the Maqsad massif (OMAN) and the implications for the study of mafic environments from OMEGA data on Mars.

Kim K. J.   Boynton W. V.   Finch M.   Williams R. M. S.   Reedy R. C.   Drake D. M.
Effects of Rocks on Neutron and Gamma-Ray Production in Martian Surface Soil **[#2356]**
We studied the effects of a dry rock sitting on a 3% water-containing martian-surface soil on neutron and gamma-ray fluxes. Rocks with radii of ~25 cm and bigger significantly affect these fluxes and the flux ratios of certain gamma rays.

Drost C. A.   Wynne J. J.   Chapman M. G.   Kargel J. S.   Titus T. N.   Toomey R. S.
Remotely Sensed Cave Detection on Earth and Mars **[#2103]**
The goal of this project is to improve capabilities for identifying caves on Mars, through: 1) studies of thermal properties and imaging of terrestrial caves; 2) computer modeling of cave thermal properties; and 3) GIS-aided analysis of Mars imagery for cave-like structures.

Putzig N. E.   Mellon M. T.
Effects of Surface Heterogeneity on the Apparent Thermal Inertia of Mars **[#2316]**
Apparent thermal inertia from 3 Mars years of MGS-TES data shows seasonal and diurnal variations as large as 200–600 $J\ m^{-2}\ K^{-1}\ s^{-1/2}$ over most of the surface. We examine surface heterogeneity as the potential root cause for these variations.

Pitman K. M.   Bandfield J. L.   Wolff M. J.
MGS-TES Phase Effects and Thermal Infrared Directional Emissivity Field Measurements of Martian Analog Sites **[#1336]**
We present a set of on- and off-nadir thermal IR field and laboratory emissivity spectra for three undisturbed Mars terrain analog sites and analyze them for presence or absence of directional emissivity effects. Comparisons to moderate and low albedo surface MGS-TES EPF sequences are discussed.

Heggy E.   Carley R. A.   Pommerol A.   Clifford S. M.   Morris R. V.
Density, Temperature and Frequency Dependent Model of the Dielectric Map of Martian Surface **[#2140]**
We present laboratory electromagnetic characterization of Mars analog soils as a function of the density, temperature and frequency. The results are integrated to form a parametric dielectric map of the martian surface.

Stillman D. E.   Olhoeft G. R.
Electromagnetic Properties of Martian Analog Minerals at Radar Frequencies and Martian Temperatures **[#2002]**
EM properties of Martian analog minerals were measured at radar frequencies (using a vector network analyzer) and Martian temperatures. Grey hematite and magnetite possessed significant EM losses that could impact future Martian radar missions.

MARS INTERIOR

Redmond H. L.   King S. D.
Are Both the Tharsis Rise and the Crustal Dichotomy a Result of Dynamic Mantle Processes? **[#2152]**
We numerically investigate an edge-driven convective instability at the crustal dichotomy boundary as a mechanism to generate volcanism at Tharsis Rise using a 3D spherical geometry.

Williams J.-P. Nimmo F. Moore W. B.
The Formation of Tharsis: What the Line-of-Sight Data is Telling Us **[#2364]**
Effective elastic thickness values for Tharsis are derived from LOS acceleration profiles from MGS. Results indicate the bulk of Tharsis was emplaced in the Noachian with continued volcanic activity persisting in the western half of the region.

Anderson R. C. Dohm J. M. Haldemann A. F. C. Pounders E. Golombek M. P.
Tectonic Evolution of Mars **[#1883]**
Detailed stratigraphic and structural mapping indicates that the Tharsis rise of the western hemisphere and the formation of Isidis Planitia and the Elysium rise of the eastern hemisphere dominate the tectonic history of Mars.

King S. D. Redmond H. L.
How Can We Reconcile Mars Thermal History with the Crustal Dichotomy, Magnetic Field, and Tharsis Volcanism? **[#1927]**
The interior heat engine is the primary driving mechanism for planetary-scale tectonic and volcanic processes; hence it is important to understand whether our picture of Martian thermal evolution is consistent with these events.

Wdowiak T. J.
A New Mechanism for H_2O Precipitation on an Earlier Mars **[#1214]**
The eruption of ancient Martian volcanoes likely resulted in the atmospheric introduction of magmatic H_2O (as water vapor) and ash aerosol substrate for its prompt nucleation and condensation under presumed low temperature early environmental conditions, with fallout over the planet.

Kargel J. S. Begét J. E. Wessels R. Skinner J. E. Jr.
"Bottom → Up" Geothermal Interactions and "Top → Down" Climatic Interactions with Permafrost and Hydrates on Mars **[#2308]**
Geothermal and volcanic heating of permafrost and climatically driven thawing result in different sets of unique processes and features on Earth and probably also on Mars. These features and thermal models explaining them will be presented.

Parsons R. A. Hustoft J. W. Holtzman B. K. Kohlstedt D. L. Nimmo F.
Surface Tension-driven Melt Flow in the Upper Mantle: An Experimental and Modeling Approach to Studying Silicate Melt Diffusion Through an Olivine Matrix **[#2446]**
In this study we focus on modeling melt diffusion resulting from surface tension during the static anneal. By matching model results to experimental data, we are able to place constraints on variables governing surface tension-driven flow.

Khan A. Connolly J. A. D.
Constraining the Composition and Thermal State of Mars **[#1283]**
We inverted a set of geophysical data to constrain martian mantle composition and thermal state. We find a mantle composition similar to the pyrolite model, except for FeO. For the core, a composition of Fe 14 wt% S and of ~1600 km radius is favoured, while CMB temperatures suggest it to be fluid.

Roberts J. H. Zhong S.
Degree-1 Mantle Convection and the Origin of the Martian Hemispheric Dichotomy **[#1447]**
The hemispheric dichotomy on Mars may have been formed by degree-1 convection. 3D models with a layered viscosity structure can generate a one-plume structure within 100 My, quickly enough to be associated with the dichotomy.

Roberts J. H. Zhong S.
Polar Wander of Mars Driven by Degree-1 Mantle Convection and Its Implications for the Formation of the Crustal Dichotomy and the Tharsis Rise **[#1206]**
The geoid associated with degree-1 mantle convection places the plume at the equator, forming an east-west crustal dichotomy. A 30 km lithosphere makes the geoid negative, moving the plume to the pole, and the dichotomy to its present position.

MARS IMPACT CRATERING

Barlow N. G.
Status Report on the "Catalog of Large Martian Impact Craters", Version 2.0 **[#1337]**
The contents of the revised "Catalog of Large Martian Impact Craters" ("Catalog 2.0") are discussed and a status report of the revision is described.

Getzandanner K. M. Frey H. V.
Western Arabia Total Population Crater Retention Age: More Like Lowlands than Highlands **[#1968]**
The cratered terrain in Western Arabia has a total population crater retention age that is identical to that of the adjacent lowlands. In elevation and age it is more similar to the martian lowlands than to the rest of the global highlands.

Benignus C. Cassiani N. Dasgupta A. Nguyen D. Saribudak A. Saribudak E. Zychowski K.
Analysis of Rayed Craters on Mars **[#1486]**
We have examined the correlation between the diameter of rayed craters on Mars and the thermal inertia of the surrounding materials of the craters by using the THEMIS images of Gratteri, Zunil, Zumba, and Dilly.

Morgan G. A. Head J. W.
Relationship Between Impact Crater Deposits, Small Scale Channels and Lineated Valley Fill at the Dichotomy Boundary in the Northern Mid Latitudes **[#2008]**
The martian northern dichotomy boundary shows evidence of an integrated LVF system emerging from a single source area, and impact-induced melting of extensive snow/ice deposits under previous climatic regimes.

Matias A. Jurdy D. M.
Martian Mid-Latitude Craters with Unusual Rim Deposits: Evidence for Volatiles or Topographic Control? **[#1091]**
We examine three ejecta craters located within a 10-degree latitudinal band on the northern plains displaying an unusual deposit on their rims. The similarities of these features suggest an analogous formation processes for all of them, perhaps due to volatiles or topographic control.

Reiss D. Hauber E. Ivanov B. A. Michael G. Jaumann R. Neukum G. HRSC Co-Investigator Team
Rampart Craters in Thaumasia Planum, Mars **[#1754]**
We measured the onset diameter, ages, and depth-diameter ratios of rampart craters in Thaumasia Planum. The first results of this study suggest that the formation of rampart craters is connected to volatile rich periods in the Hesperian.

Kadish S. J. Barlow N. G.
Pedestal Crater Distribution and Implications for a New Model of Formation **[#1254]**
Pedestal craters in the martian northern hemisphere are small, occur at high latitudes, and impacted into volatile-rich material. These characteristics suggest formation in an ice-rich material which has subsequently undergone sublimation.

McConnell B. S. Newsom H. E. Wilt G. L. Gillespie A.
Circular Features Located on Lineated Terrain, Ismenius Lacus Region, Mars: Implications for Post-Impact Crater Modification Attributed to Sub-Surface Ice Deflation **[#1498]**
Modified impact craters on lineated terrains formed by impact into ice-bearing material followed by infill and subsequent sublimation of the ice, resulting in collapsed crater rims, single and multiple inner rings and central layered deposits.

Bacastow A. L. Sakimoto S. E. H.
Martian North Polar Crater Morphology: Implication for an Aquifer **[#2239]**
The largest martian north polar impact craters with pingo-like fill features imply the presence of a punctured aquifer.

Stewart S. T. Valiant G. J.
Martian Subsurface Properties and Crater Formation Processes Inferred from Fresh Impact Crater Geometries **[#2427]**
We infer the subsurface strength and parameters for crater and ejecta formation processes from resolved crater geometry measurements.

Lanagan P. D.
Paucity of <200-m-Diameter Craters in Vastitas Borealis, Mars, and Implications for Geomorphic Processes **[#2315]**
Martian northern plains. Show very few small craters. Creep may erase them.

Korteniemi J. Aittola M. Lahtela H. Öhman T. Raitala J.
Martian Floor-fractured Craters vs. Craters with Irregular Depressions **[#2145]**
On Mars craters with floor fractured and/or irregular depressions are linked to specific locations near the dichotomy boundary and giant impact basins. They provide information on the subsurface processes.

Lahtela H. Korteniemi J. Ori G. G. Pondrelli M. Di Lorenzo S. Neukum G. HRSC Co-Investigator Team
Enigmatic Features of a Crater in Arabia Terra, Mars **[#2114]**
This HRSC study discusses the characteristics of an enigmatic ~25 km crater, located at 36.0N°, 351.8E°, in Arabia Terra. It is either of volcanic or impact origin.

Peet V. M. Ramsey M. S. Crown D. A.
Terrestrial Volcanic and Impact Analogs to Small Martian Craters: Utilizing Remote Sensing and Field-Based Datasets to Analyze Formational and Sediment Transport Processes **[#2323]**
El Elegante Crater and Meteor Crater are studied to constrain formation and sediment transport processes. Block sizes and distributions, crater rim volumes, vegetation, and a broad range of remote sensing datasets are considered.

Mest S. C.
Characteristics of Impact Crater Interior Deposits in the Southern Highlands of Mars **[#2236]**
Impact craters (D>10 km) in the highlands of Noachis Terra display morphologies and features, and contain interior deposits that indicate a variety of geologic processes modified the craters subsequent to their formation.

Anderson R. B. Kiefer W. S. Frey H. V. Roark J. H.
Morphometry of Large Martian Impact Structures and Implications for Resurfacing Processes on Mars **[#2018]**
We compare the morphometry of pristine and partially filled large impact structures on Mars to constrain the amount of fill thickness in the filled craters. The resulting fill thickness map helps constrain resurfacing process on early Mars, including the importance of ballistically emplaced ejecta.

Cohen B. A.
Quantifying the Amount of Impact Ejecta at the MER Landing Sites and Potential Paleolakes in the Southern Martian Highlands **[#1043]**
Applying previous equations for impact ejecta thickness to Mars, tens of meters of ejecta are expected over the southern hemisphere. This is not enough to explain observed depth discrepancies in Gusev Crater or in other potential Martian paleolakes.

BOSUMTWI METEORITE IMPACT CRATER DRILLING PROJECT

Ugalde H. Morris W. A. Danuor S. K.
3D Vector Magnetics at Lake Bosumtwi: Experiment and Results **[#1064]**
The Bosumtwi impact crater was drilled in September–October 2004 as part of ICDP. During the drilling program an extended dataset of 3D vector magnetic data was collected throughout the lake. Here we present the first results of the experiment.

Deutsch A.
Lake Bosumtwi Drilling Project: Shock Metamorphism in Rocks from Core BCDP-8A vs. Experimental Data **[#1327]**
Recovery experiments with carbonaceous greywackes at 34, and 39.5 GPa confirm that the generally low shock levels recorded in lithologies inside the Lake Bosumtwi crater, are not due to specific petrophysical properties of this lithology yet may be caused by the obliquity of the impact.

L'Heureux E. Ugalde H. Milkereit B.
Seismic Parameters of Impactites from Physical Property Variations — Results from Bosumtwi Borehole Logs **[#1369]**
Sonic velocity and density logs from the Bosumtwi impact crater were analyzed in terms of their stochastic variations. Differences in scale parameters are used to explain the different seismic signatures observed between lithologies.

Schmitt D. R. Milkereit B. Karp T. Scholz C. A. Danour S. K. Meilleux D. Welz M.
Wellbore Seismic Studies in the Lake Bosumtwi, Ghana, Impact Structure **[#1503]**
Wellbore seismic data was acquired in one of the hard rock wellbores drilled into the central uplift of the Lake Bosumtwi impact structure. The observed velocities are lower than those anticipated for the protolith and may be evidence for impact induced damage to the material.

Brown M. Schmitt D. R. Milkereit B. Claeys P.
Porosity in Impact Damaged Rocks: Inferences from Scientific Drilling in the Lake Bosumtwi, Ghana, Impact Structure **[#1507]**
Porosities and grain densities are measured on core and nearby surface samples from the Lake Bosumtwi impact structure. Porosity ranges from nearly nil to as much as 40%. There does not appear to be any relationship between porosity and lithology as determined on the basis of grain density.

Elbra T. Pesonen L. J.
The Bosumtwi Impact Structure: Petrophysical, Paleomagnetic and Rock Magnetic Investigations of Impactites from BCDP-7A and BCDP-8A Deep Drill Cores **[#1578]**
In 2004, the Bosumtwi Crater Drilling Project, carried out by ICDP, was performed. Hereby, we report preliminary petrophysical, paleomagnetic and rock magnetic results of impact rocks obtained from BCDP-7A and BCDP-8A deep drill cores of Bosumtwi impact crater.

Petersen M. T. Newsom H. E. Moore D. M. Nelson M. J.
Preliminary X-Ray Diffraction Evidence of Hydrothermal Alteration in the Bosumtwi Impact Crater **[#2099]**
Petrographic evidence of post-impact clay formation and XRD evidence of illite clay with 2M structure in drill core samples from the central uplift of the Bosumtwi crater is consistent with the presence of a post-impact hydrothermal system.

Qian W. Milkereit B. Kück J.
Bosumtwi Rock Porosity Depth Profile as Inferred from the Resistivity Log **[#2345]**
Resistivity log data variations from borehole LB007A and LB008A can be attributed to porosity variations in the impactite sequence. The porosity derived from resistivity is in good agreement with other measurements.

ASTROBIOLOGY

Moores J. E. Smith P. H. Tanner R.
The Effect of Martian Surface Geometry on Ultraviolet Fluxes **[#2340]**
The effect of four different small scale geometries on localized ultraviolet surface fluxes is considered for differing latitudes and atmospheric conditions using a 1D atmospheric model.

Lerman L.
Prebiotic Chemical Evolution on an Early Mars: Consequences and Artifacts of "Organic" Weather Cycles in the Noachian **[#1566]**
The conditions for life to exist are not necessarily those needed for its origin. Could basic organic molecules on an early Mars have even come together to bring about life? This paper is the first attempt to build a "universal" theory of life's (potential) origin on a warmer, wetter younger Mars.

Cabrol N. A. Hock A. N. Sunagua M. Grin E. A.
Evolution of Aqueous Habitat and Life in High-Altitude Lakes During Rapid Climate Change: Astrobiological Methods and Geo and Biosignatures **[#1016]**
Microbialites are studied from the peak stage of a paleolake to the current water level. This continuum allows to track the increased pressure from extreme factors on habitat in the geological record in an environment analogous to early Mars.

Gleeson D. F. Pappalardo R. T. Grasby S. E. Spear J. R.
Borup Fiord: A Unique Glacial Environment of Astrobiological Significance and Potential Analogue to Europa Exploration **[#1854]**
Supraglacial sulfur-rich springs located in the High Canadian Arctic are abundant in microbes, and will offer insights into possible Europa microbial niches, surface chemistry, and movement of melt within ice.

De Gregorio B. T. Sharp T. G.
Possible Abiotic Formation of Kerogen-like Carbon in the Strelley Pool Chert **[#2318]**
Black chert veins near ancient stromatolites in the 3.45 Ga Strelley Pool Chert contain kerogen-like carbonaceous material. Although it is likely biogenic, Fischer-Tropsch-type processes may have also created this carbonaceous material.

Socki R. A. Gibson E. K. Jr. Bissada K. K.
Isotope Variations in Terrestrial Carbonates and Thermal Springs as Biomarkers: Analogs for Martian Processes **[#1014]**
Stable isotope measurements in terrestrial carbonates and methane are indicators of paleoenvironmental conditions and can be used as possible biomarkers when making isotope measurements on Martian carbonates.

Stivaletta N. Barbieri R. Bosco M. Ori G. G. Marinangeli L.
Microbial Communities from Continental Sabkhas of Southern Tunisia: Terrestrial Analogues of Mars Evaporite Environments **[#1608]**
We are conducting a comparative investigation of the microbial communities and their biosignatures from modern and fossil evaporite deposits of continental sabkha environments for evaluating what and how microbial products can be delivered to the fossil record.

Prieto-Ballesteros O. Fernandez-Remolar D. C. Gómez F. Torres J. Gómez Ortiz D. Kargel J. S. Gonzalez Pastor E. Fernandez Sampedro M. Martín Redondo M. P. Gonzalez de Figueras C. Gómez-Elvira J.
The Permafrost in the Imuruk Lake Basaltic Field (Alaska) as a Martian Permafrost Analogue **[#1524]**
We are studying the permafrost in the Imuruk lake volcanic area (Alaska) in order to define biosignatures in cold environments and develop new instrumentation for detecting life that may be used in future space exploration missions.

Gómez F. Gonzalez-Pastor E. Fernandez-Remolar D. C. Torres J. Gómez-Ortiz D. Fernandez-Sampedro M. Martin-Redondo M. P. Gonzalez de Figueras C. Gómez-Elvira J. Prieto-Ballesteros O.
Microbial Diversity on a Volcano-Sedimentary Mars Analog Permafrost: Imuruk Lake **[#1760]**
Due to Mars surface environmental conditions (oxidative stress, UV radiation) there are few chances for life on the surface of the red planet. Permafrost on earth is located at circumpolar latitudes. Of special interest is permafrost on volcanic areas due to the similarities with Mars geology.

Gómez F. Fernández-Remolar D. C. Prieto O. Rodríguez-Manfredi J. A. Rodríguez N. Amils R.
Mars Analogs on Earth: Putative Habitats on Mars? Lectures from Extremophiles **[#1793]**
Mineralogy studies by NASA Opportunity Rover report iron oxides and hydroxides precipitates on Mars. Sedimentary deposits have been identified at Meridiani Planum. These deposits should have been generated in a dune aqueous acidic and oxidizing environment. Similarities appear when we study Rio Tinto.

Szynkiewicz A. Pratt L. M.
Calibration of Contamination from Soil Organic Matter in Exposed Mantle Xenoliths — Preliminary Results **[#2088]**
Concentration and distribution of organic compounds in mantle xenoliths indicate that contamination by soil organic matter is not a simple process. Inhomogeneity and low porosity appear to limit penetration of contaminants.

Chafetz H. S.
Recognition of Bacterially Induced Mineral Precipitates: Examples from Carbonate, Silicate, and Mn- and Fe-rich Deposits **[#1844]**
Bacterially induced mineral deposits range from those fairly obvious on the outcrop to those in which the bacteria only occur as the nucleus around which precipitation is initiated. Nevertheless, all of these precipitates provide evidence for the former existence of bacterial life.

Bowden S. A. Wilson R. Parnell J. Cooper J. M.
Liquid-Liquid Extraction of Included Organic Compounds from Dissolved Sulphate Minerals Performed on a Microfluidic Format **[#1616]**
Sulfates are present on the surface of Mars and could have trapped organic compounds present in their parent solution. Extraction via a microfluidic device can recover fossil-lipid biomarkers from small quantities of sulfate bearing materials.

Schieber J.   Glamoclija M.   Schimmelmann A.   Thaisen K.
Snot, Sticks, and Lots of Water: Iron Microbes as Minimalist Architects **[#2004]**
Mat textures of iron microbes (Leptothrix) are based on open scaffold structure with water pockets. Efficiently constructed from sheaths and EPS, macroscopic/microscopic structures can be preserved by diagenetic mineralization or clay infiltration.

Glamoclija M.   Schieber J.
Biotic Contributions to the Formation of Submarine Iron-rich Hydrothermal Crusts near the Panarea Islands, Tyrrhenian Sea, Italy **[#1135]**
Iron-crusts from submarine hot springs from Tyrrhenian Sea contain a wide range of morphological features and geochemical signatures that resemble fossilized microbial life forms adapted to a harsh hydrothermal environment.

Hasiotis S. T.   Walton A. A.   Roberts J. A.   Goldstein R. H.
Distinguishing Between Trace Fossils as Organism-Substratum Interactions and Traces of Chemical Fingerprints from Life **[#1522]**
If life was once part or still part of the martian landscape or that of any other extraterrestrial body, an excellent chance exists for the preservation of this evidence in the form of trace fossils, as borings, biolaminates, and inclusions.

Zahnle K. J.   Abe Y.   Abe-Ouchi A.   Sleep N. H.
Dune: How Much Sunlight is Too Much? **[#2359]**
The planet Dune is a well-known fictional example of a very dry yet habitable planet. We show that the habitable zone for dry planets like Dune is bigger than the habitable zone for wet planets like Earth.

ten Kate I. L.   Garry J. R. C.   Peeters Z.   Foing B. H.   Ehrenfreund P.
Amino Acid Destruction in the Martian Surface Environment **[#2397]**
In this paper we present the results of experiments, in which thin films of glycine have been irradiated with UV in a CO_2 atmosphere, and cooled to an average martian surface temperature of 210 K.

Wirick S.   Flynn G. J.   Jacobsen C.   Keller L. P.
Organics in the Murchison Meteorite Using Carbon XANES Spectroscopy **[#1418]**
We analyzed the organics in the Murchison meteorite using carbon XANES. The sample is prepared by crushing and suspending fine particles of the meteorite in water. Three categories of carbonaceous compounds were found: water soluble organic, water insoluble organic, and water insoluble inorganic.

Golden D. C.   Ming D. W.   Lauer H. V. Jr.   Morris R. V.   Treiman A. H.   McKay G. A.
Formation of "Chemically Pure" Magnetite from Mg-Fe-Carbontes: Implications for Exclusively Inorganic Origin of Magnetite and Sulfides in Martian Meteorite ALH84001 **[#1199]**
Pure (Mg-free) magnetite was synthesized by heating Mg-Fe-carbonate at 350°C in the presence of pyrite in an evacuated sealed glass tube. The Mg-free magnetite in the black rims of ALH84001 may have formed by a similar inorganic abiotic process from Mg-Fe-carbonates.

Steele A.   Fries M.   Amundsen H. E. F.   Mysen B.   Fogel M.   Schweizer M.   Boctor N.
A Comprehensive Imaging and Raman Spectroscopy Study of ALH84001 and a Terrestrial Analogue from Svalbard **[#2096]**
We have undertaken a comprehensive Raman microprobe study of a depth profile of ALH84001 and a terrestrial analogue. We find that ALH84001 globules contain hematite as well as magnetite. Macromolecular carbon is always associated with magnetite both in the carbonates and in the bulk matrix.

Gibson E. K. Jr.   Clemett S. J.   Thomas-Keprta K. L.   McKay D. S.   Wentworth S. J.   Robert F.   Verchovsky A. B.   Wright I. P.   Pillinger C. T.   Rice T.   Van Leer B.
Observation and Analysis of In Situ Carbonaceous Matter in Nakhla: Part II **[#2039]**
Analysis of *in situ* carbonaceous matter in the Nakhla SNC meteorite has been carried out using a variety of techniques. Laser raman data shows the carbonaceous matter to be highly complex and static mass spectrometry has shown it to have an isotopic composition of –18 to –20‰ C.

PLANETARY CARTOGRAPHY

Clark C. S.   Stooke P. J.   Clark P. E.   De Hon R. A.
A More Topological Planetary Cartography: World Maps with Constant Scale Natural Boundaries (CSNB) **[#1207]**
A novel method of cartography is described and illustrated with constant scale natural boundary maps and folded forms of Earth, Mars and 433-Eros.

Dobinson E.   Curkendall D.   Plesea L.   Hare T. M.
Adaptation and Use of Open Geospatial© Web Technologies for Multi-Disciplinary Access to Planetary Data **[#1463]**
We are adapting the fast-developing and well-supported open geospatial standards and technologies, as defined by the Open Geospatial Consortium©, for the access, processing, and display of geospatial data to the planetary domain.

Archinal B. A.   Rosiek M. R.   Kirk R. L.   Redding B. L.
Completion of the Unified Lunar Control Network 2005 and Topographic Model **[#2310]**
A new Unified Lunar Control Network has been completed, unifying the previous ULCN and the Clementine LCN. Since point locations were solved for in 3D, this also comprises a new global topographic model for the Moon. Final analysis is underway.

Archinal B. A.   Tomasko M. G.   Rizk B.   Soderblom L. A.   Kirk R. L.   Howington-Kraus E.   Cook D. A.   Becker T. L.   Rosiek M. R.   Galuszka D.   Redding B. L.   Hare T. L.   DISR Science Team
Topographic Mapping of the Huygens Landing Site on Titan: New Results and Error Analyses **[#2089]**
A new DTM of the hills near the Huygens landing site on Titan is presented, as generated from five DISR images. We describe our investigation of possible error sources, such as from the merging of DTMs from stereo pairs and from camera calibration.

Curkendall D.   Hare T.   Anderson R.   Dobinson E.   Plesea L.
Mars GIS Landing Site Suitability Models **[#2110]**
We have explored the use of GIS suitability models for the screening and analyzing of potential sites for Mars landers using engineering and scientific constraints in an iterative and interactive manner.

Skinner J. A. Jr.   Hare T. M.   Tanaka K. L.
Digital Renovation of the Atlas of Mars 1:15,000,000-Scale Global Geologic Series Maps **[#2331]**
We have manually re-digitized the Viking-based 1:15M scale geologic maps using MDIM 2.1 and MOLA shaded-relief images as base images. These efforts have produced fully-registered geologic maps with structure and associated metadata.

Roark J. H.   Seifter A. B.   Frey H. V.
Enhancements to Gridview: Software for Topography Analysis **[#1434]**
Gridview is a software application designed to aid researchers in their efforts to analyze, measure and visualize gridded data products such a planetary topography. The application can be downloaded at http://geodynamics.gsfc.nasa.gov/gridview.

Gehrke S.   Lehmann H.   Köhring R.   Wählisch M.   Albertz J.   Neukum G.   HRSC Co-Investigator Team
Iani Chaos in Three Scales — A Topographic Image Map Mars 1:200,000 and Its Subdivisions **[#1325]**
The presentation will illustrate both quality of Mars Express HRSC image and DTM data as well as cartographic concept and flexibility of the standard map series. A regular sheet (200k) and two subdivisions in larger scales (100k and 50k) are shown.

Hare T. M.   Skinner J. Jr.   Liszewski E.   Tanaka K.   Barlow N.
Mars Crater Density Tools: Project Report **[#2398]**
Crater density plots provide researchers the means to interpret the age and geologic history of planetary surfaces. We have created a Mars crater density tools for the planetary community and provide a brief progress report.

Salamunićcar G.   Lončarić S.
Estimation of Ground Truth for Evaluation of Crater Detection Algorithms **[#1137]**
Catalogue of 17582 craters was assembled, wherein each crater is aligned with MOLA topography and confirmed by three independent sources. It can be used as ground truth in future evaluations of crater detection algorithms.

Salamuniććar G. Lončarić S.
Estimation of False Detections for Evaluation of Crater Detection Algorithms **[#1138]**
A method for estimation of false detections for crater detection algorithms is proposed. In combination with known ground truth and other available analyses, the proposed method can improve evaluation of crater detection algorithms.

Bue B. D. Stepinski T. F.
Machine Detection of Martian Craters from Digital Topography **[#1178]**
An automated crater detection algorithm based on Martian DEM data is developed and its performance is compared to the image-based catalog of Martian craters manually compiled by N. Barlow.

Oberst J. Hoffmann H. Matz K. D. Roatsch T. Wählisch M. Giese B. Neukum G.
New Observations of Phobos and Its Shadow with the HRSC/SRC on Mars Express **[#1312]**
The Mars Express spacecraft occasionally approaches the martian satellite Phobos. During 25 individual flybys Phobos was observed from ranges between 5000 km and 150 km. In addition, the Phobos shadow on the surface of Mars was captured on four occasions.

Hare T. M. Archinal B. Plesea L. Dobinson E. Curkendall D.
Standards Proposal to Support Planetary Coordinate Reference Systems in Open Geospatial Web Services and Geospatial Applications **[#1931]**
The abstract outlines a proposal to improve support for planetary coordinate reference systems within existing open geospatial standards and applications. This will help on-line and local mapping applications to recognize and share planetary data.

MARTIAN METEORITES: ALTERATION, ATMOSPHERES, AND APPLICATIONS

Stopar J. D. Taylor G. J.
Martian and Lunar Meteorites: Styles of Aqueous Alteration **[#1652]**
A preliminary analysis of the different styles of aqueous alteration found in martian and lunar meteorites. We study the terrestrial alteration of lunar meteorites as an analog for aqueous alteration on Mars.

Sefton-Nash E. Anand M. Dobson D. Vocadlo L. Williams T.
The Oxygen Balance of Primordial Mars: Oxygen Fugacity of Selected SNC Meteorites, Sub-Surface H_2O Inventory, the Martian Fe^{3+}/Fe^{2+} Ratio and the Implications for Biogenic Influences **[#1748]**
The oxygen balance of primordial mars: oxygen fugacity of selected SNC meteorites, sub-surface H_2O inventory, the martian Fe^{3+}/Fe^{2+} ratio and the implications for biogenic influences.

Herd C. D. K.
Fractionation of K, U and Th During Martian Aqueous Alteration: Insights from MIL 03346 **[#2079]**
In support of a Borehole Gamma Ray Spectrometry Concept Study, the distribution of K, U and Th were examined in the MIL 03346 martian meteorite. Preliminary results show that K is heterogeneously distributed among igneous and alteration phases.

Rost D. Vicenzi E. P. Fries M.
A Host for Lithium in MIL03346 and Implications for Aqueous Alteration on Mars **[#2362]**
In nakhlites, poorly crystalline clays formed by aqueous alteration on Mars show the highest Li contents. The finding of likewise enriched olivine in the MIL03345 mesostasis revokes the need for sources outside the nakhlitic flow(s) as explanation.

Fries M. Mysen B. Vicenzi E. Rost D. Steele A.
Hydrated Phosphates in Nakhlite MIL 03346 **[#2267]**
Phosphate minerals in MIL 03346 are found both as platy grains within the mesostasis and within inclusions in cumulate pyroxene crystals. These phosphates are hydrated but unsaturated in H_2O and contain a significant fraction of bound hydrogen.

Kennedy J. D. Harvey R. P.
Petrology and Mineral Chemistry of the Antarctic Ferrar Dolerite: Implications for Martian Meteorites **[#1689]**
The Ferrar dolerite provides an excellent terrestrial analog to martian igneous lithologies and surficial processes. These rocks are exposed to some of the coldest, driest conditions on Earth, and display similar weathering features found on Mars.

Walton E. L. Spray J. G. Herd C. D. K.
Melting Rocks by Shock: Localized Shock Melting in Martian Meteorites and Target Rocks from the Manicouagan Impact Structure **[#2025]**
Localized shock melting in lherzolitic shergottites have been compared to naturally shocked rocks from the Manicouagan impact structure. Manicouagan may provide important links that enable us to place the development of *in situ* shock melting in a spatial context within an impact crater.

Bérczi Sz. Hegyi S. Hudoba Gy. Józsa S. Szakmány Gy.
Planetary Analog Metarials Studies: Martian Shergottites and Their Counterparts from the Szentbékkálla Series of Mantle Lherzolite Inclusions and the Host Basalts in Hungary **[#1122]**
Several petrographic and genetic characteristics of the host basalt and its ultramafic inclusions of Szentbékkálla, Balaton Mts., Hungary are analogs to the range of the basaltic, picritic or olivine-phyric, and lherzolitic or peridotitic shergottites.

Nekvasil H. McCubbin F. Filiberto J.
Terrestrial Ferropicritic Dunites: Implications for the Chassignites **[#1096]**
Terrestrial ferropicritic analogs to the chassignites crystallized primarily at low pressure in spite of the presence of kaersutite and Ti-biotite. The chassignite mineralogy is more consistent with a higher pressure crystallization history.

Anand M. Russell S. S. Blackhurst R. Grady M. M.
Fe Isotopic Composition of Martian Meteorites and Some Terrestrial Analogues **[#1824]**
We report Fe isotopic composition of seven martian meteorites and other terrestrial materials that may be considered martian analogues.

Filiberto J. Nekvasil H. McCubbin F. Lindsley D. H.
Are Terrestrial Ferropicrites Analogues of Martian Rocks? **[#1081]**
The ferropicrites may represent close terrestrial analogues to the SNC meteorites. Their crystallization history, associated lithologies, and tectonic environment may provide invaluable information about Martian magmatic history.

McCubbin F. Nekvasil H. Lindsley D. Filiberto J.
The Chemical Nature of Kaersutite Experimentally Produced at 0 kbar **[#1097]**
Fluor-oxykaersutite with fluorine contents ranging from 3.5 wt% to 2 wt% was crystallized at 0 kbar. This suggests that kaersutite is stable over a wide pressure range and that its presence does not imply elevated crystallization pressure.

Norris J. R. Herd C. D. K.
The Yamato 980459 Liquidus at 10 to 20 Kilobars **[#1787]**
Piston-cylinder runs at pressures in the 10–20 kbar range give a liquidus for the Y980459 composition that is approximately 100°C less than previous work.

Beck P. Ferroir T. Gillet P. Montagnac G. Bohn M. Lesourd M.
Shock-Melting of Martian Basalts and the Entrapment of Atmospheric Gases **[#1939]**
We suggest here that melt pockets, which are commonly observed in shergottites, were formed by shock-induced melting of pre-existing porosity.

Park J. Nagao K.
New Insights on Martian Atmospheric Neon from Martian Meteorite, Dhofar 378 **[#1110]**
This is the first report of a reliable $^{20}Ne/^{22}Ne$ ratio obtained from a unique Martian meteorite Dhofar 378. The Ne shows clear evidence of very low $^{20}Ne/^{22}Ne$ ratio (7.3±0.1) for the present-day Martian atmosphere.

Parente M. Bishop J. L.
Deconvolution of Reflectance Spectra Using Nonlinear Least Squares Curve Fitting: Application to Martian Meteorites **[#1535]**
We present a novel spectral deconvolution model based on the description of absorption bands due to electronic transition processes in continuum-removed spectra. The model allowed discrimination of highly overlapping mineral bands in martian meteorites.

Head J. N.
Martian Meteorites and Cosmic Ray Exposure: Constraints on the Role of In-Space Breakup Events **[#1870]**
The number of martian meteorite (MM) launch events can be estimated from the cosmic ray exposure (CRE) and ages. Known CRE histories for MMs are difficult to reconcile with in-space breakup events. MM CRE ages are likely indicative of launch events.

MARTIAN METEORITES: ON THE ROCKS

Wittke J. H.   Bunch T. E.   Irving A. J.   Farmer M.   Strope J.
Northwest Africa 2975: An Evolved Basaltic Shergottite with Vesicular Glass Pockets and Trapped Melt Inclusions **[#1368]**
Yet another basaltic shergottite has been found in Algeria — an evolved martian lava containing partially crystallized melt inclusions.

Calvin C.   Rutherford M.   Sullivan N.
Comparing Primitive EETA79001 Melts with Those from Other SNC Meteorites **[#1697]**
The major and minor element chemistry of fused ground mass from EETA79001 lithology A is compared with rehomogenized melt inclusions from ALH 77005 in order to understand the petrogenesis of the shergottites.

Burgess K. D.   Musselwhite D. S.   Treiman A. H.
Experimental Petrology of Olivine-Phyric Shergottite NWA 1068: Toward Defining a Parental Melt **[#1972]**
We have determined experimentally the phase relations for the olivine-phyric basaltic shergottite NWA 1068 at martian upper mantle conditions. We have used these results to infer a model parent-melt composition for this important martian meteorite.

Nagao K.   Park J.   Bartoschewitz R.
Terrestrial Weathering Effects on Noble Gases of Martian Meteorites **[#1800]**
Noble gas compositions of weathering products are compared with those of martian meteorites. Terrestrial noble gases trapped on martian meteorites by weathering processes might be the "Chassigny-type" end member observed for some shergottites.

Thompson J. R.   Wiens R. C.   Clegg S. M.   Barefield J. E.   Vaniman D. T.   Newsom H. E.
Remote Laser Induced Breakdown Spectroscopy (LIBS) Analyses of DaG 476 and Zagami Martian Meteorites **[#1761]**
LIBS was selected as part of the ChemCam instrument package for the MSL rover. Here we investigate the ability of LIBS to remotely determine differences between basaltic rock types on Mars by analyzing two Martian basaltic shergottite meteorites in a simulated Martian environment.

Gaffney A. M.   Borg L. E.   Connelly J. N.
U-Pb Isotope Systematics of Shergottite Queen Alexandra Range 94201: Seeing Through Terrestrial Lead Contamination to Identify an Even Lower-Mu Source on Mars **[#1483]**
New U-Pb isotopic results for martian meteorite QUE 94201 show evidence for a very low-μ (<2) source in the martian mantle, as well as Pb contamination by Antarctic ice.

Rao M. N.   McKay D. S.   Wentworth S. J.   Garrison D. H.
Martian Brines: Clues from Sulfur and Chlorine in Salts from Some Martian Meteorites and MER Samples **[#1969]**
S and Cl in salts from Nakhla and from the gas-rich impact-melt ("grim") glasses in Shergotty and EET79001 suggest that these salts are produced from neutral-chloride and acid-sulfate solutions on Mars. Interaction with similar solutions generated salts occurring in Meridiani rock- rinds.

Chennaoui Aoudjehane H.   Jambon A.
Occurence of Post Stishovite in Shergottites NWA 856 and Zagami: A Cathodoluminescence Study **[#1036]**
We used cathodoluminescence images and spectra for identifying silica phases: High pressure silica glass, stishovite and particularly post stishovite in shergottites NWA 856 and Zagami. CL appears an easy and powerful technique especially for post stishovite.

Chennaoui Aoudjehane H. Jambon A. Boudouma O.
Cristobalite and K-Feldspar in the Nakhlite MIL03346: A Cathodoluminescence Study **[#1037]**
We used cathodoluminescence images and spectra for identifying cristobalite and K-feldspar in the mesostasis of MIL03346 nakhlite. The presence of cristobalite suggest that the shock intensity in MIL03346 is low in agreement with that of other nakhlites, much weaker in comparison to shergottites.

Makishima J. McKay G. Le L. Miyamoto M. Mikouchi T.
Calibration of the Eu Oxybarometer for Nakhlites **[#1589]**
We report preliminary results of our experimental calibration of the depth of Eu anomaly in pyroxene vs. oxygen fugacity for nakhlites. Our results suggest that Nakhla may have formed under fairly reducing conditions.

Mikouchi T. Miyamoto M. Koizumi E. Makishima J. McKay G.
Relative Burial Depths of Nakhlites: An Update **[#1865]**
We updated our model of the nakhlite igneous body in terms of their relative burial depths. Olivine chemical zoning gave burial depths of 1–2 m for NWA817, 4 m for MIL03346, 7 m for Y000593, 10 m for Nakhla/Gov. Val. and >30 m for Lafayette/NWA998.

McKay G. Mikouchi T. Schwandt C.
Additional Complexities in Nakhlite Pyroxenes: A Progress (?) Report **[#2435]**
Al zoning in nakhlite pyroxenes correlates with cooling rate. Melt inclusions occur predominately in Al-rich zones. These observations are puzzling. If zoning formed in the magma chamber, why does it correlate with post-eruption cooling rate?

McCanta M. C. Dyar M. D. Treiman A. H. Pieters C. M. Hiroi T. Lane M. D. Bishop J. L.
Mössbauer and Synchrotron MicroXANES Analysis of NWA2737 **[#1751]**
We report on the distribution of Fe^{3+} between the mineral phases in NWA 2737 as measured with Mössbauer and synchrotron microXANES spectrometry. The brown olivine in NWA 2737 implies that it has been subject to different processes than Chassigny.

Mohapatra R. K. Crowther S. A. Gilmour J. D. Marty B.
Xenon Isotopic Components in NWA 2737 — A Chassignite from the Hot Desert **[#1840]**
We present here preliminary xenon isotopic data from mineral separates from a 10 mg sample of NWA 2737, and discuss their implications for the volatile components in this meteorite.

Reynard B. Beck P. Barrat J.-A. Bohn M.
Pyroxene Crystal-Chemistry and the Late Cooling History of NWA 2737 **[#1963]**
The chassignite NWA 2737 display a specific pattern of pyroxene compositions with Fe/Mg ratios following equilibrium tie-lines. This pattern can be explained in the context of late crystallization in the interstitial liquid of a dunitic cumulate, and sets constrains on the late cooling history.

Bogard D. D. Garrison D. H.
Ar-Ar Dating of Martian Chassignites, NWA2737 and Chassigny, and Nakhlite MIL03346 **[#1108]**
Ar-Ar ages determined for chassignites Chassigny and NWA2737 and nakhlite MIL03346 are ~1.35 Gyr and are similar to various radiometric ages reported for these martian meteorites and for other nakhlites.

Domeneghetti M. C. Fioretti A. M. Camara F. Molin G. McCammon C.
Constraints on the Thermal History and Oxidation State of MIL03346 Martian Meteorite: Single-Crystal XRD, Electron Microprobe and Mossbauer Analyses of Clinopyroxene **[#1238]**
Augite from MIL03346 was studied by single crystal X-ray diffraction, electron microprobe and single crystal Mössbauer spectroscopy to measure the Fe^{2+}-Mg order degree and to retrieve information on thermal history and redox state of this meteorite.

Domeneghetti M. C. Fioretti A. M. Camara F. Molin G. Tazzoli V.
Closure Temperature of Fe^{2+}-Mg Ordering in Orthopyroxene: Implications for Thermal History of ALH84001 Meteorite **[#1237]**
The closure temperature of Fe^{2+}-Mg ordering state, expressed by kD, was calculated in ALH84001 orthopyroxene using X-ray single-crystal diffraction and electron microprobe data.

Gildea K. J.   Holland G.   Lyon I. C.   Chatzitheodoridis E.   Burgess R.
High Calcium (~80mol%) Late Stage Carbonate in ALH84001 **[#1776]**
Brief petrological, chemical and textural description of previously undescribed high Ca late stage carbonate in Martian meteorite ALH84001. This carbonate surrounds Mg rich carbonates and rosette fragments.

Schwenzer S. P.   Ott U.
Evaluating Kr- and Xe-Data in the Nakhlites and ALHA84001 — Does EFA Hide EFM? **[#1614]**
We evaluate the noble gas components contributing to the nakhlite Lafayette, estimate the Kr/Xe ratio of fractionated martian atmosphere and apply our results on literature data and a model taken from petrological studies.

Morlok A.   Anand M.   Grady M. M.
Dust from Collisions: Mid-Infrared Absorbance Spectroscopy of Martian Meteorites **[#1512]**
Mid-infrared transmission/absorbance spectra of a representative range of martian meteorites are presented. The data is used for mineralogical bulk studies, but also for the comparison with astronomical dust spectra.

HIGH ON CARBS

Huber H.   Rubin A. E.   Wasson J. T.
Bulk Compositions and Petrographic Characteristics of Ten Unusual Carbonaceous Chondrites **[#2381]**
We used INAA to determine the bulk compositions of 10 carbonaceous chondrites of uncertain classification. Thin sections were examined microscopically. Averaged results of duplicate analysis and Mg- and Cr-normalized abundance patterns show clear identifications for four specimens.

Chizmadia L. J.   Bendersky C. N.
Asuka-881632: The First CO3.1? **[#2255]**
AOAs in the CO3 chondrite, A-881632, contain forsteritic olivine ($Fa_{1.4}$) and 0.8 µm Fe-olivine veins. The olivine composition and vein thicknesses in AOAs is intermediate between 3.0 and 3.2 and is consistent with what was predicted for a 3.1 by Chizmadia et al. (2002).

Berlin J.   Jones R. H.   Brearley A. J.
Determining the Bulk Chemical Composition of Chondrules by Electron Microprobe: A Comparison of Different Approaches **[#2370]**
In this abstract, we point out problems with various electron microprobe methods that have been used to determine bulk chemical compositions of chondrules.

Bloom J. L.   Bland P. A.   Kearsley A. T.   Watt L. E.
Studies of Minor Phases in Primitive Chondrite Matrix **[#1714]**
We use large, high-resolution ED maps of primitive chondrites to constrain the nature of trace and minor element carrier phases in matrix. These data are relevant to understanding condensation, and volatile depletion in the early solar system.

Fries M.   Butterworth A.   Snead C.   Steele A.
Complementary STXM and Confocal Raman Imaging of Murchison CM2 Particle Embedded in Sulfur **[#2419]**
Scanning transmission X-ray microscopy (STXM) and confocal Raman imaging have been utilized on a sample of the Murchison CM2 meteorite in order to examine the structure and composition of carbonaceous material with a minimal degree of alteration due to sample preparation.

Ivanova M. A.   Lorenz C. A.   Greenwood R. C.   Franchi I. A.   Nazarov M. A.   Morris A. A.   Baker L.   Brandstaetter F.
Experimental Study of Laboratory-heated CM2 Chondrites Mighei and Murchison **[#1086]**
We conducted experimental heating of two CM2 chondrites, Murchison and Mighei, to study changes in their oxygen isotopic compositions and mineralogy and explore possible genetic relationships between MCCs and normal CMs.

Komatsu M. Fagan T. Miyamoto M. Krot A. N. Mikouchi T.
Amoeboid Olivine Aggregates in the Yamato-86009 CV3 Chondrite **[#1523]**
Based on the mineralogical study of AOAs in Y-86009, we infer that AOAs in Y-86009 were originally similar to those in reduced CVs, and subsequently experienced low-temperature aqueous alteration; they largely escaped Fe-alkali metasomatic alteration.

Sugiura N. Miyazaki A. Hiyagon H. Kimura K. Petaev M. I.
Nebular History of Amoeboid Olivine Aggregates **[#1266]**
Trace element (Ca, Cr and Mn) concentrations were measured in amoeboid olivine aggregates in Acfer 094 and Yamato 81020. Cr and Mn concentrations are negatively correlated with Ca concentrations.

Butterworth A. L. Benedix G. K. Tamura N. Menzies O. N. Bland P. A.
Chondrule Olivine: Relationship Between Structure and Composition Using Synchrotron X-Ray Laue Microdiffraction **[#2144]**
The composition, crystal orientation and strain of a chondrule zoned olivine in EET 83389 (CM2) was mapped using microfocus, white beam synchrotron XRD.

Neff K. E. Righter K.
Opaque Assemblages in CK and CV Carbonaceous Chondrites **[#1320]**
Using the oxide, metal and sulfide assemblages of CK and CV chondrites, constraints can be placed on the temperature and oxygen fugacity at which the meteorites equilibrated, which can be compared in order to help define their formation history.

Nakamura T. M. Sugiura N. Kimura M. Miyazaki A. Krot A. N.
Condensation and Accretion of Corundum and Corundum-Hibonite Grains in the Solar Nebula **[#1267]**
Accretion of corundum aggregates in the solar nebula was investigated. In a monotonically cooling nebula with a solar composition, formation of such aggregates is difficult because hibonite is formed on corundum grains before formation of aggregates.

Tronche E. J. Hewins R. H. MacPherson G. J.
Formation Conditions of Aluminium-rich Chondrules **[#1159]**
Dynamic crystallization experiments have been performed with five synthetic Al-rich chondrules compositions. For natural Al-rich chondrules, peak temperatures of ~1400°–1500°C (up to 1600°C for Al-rich BO) and cooling rates of 50°–1000°C/hr are appropriate.

Paque J. M. Burnett D. S. Beckett J. R. Hutcheon I. D. Weber P. K.
Origin of Trace Elements in Spinel from Ca-Al-rich Inclusions: Constraints from NanoSIMS Analyses of Spinel and Enclosing Melilite **[#1823]**
Ti valence state changes during initial crystallization appears to be the most plausible explanation for the center peaked Ti zoning profiles in spinel. Preliminary NanoSIMS analysis did not reveal any direct evidence for diffusion of trace elements from spinel to the melilite.

Hiyagon H. Sasaki M.
Rare Earth Element Abundances in Refractory Inclusions from Y-81020 (CO3.0) Chondrite: Evidence of REE Fractionation Under Variable Conditions **[#1514]**
REE analyses were performed for refractory inclusions from Y-81020 chondrite. One inclusion shows HREE-depletion with large positive anomalies in Eu and Yb. Fractionation conditions to produce such REE patterns are discussed.

Krot A. N. Ulyanov A. A. Ivanova M. A.
Refractory Inclusions and Aluminum-rich Chondrules in the CB/CH-like Carbonaceous Chondrite Isheyevo **[#1226]**
The CAIs and Al-rich chondrules in Isheyevo are texturally and mineralogically similar to those in other previously studied CH chondrites and to a lesser degree to those in the CB chondrites and different from those in CO, CM, CR, and CV chondrites.

Plagge M. Ott U. Hoppe P.
Search for Extinct Chlorine-36 in an Allende CAI **[#1287]**
Using the Nano-SIMS, we have searched for enhanced ^{36}S abundances due to decay of shortlived ^{36}Cl ($T½ = 0.3$ Ma) in sodalite grains from a fine-grained Allende CAI. With $^{35}Cl/^{34}S$ ranging up to ~30,000, no evidence was found.

Ushikubo T. Guan Y. Leshin L. A.
^{10}Be-^{10}B Systematics of Hibonite-bearing Inclusions from Murchison (CM2) and Kainsaz (CO3) **[#2368]**
^{10}Be-^{10}B systematics of hibonite inclusions were measured. Although their δ^{50}Ti range from –20‰ to +20‰, all the samples tend to show ^{10}B-excesses.

Fujii T. Moynier F. Telouk P. Albarède F.
Mass-independent Isotope Fractionation of Molybdenum and Ruthenium in Murchison **[#1656]**
We propose that isotopic anomalies of Mo and Ru found in Murchison (CM2) may be due to the nuclear field shift effect. This shift results from a mass-independent character via the nuclear charge distribution.

Quitté G. Zanda B. Halliday A. N. Latkoczy C. Günther D.
Search for ^{60}Fe in Chondrules from Allende and Tieschitz **[#1856]**
A new technique using MC-ICPMS permits to measure Ni isotopes with high precision in individual chondrules. Allende (CV3.7) and Tieschitz (H3.6) chondrules generally show no ^{60}Ni-excess because Fe and Ni have been redistributed during metamorphism.

Sugiura N. Krot A. N.
Al-Mg Dating of Ca-Al-rich Inclusions in Acfer 094 Chondrite **[#1265]**
Al-Mg dating of Ca-Al-rich inclusions in Acfer 094 chondrite was made. Out of 14 CAIs, 11 show nearly canonical initial ^{27}Al/^{27}Al ratios, whereas 3 show no resolvable excesses in ^{26}Mg.

Schoenbeck T. W. Kleine T. Irving A. J.
Chemical and Hf-W Isotopic Composition of CV Metachondrite NWA 3133 **[#1550]**
We present petrographic features, mineral composition, oxygen isotopes, bulk chemistry and Hf-W data of the metachondrite NWA 3133. This data suggests that NWA 3133 formed from a CV chondrite precursor and was metamorphosed early in the solar system.

Shahar A. Young E. D.
Silicon Isotope Ratios in CAIs: In-Situ Laser-Ablation MC-ICPMS Measurements and Comparisons with Magnesium Isotope Ratios **[#1493]**
In-situ Si isotope ratios were measured in an Allende CAI using LA-MC-ICPMS and the results were compared with Mg isotope ratios. The new Si isotope data constrain parameters related to the diffusion of Si isotopes in CAI liquids.

de Leuw S. Wasson J. T. Rubin A. E. Papanastassiou D. A.
Petrographic Search for the Carriers of Isotopically Anomalous Chromium in Carbonaceous Chondrites **[#1352]**
Electron probe studies were performed on a thin section from the Kainsaz meteorite in order to identify phases for Cr isotopic studies with the purpose of identifying the carrier phase of the observed ^{54}Cr anomalies in carbonaceous chondrites.

Jogo K. Shih C.-Y. Reese Y. D. Nyquist L. E.
^{53}Mn-^{53}Cr Systematics of R-Chondrite NWA 753 **[#1518]**
We report the study of the Mn-Cr systematics of the R-chondrite NWA753. The conclusions are an initially heterogeneous distribution of ^{53}Mn in the early solar system, or variations in initial Cr-isotopic compositions, possibly correlated to O-isotope variations.

Koiwa Y. Shirai N. Ebihara M.
Fractionation of Platinum Group Elements in Carbonaceous Chondrites **[#1928]**
We analyzed platinum group elements (PGEs: Os, Ir, Ru, Pt, Rh and Pd) in carbonaceous chondrites. We consider whether the PGEs data indicate the record of nebula conditions and processes.

Yamamoto Y. Nakamura T. Noguchi T. Okazaki R. Nagao K.
Temperature Dependence of Mineralogical and Noble Gas Compositional Changes During Experimental Aqueous Alteration of Ningqiang **[#1520]**
Aqueous alteration experiment of Ningqiang carbonaceous chondrite at 100°C and 200°C shows that mineralogical and noble gas compositional changes during aqueous alteration greatly depend on the temperature of alteration.

Bonal L. Rouzaud J.-N. Quirico E.
Metamorphic Control of Noble Gas Abundances in Pristine Chondrites **[#1792]**
The structure and texture of IOM was studied by HRTEM in Kaba, Leoville, Mokoia, Allende,Tieschitz. We revisit the question of the metamorphic control of the Q (P1), P3 and P6 components, the carrier of the Q phase.

Yabuta H. Cody G. D. Alexander C. M. O'D.
Quantitative Study of Ether Group Molecules in Insoluble Organic Matter from Carbonaceous Chondrites by CuO-NaOH Selective Degradation **[#1820]**
CuO-NaOH degradation of the insoluble organic matter (IOM) from the Murchison meteorite was conducted. A variety of carboxylic acids were indentified. Oxalic acid was most abundant. It was estimated that approximately ~30% of the IOM included ether groups containing molecules.

Derenne S. Rouzaud J.-N. Robert F. Pizzarello S.
Polyaromatic Units from Tagish Lake Insoluble Organic Matter **[#1251]**
Aromatic units in Tagish Lake insoluble organic matter are of similar size as those of Orgueil and Murchison in spite of a higher aromaticity.

Huang Y. Alexandre M. R. Wang Y. Brearley A. J. Cody G. Alexander C. M. O'D.
Molecular and Isotopic Distributions of Aliphatic Side Chain Carbonaceous Chondrites **[#2122]**
The aim of this work is to understand the chemical structures and isotopic variations of the aliphatic side chains in the Insoluble Organic Matter (IOM) of different meteorites.

Okazaki R. Nakamura T.
Mineralogy and Oxygen Isotopes of Unmelted Antarctic Micrometeorites **[#1510]**
We report mineralogical characteristics and oxygen isotope compositions determined for unmelted micrometeorites collected from Kuwagata Nunataks in Antarctica.

ORDINARY AND ENSTATITE CHONDRITES

Schoenbeck T. W. Zipfel J. Palme H.
Bulk Chemistry of Carbonaceous and Ordinary Chondrites, A Comparison **[#1817]**
New XRF data for ordinary and carbonaceous chondrites indicate lower Cr for L and LL chondrites. This allows calculation of the Cr of the removed metal. Differences in Al/Ti between OC and CC suggesting the addition of a Ti-rich component in OC.

Sandel L. E. Strait M. M. Durda D. D. Flynn G. J.
Methods for Quantifying Results of Impact Disruption Experiments of Chondritic Meteorites **[#1359]**
Data from impact experiments on meteorites and meteorite simulants was processed and analyzed to look for patterns. Foils were measured using a computer program and meteorite remnants were sieved and weighed. Both sets of data are discussed.

Kohout T. Kletetschka G. Pesonen L. J. Wasilewski P. J.
Magnetic Studies of Avanhandava H4 and Bjurböle L4 Chondrules **[#1601]**
The laboratory study shows that the chondrules of Avanhandava H4 and Bjurböle L4 chondrites show randomly oriented magnetizations. This suggests that the magnetizing event (5–45 μT) occurred before aggregation of those meteorites.

Adachi T. Kletetschka G. Wasilewski P. J.
Magnetic Record of Bjurbole Meteorite — Preliminary Report **[#2205]**
The magnetic record of the Bjurbole meteorite suggests the absence of a recordable magnetic field during matrix formation. Chondrules indicate a large range of paleofields, perhaps indicating distance from the nebula during chondrule formation.

Cervantes-de la Cruz K. E. Ortega-Gutiérrez F.
The Mexican Meteorite Nuevo Mercurio (H5): Characteristics of Chondrules **[#1198]**
A study of the chondrules of Nuevo Mercurio (H5). There are some primary characteristics that can be observed, such as the relationship between chondrule size and their texture, and presence of opaque minerals (troilite and/or Fe-Ni alloys).

Niemeier M.   Bischoff A.
Glanerbrug — An LL4–6 Fragmental Breccia with Huge L Chondritic Clasts **[#1625]**
Glanerbrug is a very complex fragmental breccia and has been previously classified as an LL breccia or L/LL5 chondrite. We classify Glanerbrug as an LL4–6 fragmental breccia with huge L-chondritic clasts.

Dunaway J. K.   Moersch J.   Taylor L. A.
Petrogenesis and Potential Pairing of the Kunashak and Park Forest Chondrites **[#1891]**
The Kunashak L chondrite is characterized and compared to the Park Forest chondrite.

Pack A.   Hezel D.
Phase Relations in Two Na- and Al-rich Chondrules and the Formation of the Chondrule Precursor Material **[#1353]**
We present chemical and mineralogical evidence for a primary origin in two Na- and Al- rich chondrules from ordinary chondrites.

Llorca J.   Trigo-Rodríguez J. M.
Raman Spectroscopy of Merrillite in Villalbeto de la Peña L6 Ordinary Chondrite **[#1055]**
Ca-phosphates were studied by means of Raman spectroscopy in the Villalbeto de la Peña L6 chondrite, which fell recently in Spain (2004). The presence of merrillite in the shock veins of the meteorite indicates that it was not severely shock-metamorphosed.

Nettles J. W.   McSween H. Y. Jr.
A Comparison of Metal-Troilite Grain Size Distributions for Type 3 and Type 4 Ordinary Chondrites Using X-Ray CT Data **[#1996]**
We compare mean metal-troilite grain volumes of type 3 and 4 ordinary chondrites using X-ray CT data to quantify grain coarsening between these two petrologic types.

Tronche E. J.   Mostefaoui S.   Meibom A.   Robert F.   Sautter V.   Guilhaumou N.   Libourel G.   Duhamel R.
Chondrule Thermal History: An Approach Based on NanoSIMS Analysis of Short Diffusion Profiles in Melt Inclusions **[#1644]**
NanoSIMS technique has been used to constrain diffusion profiles in small (<15 μm) melt inclusions in olivines of type II chondrules in Semarkona. These profiles will enable us to deduce cooling rates for these olivines.

Tachibana S.   Nagahara H.   Mizuno K.
Constraints on Cooling Rates of Chondrule from Metal-Troilite Assemblages **[#2263]**
We performed dynamic crystallization experiments of Fe-Ni-S melt in order to constrain the cooling rate of chondrules at temperatures below the solidus of chondrule silicates.

Pravdivtseva O.   Meshik A.   Hohenberg C. M.   Amelin Yu.
New I-Xe Ages of Chondrules from the Ordinary L4 Chondrite Saratov **[#2418]**
New I-Xe ages reported for two chondrules from the ordinary L4 chondrite Saratov. The ages are consistent with the mineralogy of the chondrules and with methamorphic grade of the Saratov meteorite.

Guan Y.   Ushikubo T.   Leshin L. A.
^{10}Be-^{10}B in Enstatite and Ordinary Chondrites: A Preliminary Study **[#2360]**
We carried out a search for ^{10}Be in CAIs and Al-rich chondrules from UECs and UOCs. No resolvable ^{10}B excesses were observed in five CAIs. Marginally resolved ^{10}B excesses in one Al-rich chondrule hint the pre-existence of ^{10}Be in UEC forming region.

Nakashima D.   Herrmann S.   Ott U.   El Goresy A.   Nakamura T.
Noble Gases and Nitrogen in the KLE98300 EH3 Chondrite **[#1119]**
We report on the analysis of KLE98300 (EH3) simultaneously for its nitrogen and noble gas isotopic compositions, as part of a comprehensive study of KLE98300.

Schönbächler M. Carlson R. W. Hauri E. H.
Silver Isotope Fractionation in Chondrites **[#2157]**
Precise Ag isotope data are presented for different chondrites classes. In particular, ordinary chondrites show large Ag isotope fractionations ranging from –11.9 to + 4 for e107Ag. A correlation of Ag and Cd isotope fractionation is observed.

Botta O. Martins Z. Emmenegger C. Dworkin J. P. Glavin D. P. Harvey R. P. Zenobi R. Bada J. L. Ehrenfreund P.
Reassessing the Organic Content of Antarctic Ice and Meteorites **[#1464]**
Meteorites and Antarctic ice samples collected at the same time and location were analyzed for their PAH and amino acid composition using L2MS and HPLC, respectively. Very low levels of these compounds were found.

RESULTS OF THE HAYABUSA MISSION

Franzen M. A. Haseltine J. D. Kramb J. Ostrowski D. R. Sears D. W. G.
Fluidization as a Potential Mechanism for Formation of Polar Surface Features on Asteroid Itokowa **[#1022]**
The Hayabusa mission imagery of asteroid Itokowa has revealed smooth textures in the polar regions that may have been caused by fluidization.

Yoshikawa M. Michel P.
Orbital Evolution of Asteroid (25143) Itokawa: Its Past, Present, and Future **[#1545]**
The orbital evolution of asteroid Itokawa was studied. It is found that Itokawa most likely comes from the inner part of the main belt, and will collide with the Sun or terrestrial planets. This is the typical evolution of Near Earth Objects.

Maruya M. Ohyama H. Uo M. Muranaka N. Morita H. Kubota T. Hashimoto T. Saito J. Kawaguchi J.
Modeling and Analyzing Itokawa Topography for Hayabusa Touchdown and Sample Collection **[#1702]**
This paper describes the 3-D model of Itokawa constructed during the Hayabusa proximity observation, and it also describes the topographical aspect of site selection for safe touchdown.

Michikami T. Nakamura A. M. Honda C. Saito J. Hiraoka K. Nakamura R. Demura H. Ishiguro M. Hirata N. Miyamoto H.
The First Look of Blocks on Asteroid 25143 Itokawa by the Hayabusa Spacecraft: A Comparison of the Observed Number Density with the Estimated **[#1843]**
We examine the origin of blocks on surface of Itokawa, by comparing the observed number with the estimated number of blocks. Our results mean that the blocks of Itokawa are not direct consequences of impact cratering process.

Gaskell R. Saito J. Ishiguro M. Kubota T. Hashimoto T. Hirata N. Abe S. Barnouin-Jha O. Scheeres D.
Global Topography of Asteroid 25143 Itokawa **[#1876]**
Digital maps of the asteroid Itokawa have been constructed using multi-image photoclinometry from 600 Hayabusa images. They are combined to construct high resolution global and local topography, and are used as control points for determining the pole and spacecraft position and orientation.

Tholen D. J. Hirata N. Gaskell R. W. Ishiguro M. Saito J.
Comparison of Ground-based Lightcurve Observations of (25143) Itokawa with Synthetic Lightcurves Generated from Asteroid Shape Models **[#2223]**
The light scattering properties of the surface of Itokawa are being constrained by matching the observed rotational lightcurve behavior with synthetic lightcurves based on shape models derived from both radar and Hayabusa spacecraft observations.

Yokota Y. Ishiguro M. Nakamura A. M. Nakamura R. Tholen D. Smith P. Saito J. Kubota T. Hashimoto T.
Opposition Effect on Itokawa: Preliminary Report from Hayabusa Images **[#2445]**
Opposition surge of the airless body surface is thought as a useful tool to investigate the property of the regolith. Hayabusa has three Optical Navigation Cameras. We will present the current status of the analysis of data.

Abe S. Mukai T. Hirata N. Barnouin-Jha O. S. Cheng A. Mizuno T. Nakamura R. Scheeres D. Yoshikawa M. Gaskell R. Demura H. Hashimoto T. Kubota T. Matsuoka M.
Determination of Gravity and Density of Asteroid 25143 Itokawa by Light Detection and Ranging Instrument on Hayabusa Spacecraft **[#2461]**
The LIght Detection And Ranging instrument (LIDAR) onboard the Hayabusa spacecraft provided the scientific data of the gravity estimation. In this paper, we will describe the mission specifications for the LIDAR instrument and the gravity and density results obtained by LIDAR.

Abell P. A. Vilas F. Jarvis K. S. Gaffey M. J. Kelley M. S.
Mineralogical Composition of (25143) Itokawa 1998 SF_{36} from Visible and Near-Infrared Reflectance Spectroscopy: Evidence for Partial Melting **[#1513]**
Spectral reflectance ground-based observations of (25143) Itokawa were obtained to support the Japanese Hayabusa mission. Detailed analyses of the spectra indicate that this object is likely a primitive achondrite with a 70:30 olivine/pyroxene ratio.

Okada T. Yamamoto Y. Inoue T. Shirai K. Arai T. Ogawa K. Hosono K. Kato M.
Thermal Radiometry of Asteroid Itokawa by the XRS Onboard Hayabusa **[#1965]**
Thermal radiometry of asteroid Itokawa has been conducted by the XRS onboard Hayabusa. Preliminary results show the global averaged temperature in the daytime is 340±10 K, consistent with relatively high thermal inertia by Mueller et al. (2005).

RESULTS FROM THE DEEP IMPACT MISSION

Belton M. J. S. Thomas P. C. Carcich B. Crockett C. J. Deep Impact Science Team
The Spin State of 9P/Tempel 1 **[#1487]**
A high precision spin state for the nucleus of 9P/Tempel 1 is determined. The spin is fully relaxed and in the direct sense. The pole is a RA, Dec (J2000) = 293.8, +72.6° with an absolute uncertainty of 5°. The diurnal spin period in 1.6976 ± 0.00006 d.

Li J.-Y. A'Hearn M. F. McFadden L. A. Sunshine J. M. Crockett C. J. Farnham T. L. Lisse C. M. Thomas P. C. Deep Impact Science Team
Deep Impact Photometry of the Nucleus of Comet 9P/Tempel 1 **[#1839]**
We studied the disk-resolved photometry of comet 9P/Tempel 1 from Deep Impact images. The surface of Tempel 1 is dark and red. Both albedo variations and color variations are very small.

Mori Y. Sekiguchi T. Sugita S. Matsunaga N. Fukushi H. Kaneyasu N. Kawadu T. Kandori R. Nakajima Y. Tamura M.
Near-IR Monitoring Observation of Comet 9P/Tempel 1 **[#2458]**
We performed a long-term observation of comet 9P/Tempel 1, the target of NASA's Deep Impact mission using the near-IR camera on a 1.4 m telescope. We present the observed change of the comet activity and the motion of the dust ejected by the impact.

Capria M. T. Cremonese G. De Sanctis M. C. Boattini A. Epifani E. Lorenzi V. Saba L. Licandro J.
High Resolution Monitoring of 9P/Tempel 1 with SARG at La Palma During the Flyby of Deep Impact **[#1275]**
Comet Tempel 1 was observed before and after the impact with the echelle spectrograph SARG on the TNG telescope in La Palma. We are cataloguing the lines visible in the spectra and comparing the spectra between them.

Wellnitz D. D. Deep Impact Science Team
Observations of the Inner Coma and Activity near the South Pole on the Nucleus of Comet 9P/Tempel 1 **[#2465]**
Surprisingly, one of the largest areas of near-surface coma enhancement of comet 9P/Tempel 1 appears to be associated with the area near the south rotational pole. In this region there are diffuse brighter areas which look like they may be associated with activity on the unilluminated surface.

Ipatov S. I. A'Hearn M. F.
Velocities of Material Ejected from Comet Tempel 1 **[#1462]**
The brightest material ejected from Comet Tempel 1 after the collision of Deep Impact with the comet moved with velocity ~100 m/s, but velocities of some particles exceeded several km/s.

EARLY SOLAR SYSTEM EVOLUTION: AN ISOTOPIC PERSPECTIVE

Ozima M. Podosek F. A. Higuchi T. Yin Q. Z. Yamada A.
Oxygen Isotopes in the Solar System **[#1130]**
Bootstrap statistical examination of O isotopes in planetary objects such as meteorites, Mars (SNC), and Earth suggests that they formed by random accretion of planetesimals from the protosolar nebula, and have the same O isotopes as the Sun.

Chakraborty S. Thiemens M. H. Kimura Y. Nuth J. A. III
Non-Mass Dependent Oxygen Isotopic Fractionation of Refractory Oxide Dust Produced by a Chemical Process **[#1389]**
The results of the observed non-mass dependent oxygen isotopic effect in solid oxides formed in a smoke experiment was discussed and interpreted based on symmetry based chemical reaction scheme.

Yin Q.-Z. Jacobsen B. Hutcheon I. D.
Toward Tracing Redox State Evolution in the Protoplanetary Disk with High Resolution ^{26}Al-^{26}Mg Chronometry **[#1531]**
The goal of the study is to apply high-resolution ^{26}Al-^{26}Mg chronometry to trace the redox state evolution in the protoplanetary disk. We have discovered one chondrule with negative ε^{26}Mg (-57 ± 14 ppm). Significance of this finding will be discussed together with new data.

Ganguly J. Ito M. Zhang X.
Mn-Cr Thermochronology of Early Solar System Processes **[#1339]**
Cr diffusion was determined in olivine and enstatite and used to develop thermochronologic formulations of Mn-Cr decay system. The latter was used to estimate high temperature cooling rates and initial burial depth of a pallasite and cumulate eucrites.

Meyer B. S. Adams D. C.
Neutron Burst Production of ^{60}Fe Necessarily Implies Production of ^{182}Hf **[#1403]**
Supernova neutron burst production of Fe-60 necessarily co-produces Hf-182. Our calculations demonstrate that the yield of Fe-60 is quite sensitive to the peak temperature and density in the burst, but that of Hf-182 is not. Detailed results are available on the Web.

Moynier F. Fujii T. Albarède F.
Nuclear Field Vs Nucleosynthetic Effects as Cause of Isotopic Anomalies in FUN Inclusions **[#1629]**
Mass-independent isotope effect due to nuclear field can lead to a number of isotope anomalies found in CAIs. A whole class of isotopic heterogeneities therefore reflect evaporation/condensation processes rather than nucleosynthetic effects.

PRESOLAR GRAINS

Yada T. Stadermann F. J. Floss C. Zinner E. Nakamura T. Noguchi T. Lea A. S.
High Abundances of Presolar Silicates in Antarctic Micrometeorites; Implications for Their Cometary Origins **[#1470]**
The abundance of presolar silicates in Antarctic micrometeorites (AMMs) has been revised to be 50 ppm. That in one of the AMMs is 900 ppm, comparable to that in primitive interplanetary dust particles, indicating that it might be of cometary origin.

Morlok A. Köhler M. Grady M. M.
Infrared Spectroscopy of Circumstellar Dust: Signs of Differentiated Materials? **[#1519]**
Mid-infrared absorption spectra of powdered achondrites are compared with the astronomical spectra of dust around young, evolving stars, to find evidence (or not) of dust formed in collisional cascades of material from planetesimals.

Tonotani A. Kobayashi S. Nagashima K. Sakamoto N. Russell S. S. Itoh S. Yurimoto H.
Presolar Grains from Primitive Ordinary Chondrites **[#1539]**
We discovered 21 presolar silicate grains and 16 presolar carbonaceous grains from five primitive ordinary chondrites. We determined presolar grain abundance in the ordinary chondrites and discussed alteration effects for the abundances.

Le Guillou C. Rouzaud J. N. Brunet F.
Characterization of the Carbon to Diamond Transition by X-Ray Diffraction, Raman Microspectroscopy, and High Resolution Transmission Electron Microscopy (HRTEM): A Way to Better Constrain the Formation of Diamond in Space **[#1635]**
Nanodiamonds are found in carbonaceous chondrites and contain different isotopically anormous noble gases. The coupling of X-ray diffraction, Raman, and high-resolution TEM raises the importance of carbon precursors for diamond formation.

Stadermann F. J. Floss C. Lea A. S.
Using Auger Spectroscopy to Characterize Sub-Micrometer Presolar Grains In Situ: An Overview **[#1663]**
We have used the combination of NanoSIMS and Auger spectroscopy for *in situ* isotopic and elemental characterizations of presolar grains in primitive meteorites, Antarctic micrometeorites, and interplanetary dust particles.

Henkel T. Tizard J. Lyon I.
Comprehensive Analyses of Gentle Separated Presolar SiC-Grains **[#1700]**
Evidence for a coat-core structure of presolar SiC-grains was found in a comprehensive study of acid-free extracted grains. Comparison with acid-residue grains showed alterations these ones have experienced in the extraction process.

Lyon I. Tizard J. Henkel T.
Li and B in Gently Separated Pre-Solar SiC Grains, Evidence of Material from Interstellar Clouds **[#1750]**
Lithium and Boron isotope and elemental analyses have been acquired from pristine pre-solar silicon carbide grains, separated from the Murchison meteorite by a new acid-free technique. Results indicate acquisition of a rim on the grain from interstellar space.

Crowther S. A. Kehm K. Mohapatra R. K. Gilmour J. D.
Single Grain Xenon Measurements Using RELAX: First Results from Murchison Grains, IDPs and Presolar SiC **[#1942]**
We present first results from xenon analysis of individual IDPs and presolar grains yielding upper limits on gas concentrations.

Ofan A. Ahmad I. Greene J. P. Paul M. Pellin M. J. Savina M. R.
A Search for Live 244Pu in Deep-Sea Sediments: Development of an Efficient Detection Method **[#2133]**
Live Pu-244 (half-life = 81 Ma) is expected to be present in the interstellar medium from ongoing nucleosynthesis. We are developing a method for detecting extremely low levels of Pu-244 that may have accreted onto Earth from the ISM.

Amari S. Gallino R. Pignatari M.
Presolar Graphite from the Murchison Meteorite: Noble Gases Revisited **[#2409]**
Presolar graphite is the carrier of Ne-E(L). Novae have traditionally been thought a source of ^{22}Na in Ne-E(L). However, supernovae are a major source of ^{22}Na in low-density graphite grains. s-Process Kr in the grains was most likely produced in supernovae.

GALILEAN SATELLITES AND TRANS-KRONIAN OBJECTS

Moore C. H. Goldstein D. B. Varghese P. L. Trafton L. M. Stapelfeldt K.
Monte Carlo Modeling of Io's [OI] Aurora in Eclipse **[#2281]**
A 3D direct Monte Carlo simulation is used to simulate Io's atmospheric interaction (upon entering eclipse) with electrons from the plasma torus. It is found that the flux tube depletion across Io controls the latitude of the bright wake feature.

Moore C. H. Goldstein D. B. Varghese P. L. Trafton L. M. Larignon B. Walker A.
1-D Monte Carlo Modeling of Io's Atmospheric Collapse in Eclipse **[#2266]**
The collapse of Io's dayside SO_2 atmosphere was simulated using the DSMC method. It was found that the presence of a non-condensible species (SO) greatly increases the collapse timescale through the formation of a diffusion layer near the surface.

Keszthelyi L. Milazzo M. Davies A. G. Wilson L.
A Simple Thermal Model for Lava Fountains: Application to Io **[#2216]**
A simple model for the thermal emission from lava fountains helps explain the high lava temperatures seen at Io.

Lougen J. A. Gregg T. K. P. Lopes R.
Behavior of Loki Patera, Io Revealed Through Mathematical and Laboratory Modeling **[#2179]**
Laboratory simulations and mathematical models test lava lake hypotheses for the formation of Loki Patera, Io.

Kirchoff M. R. McKinnon W. B.
Mountain Building on Io – Part 2: Effects of Preexisting Faults and Pore Sulfur on Thermal Stresses **[#2120]**
We examine mountain formation on Io by thermoelastic stresses when the crust is allowed to expand laterally on preexisting faults, and in the presence of liquid sulfur pore pressure. The potential for mountain formation is enhanced.

Black S. R. Gregg T. K. P.
The Origin and Evolution of "Islands" in Ionian Paterae **[#2180]**
A morphological investigation of the Ionian paterae containing islands suggests that the islands are not solidified rafts of crust.

Davies A. G. Kyle P.
Spacecraft and In-Situ Observations of the Mt. Erebus, Antarctica, Lava Lake: A Terrestrial Analogue for Pele on Io **[#2284]**
In December 2005 we observed strombolian activity at an active lava lake in Antarctica, ground-truthing VIS/IR spacecraft observations (four instruments on two spacecraft) using Forward Looking Infrared (FLIR) cameras.

Groenleer J. M. Kattenhorn S. A.
Implications of Cycloid History in the Northern Trailing Hemisphere of Europa **[#2071]**
A CW rotation of cycloids through time is compatible with 600 degrees of nonsynchronous rotation of the Europan ice shell. Up to eight cycloids formed in a single rotation cycle. Non-cycloidal cracks continued to form after cycloids first developed.

Crawford Z. A. Pappalardo R. T.
Evidence for Episodic Formation of Europa's Global Lineaments Via Non-Synchronous Rotation **[#2264]**
By comparing mapped and synthetic global lineaments on Europa to non-synchronous rotation stresses at a variety of westward translations, we show that the observed features are consistent with episodic lineament formation.

Mullen M. E. Crawford Z. Pappalardo R. T. Wahr J.
Visco-Elastic Surface Stress on Europa **[#2350]**
Accurate modeling of long-period stresses on Europa's surface requires incorporating period-dependent Love numbers and Maxwell rheology terms. Visco-elastic surface stress is reduced significantly relative to purely elastic stress at NSR time scales.

Bills B. G. Nimmo F.
Limits to Non-Synchronous Rotation for Maxwell Viscoelastic Bodies **[#2131]**
It has been argued that Europa may rotate at a slightly non-synchronous rate, due to non-vanishing tidal torques. We show that, in self-consistent calculations, rigid body torques can easily prevail and enforce synchroneity.

Lichtenberg K. A. McKinnon W. B. Barr A. C.
Heat Flux from Impact Ring Graben on Europa **[#2399]**
Measurements of graben widths in the vicinity of Tyre and Callanish impact structures on Europa are used to constrain the surface heat flux from the satellite at the time of impact.

Bierhaus E. B.
Europa's Surface Properties from Small Craters **[#2436]**
This abstract describes how observations of small crater morphology reveal information regarding Europa's surface and near-surface properties.

Patterson G. W. Head J. W.
Plate Motion and the Rigidity of Europa's Lithosphere **[#1813]**
We examine the offset magnitudes of eight plate boundaries associated with a band complex located on the equatorial trailing hemisphere of Europa to determine the rigidity of the icy satellite's lithosphere when the feature was actively forming.

Doggett T. C. Davies A. G. Greeley R.
Detectability of Cryo-Volcanism with Thermal Infrared Spectroscopy **[#2243]**
This study modeled the thermal emission of putative cryovolcanic features to determine the minimum requirements of resolution and spectral range for the detection of cryovolcanism.

Dougherty A. J. Hogenboom D. L. Kargel J. S. Zheng Y. F.
Volumetric and Optical Studies of High Pressure Phases of Na_2SO_4-$10H_2O$ with Applications to Europa **[#1732]**
We present optical images of high-pressure phases of the Na_2SO_4-H_2O system, associated volume changes of the sample, and the experimental eutectic and liquidus transitions for pressures up to 300 MPa, with implications for modeling Europa's ocean.

Brand H. E. A. Fortes A. D. Wood I. G. Alfredsson M. Vocadlo L.
High Pressure Properties of Planetary Sulfate Hydrates Determined from Interatomic Potential Calculations **[#1310]**
We present the results of simulations of magnesium, sodium and ammonium sulfates and their hydrates, for comparison with experimental studies, and incorporation into planetary models.

Fortes A. D. Wood I. G. Voèadlo L. Brand H. E. A. Grindrod P. M. Joy K. H. Tucker M. G.
The Phase Behaviour of Epsomite ($MgSO_4{\bullet}7H_2O$) to 50 Kbar: Planetary Implications **[#1029]**
We describe the polymorphism of epsomite from a high-pressure powder neutron diffraction study, and relate these findings to the interiors of icy moons and to impact metamorphism.

Goguen J. D. Orzechowska G. E. Johnson P. V. Tsapin A. I. Kanik I.
UV Photolysis of Amino Acids in Water Ice: How Long Can They Survive on Europa? **[#2006]**
We report the rate of decomposition by ultraviolet photolysis of 4 simple amino acids in a ~mm-thick crystalline water ice at T=100K to constrain the survivability of these important organic molecules.

Hibbitts C. A. Szanyi J
Physisorption of CO_2 on Non-Ice Materials of Relevance to Icy Satellites **[#1753]**
Physisorption may explain some of the characteristics of the CO_2 in the surfaces of the Galilean and Saturnian satellites. Spectral characteristics of adsorbed CO_2 depend on mineralology, composition of the major cation, and temperature.

Patterson G. W. Head J. W. Collins G. C. Pappalardo R. T. Prockter L. M. Lucchitta B. K.
Global Geologic Mapping of Ganymede Light and Dark Material at 1:15M **[#1724]**
We are in the process of compiling a global geologic map of Ganymede at 1:15M utilizing a revised DOMU described herein. Our progress toward the completion of this mapping effort is summarized here.

Katz-Wigmore J. Barlow N. G.
The "Catalog of Impact Craters on Ganymede" **[#1387]**
We are producing a catalog of all impact craters larger than 3 km on Ganymede. The catalog include information on crater location, diameter, geologic unit, type of crater, ejecta and interior morphologies, and crater preservational state.

Klaybor K. Barlow N. G.
Interior Morphologies of Impact Craters on Ganymede **[#1360]**
We are analyzing the interior morphologies of impact craters on Ganymede. We are finding evidence of regional variations in the distributions of dome, central peak, and central pit craters.

Martin E. S. Collins G. C. Crawford Z. A. Pappalardo R. T.
Computer Assisted Time Sequence Sorting of Grooves in Eastern Mysia Sulci, Ganymede **[#1204]**
We examine the sequence of deformation in a complex area of Ganymede grooved terrain, using a new computer technique to sort the groove sets.

Collins G. C.
Global Expansion of Ganymede Derived from Strain Measurements in Grooved Terrain **[#2077]**
Global expansion is estimated by combining high-resolution strain estimates with global image and groove data. The ~3% radial expansion result is consistent with interior differentiation, but too large for melting in a thermal runaway event.

Sims D. W. Wyrick D. Y. Morris A. P. Ferrill D. A. Pappalardo R. T. Colton S. L.
Physical Models of Tectonic Resurfacing on Ganymede **[#1774]**
Physical analog modeling of grooved terrain has produced geometrically similar morphology to the fault systems on Ganymede. Models suggest that the grooved terrain on Ganymede formed by imbricate normal faulting at 25% or greater extension.

Murphy N. W. Khurana K. K. Pappalardo R. T. Denk T.
Ganymede's Polar Caps and Field Line Boundaries **[#2186]**
We find strong correlations between the locations of Ganymede's polar caps and open/closed field line boundaries based on modeling of Ganymede's induced and intrinsic magnetic fields. This supports a plasma bombardment origin for the polar caps.

De Sanctis M. C. Coradini A. Gavrishin A.
G-Mode Classification of Trans Neptunian Objects **[#1109]**
TNO population show a wide colour diversity. Since the population is characterized by several parameters it is important to use a multivariate statistics in order to understand if different types of objects exist.

Cook J. C. Desch S. J. Roush T. Geballe T. R. Trujillo C. A.
Near-Infrared Spectra of Charon: Support for Cryovolcanism on Kuiper Belt Objects? **[#2107]**
We present spectra of Charon which show crystalline water and ammonia hydrate, suggesting geological activity. The presence of ammonia hydrate enables cryovolcanism. We discuss how cryovolcanism may be possible on Charon, and other icy bodies.

MARS: FLUVIAL GEOMORPHOLOGY: RIVERS, OUTFLOWS, AND GULLIES
Friday, 8:30 a.m., Crystal Ballroom A

Chairs: D. M. Burr and W. Luo

8:30 a.m. Harrison K. P. * Grimm R. E.
Groundwater-controlled Valley Networks and the Decline of Surface Runoff on Early Mars **[#1908]**
We suggest a broad, first-order dynamical history of valley network formation on Mars centered on the waning influence of surface runoff in the late Noachian and early Hesperian, and on the consequent emergence of groundwater-dominated erosion.

8:45 a.m. Schon S. C. * Tanaka K. L.
Warrego Valles Revisited: Valley Network Formation, Modification, and Climatic and Structural Controls **[#1446]**
New mapping analyses indicate that Warrego Valles underwent precipitation-fed valley network incision during the Noachian followed by local, structurally controlled sapping and eolian degradation.

9:00 a.m. Stepinski T. F. * Carriere M. Molloy I.
Properties of Martian Highlands Drainage from THEMIS Images and MOLA Topography **[#1181]**
Valley networks are mapped from 100 m/pixel THEMIS mosaics for eight sites in Martian highlands. Drainage basins are delineated and terrain parameters are calculated for each basin. This higher resolution mapping does not reveal smaller scale valleys.

9:15 a.m. Luo W. * Howard A. D.
Quantitative Morphometric Analysis of Simulated Martian Landforms at Watershed Basin Scale **[#1511]**
This initial result showed that the computer simulation model can generate sapping and fluvial landforms that can be quantitatively separated based on basin scale morphometry.

9:30 a.m. Gregoire-Mazzocco H. * Mangold N. Costard F. Ansan V. Masson P. Neukum G. HRSC Team
Estimate of Discharge Rates in Nanedi Vallis, Mars **[#1806]**
Interior channels were observed at two locations on Nanedi Vallis. Discharges were calculated at both sites, using two different methods, to look for consistency between the overall morphology of the canyon and the characteristics of interior channels.

9:45 a.m. Di Achille G. * Marinangeli L. Ori G. G. Hauber E. Gwinner K. Reiss D. Neukum G. HRSC Co-Investigator Team
Geological Evolution of the Tyras Vallis Paleolacustrine System, Mars **[#1710]**
A potential paleolake, formed by the Tyras Vallis and a complex crater, contains a delta-like feature developed at the mouth of the inlet channel. The sedimentological analysis of this deposit allowed to infer the hydrological evolution of the basin.

10:00 a.m. Pondrelli M. * Rossi A. P. Marinangeli L. Ori G. G. Di Lorenzo S. Baliva A. Hauber E. Neukum G. HRSC Team
Morphofacies Analysis of the Eberswalde Crater (Mars) **[#1555]**
The Eberswalde delta has been investigated through geological mapping and stratigraphic survey. The mapped morphologies suggest formation in correspondence of a lacustrine system. Delta plain, delta front and prodelta facies can be recognized.

10:15 a.m. Kostama V.-P. * Ivanov M. Törmänen T. Raitala J. Neukum G.
Reull Vallis — Evolution of a Fluvial System in Eastern Hellas Region, Mars **[#1649]**
The study presents a possible evolution of Reull Vallis fluvial system. The system consists of several distinct parts that have formed in three major episodes.

10:30 a.m. Burr D. M. * Williams R. M. E. Nussbaumer J. Zimbelman J. R.
Multiple, Distinct, (Glacio?) Fluvial Paleochannels Throughout the Western Medusae Fossae Formation, Mars **[#1367]**
Morphologically and contextually diverse raised curvlinear features in the western MFF are interpreted as paleochannels resulting from a variety of processes. These features indicate surficial flow of water near Mars' equator during the Amazonian.

10:45 a.m. Coleman N. M. *
Formation of Lakes in the Ancestral Valles Marineris in the Epoch of Allegheny Vallis, Mars **[#1879]**
High outflow channels provide paleo-indicators of climax groundwater elevations on Mars. Analysis of hydraulic pressures beneath canyon floors shows that lake formation in the Valles Marineris may have been inevitable as a consequence of rising regional groundwater levels.

11:00 a.m. Hanna J. C. * Phillips R. J.
Tharsis-driven Hydrology and the Martian Outflow Channels **[#2373]**
The location of the Martian outflow channels within the Tharsis trough suggests that Tharsis played a key role in their formation. We present a global hydrologic model exploring the effects of Tharsis formation during early Mars history.

11:15 a.m. Morgan R. S. * Treiman A. H.
Geographic Settings of Gullies in the Newton-Copernicus Region of Mars: Implications for Groundwater, Snow, and Dust **[#1304]**
Gullies in the Newton-Copernicus region (Mars) face in all directions, more equatorward to the south; their facings are independent of regional elevations and slopes. Current theories of gully formation do not predict these facings.

11:30 a.m. Soare R. J. * Wan Bun Tseung J. M. Osinski G. R.
Gully Formation, Periglacial Processes and Possible Near-Surface Ground-Ice in Utopia Planitia **[#1666]**
Here, we show crater-wall gullies in Utopia Planitia, point to landforms suggesting that near-surface ground-ice extends tens of metres to depth in the UP landscape and argue that gully formation could be related to the melting of this near-surface ground-ice during periods of high obliquity.

SPECIAL SESSION: RESULTS OF THE HAYABUSA MISSION
Friday, 8:30 a.m., Crystal Ballroom B

Chairs: **A. Fujiwara and D. Yeomans**

8:30 a.m. Fujiwara A. * Kawaguchi J. Uesugi K. Yeomans D. Saito J. Abe M. Mukai T. Kato M. Okada T. Yoshikawa M. Yano H. Demura H. Scheers D. Gaskel R. Barnouin-Jha O. Cheng A. Miyamoto H. Hirata N. Nakamura R. Sasaki S. Nakamura A. M.
Global Properties of 25143 Itokawa Observed by Hayabusa **[#1575]**
The outline of the Hayabusa asteroid mission and its first quick report of the science results will be presented.

8:50 a.m. Demura H. * Kobayashi S. Nemoto E. Matsumoto N. Furuya M. Yukishita A. Muranaka N. Morita H. Shirakawa K. Maruya M. Ohyama H. Uo M. Kubota T. Hashimoto T. Kawaguchi J. Fujiwara A. Saito J.
Stereogrammetric Shape Modeling for (25143) Itokawa, Hayabusa Mission **[#1716]**
A task team of shape modeling gives Itokawa's pole and properties with AMICA images. GNC's pole of 200EC is (123.5, –89.53) and Aizu's one is (128.5, –89.66). Itokawa's surface area is 0.393 km^2, volume is 0.018378 km^3, X=0.535, Y=0.294, Z=0.209[km].

9:05 a.m. Sasaki S. * Saito J. Ishiguro M. Hirata N. Miyamoto H. Demura H. Hashimoto T. Higuchi Y. Hiraoka K. Honda C. Honda T. Kitazato K. Kubota T. Michikami T. Nakamura A. M. Nakamura R. Nakamura T. Smith P. Terazono J. Tholen D. J. Yamamoto A. Yokota Y. Akiyama H. Dermawan B. Fuse T. Shinohara C. Sogame A. Yoshida F. AMICA Team
Observations of 25143 Itokawa by the Asteroid Multiband Imaging Camera (AMICA) of Hayabusa: Morphology of Brighter and Darker Areas **[#1671]**
Asteroid Multiband Imaging CAmera (AMICA) on Hayabusa showed that Itokawa's surface is divided into brighter and darker areas. Brightness may be controlled by space weathering; a darker boulder-rich layer covers underlying brighter fresh materials.

9:20 a.m. Miyamoto H. * Yano H. Scheeres D. Sasaki S. Barnouin-Jha O. Gaskell R. W. Cheng A. Demura H. Fujiwara A. Hashimoto T. Hirata N. Honda C. Ishiguro M. Kubota T. Michikami T. Nakamura A. M. Nakamura R. Saito J. Yokota Y. Hayabusa Team
Regolith on a Tiny Asteroid: Granular Materials Partly Cover the Surface of Itokawa **[#1686]**
Images of Itokawa taken by the Hayabusa spacecraft reveal that a sub-kilometer-sized asteroid can have a significant amount of regolith over its surface. The regolith of Itokawa is not globally distributed but partially concentrated only at the smooth terrains.

9:35 a.m. Hirata N. * Barnouin-Jha O. S. Honda C. Nakamura R. Nakamura A. M. Demura H. Michikami T. Ishiguro M. Hashimoto T. Kubota T. Saito J.
Morphology of Craters on Itokawa and Its Possible Implication **[#1911]**
Observations of Itokawa by Hayabusa reveal various features on the asteroid surface. These possess unfamiliar morphologies that could indicate a unique cratering process and subsequent geological modification.

9:50 a.m. Ishiguro M. I. Hiroi T. H. Tholen D. J. T. Yamamoto A. Y. * Sasaki S. S. Yoshida F. Y. Clark B. E. C. Nakamura R. N. Saito J. S.
Detection of a Large Variation in the Degree of Space Weathering on the Surface of Itokawa by Hayabusa/AMICA Observations **[#1533]**
We examined the space weathering on the surface of Itokawa taken by AMICA onboard the Hayabusa spacecraft.

10:05 a.m. Honda C. * Nakamura R. Ishiguro M. Saito J. Hashimoto T. Kubota T. Nakamura A. M. Hirata N. Hiraoka K. Demura H. Michikami T.
Crater Counting on Asteroid 25143 Itokawa: Preliminary Results **[#1620]**
Using the AMICA data, we derived the crater size-frequency distribution on Itokawa. We explain the projectile size-frequency distribution in the MAB, assuming the constraints of the orbital evolution and collisional lifetime of Itokawa.

10:20 a.m. Abe M. * Takagi Y. Kitazato K. Hiroi T. Abe S. Vilas F. Clark B. E. Abell P. A. Lederer S. M. Jarvis K. S. Nimura T. Ueda Y. Fujiwara A.
Preliminary Results from the Hayabusa Near Infrared Spectrometer (NIRS) of Asteroid (25143) Itokawa **[#1547]**
The Hayabusa Near Infrared Spectrometer (NIRS) obtained more than 80,000 spectra of asteroid (25143) Itokawa successfully during the rendezvous phase of the asteroid. We will present and discuss preliminary results from NIRS.

10:35 a.m. Kitazato K. * Clark B. E. Abe M. Abe S. Takagi Y. Hiroi T.
Near-Infrared Photometry of Asteroid 25143 Itokawa by the NIRS Onboard Hayabusa **[#2258]**
We present the results of near-infrared photometry of asteroid 25143 Itokawa obtained by the near-infrared spectrometer (NIRS) onboard the Hayabusa spacecraft.

10:50 a.m. Barnouin-Jha O. S. * Cheng A. Mukai T. Hirata N. Abe S. Nakamura R. Saito S. Gaskell B. Demura H. Miyamoto H. Fujiwara A.
Small-scale Topography on 25143 Itokawa from the Hayabusa LIDAR **[#1773]**
We present preliminary results from the laser altimeter (LIDAR) aboard the Japanese HAYABUSA spacecraft which recently hovered above and landed on the surface of the near-Earth asteroid 25143 Itokawa.

11:05 a.m. Okada T. * Shirai K. Yamamoto Y. Arai T. Ogawa K. Hosono K. Kato M.
X-Ray Fluorescence Experiments of Asteroid Itokawa by the XRS Onboard Hayabusa **[#1596]**
Remote XRF spectrometry of asteroid 25143 Itokawa has been performed by the XRS onboard Hayabusa for major elemental analysis. The preliminary results indicate that Itokawa has chondritic composition and LL- or L-chondrites are most likely.

11:20 a.m. Yano H. * Kubota T. Miyamoto H. Okada T. Scheeres D. Takagi Y. Yoshida K. Abe M. Abe S. Barnouin-Jha O. Fujiwara A. Hasegawa S. Hashimoto T. Ishiguro M. Kato M. Kawaguchi J. Mukai T. Saito J. Sasaki S. Yoshikawa M.
Hayabusa's Touch Down Sites at the Smooth Terrain on Asteroid 25143 Itokawa **[#2463]**
Hayabusa conducted high resolution imagery, thermal, and spectral measurements during touch down sequences to the smooth terrain Muses Sea. Physical property of the gravel filled regolith was also derived from free-fall bouncing.

ON CHONDRULES
Friday, 8:30 a.m., Marina Plaza Ballroom

Chair: **R. H. Jones**

8:30 a.m. Cuzzi J. N. * Alexander C. M. O'D.
Size and Density of Chondrule Formation Regions from Missing Isotopic Fractionation **[#1256]**
We present a simple model to explain the lack of isotopic fractionation in chondrules, which gives constraints on the spatial scale (roughly 50–1500 km radius) and precursor volume density (roughly 10–20 m^{-3}) of formation regions.

8:45 a.m. Libourel G. * Krot A. N.
Origin of Olivines in Type I Chondrules: Petrologic and Chemical Constraints **[#1334]**
Type I chondrules from the chondrite Vigarano contain lithic clasts having granoblactic texture and composed of forsterite and Fe,Ni-metal. The clasts originated from dunite-like mantle material of earlier generations of differentiated planetesimals.

9:00 a.m. Chaussidon M. * Libourel G. Krot A. N.
Origin of Olivines in Type I Chondrules: Constraints from Oxygen and Magnesium Isotopic Compositions **[#1335]**
O and Mg isotopes in Vigarano type I chondrules containing olivine-rich granoblasctic clasts are consistent with an origin by melting of a mixture of relict olivines and CAI-like material with melt continuously interacting with the nebular gas.

9:15 a.m. Jones R. H. * Carey E. R.
Identification of Relict Forsterite Grains in Forsterite-rich Chondrules Using Cathodoluminescence **[#1783]**
We used cathodoluminescence to identify relict forsterite grains that have similar compositions to their host chondrules. This helps to understand the nature of chondrule precursors and chondrule thermal histories.

9:30 a.m. Alèxander C. M. O'D. * Desch S. J.
Evaporation/Condensation of Chondritic Chondrule Precursors in Nebular Shocks **[#2303]**
Here we exlore the elemental and isotopic evolution of initially chondritic chondrule precursors in nebular shocks.

9:45 a.m. Fedkin A. V. Grossman L. * Ghiorso M. S.
Model Evaporation of Chondrule Precursors in Nebular Shocks **[#2249]**
Evaporation rates from silicate liquids of model chondrule compositions into a complementary solar gas rise with decreasing fO_2 of formation of the precursor. Minor evaporative losses of Fe, Mg and Si do not require elevated ambient pressure or fO_2.

MARTIAN METEORITES: SHERGOTTITES
Friday, 10:15 a.m., Marina Plaza Ballroom

Chair: **S. J. Symes**

10:15 a.m. Shearer C. K. * McKay G. A. Papike J. J. Karner J.
Oxygen Fugacity of the Upper Mantle of Mars. Evidence from the Partitioning Behavior of Vanadium in Y980459 (Y98) and Other Olivine-Phyric Shergottites **[#1295]**
Using partitioning behavior of V between olivine and basaltic liquid precisely calibrated for martian basalts, we determined the redox state of primitive (olivine-rich, high Mg#) martian basalts near their liquidus.

10:30 a.m. Shirai N. * Ebihara M.
The Magmatism of Mars Inferred from Chemical Composition of Shergottites **[#1917]**
We analyzed olivine-phyric shergottites using PGA, INAA, IPAA and ICP-MS. Based on analysis data, we estimate Zr and Hf contents of the Martian crust. We discuss the magmatism of Mars.

10:45 a.m. Jagoutz E. * Jotter R. Kubny A. Zartman R.
New U-Th and Pb Isotope Data of SNC Meteorites **[#1577]**
The U-Pb isotopes reveal that olivine phyric shergottites and nakhlites are coming from the same source.

11:00 a.m. Symes S. J. * Borg L. E. Shearer C. K.
Major and Trace Element Modeling of LREE-depleted Shergottites Via Fractional Crystallization from a Y980459-like Parent **[#2043]**
Fractional crystallization models reproduce the major and trace element abundances of the LREE-depleted shergottites assuming a parent liquid similar to Y980459. These models suggest that assimilation of evolved crustal material is not required.

11:15 a.m. Nyquist L. E. * Shih C.-Y. Reese Y. D. Irving A. J.
Concordant Rb-Sr and Sm-Nd Ages for NWA 1460: A 340 Ma Old Basaltic Shergottite Related to Lherzolitic Shergottites **[#1723]**
Rb-Sr and Sm-Nd isotopic data for NWA 1460 give concordant crystallization ages of ~340 Ma. Published Pb isotopic data for nakhlites are consistent with ages of ~1.36 Ga. Published Pb isotopic data for shergottites are complex, but are interpreted as consistent with young ages.

11:30 a.m. Misawa K. * Yamada K. Nakamura N. Morikawa N. Kondorosi G. Yamashita K. Premo W. R.
Sm-Nd Isotopic Systematics of Lherzolitic Shergottite Yamato-793605 **[#1892]**
The Sm-Nd age (156 ± 14 Ma) and initial ε^{143}Nd value (+7.5 ± 0.2) of Y-793605 are in good agreement with those reported for LEW88516, suggesting they are genetically closely related. ALH77005 shows a slightly higher initial ε^{143}Nd value of +11.0 ± 0.2.

11:45 a.m. Reynolds V. S. * McSween H. Y. Jr. McDonough W. F. McCoy T.
Lithium Isotopes in Basaltic Shergottites: Evidence for a Hydrated Assimilant **[#2206]**
Basaltic shergottites represent a mixture of enriched and depleted components. Measurements of Li and Be abundances and Li isotopes suggest the enriched component was crustal material that was altered at low temperatures prior to assimilation.

SOLAR NEBULA AND PLANETARY RESERVOIRS
Friday, 8:30 a.m., Amphitheater

Chairs: F. J. Ciesla and M. C. Ranen

8:30 a.m. Ouellette N. * Desch S. J.
Efficiency of Mixing of Supernova Ejecta into Nearby Protoplanetary Disks **[#2348]**
The one-time presence of ^{60}Fe in our solar system implies it formed in close proximity to a supernova. We investigate the effects of supernova ejecta hitting a protoplanetary disk, and the efficiency with which ejecta gas mixes into the disk.

8:45 a.m. Boss A. P. *
Isotopic Heterogeneity Associated with Mixing and Transport in the Solar Nebula **[#1066]**
Spatial heterogeneity at the level of 10% is to be expected for short-lived radioisotope ratios such as ^{26}Al/^{27}Al resulting from injection of ^{26}Al into the solar nebula by a supernova shock.

9:00 a.m. Bizzarro M. * Ulfbeck D. Thrane K.
Nickel Isotopes in Meteorites: Evidence for Live ^{60}Fe and Distinct ^{62}Ni Isotope Reservoirs in the Early Solar System **[#2020]**
We report Ni isotope data for various meteorites indicating early planetesimal differentiation and the presence of large-scale coupled Ni and Cr isotope heterogeneity within the accretion disc.

9:15 a.m. Ranen M. C. * Jacobsen S. B.
Barium Isotope Heterogeneities in Early Solar System Materials: Applications to Planetary Reservoir Models **[#1832]**
We find small variations in barium isotopes in bulk chondrites compared to the Earth. These r-process enrichments show that the early solar system may be incompletely mixed in terms of r- and s-process nucleosynthetic components.

9:30 a.m. Seitz H.-M. * Brey G. P. Weyer S. Zipfel J. Ott U. Durali S.
Lithium Isotope Composition of Ordinary and Carbonaceous Chondrites, and Differentiated Planetary Bodies: Bulk Solar System and Solar Reservoirs **[#1708]**
Li isotopes for H-, L-, LL-, and C-chondrites, IABs, pallasite and HEDs indicate the existence of distinct Li isotope reservoirs in the early solar system.

9:45 a.m. Lyons J. R. *
Photooxidation in the Inner Solar Nebula **[#2374]**
Photochemical kinetics calculations of water and related species have been performed for the inner solar nebula. At 800 K, a low fraction of O_2 is predicted at the midplane, with higher values in a region above the midplane.

10:00 a.m. Young E. D. *
Evaluating CO Self-Shielding and the Oxygen Isotopic Evolution of the Solar Protoplanetary Disk with Astrochemical Reaction Networks **[#1790]**
A quantitative model for the oxygen isotopic evolution of the early solar system is presented. The model is based on combining a detailed reaction network with mass transport among reservoirs in the protoplanetary disk.

10:15 a.m. Ziegler K. * Chambers J. E. Young E. D.
High-Precision $\Delta^{17}O$ Data: Querying the Meaning of $\Delta^{17}O$ in the Inner Solar System **[#1894]**
As evidenced by different meteorite groups, $\Delta^{17}O$ signatures of planetesimals vary, but what, if anything, do these variations tell us about the structure and the dynamics of the inner solar system prior to and during planet formation?

10:30 a.m. Ciesla F. J. * Krot A. N. Lyons J. R.
Water Transport in the Solar Nebula: Implications for the Mixing of Oxygen Isotopic Reservoirs **[#1627]**
We are studying how water transport in the solar nebula would have led to the mixing of different oxygen isotopic reservoirs produced by CO self-shielding.

10:45 a.m. Zanda B. * Hewins R. H.
A Mixing Origin for Chondrite Groups **[#2199]**
We find correlations between the abundances of metal, type I chondrules, CAIs and matrix in chondrites. From the correlations we extract the compositions of the few primary reservoirs which explain chondrite goups by mixing.

11:00 a.m. Chakraborty S. * Thiemens M. H.
Isotopic Fractination Associated with Photochemistry of CO: Experimental Findings Relevant to the Solar Nebula **[#1436]**
The present experiments provide details of the fractionation associated with specific excited states of CO and demonstrate that along with CO self-shielding, excited state chemistry is important and must be considered.

11:15 a.m. Nuth J. A. III * Kimura Y. Thiemens M. H. Chakraborty S.
Non-Mass Dependent Oxygen Isotopic Fractionation of Refractory Oxide Dust Produced in an Electrical Discharge **[#1077]**
We report production of non-mass dependently fractionated iron and silicate smokes, condensed from silane and pentacarbonyl iron in a molecular hydrogen flow mixed with molecular oxygen at total pressures less than 100 Torr in an electrical discharge.

11:30 a.m. Rai V. K. * Thiemens M. H.
Mass Independently Fractionated Sulfur Component in Primitive Chondrites **[#1392]**
Here we report the first reproducible evidence of mass independent sulfur component in primitive chondrites which is most likely produced by photochemical processes in the early solar nebula.

MARTIAN NEAR-SURFACE ICE: PROPERTIES AND PROCESSES
Friday, 1:30 p.m., Crystal Ballroom A

Chairs: T. K. P. Gregg and K. L. Tanaka

1:30 p.m. Mellon M. T. * Feldman W. C.
The Global Distribution of Martian Subsurface Ice and Regional Ice Stability **[#2204]**
We examine the latest global-scale distribution of subsurface ice inferred from Mars Odyssey measurements and compare it with theoretical estimates of ice stability under various climate conditions.

1:45 p.m. Fastook J. L. * Shean D. E. Head J. W. Marchant D. R.
Ice Sheet Modeling During High-Obliquity Climates on Mars: Application to Tharsis Montes Tropical Mountain Glaciation **[#1794]**
Terrestrial ice sheet models are used to model formation and evolution of Tharsis Montes tropical mountain glaciers to assess obliquity scenarios and to help establish a geologically based reconstruction of the orbital and climate history of Mars.

2:00 p.m. Winebrenner D. P. * Koutnik M. Waddington E. D. Pathare A. V. Murray B. C. Byrne S. Bamber J. L.
Evidence for Past Flow in the Martian North Polar Layered Deposits from Ice Flow Inverse Modeling **[#1875]**
We analyze MOLA data on the NPLD and find that the inter-trough surface is consistent with ice flow equilibration of accumulation above present-day troughs and ablation below. We interpret this as evidence for ice flow prior to trough formation or persistence.

2:15 p.m. Hvidberg C. S. * Fishbaugh K. E.
Recent Flow Rates of the Martian North Polar Layered Deposits **[#2053]**
We have correlated layers exposed in trough walls across the martian north polar layered deposits. We compare the resultant stratigraphy with model predictions to assess whether large-scale flow has significantly affected the layers.

2:30 p.m. Fishbaugh K. E. * Hvidberg C. S.
Martian North Polar Layered Deposits: Stratigraphy and Relative Accumulation Rates **[#1647]**
Using MOC images and MOLA data, we correlate individual layers within the North Polar Layered Deposits up to a depth of ~500 m to gain stratigraphic information which is used to derive relative accumulation rates across the PLD and through time.

2:45 p.m. Tanaka K. L. * Mullins K. F. Skinner J. A. Jr. Rodriguez J. A. P. Fortezzo C. M.
Stratigraphy of North Polar Deposits on Mars: Major New Findings **[#2344]**
Analyses based on recent imaging and topographic data of parts of the north polar region on Mars are resulting in significant new understandings in the characterization and development of stratigraphy and landforms as related to sediment and volatile supply, climate variations, and eolian processes.

3:00 p.m. Kolb E. J. * Tanaka K. L. Greeley R. Neukum G. HRSC Co-Investigator Team
The Residual Ice Cap of Planum Australe, Mars: New Insights from the HRSC Experiment **[#2408]**
In this abstract we present results of our geologic mapping of the south polar residual ice cap deposits.

3:15 p.m. Gregg T. K. P. * Briner J. R. Paris K. N.
Glaciated Terrain in Gusev Crater, Mars **[#1752]**
Detailed investigation of hummocky terrain on the floor of Gusev crater, Mars, reveals robust similarities with terrestrial glaciated landscapes.

3:30 p.m. Rossi A. P. * Chicarro A. Pacifici A. Pondrelli M. Helbert J. Benkhoff J. Zegers T. Foing B. Neukum G.
Widespread Periglacial Landforms in Thaumasia Highland, Mars **[#1568]**
Recent glacial and periglacial landforms appear widespread in Thaumasia Highland. We are mapping them using HRSC data and, locally, MOC NA and Themis VIS. We started ice stability modeling for these landforms.

3:45 p.m. McMenamin D. S. * McGill G. E.
Martian Glacial Melt and Atmospheric Methane **[#1307]**
We compare possible sources of basal melt in martian glaciers and find that methane hydrate clathrate is an interesting possibility. If present in modern remnants of glacial ice, methane hydrate may also be a reservoir for atmospheric methane.

4:00 p.m. Shean D. E. * Head J. W. Kreslavsky M. Neukum G. HRSC Co-I Team
When Were Glaciers Present in Tharsis? Constraining Age Estimates for the Tharsis Montes Fan-shaped Deposits **[#2092]**
The fan-shaped deposits at Arsia and Pavonis Mons show evidence for multiple phases of late Amazonian glaciation under differing climate conditions. New crater age estimates from HRSC data provide a framework for recent climate change on Mars.

4:15 p.m. Helbert J. * Head J. W. Marchant D. Shean D. Kreslavsky M.
First Prospecting for Ice in the Flank Deposit at Arsia Mons **[#1371]**
There are several units on Mars which have been interpreted as glacial deposits based on morphological evidence. Our current focus is the Arsia Mons fan-shaped deposit. We will report some preliminary results of our prospecting for ice in one of the young units of the Arsia Mons deposit.

4:30 p.m. Crown D. A. * Chuang F. C. Berman D. C. Miyamoto H.
Ice-Driven Degradation Styles in the Martian Mid-Latitudes: Constraints from Lobate Debris Aprons, Lineated Valley Fill, and Small Flow Lobes **[#1861]**
This investigation examines the geomorphic characteristics of lobate debris aprons, lineated valley fill, and small flow lobes found on crater rims and massifs in order to characterize emplacement styles for ice-rich flows on Mars.

LUNAR REMOTE SENSING
Friday, 1:30 p.m., Crystal Ballroom B

Chairs: **M. S. Robinson and D. Domingue**

1:30 p.m. Gillis-Davis J. J. * Lucey P. G. Hawke B. R.
Mare Moscoviense a Window into the Interior of the Moon **[#2454]**
Investigating different mare units within Mare Moscoviense we find spectral evidence for low-calcium, high pyroxene. Is it possible that this is a surface exposure of the Mg-suite?

1:45 p.m. Hagerty J. J. * Lawrence D. J. Hawke B. R. Vaniman D. T. Elphic R. C. Feldman W. C.
Estimating Thorium Abundances of Basalt Ponds in South Pole Aitken Basin: Implications for the Composition of the Farside Lunar Mantle **[#1770]**
We use forward modeling of thorium data from the Lunar Prospector Gamma Ray Spectrometer to estimate thorium abundances of individual basalt ponds in South Pole Aitken Basin.

2:00 p.m. Kramer G. Y. * Jolliff B. L. Neal C. R.
Searching for High-Al Mare Basalts: Mare Imbrium and Apollo 14 **[#2221]**
Clementine and Lunar Prospector data are used to search for high-Al basaltic units in Mare Imbrium that may be related to the Apollo 14 high-Al mare basalts.

2:15 p.m. Garvin J. B. * Robinson M. S. Hapke B. Bell J. F. III Skillman D. Ulmer M. Pieters C.
UV Imaging of the Moon from the Hubble Space Telescope **[#2100]**
Hubble Space Telescope UV observations of three targets on the Moon have been successfully acquired (Apollo 15, Apollo 17, Aristarchus). These UV and Visible wavelength images demonstrate that lunar compositional mapping can be achieved via the HST's ACS instrument.

2:30 p.m. Wilcox B. B. * Lucey P. G. Hawke B. R.
Radiative Transfer Modeling of Compositions of Lunar Pyroclastic Deposits **[#1490]**
We use radiative transfer theory to model the compositions of three regional pyroclastic deposits for which high-quality spectra are available: Aristarchus, Humorum, and Sulpicius Gallus.

2:45 p.m. Robinson M. S. * Garvin J. B. Hapke B. Bell J. F. III Ulmer M. Skillman D. Pieters C. M.
HST UV–Visible Observations of the Apollo 17 Landing Area **[#2282]**
From Hubble Space Telescope (HST) Advanced Camera for Surveys High Resolution Camera (ACS/HRC) images we demonstrate the efficacy of UV imaging to map TiO_2 abundances within mature regolith in the region of the Apollo 17 landing site.

3:00 p.m. Campbell B. A. * Carter L. M. Campbell D. B. Hawke B. R. Ghent R. R. Margot J. L.
20-m Resolution Radar Studies of the Aristarchus Plateau and Reiner Gamma Formation **[#1717]**
We are collecting 20-m resolution, dual circular-polarization, Earth-based radar images of areas on the Moon that may contain useful resources, such as pyroclastic deposits, and to address the detailed geology of enigmatic features.

3:15 p.m. Domingue D. * Vilase F.
Photometric Effects on Spectral Interpretations: A Lunar Case **[#1924]**
Spectral variations due to photometry can mimic those attributed to composition in remote sensing data of planetary surfaces.

3:30 p.m. Cahill J. T. * Lucey P. G. Gillis-Davis J. J.
Mapping the Spatial Distribution, Mineralogy, and Geochemistry of Lunar Highlands Spectral Types **[#1453]**
Knowledge of lunar surface mineralogy and chemistry is central to understanding the evolution of the lunar crust. Here we present and evaluate central uplift maps of predefined spectral archetypes using modeling to determine mineralogy and chemistry.

3:45 p.m. Ghent R. R. * Campbell B. A. Hawke B. R. Campbell D. B.
Remote Sensing and Geologic Studies of the Southeastern Quadrant of the Moon **[#1815]**
We report on remote sensing studies of an area extending from Tycho crater to Mare Australe, and south to the pole. We use new 70-cm Earth-based radar observations and Clementine compositional data to investigate regional stratigraphy and geology.

4:00 p.m. Hughes C. G. * Blewett D. T. Hawke B. R. Richmond N. C.
Optical Maturity and Magnetic Studies of Lunar Swirls **[#1230]**
Lunar swirls are sinuous bright markings often associated with magnetic anomalies. Optical and magnetic study of selected swirls, including a previously undescribed swirl-like feature neary Airy, may lead to a better understanding of space weathering.

4:15 p.m. Lucey P. G. * Cahill J.
Magnesian Rock Types in the Lunar Highlands: Remote Sensing Using Data from Lunar Prospector and Clementine **[#1660]**
The distribution of magnesian anorthositic rocks are found to be consistent with inferences drawn from lunar meteorites. Mafic magnesian rocks are found in the PKT and SPA terranes, but are absent from the magnesian anorthosite regions.

4:30 p.m. Byrne C. J. *
The Near Side Megabasin of the Moon **[#1930]**
A very old, very large basin has been found through analysis of Clementine elevation data. Its ejecta is quantitatively modeled and accounts for the farside topography. Centered at 7°N, 21°E, it is 101 arc degrees in radius.

MARTIAN METEORITES: CHASSIGNITES AND NAKHLITES
Friday, 1:30 p.m., Marina Plaza Ballroom

Chairs: **R. C. F. Lentz and A. H. Treiman**

1:30 p.m. McCubbin F. M. * Nekvasil H. Lindsley D. H.
Apatite as a Key to Evaluating the Volatile Budget of Martian Magmas: Implications from the Chassigny Meteorite **[#1098]**
In Chassigny, olivine-hosted melt inclusions contain fluor-apatite; chlor-fluor-apatite is maskelynite-hosted, suggesting that magmatic volatile concentrations underwent significant changes from early to late stages of the crystallization history.

1:45 p.m. Pieters C. M. * Dyar M. D. Hiroi T. Lane M. D. Treiman A. H. McCanta M. Bishop J. L. Sunshine J.
Optical Properties of Martian Dunite NWA 2737: A Record of Martian Processes **[#1634]**
Although mid-IR spectra indicate NWA2737 is a well crystallized dunite, visible to near-IR spectra exhibit almost no recognizable features of olivine. The "brown" color is tied to the formation and geologic history of this meteorite.

2:00 p.m. Treiman A. H. * McCanta M. Dyar M. D. Pieters C. M. Hiroi T. Lane M. D. Bishop J. L.
Brown and Clear Olivine in Chassignite NWA 2737: Water and Deformation **[#1314]**
Olivine in the NWA 2737 chassignite is brown, and cut by ribbons of visually colorless olivine. The latter formed by deformation along the system [100]021. The brown color arises from ferric iron in the olivine, probably formed by loss of dissolved H^+.

2:15 p.m. Reynard B. * Van de Moortèle B. Beck P. Gillet P.
Shock-induced Transformations in Olivines of the Chassignite NWA 2737 **[#1837]**
Olivines of the second chassignite NWA 2737 display shock-induced transformations and in particular a black color, which is due to subsolidus reduction likely associated with high post-shock residual temperature. These microstructures are evidenced using TEM.

2:30 p.m. Boctor N. Z. * Wang J. Alexander C. M. O'D. Hauri E.
Volatile Abundances and H Isotope Signatures of Melt Inclusions and Nominally Anhydrous Minerals in the Chassignites and ALH84001 **[#1412]**
We determined the volatile abundances and H isotope signatures of melt inclusions and nominally anhydrous minerals in the chassignites and ALH 84001 by SIMS.

2:45 p.m. Wadhwa M. * Borg L. E.
Trace Element and ε^{142}Nd Systematics in the Nakhlite MIL 03346 and the Orthopyroxenite ALH 84001: Implications for the Martian Mantle **[#2045]**
We report new REE and ε^{142}Nd data for the nakhlite MIL 03346 and orthopyroxenite ALH 84001. Implications are presented for the Sm-Nd and Hf-W characteristics and the redox conditions in the source reservoirs of the martian meteorites.

3:00 p.m. Dreibus G. * Huisl W. Spettel B. Haubold R.
Halogens in Nakhlites: Studies of Pre-Terrestrial and Terrestrial Weathering Processes **[#1180]**
The comparison of halogen, C and S contents with those of trace elements like La, Ba, Th and U allows us to distinguish between terrestrial and martian weathering processes in nakhlites.

3:15 p.m. Schwenzer S. P. * Herrmann S. Ott U.
Pyroxenes from Governador Valadares and Lafayette: A Nitrogen and Noble Gas Study **[#1612]**
We present new noble gas and nitrogen data on pyroxene separates from Lafayette and Governador Valadares [rad. ^{4}He, cosmogenic nuclides (in Ne, Ar), martian interior, fractionated and unfractionated martian, and fractionated terrestrial atmosphere].

3:30 p.m. Walton E. L. * Herd C. D. K.
Crystallization of Mesostasis in Two Nakhlite Meteorites: The Fractal Approach **[#1988]**
Fractal analysis has been used to characterize the mesostasis of two nakhlite meteorites. Using the fractal dimension, in conjunction with previous crystallization experiments, we conclude that, upon eruption of a crystal-rich magma, MIL 03346 cooled at a faster rate compared to Nakhla.

3:45 p.m. Shih C.-Y. * Nyquist L. E. Reese Y.
Rb-Sr and Sm-Nd Isotopic Studies of Antarctic Nakhlite MIL 03346 **[#1701]**
Rb-Sr and Sm-Nd mineral isochron results of nakhlite MIL 03346 indicate that it was produced by clinopyroxene accumulation from a depleted martian mantle source with ^{147}Sm/^{144}Nd = ~0.23 and ^{87}Rb/^{86}Sr = ~0.078 about 1.36 ± 0.03 Ga ago.

4:00 p.m. Morris R. V. * McKay G. A. Ming D. W. Klingelhöfer G. Schröder C. Rodionov D. Yen A.
Magnetite in Martian Metorite MIL 03346 and Gusev Adirondack Basalt: Mössbauer Evidence for Variability in the Oxidation State of Adirondack Lavas **[#1594]**
Magnetite in martian meteorite MIL 03346 and Gusev Adirondack basalt is evidence for variable oxidation states for Adirondack lavas. As in the meteorite, the magnetite in Adirondack basalt is possibly present as a mesostasis phase.

4:15 p.m. Sautter V. * Jambon A. Boudouma O.
Cl-rich Amphibole in MIL 03346: Trace of Martian Soil in a Martian Meteorite **[#1318]**
The spacecraft missions revealed that Martian soils are enriched in Cl. We describe the first extra-terrestrial Cl-hastingsite (up to 7 wt % Cl), in melt inclusion from the nakhlite MIL 03346. It evidences contamination of the parent magma by Cl-rich evaporitic debris from the Martian soil.

4:30 p.m. Lentz R. C. F. * Taylor G. J. Hamilton V.
Modeling, Defining, and Searching for a Nakhlite-related Gabbro **[#2117]**
We modeled modes and mineral compositions for a proposed nakhlite-related gabbro using MELTS to crystallize published nakhlite parent magmas. We then derived thermal infrared spectra from these compositions for comparison to martian surface spectra.

PRESOLAR GRAINS
Friday, 1:30 p.m., Amphitheater

Chairs: **M. J. Pellin and H. Busemann**

1:30 p.m. Vollmer C. * Hoppe P. Brenker F. E. Palme H.
A Complex Presolar Grain in Acfer 094 — Fingerprints of a Circumstellar Condensation Sequence? **[#1284]**
We have identified 14 presolar silicates in the Acfer 094 meteorite with one complex grain consisting of an Al-rich core and a silicate rim. EDX measurements of this grain and results from a subsequent NanoSIMS study are presented.

1:45 p.m. Marhas K. K. * Hoppe P. Stadermann F. J. Floss C. Lea A. S.
The Distribution of Presolar Grains in CI and CO Meteorites **[#1959]**
Comparison of presolar silicate abundances from the Tagish Lake meteorite (CI2) and Yamato 81025 (CO3).

2:00 p.m. Ebata S. * Nagashima K. Itoh S. Kobayashi S. Sakamoto N. Fagan T. J. Yurimoto H.
Presolar Silicate Grains in Enstatite Chondrites **[#1619]**
We report the first finding of presolar silicates grains from three primitive enstatite (EH3) chondrites: Yamato-691, Allan Hills 81189, and Sahara 97072. We discovered 12 presolar silicates and discussed metamorphism effects for the abundances.

2:15 p.m. Kimura Y. * Nuth J. A. III
New Formation Route for Carbide-Core, Graphitic-Carbon Mantle Grains Based on Fullerenes **[#1073]**
We demonstrate a new formation route for core-mantle grains. The grains could have been produced by the deposition of large pre-nucleated carbon cages, formed via the Boudouard reaction from CO, that were then deposited onto carbide grain cores.

2:30 p.m. Jadhav M. * Maruoka T. Amari S. Marhas K. K. Zinner E.
Si and Mg-Al Isotopic Studies of Presolar Graphite from Orgueil **[#2177]**
We present Si and Mg-Al isotopic data for presolar graphite grains from Orgueil. The analyses indicate that the low-density graphite grains have a supernova origin, while the high-density grains appear to originate from low-metallicity AGB stars.

2:45 p.m. Busemann H. * Alexander C. M. O'D. Nittler L. R. Zega T. J. Stroud R. M. Cody G. D. Yabuta H. Hoppe P.
Correlated Microscale Isotope and Scanning Transmission X-Ray Analyses of Isotopically Anomalous Organic Matter from the CR2 Chondrite EET 92042 **[#2005]**
We discuss correlated examinations of organic matter from the CR2 chondrite EET 92042, using SIMS, STXM and other methods. We found a large, isotopically highly anomalous region of probable presolar origin that is C- and ^{13}C-poor and ^{15}N-rich.

3:00 p.m. Croat T. K. * Stadermann F. J.
Silicon Carbide Within Presolar Graphite **[#2048]**
Composite presolar grains (e.g., silicon carbide within graphite) can place constraints on circumstellar environments in which both of these phases form. We present results from a TEM and nanoSIMS study of a Murchison graphite with internal SiCs and iron grains.

3:15 p.m. Hynes K. M. * Croat T. K. Amari S. Mertz A. F. Bernatowicz T. J.
A Transmission Electron Microscopy Study of Ultramicrotomed SiC-X Grains **[#2202]**
We report the results of a NanoSIMS and TEM study of four SiC X-grains, which have a supernova origin. Like mainstream SiCs, initial polytype determinations indicate 3C-SiC is common, but with smaller domain size and higher Mg content from decayed ^{26}Al.

3:30 p.m. Gyngard F. * Amari S. Jadhav M. Zinner E. Lewis R. S.
Carbon, Nitrogen, and Silicon Isotopic Ratios in KJG Presolar Grains from Murchison **[#2194]**
Most previous measurements of Ti isotopes in SiC have suffered from various selection effects. To rectify this situation, we report C, N, and Si data for 247 randomly chosen SiC grains on which we plan to soon obtain Ti isotopic measurements.

3:45 p.m. Pellin M. J. * Savina M. R. Calaway W. F. Tripa C. E. Barzyk J. G. Davis A. M. Gyngard F. Amari S. Zinner E. Lewis R. S. Clayton R. N.
Heavy Metal Isotopic Anomalies in Supernovae Presolar Grains **[#2041]**
Isotopic anomalies in supernovae presolar grains do not show a canonical r-process. Rather they appear to have been exposed to an intense, but relatively brief neutron exposure.

4:00 p.m. Barzyk J. G. * Savina M. R. Davis A. M. Gallino R. Gyngard F. Amari S. Zinner E. Pellin M. J. Lewis R. S. Clayton R. N.
Measurement of the Isotopic Compositions of Six Elements in Individual Presolar SiC Grains **[#1999]**
We measured isotopic compositions of up to six elements (Mo, Zr, Ba, C, N, Si) in presolar SiC grains, allowing identification of contamination with material of solar system composition and constraining ^{13}C pockets abundance in AGB stars.

4:15 p.m. Kashiv Y. * Davis A. M. Cai Z. Lai B. Sutton S. R. Lewis R. S. Gallino R. Clayton R. N.
Extinct ^{93}Zr in Single Presolar SiC Grains and Condensation from Zirconium-depleted Gas **[#2464]**
The abundances of Zr and Nb in single presolar SiC grains were measured by SXRF. The data suggest that the s-process radioisotope ^{93}Zr ($t_{1/2} = 1.5 \times 10^6$ yr) condensed into the grains and that many of the grains condensed from Zr-depleted gas.

4:30 p.m. Heck Ph. R. * Hoppe P. Gröner E. Marhas K. K. Baur H. Wieler R.
Automated Search for Rare Presolar Silicon Carbide from Novae and of Type A/B: A Combined Isotopic Study of Single Grains with NanoSIMS and Noble Gas Mass Spectrometry **[#1355]**
We discuss new presolar nova grain candidates and A/B type grains found during an automated search for single presolar SiC grains with low C-12/C-13 ratios with the NanoSIMS and during a combined study with NanoSIMS and noble gas mass spectrometry.

PRINT-ONLY PRESENTATIONS

MOON

Goswami J. N. Thyagarajan K. Annadurai M.
Chandrayaan-1: Indian Mission to Moon **[#1704]**
The Indian mission to moon, Chandrayaan-1, to be launched in late 2007, will carry a host of Indian, European and U.S. payloads for selenological and chemical mapping of the lunar surface to further our understanding of the origin and evolution of the Moon.

Khavroshkin O. B. Tsyplakov V. V.
The Interstellar Dust Streams and Lunar Seismicity: Detection, Analysis, First Results **[#1008]**
The kinds of lunar seismicity are existing from Earth-solar tides, meteoroid streams, interplanetary dust streams, interstellar dust, solar wind and cosmic rays. The research of these objects is a modern task for planetologists. The first steps for that are described.

Stooke P. J.
Locating Landed Spacecraft and Artificial Impact Craters in LRO Images **[#1341]**
LRO will try to image some landed spacecraft and artificial impact craters from past missions. The greatest difficulty will come from positional uncertainty. Ejecta or nearby features will sometimes help. Luna 9 and Ranger 6 sites are illustrated and discussed.

Berezhnoy A. A. Gasnault O. Hasebe N. Kobayashi M. Michael G.
Correction of Lunar Prospector Elemental Maps **[#1032]**
Lunar Prospector Si content is underestimated, while Mg and Al contents are overestimated in Fra Mauro region. Corrected Si, Mg, and Al data were obtained and analyzed. Petrologic technique was used for checking the quality of Mg and Al elemental maps.

VENUS

Burba G. A.
Large Ring Structure Around Colorado Plateau in North America Looks Similar to Coronae on Venus **[#1052]**
Colorado Ring Structure is located between 33–41°N and 105–115°W. Its outer diameter is ~850 km, the rim width is ~170 km. The overall topographic shape is similar to the typical topography of the large circular features on Venus termed corona.

Krassilnikov A. S.
Relationship Between Radial/Concentric Volcanic/Tectonic Features on Venus (Coronae, Novae, Arachnoids and Calderas) **[#1853]**
Coronae, novae, arachnoids and calderas were formed due to similar processes controlled by few geological factors that determine main characteristics of the structures. Gradual tectonic and morphologic transition between features takes place.

IMPACTS

Basu A. R. Chakrabarti R. Peterson J. Poreda R. J. Becker L
Laser Raman Spectra of Bedout 'Maskelynite': Comparison with Shocked Plagioclases from Martian Meteorite (SaU 005), and the Lonar Impact Crater, and Synthetic Albite (CIT# 1424) and Anorthite (CIT# 1301) **[#2307]**
Laser Raman spectra of Bedout "maskelynite" shows remarkable resemblance with shocked plagioclases from Martian meteorite (SaU 005), Lonar impact crater, and synthetic albite and anorthite glasses.

Chakrabarti R. Basu A. R. Peterson J.
Trace Element-Isotope Geochemistry of Impact Breccia, Target Basalts and Laser Raman Spectroscopy of Shocked Plagioclase from Lonar Crater, India **[#2248]**
Trace element and isotopic data indicate Archean basement component in the impact breccia of the Deccan basalt-hosted Lonar Crater. Raman spectral study of Lonar and Manicouagan maskelynites indicate different modes of origin of maskelynites.

Feldman V. I. Sazonova L. V. Kozlov E. A.
Some Peculiarities of Impact Melts (Natural and Experimental Data) **[#1020]**
All impact melts are very specific formations distinctly differing from any other endogenous magmatic formations by sum of features. This publication presents our results obtained by studying the impact melts in the nature and experiments.

Gibsher N. A. Vishnevsky S. A.
The Popigai Impact Fluidizites, Water Fluid Inclusions in Lechatelierite Schlieren: Estimation of Conservation Pressures **[#1234]**
Description and genetic interpretations (conservation pressures) of water fluid inclusions in lechatelierite schlieren from the Popigai impact fluidizites.

Milyavskiy V. V. Sazonova L. V. Borodina T. I. Sokolov S. N. Beljatinskaja I. V. Zhernokletov D. M.
Plagioclase and Amphibole Transformations in Conditions of Step-like Shock Compression of Crystal Schist **[#1076]**
Transformations of different schists have been studied using of recovery assemblies of planar geometry (26–52 GPa). Our research centered on the comparison of the behavior in shock waves of minerals of the same groups but different compositions.

Povenmire H. Strange R. L.
The First Tektite from Dooly Crisp Counties, Georgia **[#1002]**
Newly discovered GA tektite expanding the known GA strewn field.

Sazonova L. V. Beljatinskaja I. V.
Shock and Thermal Transformation of Andalusite in Impactites of the Janisjarvi Astrobleme, Karelia, Russia **[#1019]**
This publication presents our results obtained by studying the impact and thermal metamorphism of andalusite from andalusite-plagioclase-quartz-muscovite-biotite schists that are the target rocks of the Janisjarvi astrobleme.

Svetsov V. V.
Thermal Radiation on the Ground from Large Aerial Bursts Caused by Tunguska-like Impacts **[#1553]**
Numerical simulations were made for the impacts of relatively small comets which produce explosions at altitudes of 5–10 km. Impact velocities were 20 and 50 km/s, comet diameters from 40 to 200 m, and incidence angles from 15° to 90°.

Vishnevsky S. A. Raitala J. Gibsher N. A. Palchik N. A. Simakin S. G.
The Popigai Impact Fluidizites **[#1268]**
Brief overview and new data on the Popigai impact fluidizites.

Williams K. E. Pappalardo R. T.
Variability in the Small Crater Population on Callisto **[#1202]**
We analyze Callisto imagery and find that much of the variability in small crater population on Callisto can be attributed both to secondary cratering and local resetting events.

METEORITES

Barrat J. A. Benoit M. Cotten J.
Bulk Chemistry of the Nakhlite Miller Range 03346 (MIL 03346) **[#1569]**
We report on the composition of MIL 03346 and have determined the concentrations of 45 elements using a combination of ICP-AES and ICP-MS procedures.

Gorin V. D. Alexeev V. A.
Radionuclides in the Bukhara CV3 and Kilabo LL6 Chondrites **[#1034]**
Contents of cosmogenic Mn-54, Na-22, Al-26, and natural potassium in chondrites Bukhara CV3 and Kilabo LL6 are submitted.

Hewins R. H. Zanda B. Bourot-Denise M. Albarède F. Bland P. A.
Formation of Oxygen Isotope Reservoirs by Mixing Chondritic Components **[#1944]**
$\Delta^{17}O$ is controlled by the abundance of CAIs in CC and of type II chondrules in OC, and $\Delta^{18}O = \delta^{18}O - \delta^{17}O$ by the abundance of matrix in all groups. Calculated $\Delta^{17}O$ and $\Delta^{18}O$ reproduce measured values. Chondrite groups originated by mixing isotopically distinct petrologic components.

Huber L.   Hofmann B.   Gnos E.   Leya I.
The Exposure History of the JaH 073 Meteorite **[#1628]**
We measured noble gases in fragments of the JaH 073 strewnfield meteorites. The data confirm that large meteorites usually suffer complex exposure with a first stage exposure on the parent body.

Ivliev A. I.   Alexeev V. A.
Estimation of the Meteorite Orbits by the Thermoluminescence Method **[#1047]**
Estimation of the meteorite orbits by the thermoluminescence method is considered.

Jacobsen S. B.   Ranen M. C.
The ^{135}Cs-^{135}Ba Chronometer and the Origin of Extinct Nuclides in the Solar System **[#2241]**
High precision Cs-Ba isotopic data for chondrites yield an upper limit of about 0.00001 for the $^{135}Cs/^{133}Cs$ ratio in the early solar system. This value is consistent with galactic average production but not with injection from a young stellar source.

Kashkarov L. L.   Shilobreeva S. N.   Kalinina G. V.
Chemical Modification of the Luna 24 Olivine Grains Under Solar Cosmic Ray Irradiation **[#1080]**
The new results of the radiation parameters in the silicate micrograins of the Luna 24 soil matter and the first results of the chemical modification inside an individual lunar regolith olivine microcrystals subjected to different exposure SCR protons and α-particles dose are presented.

Lavrentjeva Z. A.   Lyul A. Yu.   Shubina N. A.   Kolesov G. M.
Siderophile, Rare Earth and Some Other Trace Element Distributions in Components of Abee Enstatite Breccia **[#1035]**
Siderophile, rare earth and some other trace element distributions in components of Abee enstatite breccia are considered.

Miyamoto M.   Koizumi E.   Mikouchi T.
Verification of a Model to Calculate Cooling Rates in Olivine by Consideration of Fe-Mg Diffusion and Olivine Crystal Growth, II **[#1538]**
We developed a model to calculate the olivine cooling rate by analyzing zoning on the basis of Fe-Mg diffusion during crystal growth. We verify this model by using zoning profiles produced by dynamic crystallization for Martian and lunar meteorites.

Petford N.   Rushmer T.   Lansdown G.
Numerical Modelling of Liquid Metal Transport in Partially Molten H5 Ordinary Chondrite **[#1603]**
An equation-based model of liquid metal segregation in Fe-bearing chondrite meteorites is presented. Textural data from natural samples provide the input conditions. Initial results confirm porous flow of Fe-Ni-S liquid alloy as an important metal segregation mechanism in planetary interiors.

Sharygin V. V.   Kovyazin S. V.   Podgornykh N. M.
Mineralogy of Olivine-hosted Inclusions from the Omolon Pallasite **[#1235]**
This paper is concerning mineralogy of olivine-hosted inclusions from the Omolon pallasite. Troilite, kamacite, nickelphosphide, taenite, stanfieldite, chromite, whitlockite, eskolaite and Si-O-bearing phase were found in metal-sulfide blebs.

Smoliar M. I.   Alexander C. M. O'D.   Walker R. J.   Jacobsen S. B.
Re-Os Isochron for Allegan (H5): Reconciling Re-Os and U-Pb Chronologies **[#1468]**
New precise Re-Os isochron for Allegan (H5) allows to reconcile Re-Os and U-Pb chronometers with ~2 times improved precision. Also, due to record-low Re/Os ratio in several samples, isochron gives the most reliable value for the initial $^{187}Os/^{188}Os$ ratio of the solar system.

Wang Y.   Hua X.   Hsu W.
Phosphoran-Olivine in Opaque Assemblages of the Ningqiang Carbonaceous Chondrite: Implication to Their Precursors **[#1504]**
We report the first occurence of phosphoran-olivine in opaque assemblages of the Ningqiang carbonaceous chondrite and discuss its implications to the precursor of opaque assemblages.

Zhang A. Hsu W. Wang R. Ding M.
Assemblage of Diopside, Pyroxene, Akimotoite, and Ringwoodite in the Heavily Shocked Sixiangkou L6 Chondrite: Further Constraints of Shock Metamorphism **[#1069]**
This study reports the occurrence of diopside, pyroxene, akimotoite, and ringwoodite in the shock-induced melt veins of Sixiangkou and discuss its implication to the shock metamorphism.

MER: SPIRIT AND OPPORTUNITY

Knoll A. H. Arvidson R. E. Bell J. F. III Clark B. C. Grotzinger J. P. Jolliff B. McLennan S. M. Squyres S. W. Tosca N. Athena Science Team
Toward an Integrated Understanding of Outcrop Rocks Observed by Opportunity in Meridiani Planum **[#1655]**
Observations on outcrop rocks at Meridiani Planum range from the microscopic to regional in scale. Collectively, they support interpretation of Meridiani rocks as predominantly eolian sandstones, with alteration of precursor basalts before deposition and groundwater diagenesis afterward.

Moggi-Cecchi V. Salvadori A. Pratesi G. Franchi I. Greenwood R.
A New CH Carbonaceous Chondrite from Acfer, Algeria **[#1909]**
A single stone weighing 1456 g was found in November 2002 in the Acfer area, Algeria. Oxygen isotope, chondrules-matrix ratio as well as other petrographic features point to a classification as CH carbonaceous chondrite.

Pratesi G. Salvadori A. Moggi-Cecchi V. Franchi I. Greenwood R.
A New CK Carbonaceous Chondrite from Hammada Al Hamra, Libya **[#1899]**
A single stone weighing 198 g was found in 2001 in the Hammada al Hamra region of Libya. Petrographic features (mean chondrules dimensions, coarse grained matrix and presence of AOIs and CAIs) point to a classification as CK carbonaceous chondrite.

Salvadori A. Moggi-Cecchi V. Pratesi G. Franchi I. Greenwood R.
A New CO Carbonaceous Chondrite from Acfer, Algeria **[#1925]**
Many small fragments, totally weighing 118 g were found in the Acfer area by an Italian dealer. Chondrules size and types (predominance of granular olivine type), occurrence of twinned clinoenstatite and absence of plagioclase suggested a classification as CO carbonaceous chondrite.

MARS EXPRESS: PROBING THE DEPTHS

Melchiorri R. Encrenaz T. Drossart P. Fouchet T. Forget F. Langevin Y. Gondet B. Bibring J.-P. OMEGA Team
OMEGA/Mars Express Data Analysis: Possible Correlation Between Water Vapor and Presence of Gypsum in the North Polar Cap Region? **[#1561]**
We report on the detection of a seasonal variation of the water vapor content over a north polar region. A neighbouring region has been the subject of the spectral identification of gypsum. Further studies are necessary to identify the nature of this possible correlation.

MARS

Kress A. Head J. W. Marchant D. R.
The Nature of the Transition from Lobate Debris Aprons to Lineated Valley Fill: Mamers Valles, Northern Arabia Terra-Deuteronilus Mensae Region on Mars **[#1323]**
Mamers Valles lobate debris aprons (LDA) form in alcoves, meet and flow laterally to become lineated valley fill (LVF) suggesting a related mode of origin: individual debris-covered glaciers creating larger glacial landsystems.

López V. Tejero R. Ruiz J. Gómez-Ortiz D.
The Elevation Range of the Possible Meridiani/Arabia Paleoshoreline, Mars **[#1810]**
The whole topographic range along the Meridiani/Arabia shoreline would be ~1.6 km, between –0.5 and –2.1 km. This is still far of an equipotential surface, but it is a reasonable elevation range for a very old paleoshoreline.

Maxe L. P.
An Application of New Experimentally Received FTIR-Spectra to the Analysis and Comparison with Martian Spectra **[#1850]**
Using non-KBr method it was possible to recorder spectra of different powdered mineral substances, materials and gas components simultaneously, water solution and suspensions. The new method can be applied practically to simulate IR-spectra of components of martian surface and dust composition.

McGrane B. S. Golombek M. P.
Geomorphology Context and THEMIS Appearance of Boulder Fields in Phoenix Landing Region B **[#1541]**
A study of boulder fields in Region B, as identified in MOC images, that describes the geomorphology units that are most associated with boulder field occurrence and the appearance of those boulder fields in visible THEMIS images.

Metzger S. M.
Modifications to Dust Drapes on Soil at the MER Spirit Gusev Site **[#2296]**
Dust drapes are observed on rocks and soils at the MER Spirit Gusev site. Dust devil vortices, rover compression and disruption are examined to explore the response of dust deposits exposed to surficial processes.

Nahm A. L. Head J. W. III Marchant D. R.
Lobate Debris Aprons Surrounding Mesa Clusters North of Ismeniae Fossae, Mars: Characteristics and Transition to Lineated Valley Fill **[#1186]**
Lobate debris aprons examined in new high resolution images show evidence for origin in alcoves as debris-covered glaciers and merging to form lineated valley fill. These deposits suggest periods of glaciation in the Amazonian.

Papike J. J. Karner J. M. Shearer C. K.
Implications of Martian and Terrestrial Jarosite. A Crystal Chemical Perspective **[#1115]**
The importance of the discovery of jarosite at Meridiani Planum is discussed.

Plesko C. S. Werner S. C. Brumby S. P. Asphaug E. A. Neukum G. HRSC Investigator Team
A Statistical Analysis of Automated Crater Counts in MOC and HRSC Data **[#2012]**
We describe continuing efforts to develop automated crater counting algorithms for Mars surface images. Comparison of automated to manual counts yield automated counts that are within the 1-σ error of the manual counts in several adjacent diameter bins.

Popa I. C.
Salt Triggered Melting of Permafrost in the Chaos Regions of Mars **[#2218]**
An investigation of energy provided by ice-salt interaction as an alternative cause for permafrost melting in chaos regions on Mars. This process, along with the fluid freezing point depression, could explain the way water originated from chaos regions as source for outflow channels.

Pupysheva N. V. Basilevsky A. T. Ivanov B. A. Neukum G. Werner S. van Gasselt S.
Channel Network South-East of Olympus Mons, Mars, as seen in MEX HRSC Images: Morphology, Depths, Area and Volume **[#1144]**
SE of Olympus Mons there is a channel network studied using HRSC and MOC images and MOLA profiles. The network area was found to be ~273 km^2, depth from 8 to 40 m (24 m on average), volume 6.4 to 7.3 km^3 and volume of the carving liquid, 18 to 73 km^3.

Royer D. Nelson J. Wallace H. C.
Mars Spherule Size Distribution from Panoramic Camera Images **[#1001]**
Statistics performed on spherules images from the Opportunity's Pancam provides size distributions at two locations of Meridiani Planum. The distributions appear close together with in both cases a significant asymmetry towards lower spherule sizes.

Saraiva J. Bandeira L. P. C. Pina P.
A Structured Approach to Automated Crater Detection **[#1142]**
A structured methodology for automated recognition of impact craters is presented, comprising three phases: edge detection; template matching; and analysis of a probability volume to identify centers and dimensions of craters.

Seabrook A. M. Bridges J. C. Rothery D. A. Wright I. P.
Eskers in Isidis Planitia, Mars **[#2035]**
We have identified eskers in Isidis Planitia. Along with evidence of other ice-related features in the basins such as recessional moraines and pingos, they strongly suggest that the basin had a covering of ice in the past. This most likely occurred in the late Hesperian epoch.

Sprenke K. F.
A Gnome's-Eye View of Giant Impact Locations on Mars **[#1099]**
Impact basins on Mars of the size of Isidis and larger can be fit by three great circles, two of which, if they do represent ancient equators, are consistent with other studies of polar wander on Mars.

Tichy M.
Dry Flows on Mars **[#1240]**
Landforms on Mars are currently explained by the activity of water in fluid or firm state. An explanation based on the concept of soil movements is offered. It is founded on the physical properties of soil in martian conditions, mechanics of particulate materials, and observed martian morphology.

PLANETARY CARTOGRAPHY

Smith M. J. Petford N. Xiao L.
Planetary Remote Sensing and GIS: The Convergence of Software, Techniques and Data **[#1675]**
GIS has been used extensively within geoscience, however this has not been mirrored within the planetary science. We briefly explore the convergence between GIS, application of new techniques and availability of data within the planetary sciences.

Vaz D. A. Barata M. T. Alves E. I.
Automatic Detection and Classification of Fault Scarps on MOLA Data **[#1571]**
Wavelet analysis and mathematical morphology are applied to MOLA altimetry data to automatically extract tectonic features from Mars' surface.

ASTROBIOLOGY

Brown I. Mummey D. Sarkisova S. Allen C. McKay D. S.
Iron-Tolerant Cyanobacteria as an Effective Tool to Study Early Evolution of Life and the Development of Biosignatures **[#2342]**
Modern understanding of microbial ecology provides a lens through which the accumulating knowledge of physiology, molecular phylogeny and Earth's history can be integrated and focused on the phenomenon of prokaryotic evolution.

Furfaro R. Dohm J. M. Fink W. Schulze-Makuch D. Fairén A. G. Tarbell M. A. Hare T. M. Baker V. R.
Multi-Layer Fuzzy Logic-based Expert System for Conducting Tier-Scalable Planetary Reconnaissance **[#1257]**
A fuzzy logic approach is proposed to design a multi-layer expert system that can be used to autonomously operate the deployment of a novel mission architecture termed "tier-scalable" for life-containing assessment of planetary bodies.

Méndez A.
The Planetary Habitability Classification **[#2396]**
The suggested Planetary Habitability Classification (PHC) system provides a simple mechanism to compare the potential habitability of terrestrial-sized extrasolar planets with Earth and themselves.

Perry R. S.   Lynne B. Y.
New Insights into Natural Recorders of Planetary Surface Environments: The Role of Silica in the Formation and Diagenesis of Desert Varnish and Siliceous Sinter **[#1272]**
Desert varnish from the USA and sinter from NZ form in extreme environments and silica may play a significant role in their formation. If they follow similar preservation and diagenetic pathways, it is important to understand how their paleoenvironmental biosignatures change with time.

Phillips S. J. M.   Parnell J.
The Cairngorms as a Proposed Site for the Evaluation of Biosensing Equipment and Astrobiological Instrumentation **[#1027]**
The Cairngorms provides a good initial evaluation site for biosensing equipment and astrobiological instrumentation due to the variety and extremes of weather, ecology and terrain within a small, accessible area.

ASTEROIDS, COMETS, SMALL BODIES

Filonenko V. S.
Some Properties of Secular Variations of Brightness of Some Periodic Comets **[#1597]**
The results of the study of secular fading of some short-periodic comets during their all observed returns are presented. An influence of the 90-year solar activity cycle upon the changes of secular variations of these comets had been found.

Golubeva L.   Shestopalov D.
Are There Pyroxenes on A-Asteroid Surfaces? **[#1228]**
The 500-nm absorption feature in the reflectance spectra of the A-asteroids 289 Nenetta and 446 Aeternitas indicates that pyroxenes are present on these asteroids. By the "olivine minimum" of the 500-nm band we estimated that olivine for these asteroids contains approximately 55 wt.% forsterite.

Greenspon J. A.   Mardon A. A.   Mardon E. G.
Representations of Halley's Comet in April 1066 A.D. Found in the Bayeaux Tapestry and Other Contemporary Written Accounts **[#1527]**
Halley's Comet has been a significant character in global history — foretelling of events serving as a forecast tool to astrologers for centuries. A look at its significance in 1066 is presented herein.

Mardon E. G.   Mardon A. A.
References to Historical Comets from 497 A.D. to 1402 A.D. in English Manuscripts **[#1092]**
The following abstract is a compilation of the cometary references found in English Medieval Manuscripts from the 5th Century to the 14th Century AD. The references to comets in England over the Medieval period shows an interest in cometary astronomy in England.

Perov N. I.
Forecasting the Closest Approach of Undiscovered Before Now Comets with the Earth **[#1018]**
In terms of a pairwise three-dimensional two-body problem–Sun-comet and planet-comet–the space-time domains for new comets are localized. Jupiter and Saturn are considered as detectors of the epochs of appearances near the Earth of undiscovered hazardous comets.

Shestopalov D.   Golubeva L.
Compositional Variations of the 495-nm Absorption Band in Olivine Reflectance Spectra **[#1227]**
The long-wavelength shift of the 495-nm absorption band center in the olivine reflectance spectra is observed when forsterite content decreasing. The shift of band center depends on grain size and gives error of forsterite estimation amounting to ±10 wt%.

Slyuta E. N.
Shapes of Small and Planetary bodies: Case of Phoebe **[#1088]**
Shapes of small and planetary bodies principal differ from each other. Phoebe on the shape parameters is not a small body and belongs to planetary bodies.

Tikhomirova E. N. Perov N. I.
Perturbations of Meteors' Particles Motion Under Action of Photons and Protons **[#1089]**
The new integrals of meteors motion with taking into account the effect of Poynting-Robertson and drag caused by solar wind are deduced and used in practice. The life-time of future meteor showers of comet Tempel I is estimated (after explosion made July 4, 2005).

PRESOLAR GRAINS

Fisenko A. V. Semjonova L. F.
Helium and Neon in Grain-Size Fractions of the Boriskino CM2 Nanodiamond **[#1045]**
The analysis of grain-size fractions of the Boriskino nanodiamond has shown either (a) processes of acceleration of ions of P3 and HL components were various or (b) the He and Ne contents in nanodiamond are caused by noble gas component.

INTERPLANETARY DUST PARTICLES

Davoisne C. Leroux H. Grimblot J. Gengembre L. Frere M. Feirreiro V. Djouadi Z.
Jones A. P. d'Hendecourt L.
Morphological and Chemical Silicate Evolution Under Ion Irradiation **[#1715]**
Ionizing irradiations on samples with olivine composition are investigated. Chemical and morphological modifications are observed and studied. These changes may contribute to a better understanding of gas species actions on grain surface in the ISM.

Tsou P. Brownlee D. E. Chi Z. H.
Nondestructive Characterization of Samples Captured in Aerogel **[#1479]**
Due to the dimensions of the aerogel capture cell ($2 \times 4 \times 3$ cm), nondestructive SEM and IR cannot be applied on embedded particles. Our efforts to evaluate the Raman spectroscopy for this *in situ* characterization capability are described here.

Von Korff J. S. Westphal A. J. Anderson D. P.
A Method for Combining Judgements in Distributed Decision Making, Applied to the Stardust Project **[#1985]**
Interstellar dust grains, captured in aerogel by the Stardust mission, will be located by volunteers recruited over the Internet. We describe a statistical method for determining the number of volunteers who must examine each image.

EARLY SOLAR SYSTEM EVOLUTION AND PLANETARY FORMATION

Alibert Y. Mousis O.
Structure and Evolution of the Saturn's Subnebula — Implications for the Formation of Titan **[#1141]**
We calculate the structure and the evolution of the Saturn's subnebula, in a way consistent with the formation process of the planet, by using a two-dimensional evolutionary turbulent alpha-model. We also discuss the implications for the formation of Titan in the subnebula.

Canup R. M. Pierazzo E.
Retention of Water During Planet-Scale Collisions **[#2146]**
Results of SPH simulations of impacts between large, ice-rich impactors and an Earth-like planet are presented, in particular the predicted fraction of water retained as a function of impact velocity and angle.

Gusev A. V. Petrova N. K.
Normal Modes in Rotation of the Earth-like Planets **[#1669]**
For a planet with a solid inner core and a liquid outer core, there are four rotational normal modes. This numbers is reduced to two for a planet without inner core, and to one for a planet without liquid core.

Holin I. V.
Earth-based OREPS to Measure Variations in Planetary Spin **[#1118]**
The synthesis and analysis of the OREPS approach is described to measure variations in planetary spin vectors.

Horner J. Mousis O. Hersant F.
Deuterium and Cometary Reservoirs **[#1041]**
Using a deuterium-enrichment profile, which offers a relationship between the D:H ratio incorporated in grains and their formation place in the nebula, we examine the possible effect that formation in different regions could have on the values of this ratio observed in comets today.

Kortenkamp S. Weidenschilling S. J. Marzari F.
Perturbed Planet Formation: Accounting for Massive Companions in Simulations of Planetesimal Growth **[#2034]**
We study planet formation in perturbed systems where planetesimal growth occurs under the influence of massive companions, either additional stars (e.g., Gamma Cephei) or pre-existing giant planets (e.g., Jupiter and Saturn in our own solar system).

Mousis O. Alibert Y. Sekine Y. Sugita S. Matsui T.
Fischer-Tropsch Catalysis in a Turbulent Model of the Jovian Subnebula **[#1139]**
We examine the production of methane through the Fischer-Tropsch catalysis in the Jovian subnebula and its implications for the composition of produced satellitesimals by using an evolutionary turbulent accretion disk model.

Pauzat F. Ellinger Y. Mousis O.
Sequestration of Noble Gases by H_3^+ in the Outer Solar Nebula — Implications for the Formation of Comets **[#1331]**
We discuss the implications of the production of stable complexes formed by H_3^+ and noble gases in the gas-phase for the formation of comets in the outer solar nebula.

Petit J.-M. Mousis O. Alibert Y. Horner J.
Photophoresis as a Source of Crystalline Silicates in Comets **[#1558]**
We show that photophoresis is an effficient transport mechanism that allows crystalline silicates formed in the inner nebula to move outward in the formation regions of comets. This mechanism is found consistent with the heterogeneity of crystalline silicates abundances observed in comets.

Rushmer T. Petford N. Humayun M.
Can Deformation Induced Core-Mantle Interaction Account for the "Late Veneer"? **[#1936]**
Results from our model of shear-enhanced dilatancy and return flow suggest that at least some of the "late veneer" component in the present day Earth could be internal in origin, but triggered by external impacts.

Sahijpal S.
Numerical Simulations of the Planetary Differentiation of Planetesimals **[#1688]**
Numerical simulations of planetary differentiation of planetesimals with ^{26}Al and ^{60}Fe as the heat sources have been carried out.

Ustinova G. K.
The Key Role of the Type Ia Supernova in Origin of the Solar System **[#1070]**
Injection of the iron enriched matter of the Type Ia Supernova into the protosolar nebula has created the initial large-scale chemical heterogeneity of the accreting matter, which in conditions of the supersonic turbulence has resulted in the initial metal-silicate separation of the matter.

Vityazev A. V. Bashkirov A. G. Pechernikova G. V.
Gravito-MHD of Gas-Dust Disk Near Young Sun: Dissipative Stage **[#1860]**
Layered models of post-accretion disk are investigated where an accumulation of bodies occurs. At the same time, a turbulent outward transport of an angular momentum and gas to the periphery of the disk is accounted in the MHD-active upper layer.

Ward Wm. R. Canup R. M.
Tidal Interactions Between a Planet and a Circumplanetary Disk **[#2169]**
The tidal interaction between a planet and a circumplanetary disk with spiral wave structures is considered. The process can deposit angular momentum from the planet's rotation into the disk, inhibiting inward diffusion and increasing the fraction of material available for satellite formation.

OUTER PLANETS, SATELLITES, AND RINGS

Adriani A. Moriconi M. Colosimo F. Coradini A. Filacchione G. Orosei R. D'Aversa E. Capaccioni F. Cerroni P. Bellucci G. Brown R. H. Baines K. H. Bibring J.-P. Buratti B. J. Clark R. N. Combes M. Cruikshank D. P. Drossart P. Formisano V. Jaumann R. Langevin Y. Matson D. L. McCord T. B. Mennella V. Nelson R. M. Nicholson P. D. Sicardy B. Sotin C.
Determination of the Haze Layer Parameters in the Saturn Atmosphere from Cassini-VIMS Images **[#1584]**
The main goal of this study is the determination of the altitude of the upper clouds in Saturn atmosphere with some of optical parameters of them. The images that we analyzed were taken by Cassini-VIMS in April 15, 2005.

Filacchione G. Coradini A. Capaccioni F. Cerroni P. Bellucci G. Brown R. H. Baines K. H. Bibring J.-P. Buratti B. J. Clark R. N. Combes M. Cruikshank D. P. Drossart P. Formisano V. Jaumann R. Langevin Y. Matson D. L. McCord T. B. Mennella V. Nelson R. M. Nicholson P. D. Sicardy B. Sotin C. Adriani A. Moriconi M. D'Aversa E. Tosi F. Colosimo F.
VIS-NIR Spectral Properties of Saturn's Minor Icy Moons **[#1271]**
This work contains a comparative study of Cassini/VIMS VIS-NIR spectra of the minor moons of Saturn Atlas, Pandora, Prometheus, Janus, Epimetheus, Telesto and Calypso.

Hahn J. M.
Small Shepherd Satellites in Saturn's Encke Gap? **[#1025]**
The Cassini spacecraft has detected several ringlets residing in Saturn's Encke gap. Small unseen moonlets also inhabiting the Encke gap are suspected, since they might confine particles in ringlets; this possibility is assessed herein.

Moriconi M. Adriani A. Gardini A. Coradini A. Filacchione G. Orosei R. D'Aversa E. Capaccioni F. Cerroni P. Bellucci G. Brown R. H. Baines K. H. Bibring J. P Buratti B. J. Clark R. N. Combes M. Cruikshank D. P. Drossart P. Formisano V. Jaumann R. Langevin Y. Matson D. L. McCord T. B. Mennella V. Nelson R. M. Nicholson P. D. Sicardy B. Sotin C.
Considerations on the Titan Topography Based on the Cassini-VIMS Measurements in the NIR Range **[#1579]**
A technique based on the band ratio method for in-band and out-band reflectances has been set to estimate surface topography of Titan. This technique was applied to the images taken by Cassini-VIMS during the March 31, 2005, flyby.

Owen T. C. Aksnes K. Beebe R. Blue J. Brahic A. Burba G. A. Smith B. A. Tejfel V. G.
Titan: Nomenclature System and the Very First Names for One More World **[#1082]**
Description of feature types on Titan is made as first approach. Ten feature types and Latin terms for naming, and seven categories of proper names are established. Forty-five features obtained their names — the first names ever given on the surface of Titan.

Rosaev A. E.
Notes to Ijiraq and Kiviuq Orbital Evolution Reconstruction **[#1134]**
The unique orbital characteristics of small irregular Saturn satellites Ijiraq and Kiviuq provide very rare mutual close encounters. It is possible to calculate main periods in studied system. The epoch of most recent close encounter is calculated.

Shalygina O. S. Korokhin V. V. Akimov L. A. Starodubtseva O. M. Marchenko G. P. Shalygin E. V. Velikodsky Yu. I.
Causes of Observed Long-Period Variations of the Polarization at Polar Regions of Jupiter **[#1599]**
Using new data the anticorrelation between linear polarization asymmetry and insolation in jovian polar areas has been found. The mechanism of influence of seasons' changing (through temperature variations) on polarization formation has been proposed.

Stern S. A. Weaver H. A. Steffl A. J. Mutchler M. J. Merline W. J. Buie M. W. Young E. F. Young L. A. Spencer J. R.
The Origin of the Quadruple System at Pluto **[#1241]**
We argue that P1 and P2's proximity to Pluto and Charon, their circular orbits coincident Charon's orbital plane, and their apparent locations in or near high-order mean-motion resonances with Charon, all result from their formation with Charon.

Veeder G. J. Matson D. L. Davies A. G. Johnson T. V. Castillo J. C.
Loki Patera: The Bottom of a Sea Story? **[#1767]**
So far, our sea story considers Loki Patera on Io as a large uniform body of magma. The dark region is a crust which founders, pieces sink and are replaced by fresh, liquid lava. The fate of the recycled material is linked to conditions near the bottom.

Volent R. Kereszturi A.
Comparison of Ice Blocks on Earth, Mars, Europa and Ganymede **[#1316]**
We have analyzed areas with disrupted blocks on Earth, Mars, Europa and Ganymedes, probably made of ice. We found that some Martian blocks regarding their basic morphometric parameters show resembling characteristics to ice rafts on Europa chaotic and Earth polar terrains.

EDUCATION AND PUBLIC OUTREACH

Bérczi Sz. Gál-Sólymos K. Gucsik A. Hargitai H. Józsa S. Szakmány Gy. Kubovics I. Puskás Z.
How We Used NASA Lunar Set in Planetary and Material Science Studies: Experiences of 10 Years of Studies in Eötvös University, Hungary **[#1298]**
Our 10 year program on the NASA Lunar Sample Set included: petrographic studies and comparisons (with terrestrial rocks, meteorites, SNC samples, industrial materials), educational (films, CD, atlases, maps) and complex (analog, space robotic) studies.

Hegyi S. Drommer B. Hegyi A. Biró T. Kókány A. Hudoba Gy. Bérczi Sz.
Analog Planetary Material Studies of Igneous Rocks in Field Trips at Hungarian Sites of North-Balaton and Mecsek Mountains with University Space Probe Models Hunveyor and Husar **[#1136]**
We used the educational lander Hunveyor and rover Husar units of Pécs and Székesfehérvár Colleges to visit the North-Balaton and Mecsek Mountains where igneous rocks, basalt tuff and its ultramafic inclusions, and phonolite are exposed.

Kabai S. Bérczi Sz.
Space Stations Construction by Mathematica: Interactive Programs to Use the Double Role of the Golden Rhombohedra Modules (The Crystallography of a Space Station) **[#1121]**
We prepared an interactive Mathematica program to study crystallography and technology of constructing a space station with modular units capable of attaching them both with regular crystallographic and with quasi-crystalline method in 3D space.

Proshletsova M. V. Perov N. I.
Astronomy: Research Methods of Teaching **[#1105]**
Astronomy is a subject to provide the educational process based on using of significant discoveries of students and research methods of teaching. These discoveries consolidate the social status of astronomy. Such teaching of astronomy is fundamental and superior to the classic one.

Szikra I. Ferenczi Gy. Varga T. Darányi I. Hudoba Gy. Földi T. Hegyi S. Bérczi Sz.
A New Form of Space Science Education: Preparations for Phoenix Lander Mission Simulations by Hunveyor in Terrestrial Conditions **[#1169]**
Using the Phoenix near future landing on Mars, we prepared the Hunveyor model for simulations of various atmospheric measuring instruments on Phoenix, as a new form of space science education with analog studies by simulations in terrestrial conditions.

OTHER

Alexeev V. A.
Changes of the Solar Activity and Terrestrial Climate **[#1033]**
The changes of the solar activivity and terrestrial climate for last 125 years are compared.

Davis K. A. Dykman C. A.
The Need for Knowledge Management in the Multifaceted World of Robotics **[#1072]**
This is a position paper advocating the need for a knowledge management approach to integrating the independent areas of robotics research and development.

Program Author Index

** Denotes speaker*